Modelling and analysis of smart localised energy system for a sustainable future power network

Ye-Obong Udoakah

School of Engineering

Cardiff University

A THESIS SUBMITTED IN PARTIAL FULFILMENT OF THE REQUIREMENTS FOR THE DEGREE OF DOCTOR OF PHILOSOPHY IN ELECTRICAL ENGINEERING

October 2023

Abstract

Combating the increasing effect of climate change and averting future energy crisis resulting partly due to our continued dependence on conventional energy sources requires exploring aggressively more sustainable means of generating and utilising energy. Currently, most developed countries are transitioning slowly from a fossil fuel dominated energy system to a sustainable and renewable energy based system. However, for the results of these transitions to be impactful and reduce the global temperature rise to the expected 1.5^{o}C, the approach must be wholistic and encompassing. Although there are a lot of ongoing research in the areas of renewable energy integration into the grid, however, there seems to be a dearth of such studies in some specific aspect of the power system application. Consequently, this thesis models and performs several analyses on a smart localised energy system with the aim of decarbonising some aspects of the future power network.

The study investigated the dynamics of residential power demand in Nigeria and modelled the residential energy consumption profile. An excel-based algorithm was developed and applied to the developed model. The results of the residential energy consumption was based on the appliance energy end use methodology. This was used to develop a load profile indicative of a typical urban residential energy demand in Nigeria and employed to predict the effects of residential loads on the power system. Following the frequent use of diesel generators by municipal councils to power street lighting, several case studies demonstrating how to optimise street lighting energy consumption and improve energy efficiency were carried out using simple economic analysis indices such as Life Cycle Cost (LCC), Annualized Life Cycle Cost (ALCC), Net Present Cost (NPC), Cost of Energy (COE), and

Return on Investment (ROI). The solar photovoltaic (SPV) system had the lowest LCC and ALCC, thus making it the most economically viable option.

The response of the power system to Distributed Energy Resources (DERs) integration was also investigated. Data from a real low voltage (LV) distribution network in Nigeria was obtained and used in modelling the network using PSCAD/EMTDC software package. Different impact studies considering addition of distributed generation sources and increase in the load were performed. Volt-VAr optimisation (VVO) was performed to enable the inverter-based PV systems participate actively in voltage regulation by the provision of flexible reactive power support. A net total of 1.359 MVAr and 1.301 MVAr respectively are utilised from the inverter to regulate voltage within the acceptable limits, hence reducing the substation reactive power by 19.8% and 18.9% respectively during the controlled case study. Also, the total active power loss did reduce from 0.437 MW to 0.172 MW while the deviation of consumer voltages from the nominal system voltage was reduced by 33.4% during the controlled case studies. Overall, the VVO did enhance power quality and reliability by improving the feeder voltage profile and reducing the active power losses in the network.

Lastly, to decarbonise some operation of the power system and improve the system resilience, DERs integrated black start restoration (BSR) strategy was implemented. The formulated BSR problem was implemented as a dynamic optimisation problem and the simulation was performed on the Nigerian 330 kV 48-bus system. The mixed-integer linear programming (MILP) technique was adopted and modelled to suit the nature of the BSR method developed. The black start power restoration sequence and the development of a viable restoration strategy were actualised. The simulation of the MILP model was achieved in MATLAB® using the IBM CPLEX™ solver. For the Nigerian 330 kV 48-bus system analysed, it was observed that most

loads were optimally restored before the 30^{th} time step for a black start operation. Both the experimental and numerical methodology were adopted in the validation of energy storage system (ESS) adopted for the proposed BSR simulated study. The optimal battery power availability for participating in restoration was reached in less than 50 minutes, with ESS optimally contributing to power restoration achieving 4.3% & 18.1% for Kaduna and Jos respectively.

List of Tables

List of Figures

List of Publications

Journal Publications Under Review – <u>first-author</u>

Udoakah, Y., Sonder, Hasan., Liang, Jun., Cipcigan, Liana., "Battery state of charge analysis of PV and grid connected energy storage systems used in power system black start applications," (Renewable and Sustainable Energy Reviews)

Udoakah, Y., Liang, Jun., Cipcigan, Liana., "Enhancing Power System Resilience by Distributed Energy Resources Deployment as Black Start Units," (Applied Energy)

Udoakah, Y., Liang, Jun., Cipcigan, Liana., "Decarbonising Power System Operations by DER Application in the Provision of Black Start Services," (IEEE Transactions on Power Systems)

<u>Journal as co-author</u>

Mudaheranwa, E., Sonder, Hassan Berkem, **Udoakah, Y.,** Cipcigan, Liana, Ugalde-Loo, Carlos. Participation of load aggregator in grid frequency stabilization with consideration of renewable energy resources integration, Energy Reports, 9, 2023, pp. 3967-3988.

H. B. Sonder, **Udoakah, Y.,** Cipcigan, Liana, "Real-time analysis and state of charge estimation of battery energy storage systems connected to rapid charging hubs," (Under Review in Journal of Power Sources)

Published Conferences

First author

Udoakah, Y., Mudaheranwa, E., Liang, Jun., Cipcigan, Liana. Black Start Application in Power System Restoration using Distributed Energy Resources. (A paper presented at the 14th International Conference on Applied Energy-ICAE2022, in Bochum, Germany, August, 2022. Pp. 1-6, DOI: https://doi.org/10.46855/energy-proceedings-10190

Udoakah, Y., Adedoyin, Inaolaji, Cipcigan, Liana, Sumit Paudyal. Volt-VAr Optimisation of a Low Voltage Distribution Network in Nigeria. (A paper presented at the IEEE PES & IAS Conference {POWERAFRICA CONFERENCE} in Kigali, Rwanda, August, 2022)) pp. 1-5. DOI: 10.1109/PowerAfrica53997.2022.9905368 (Publisher: IEEE) (This paper won the **1st Runner-up Award** at the Conference)

Udoakah, Y., Sonder, Hasan., Cipcigan, Liana. Development of a Viable Black Start Restoration Pathway and Problem Formulation Sequence. (A paper presented at the IEEE International Energy Conference (ENERGYCON 2022), in Riga, Latvia, May, 2022) pp. 1-6. DOI: https://doi.org/10.1109/ENERGYCON53164.2022.9830473 (Publisher: IEEE)

Udoakah, Y., Sonder, Hasan., Cipcigan, Liana. Nigerian Distribution Network Feeder Impact Assessment with Electric Vehicle Integration. (A paper presented at the IEEE International Energy Conference (ENERGYCON 2022), in Riga, Latvia, May, 2022) pp. 1-6. DOI: https://doi.org/10.1109/ENERGYCON53164.2022.9830280 (Publisher: IEEE)

Udoakah, Y., Sonder, Hasan., Cipcigan, Liana. Low Voltage Distribution Network Simulation and Analysis for Electric Vehicle and Renewable Energy Integration. (A paper presented at the PES Innovative Smart Grid Technologies North America {ISGT-North America} in Washington, DC, USA, February, 2021) DOI: 10.1109/ISGT49243.2021.9372184 (Publisher: IEEE)

Udoakah, Y., Saad, Khalaf., Cipcigan, Liana. Blackout and Black Start Analysis for Improved Power System Resilience: The African Experience (A paper presented at the IEEE PES & IAS Conference {POWERAFRICA VIRTUAL CONFERENCE} in Nairobi, Kenya, August, 2020) **DOI:** 10.1109/PowerAfrica49420.2020.9219884 (Publisher: IEEE)

Udoakah, Y., Mudaheranwa, E., Cipcigan, Liana. Dynamic Modeling of Energy Consumption Pattern of a Typical Nigerian Average Urban and Rural Household for Microgrid PV Design. (A paper presented at the IEEE PES Innovative Smart Grid Technologies Europe {ISGT-Europe} in Bucharest, Romania, September, 2019) pp. 1-5. http://dx.doi.org/ 10.1109/ISGTEurope.2019.8905464 (Publisher: IEEE)

Udoakah, Y., Mudaheranwa, E., Cipcigan, Liana. Municipal Street Lighting Systems Energy Cost and Carbon Footprint Estimation in Uyo, Nigeria. (A paper presented at the IEEE PES & IAS Conference {POWERAFRICA CONFERENCE} in Abuja, Nigeria, August, 2019) pp. 476-481. http://dx.doi.org/10.1109/PowerAfrica.2019.8928661 (Publisher: IEEE)

Co-author

Mudaheranwa, E., Sonder, Hassan Berkem, **Udoakah, Y.,** Cipcigan, Liana, Ugalde-Loo, Carlos. Dynamic Demand Control for Grid Frequency

Stabilization. (A paper presented at the IEEE PES & IAS Conference {POWERAFRICA CONFERENCE} in Kigali, Rwanda, August, 2022)) pp. 1-5. DOI: 10.1109/PowerAfrica53997.2022.9905361 (Publisher: IEEE)

Mudaheranwa, E., Masnego, G., **Udoakah, Y.,** Cipcigan, Liana. Development and Analysis of Rwanda's Future Energy Scenarios as input for Long Term Regulated Investment in Electricity System Planning. (A paper presented at the AEEES Conference {The 3rd Asia Energy and Electrical Engineering Symposium} in Chengdu, China, March, 2021) pp. 1124-1129. DOI: http://dx.doi.org/10.1109/AEEES51875.2021.9403043 (Publisher: IEEE)

Mudaheranwa, E., **Udoakah, Y.,** Cipcigan, Liana. Rwanda's Energy Profile and Potential Renewable Energy Resources Mapping towards Sustainable Development Goals. (A paper presented at the IEEE PES & IAS Conference {POWERAFRICA CONFERENCE} in Abuja, Nigeria, August, 2019) pp. 533-538. http://dx.doi.org/10.1109/PowerAfrica.2019.8928834 (Publisher: IEEE)

Nomenclature

Abbreviations

ADN	Active distribution network
ADMS	Advanced distribution management systems
ALCC	Annualized life cycle cost
AMI	Advanced metering infrastructure
AMF	Average monthly fuel in liters used
BR	Battery replacement
BSR	Black start restoration
BSI	British Standards Institution
CBN	Central bank of Nigeria
CCR	Charge controller replacement
DisCos	Distribution companies
CO_2	Carbon dioxide
CHP	Combine heat and power
CIS	Customer information system
CLPU	Cold load pick up
COE	Cost of Energy
CTC	Carbon Trust and Crown
DERs	Distributed energy resources
DERMS	Distributed energy resources management systems
DG	Distributed generation
DMS	Distribution management system
DOPF	Distribution grid optimal power flow
DR	Demand response
DSR	Demand side response
ECN	Energy Commission of Nigeria
EEF	Electricity emission factor

EM	Engineering method
EO	Engine overhauling
EPRI	Electric power research institute
ESS	Energy storage systems
ESO	Electricity system operators
EVs	Electric vehicles
FEF	Fuel emission factor
GB	Great Britain
GenCos	Generation Companies
GIS	Geographic information system
GHG	Greenhouse Gas
Gt	Gigatonnes
HOMER	Hybrid Optimization Model for Multiple Energy Resources
HPS	High pressure sodium
HVAC	Heating Ventilation and Air Conditioning Systems
IEA	International energy agency
If	Inflation rates
Ir	Interest rates
ISO	International Standards Organization
IVR	Interactive voice response
KCL	Kirchhoff's circuit law
LCOE	Levelised cost of energy
LCC	Life cycle cost
LED	Light emitting diode
LIP	Linear integer program
LR	Lamp replacement
LV	Low voltage
MGCC	Microgrid control center
MILP	Mixed-integer linear programming

MINLP	Mixed integer non-linear problem
MPC	Model predictive control
MW	Megawatt
NERC	Nigerian Electricity Regulatory Commission
NPC	Net present cost
O/F	Oil and filter
O/M	Operations and maintenance
OMS	Outage management system
PC	Personal computer
PVBBSs	Photovoltaic battery backup systems
PHEV	Plug-in electric vehicles
PPM	Part per million
PSR	Power system restoration
PV	Photovoltaic
PW	present worth
PWM	Present worth of maintenance
RCSs	Remote controllable switches
RE	Renewable energy
RES	Renewable energy sources
REMP	Renewable energy master plan
ROI	Return on Investment
SCADA	Supervisory control and data acquisition
SDGs	Sustainable development goals
SDP	Semidefinite program
SM	Statistical methods
SNGFG	Small natural gas fueled generators
SO	System operators
SPV	Solar photovoltaic
SPEN	SP Energy Networks

SRN	System restoration navigator
SSR	Sequential service restoration
STG	Steam turbine generator
TCN	Transmission company of Nigeria
TE	Transactive energy
T&D	Transmission and Distribution
THD	Total Harmonic Distortion
TWh	Terawatt-hours
USB	Universal serial bus
V2G	Vehicle to grid
VVO	Volt-VAr optimization
WHO	World Health Organisation
WIS	Wind information system
WW	Worker's wage
ZIP	Constant-impedance, constant-current and constant-power loads.

Symbols and Parameters

T	The length of the time horizon
Δt	The length of the time step
Nn	Total number of nodes
$N\text{br}$	Total number of lines
Nl	Total number of loads
Ng	Total number of DGs

Sets

$\mathbb{C}$	Set of complex numbers. $\mathbb{C}^{3\times1}$ is the set of 3×1 vectors of complex number
$\mathbb{R}$	Set of real numbers. $\mathbb{R}^{3\times1}$ is the set of 3×1 vectors of real number
$\mathbb{Z}$	Set of integer numbers. $\mathbb{Z}_2^{3\times1}$ is the set of 3×1 vectors of binary integer
$\mathcal{T} \coloneqq \{1,2,\dots,T\}$	The set of time steps, T is the length of horizon.

$\Phi \coloneqq \{a, b, c\}$	The set of phases for single, two, and three-phase nodes and lines
$\mathcal{N} \coloneqq \{1,2, \dots, Nn\}$	The set of all the nodes such as load buses and DG buses.
$\mathcal{NF} \subseteq \mathcal{N}$	The set of nodes that cannot be energized, e.g., fallen power line poles
$\mathscr{L} \subseteq \mathcal{N}$	The set of nodes connected to loads
$\mathscr{L}S \subseteq \mathscr{L}$	The set of loads that can be switched on or off remotely
$\mathscr{L}F \subseteq \mathscr{L}$	The set of loads that cannot be restored in a short time
$\mathcal{G} \subseteq \mathcal{N}$	The set of nodes connected to DGs
$\mathcal{G}S \subseteq \mathcal{G}$	The set of substation buses (i.e., slack buses) or DGs with black start capability
$\mathcal{G}F \subseteq \mathcal{G}$	The set of DGs that cannot be utilized for service restoration
$\mathcal{B} \coloneqq \begin{Bmatrix} (\mathrm{i},\mathrm{j}): \mathrm{i} \in \mathcal{N}, \\ \mathrm{j} \in \mathcal{N}, \mathrm{i} \neq \mathrm{j} \end{Bmatrix}$	The set of lines
$\mathscr{B}^{S} \subseteq \mathscr{B}$	The set of lines that can be controlled remotely
$\mathscr{B}^{F} \subseteq \mathscr{B}$	The set of lines which are found to be damaged or disconnected and hence requires to be isolated or fixed (e.g., trees lean on these lines, blown fuses)
$\mathcal{V} \subseteq \mathscr{B}$	The set of lines installed with voltage regulators and transformers
$\mathscr{E} \subseteq \mathcal{N}$	The set of ESS
$\mathcal{E}^{\mathrm{F}} \subseteq \mathcal{N}$	The set of ESS not participating in BSR
$\mathscr{R}$	The set of voltage regulators

Superscripts and Subscripts

"S"	Superscript to indicate that a component/set is controllable, e.g., $\mathcal{B}^{\mathrm{S}}$
"F"	Superscript to indicate that a component/set is faulty, e.g., B^{F}
"N"	Superscript to indicate that a variable is related to node set, e.g., , $s_{i,t}^{N}$
"BR"	Superscript to indicate that a variable is related to a line, e.g., $x_{ij,t}^{BR}$
"L"	Superscript to indicate that a variable is related to a load, e.g., $P_{l,t}^{L}$
"G"	Superscript to indicate that a variable is related to a DG, e.g., $P_{g,t}^{G}$
"i"	Subscript to represent the node number, e.g., , $s_{i,t}^{N}$
"ij"	Subscript to represent the two end nodes of a line, e.g., , $x_{ij,t}^{BR}$
"l"	Subscript to represent the load number, e.g., , $x_{l,t}^{L}$

"g"	Subscript to represent the DG number, e.g., , $x_{g,t}^{G}$
Variables	
$s_{i,t}^{N} \in \{0,1\}$	Energization status of node i at step t
$x_{ij,t}^{BR} \in \{0,1\}$	Energization status of line (i,j) at step t
$x_{i,t}^{L} \in \{0,1\}$	Energization status of load l at step t
$x_{g,t}^{G} \in \{0,1\}$	Energization status of DG g at step t
$x_{e,t}^{ESS\_CH} \in \{0,1\}$	Charging action for ESS e at step t
$x_{e,t}^{ESS\_DISCH} \in \{0,1\}$	Discharging action for ESS e at step t
$\boldsymbol{P}_{g,t}^{\phi}, \boldsymbol{Q}_{g,t}^{\phi} \in \mathbb{R}^{3\times1}$	Three-phase active and reactive power provided by the DG at node $g \in \mathcal{G}$ for each phase at step t
$P_{e,t}^{\text{ESS\_CH}}, P_{e,t}^{\text{ESS\_DISCH}}$	Single-phase charging & discharging active power for ESS e at step t
$Q_{e,t}^{\text{ESS\_CH}}, Q_{e,t}^{\text{ESS\_DISCH}}$	Single-phase charging & discharging reactive power for ESS e at step t
$SOC_{e,t}^{\text{ESS}}$	State of charge (SOC) for a single-phase ESS e at step t
$P_{ij,t}^{\text{BR}}, Q_{ij,t}^{\text{BR}} \in \mathbb{R}^{3\times1}$	Three-phase active and reactive power going through the line between node i and node j at time step t
$P_{l,t}^{\text{L}}, Q_{l,t}^{\text{L}} \in \mathbb{R}^{3\times1}$	Three-phase active and reactive power of load l at time step t. Note they are determined by the control variables of load status $x_{i,t}^{\text{L}}$.
$V_{i,t}$	Node voltage at time step t
$\beta_{r,t}$	Tap ratio for voltage regulator r at time step t
Operators	
$\odot$	Element-wise product for vectors and matrices
$\oslash$	Element-wise division for vectors and matrices

Acknowledgment

Studying for and successfully completing a PhD requires more than a "community" effort. I honestly wouldn't have successfully accomplished this feat without the direct and indirect help I received from members of this "community". To them I dedicate the success of this milestone to!

Prof. Liana, you are indeed a very special and rare breed. As the head of my PhD supervision "community" you made every day of my PhD research fun filled, enjoyable, fulfilling and very productive. You did not just encourage, but you spurred and facilitate all the external research related trainings and conferences I attended. You meticulously read and provided insightful feedback on every piece of wring I sent across to you. For this, you would always be appreciated. Thank you for being more than just a supervisor! I can confirm that I am among the privileged few who have had such a smooth PhD ride. Prof. Jun Liang, besides being a part of my supervisory team, you are an asset to the wider academic community. Thank you for the several timely prompts and platforms you provided for me to share my research outputs. You challenged me to maximise my potentials and I'll always be grateful for this.

I couldn't have been very successful without the relative peace and stability I enjoyed from the home "community". My dear wife as the head of the "home office" made tremendous sacrifices to ensure that I had the maximum concentration required to carry out a research of this magnitude. Interestingly, she carried on with looking after our two lovely kids Itohomfonma and Otoutibeima while also studying for her PhD. I can't overemphasis how indebted I am to you all. Thank you for bearing with me and also enduring my long period of absence. I can only reward you all by dedicating this work to you. I love you all!

My extended family is yet another "community" whose contributions are immeasurable. To my parents, Prof. and Mrs. Udoakah, you provided all the motivation I needed besides supporting my home front with child care and ensuring they were not in lack. My siblings Qs UnyimeAbasi, Mmenyeneobong, Obongodot, Abasiokpon, their spouses and children were readily available to ensure my immediate family did not really feel my absence. Thank you DayeAbasi and Dara-Abasi for keeping my son and daughter very busy. Family is everything and I love you all. My in-laws, were also amazingly helpful. To my parents in-law Mr and Mrs Ubon, I owe you a debt of gratitude.

To the Christian "community" at home and abroad, I can't thank you enough for your relentless prayers and support. I can only ask for God's blessings upon you. The support I received from this special "community" is unquantifiable and the list of persons is endless. In no particular order, I want to say a special thank you to the following persons; Prof. and Mrs Bassey Antia, Engr. and Mrs Daniel Ebong, Mr and Mrs Usen Ekpo, Mboutidem Ekpo, Nsese Ekpo, Mr and Mrs Emmanuel Boateng, Mr and Mrs Kwaku Twumasi, Mr and Mrs Marvelous Steward, Mma Ekah, Mr and Mrs David Winstanley, Mr and Mrs Iniobong Charles, Mr and Mrs John Bassey. To members of the Church of Christ community in Uniuyo campus, Stratford, and Newport, I say thank you.

The Smart Grids and EV research group is another amazing "community" I can't stop acknowledging. You guys were my primary support base and you all made the weekly meetings interesting to attend. The contributions of two outstanding persons in this community to the success of my PhD is worthy of mention. Thank you Hasan Berkem Sonder and Emmanuel Mudaheranwa

for being more than just research partners. The relationship we have built is sure to stand the test of time, as we now have become family. Also deserving of appreciation are members of my research office. They made every seconds spent in the office count. To other members of the wider research community who peer reviewed my papers and provided feedback, I am grateful. Your contribution by way of constructive criticism of my work served as the fuel needed to refine my analytical skills. To those whose work has provided the foundation for which mine is resting, I have made meticulous effort to acknowledge this by way of referencing.

These special "community" of people are those I would classify as "friends beyond limit". Their contributions in various ways went more than a mile to enhance the completion of my PhD. Some of these ones have been duly acknowledged in most or all of the published works associated with this study. In that regard, I am full of gratitude to Uduak Akpanedet, Inimfon Okure and Engr. Moses Enang. Thank you Dr. Imoh Nkan for agreeing to share all the TCN data you obtained for your PhD research with me. Dr. Gideon Umoh you have taught me what true friendship means. Despite your very busy schedules, you did not only assist with the sorting of the raw and unprocessed data, you were there in the data analysis phase as well. I honestly wouldn't have made significant progress without your assistance. I can't appreciate you enough. Dr. Ogbonnaya Agwu, your encouragement, motivation and role in perfecting the finished work deserve worthy commendation. For this, I'll always be full of gratitude.

During the course of my PhD, I met colleagues whose perseverance in their PhD pursuit was an encouragement and motivation to me. In this "community" are a host of persons including; Eferhonore Efe-Eyefia, McDonald Nyalapa, Iona, Onyeka Amiebenomo, Godwin, Martins, Davide,

Hector, Oscar. I also met and made new friends and flat mates. In this special "community" are; Esther Efe-Eyefia, John Ovuson, Katie and Jana. To my friends and colleagues in Nigeria who kept on checking on my progress, I really appreciate. Thank you Ubongete, Puma, mandy, Bliss, Amanam, Otobong and Utibe. To the Luthisco class of 98, I can't hold back my admiration of you guys. Thanks for all the fun time which provided the needed timely stress relief.

Without the funding provided by the Nigerian government through TETFund, my PhD dream would either have been delayed or made more difficult. For this I am most grateful. The ultimate acknowledgement and appreciation goes to God, the owner and giver of wisdom. To Him alone I return all the glory and praise for indeed, "Ye-Obong" all things are possible!

Table of Contents

CHAPTER 1

1.0 INTRODUCTION

1.1 The Energy System

Energy remains pivotal to the achievement of the sustainable development goals (SDGs). Specifically, access to affordable, reliable, sustainable and modern energy for all by 2030 is the core theme of the (SDG 7). In simple terms, the provision of energy is the means to an end and energy access the world over is the major driver of economic, industrial, technological and human growth. Access to sustainable energy has continued to remain one of the greatest challenges of the 21st century.

The increasing effect of climate change resulting from carbon dioxide (CO_2) and other greenhouse gases emissions associated with the use of fossil fuels (coal, oil and gas) has prompted the active search for sustainable alternative energy sources. In order to reduce the impact of climate on the environment, global climate targets have been set and countries are expected to significantly reduce their CO_2 emissions levels. To accomplish this, a gradual but steady transition from a fossil fuel dominated energy system to a sustainable and renewable energy-based system has to take place.

With the increase in the world population, the world energy consumption has continued to increase. The global primary energy consumption shown in Fig. 1.1 [1], captures the world consumption in exajoules (EJ) and shares of primary energy in percentage. By inspection, it is seen that coal, crude oil and natural gas are the three major energy resources with the highest consumption level globally. These three energy sources are also the major

emitters of CO_2, nitrous oxide, methane and other greenhouse gases emissions which according to [2] have increased the global temperatures by almost 1°C since pre-industrial times.

The effects of climate change have continued to impact negatively on the environment and have often resulted in extreme weather events such as; flooding, wild fire, storm, heat-waves, droughts, rise in sea-level [3]. Some of these events have caused severe damage to the power system resulting in blackouts. In some developing countries, non-weather related blackouts are becoming a regular occurrence. For instance, in Nigeria, frequent power outages appears to be the major reason most people tend to rely on the use of generators for their alternative power source. The economic, social, and political impact of blackouts events have been succinctly discussed in [4]. **This thesis aim to address some of the peculiar challenges facing the Nigerian Power System by the application of distributed energy resources (DERs) to improve the grid resilience**.

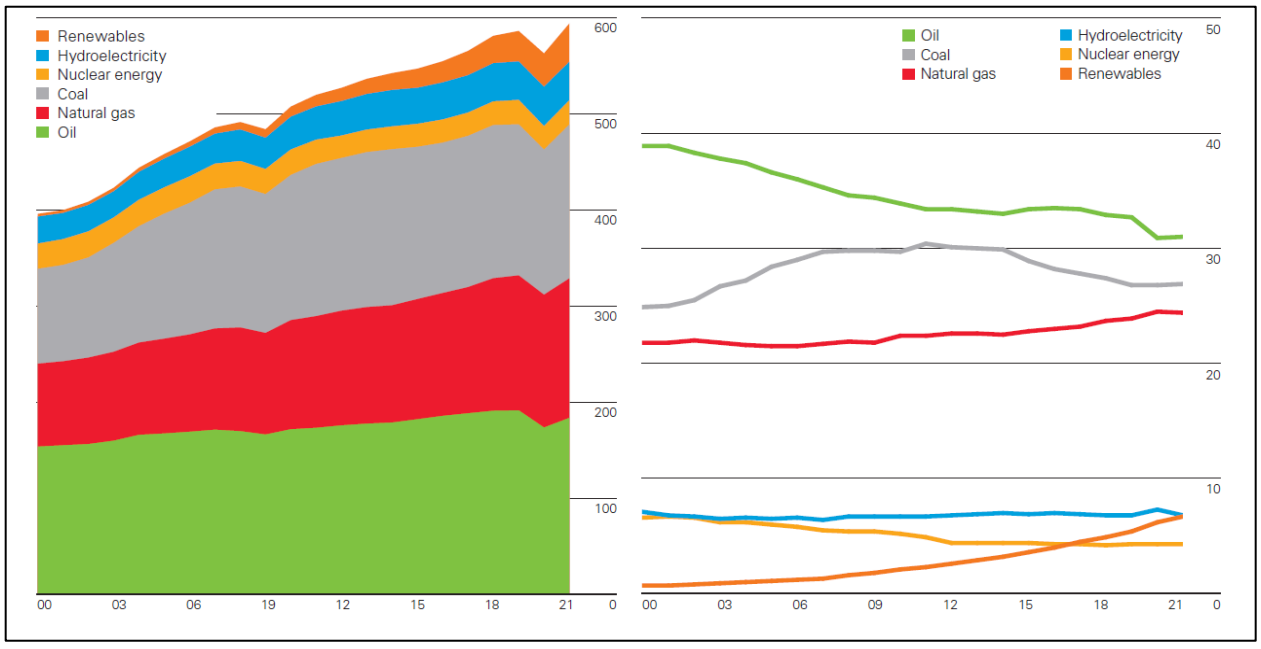

Fig. 1.1. World consumption in EJ and shares of primary energy in percentage [1].

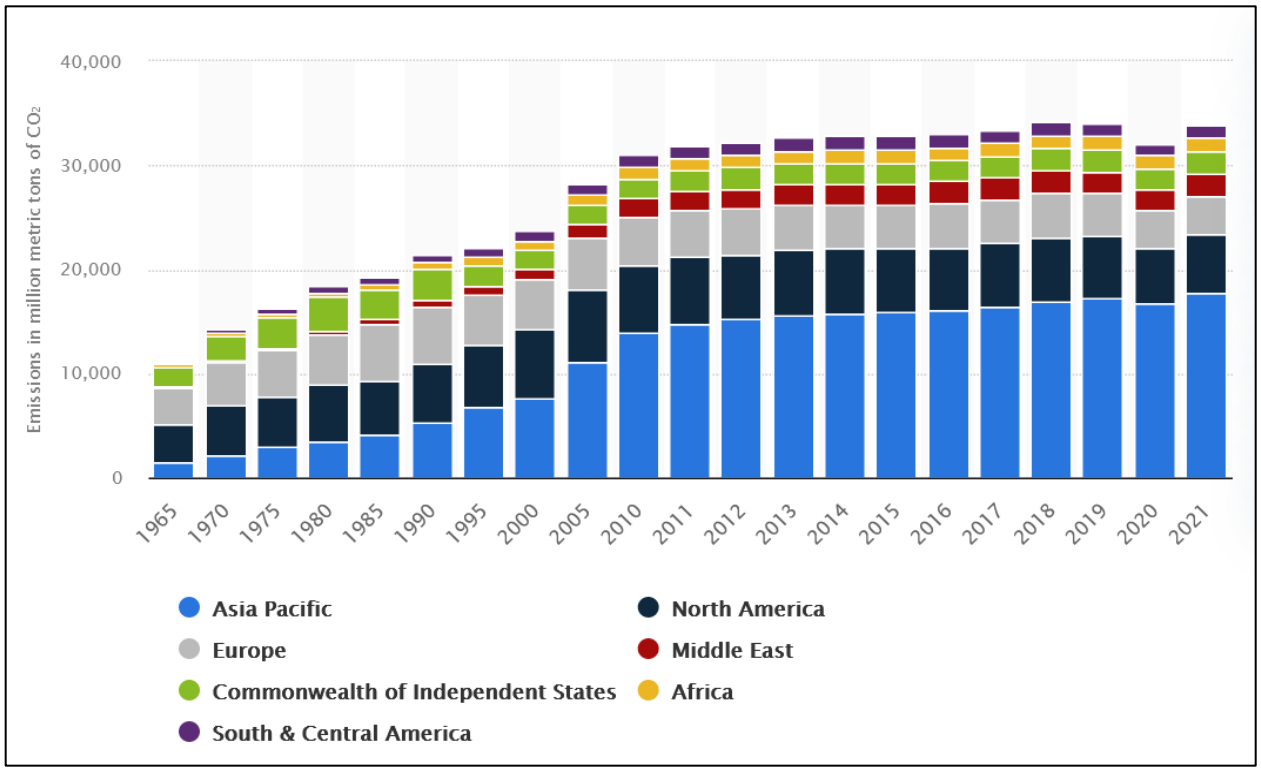

Fig. 1.2. Annual CO_2 emissions by world region [1, 5].

The annual CO_2 emissions by world region is presented in Fig. 1.2. According to [3, 5], the concentrations of CO_2 in the atmosphere which is about the highest levels in over 800,000 years are over 400 ppm. The global annual CO_2 emissions have also been estimated to be 36 billion tonnes per year with current trend projected to continue. Unfortunately, despite sustained global campaign for a sustainable energy future, analysis and future projections indicates that the world may likely not meet its agreed target of limiting global warming to 2 ^oC or less.

1.2 COVID-19 Impact on the Energy System

The world energy system was also impacted by the COVID-19 pandemic in 2020. According to [6], during the first quarter of the year, there was a

3.8% decline in the global energy demand. The energy use and demand were significantly altered resulting from government policies and lockdown which was implemented in nearly all the countries. Global electricity demand reduced by 5% and up to 10% in some regions due to service reductions in industries and other major energy demanding sectors [6]. Fig. 1.3 [6] highlight the trend in electricity demand fall in some countries. The global emission levels were also significantly reduced. As observed by [6], the global CO_2 emissions levels were expected to fall by 8% which translate to about 2.6 gigatonnes (Gt).

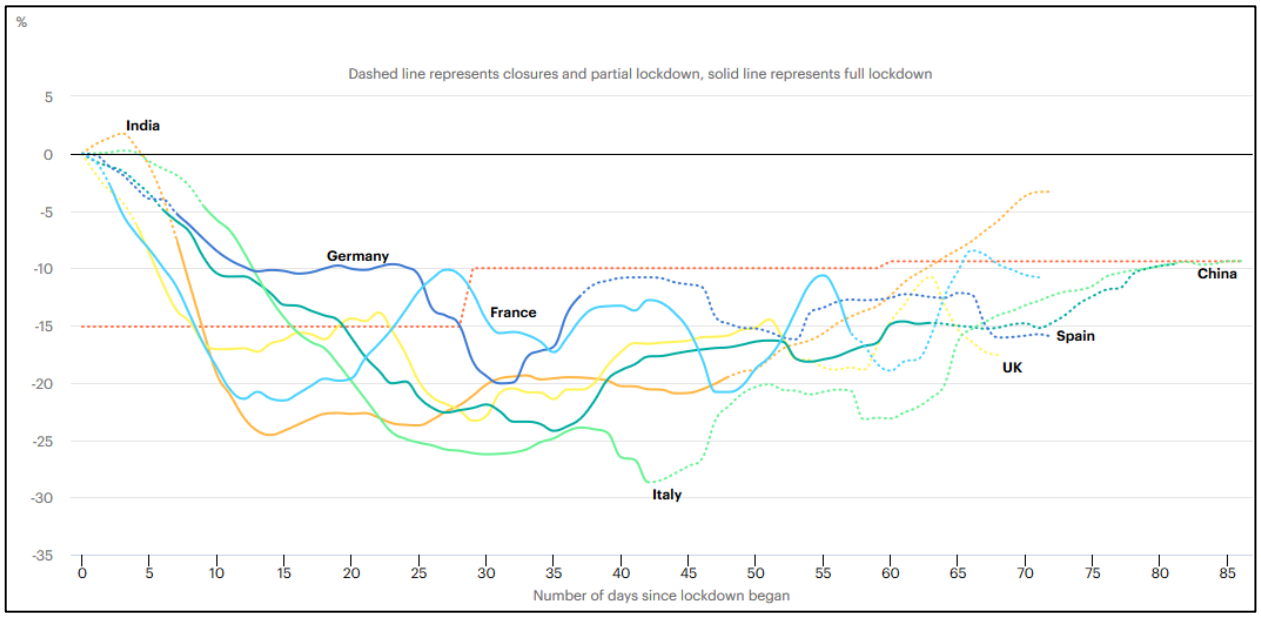

Fig. 1.3. Electricity demand trend in selected countries during lockdown 0 to 86 days [6].

The effect and impact of Covid-19 on the energy system seems to have reiterated the need to navigate towards a sustainable energy system. Ironically, as most of the other energy sectors were impacted by Covid-19, the renewable energy sector seems to have soared across the globe. The power mix across most regions was observed to have shifted towards renewable resulting from the lockdown measures taken across the globe. As

noted by [6], this was primarily due to depressed electricity demand, low operating cost and priority access to the grid through regulations.

Statistically, renewables-based generation was observed by [6] to have increased by 3% with a resultant share of renewables in electricity supply nearing 28% in the first quarter of 2020. This according to [6] was attributed to the double-digit percentage increase from wind power and a major boost in the solar photovoltaic (PV) output from projects carried out in previous years. The electricity mix by region is presented in Fig. 1.4. One major take away from the chart is that the electricity supply in most regions under lockdown underwent a significant shift towards low carbon energy sources during the first quarter of 2020 which further emphasis the need for transitioning towards a sustainable energy future [6].

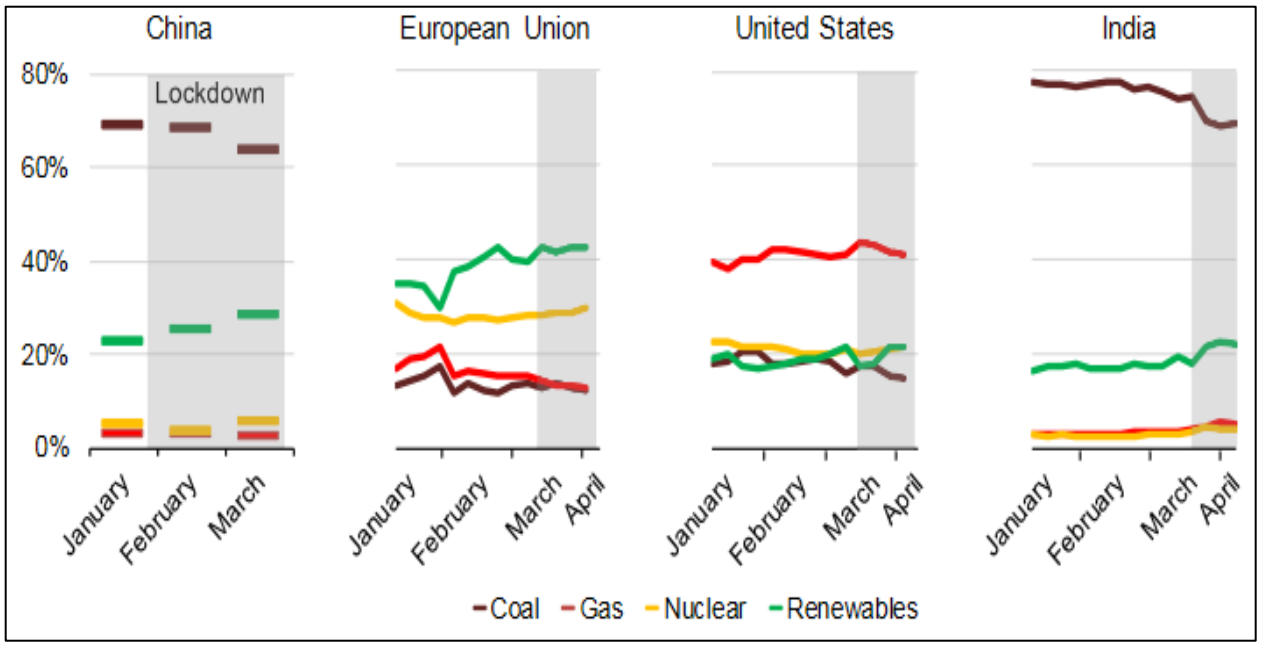

Fig. 1.4. Electricity mix by region 2020 [6].

1.3 Towards a Sustainable Energy System

As the world population continues to increase, the global energy demand is also expected to rise and meeting the growing energy demand in a sustainable manner has remained one of the greatest challenges of the 21st century. Increasing the energy supply to meet the growing demand is one of the four elements of sustainability highlighted by [7]. As observed by [8], to achieve a sustainable energy system requires the provision of affordable energy to everyone from an energy source that is devoid of high risk. It also involves improving the living standards for millions the world over.

The concept of sustainable development as defined by [7], emphasised on the importance of the present generation to meet their needs without compromising that of the future generation. In order to achieve sustainability, [7, 9] observed that the four elements of sustainability with respect to the energy system namely: (i) the ability to increase the supply of energy to meet growing human needs, (ii) energy efficiency and conservation, (iii) public health and safety, and (iv) "protection of the biosphere and prevention of more localised form of pollution" must be met. Despite the diverse views on what a sustainable energy system should be, the environment, economy and society seem to be the tripod on which sustainable energy systems sits.

Statistically, research has shown that human activities relating to energy production and consumption are the leading cause of greenhouse gas and other related emissions [10]. According to World Health Organisation (WHO), there is still high reliance on traditional cooking methods which involves the use of smoky fuels such as burning biomass (wood, animal dung and crop waste) and coal. Such cooking method not only harm the

environment, but also causes harm to the users and often times leads to premature death resulting from illness associated with air pollution [11].

Achieving a sustainable energy system would imply sustainably changing human activities relating to energy production and consumption. This would involve increasing the renewable energy shares in electricity production, decarbonising transportation through electrification, switching from fossil-based means of transportation to electric vehicles (EVs), adopting and using energy efficient devices and appliances and generally aiming to achieve the net zero target in all energy sectors. To achieve this would entail changing the dynamics of the future power and energy network.

1.4 Future Energy and Power System

The power network has been described as one of the most complex systems designed and operated. From the series of interconnected generators operating synchronously to the transmission and distribution systems spanning thousands of miles down to the millions of energy consumers spread across the various land mass. The system is continuously operated to meet the increasing load demands subject to a set of dynamic security constraints. For the traditional power system the current flow is unidirectional (Fig. 1.5) [12] and the system operation although complicated is carried out by a set of known procedures.

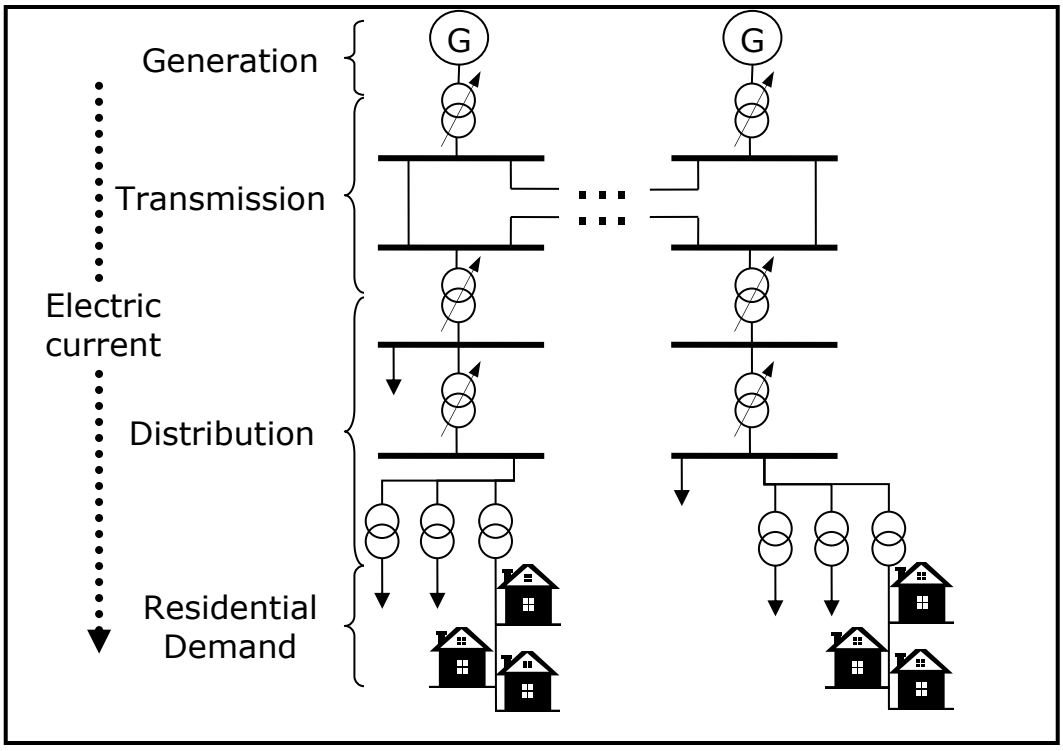

Fig. 1.5. Traditional power system with unidirectional electricity flow [12].

For most traditional or conventional power systems, the power generation is achieved using fossil-based plants. These generating stations are usually located away from the city centers or large populated areas. The rating of these generators varies from a few hundred to thousands of MW. The generated power is evacuated through the transmission lines to the various sub-transmissions stations where a series of transformation is performed before it is further distributed. Different countries operate at different transmission and distributions voltage levels and the various networks are managed by system operators (SO).

The future power system holds the promise of a sustainable, low emission and energy efficient technology, yet with more complications. The non-synchronous nature of most renewable energy technologies along with the complex power electronic interface associated with these technologies adds yet another challenges to the complex power system. Besides this, the

intermittent nature of most of the renewable energy sources that would gradually replace some of the fossil-based power generation technologies has stirred on-going debate on the resilience of the future power system.

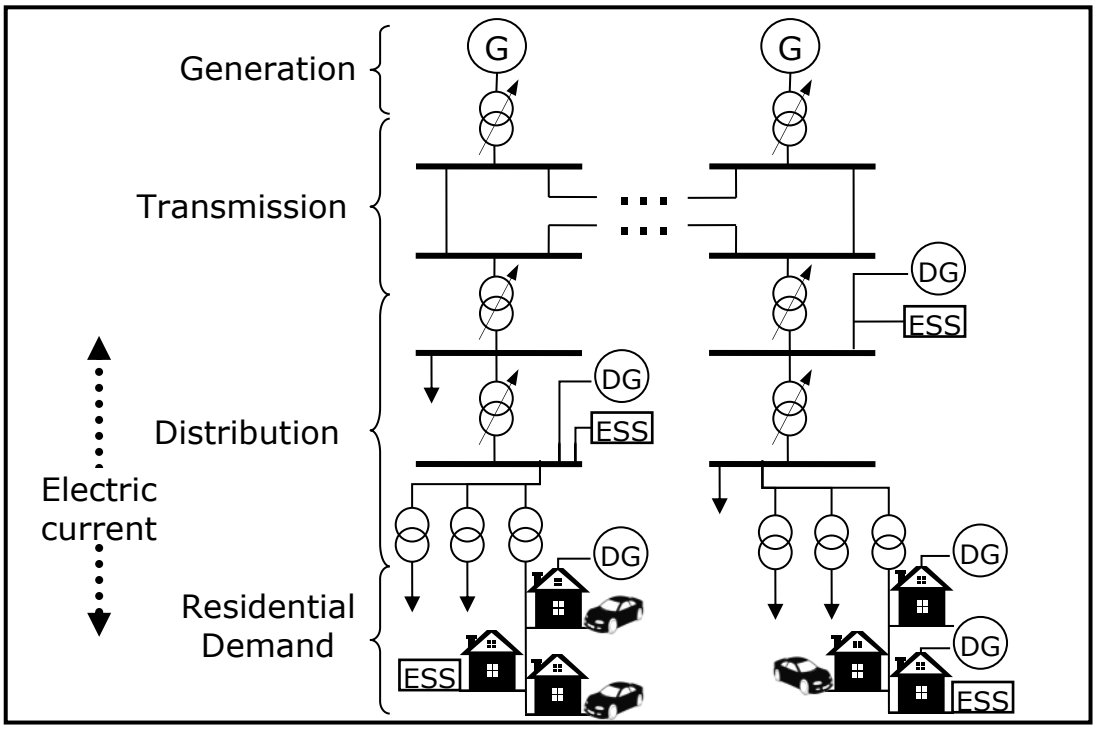

Fig. 1.6. Electricity network with DER integration [12].

Again, the bidirectional nature of current flow (Fig. 1.6) [12] that would result from integration of distributed generation (DG) technologies into the distribution network would further increase the level of complexity of the power system. Regardless of the aforementioned concerns, the benefits of the future power system seem to outweigh these concerns hence the on-going research in these areas.

1.5 Renewable Energy Sources

Around the world, with various partial or total renewable energy (RE) transitioning timelines set, the level of penetration and integration are

expected to increase. For example, reports from [13] [14] indicates that many countries were generating more than 20% of their electricity from solar and wind hence, making solar photovoltaic and wind clearly their main stream options in the power sector. Furthermore, the report observed that renewable power cost, when compared to conventional fossil fuel-fired power plant was increasingly cost competitive. Specifically, in some locations, the energy from wind and solar PV plants were more economical than power from fossil fuel-fired plants. By the end of 2022, the total global renewable power capacity was about 3,372 GW, growing the stock of renewable power by 9.6% (295 GW) [14]. Hydro power accounted for the largest share with 1,250 GW. Solar and wind contributed 90% to the share of all renewable capacity in 2022.

1.6 Renewable Energy Application in COVID-19

Renewable energy technology may play a key role in the provision of emergency power to critical infrastructures during blackout situations or any other disturbance leading to electricity disruption. The health and economic crises caused by the outbreak of COVID-19 especially in countries with low or no electricity access reiterated the need for critical facilities such as hospitals to be considered a priority for energy access. In sub-Saharan Africa, according to WHO, one in four health facilities has no access to electricity, and only a third of hospitals have reliable electricity access [15]. With most of the critical hospital facilities being energy dependent, the role of renewable energy not just as an emergency power source but also as a reliable, sustainable and environmentally friendly energy source becomes more apparent.

For instance, in Nigeria, the application of DERs in supporting energy resilience in a localised region was demonstrated in Mokoloki, a community in Ogun state. The Nigeria's first under-grid mini-grid pilot project lunched in February 2020, has the capacity to provide constant electricity to power the health clinic in Mokoloki community thereby keeping medicines stored in the clinic's refrigerators safe [16]. The resilience of the mini-grid project especially during the very difficult times and uncertainties resulting from the global COVID-19 pandemic laid credence to the credibility and viability of DERs in providing smart solutions to local energy system which can enhance a sustainable future. Besides enhancing the services of the local healthcare delivery, other business opportunities are equally created which in turn trigger development and sustained economic growth. **The integration of DERs into the Nigerian Power System, which is one of the objectives of this thesis would further enhance the resilience of the grid while also providing electricity access to more communities**.

1.7 Distributed Energy Resources and Coordination in the Future Power Network

DERs are either renewable or non-renewable technologies [17]. It is defined by [17] as "*electricity-producing resources or controllable loads that are connected to a local distribution system or connected to a host facility within the local distribution system*". These technologies when connected either as a single unit or in combination with other units to the electricity grid or as a standalone system constitute a Distributed Generation (DG).

DG is defined by [18] as "*relatively small-scale generators that produce several kilowatts (kW) to tens of megawatts (MW) of power and are generally connected to the grid at the distribution or substation levels*". The

deployment of DG has continued to increase, and indications are that the trend is likely to continue. Without doubts, the increased penetration of DG is bound to pose significant challenges in the traditional system operation [19]. With DG, the traditional unidirectional flow of electricity would change to bidirectional which most grids were not designed for, hence the need for resource coordination.

The future electricity network would incorporate large penetration of DERs and the management and coordination of these diverse energy sources would be crucial to maintaining the power system resilience. As depicted in Fig. 1.6, the integration of DERs across the various levels of the power system will ultimately change the traditional dynamics of the power system. The variable nature of most RES suggests the need for storage and the energy transformation from either the storage device or the RES also requires a power electronic interface. Besides this, the traditional distribution grid operates as a passive system and would have to transition to an active system. To achieve this, the distribution network must be subjected to advanced control, monitoring and management. Some of the advanced coordination strategies would be discussed in detail in the subsequent chapters.

1.8 Thesis Objectives

This thesis aims to model a smart localised energy system and assess the response of the future power network to DERs integration into the Nigerian Grid. The study also seeks to address the resilience of the Nigerian Power System through DERs application in power system black start restoration (BSR). To achieve this broad research objective, the following specific research objectives were set:

- To evaluate the dynamic changes in residential power demand and estimate the potential for demand response from residential loads in Nigeria.
- To evaluate the economic viability of generator-powered street lighting system in Nigeria using established metrics.
- To model a real urban Nigerian distribution network and identify the localised challenges of DERs uptake.
- To perform a Volt-VAr optimisation (VVO) of the real urban Nigerian distribution network to enable the inverter-based PV systems participate actively in voltage regulation.
- To mathematically formulate the proposed black start restoration method as a dynamic optimisation problem.
- To develop a black start restoration strategy and implementation framework for application in power system restoration.
- To model the Nigerian 330 kV 48-bus system and investigates the challenges resulting from the use of DERs as black start units.
- To experimentally validate the characteristics of the Energy storage systems (ESS) adopted for the proposed BSR simulated study.

1.9 Thesis Structure and Summary of Chapter Contributions

Chapter 2: The relevant literatures have been reviewed in this chapter starting with an overview of the dynamics of energy efficiency, energy economics, emissions and financial considerations for sustainable energy systems design. The municipal lighting system and the carbon footprints associated with diesel generator powered systems was assessed. In addition, the dynamic changes in residential power demand and its potential application in demand response was discussed. The performance of the distribution network when DERs are connected and its impact on the voltage and harmonic profile was examined. The use of DERs as black starts services, the application of DERs to improve power system resilience and in the development of an effective restoration strategy was assessed. Lastly,

research gaps were identified and would be addressed in subsequent chapters.

Chapter 3: The impact of the residential sector energy usage on the electricity distribution system is investigated and the need for energy efficiency measures along with the background of demand response discussed. Several case studies demonstrating how to optimise energy consumption and improve energy efficiency were carried out. A techno-economic analysis of energy cost of municipal street lighting system using metrics such as LCC, ALCC, NPC, COE, and ROI were performed.

The first two objectives were met in this chapter resulting in the development of an excel-based algorithm used to estimate the urban residential energy use of different residential types in Nigeria in the absence of smart meters or historical data. A load profile indicative of a typical urban residential energy demand was developed and adopted in predicting the effects of residential loads on the power system using the predicted results based on the appliance energy end use methodology.

Chapter 4: The performance of a low voltage (LV) distribution network with and without the integration of DERs is presented in this chapter. Several case studies involving both fixed and variable load profiles were carried out. The impact of DERs integration on the voltage profile of a typical LV distribution network in Nigeria was examined under different scenarios. Also, following the integration of PV systems in the network, Volt-VAr optimization was performed to enable the inverter-based PV systems participate actively in voltage regulation by the provision of flexible reactive power support.

Objectives 3 and 4 were addressed in this chapter. A model of a real LV distribution system in Nigeria consisting of a 60 MVA 3-phase 33 kV ideal voltage source, connected to a 15 MVA, 33/11 kV YY0 transformers, and seven 11 kV outgoing feeder's substation was developed and dynamic analysis conducted with the integration of DERs. A VVO was also performed to enable the inverter-based PV systems participate actively in voltage regulation by the provision of flexible reactive power support.

Chapter 5: Resulting from the frequent power outages in Nigeria and the need for a reliable restoration pathway, the mathematical formulation of a BSR problem is presented in this chapter. The formulated BSR problem was done as a dynamic optimisation problem to enable the effective coordination of the dispatching actions of the DERs along with the switching actions of remote controllable switches (RCSs) over multiple decisions time steps. The mixed-integer linear programming (MILP) technique was adopted and modelled to suit the nature of the BSR method developed. The black start power restoration sequence and the development of a viable restoration strategy were actualised.

Objectives 5 and 6 were actualised in this chapter. The BSR problem was mathematically formulated as a dynamic optimisation problem and the power flow model of the matrix equation for CPLEX was formulated in MATLAB and used for the BSR simulation. A structured restoration sequence capable of improving the resilience of the power grid was equally developed.

Chapter 6: In chapter 6, the Nigerian 48 bus system was modelled and used as a case study to assess the performance of the developed BSR method. The simulated test system and the analysis resulting from the loading of a real network is presented.

The seventh objective was achieved in this chapter. To assess the performance of proposed BSR method, the Nigerian 48-bus system was modelled in NEPLAN and used as the simulated test system. A sectional model of the 330 kV 48-bus system indicative of the various regions were further modelled and used to perform various simulated load restoration analysis. The effect of cold load pickup on the system restoration as well as voltage and frequency responses to the loading during restoration were monitored in the different regions and noted to be satisfactory.

Chapter 7: In Chapter 7, the experimental validation of energy storage system adopted for the proposed BSR simulated study carried out is discussed. The description of both the experimental and numerical methodology is presented alongside a detailed analysis of different scenarios.

The last objective was satisfied in this chapter. The contributions of both PV and ESS to system restoration were quite significant and did optimally contribute to improving the settling values of the restoration zones. The system restoration time was improved with the contribution of the battery ESS.

Chapter 8: The summary of the key findings and conclusions of the research is presented in chapter 8. Also, this chapter includes the research contributions and future research directions.

The flowchart showing the interconnectivity of the various chapters is presented in Fig. 1.7.

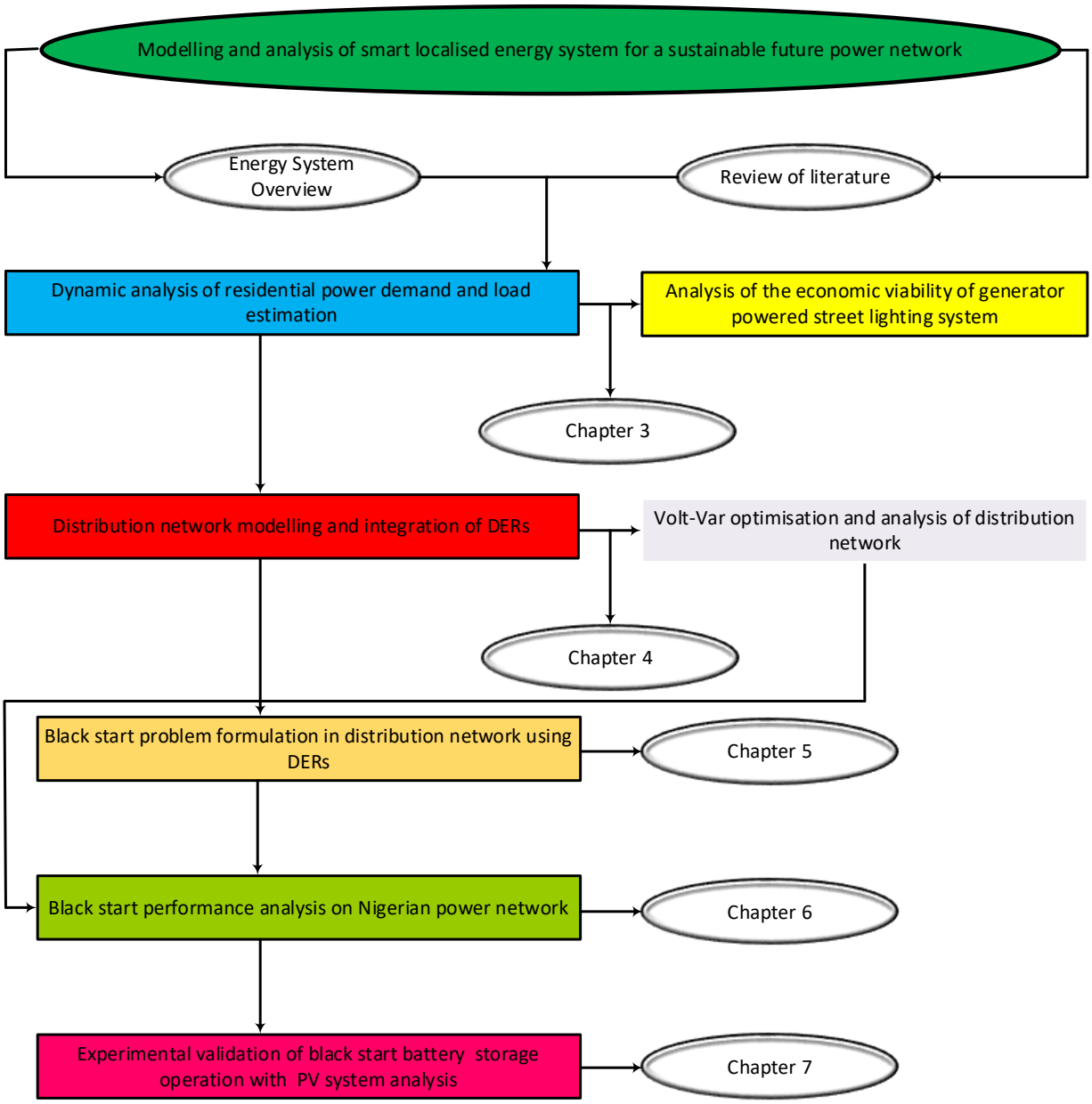

Fig. 1.7. Flowchart showing the interconnectivity of the various chapters.

CHAPTER 2

2.0 LITERATURE REVIEW

2.1 Energy Use Optimisation and Future Scenario Prediction

Renewable energy generation and its usage will continue to play a significant role in achieving a sustainable energy future. The global energy consumption has been projected to increase by 38.6% by the year 2030 [20]. This kind of predictions emphasises the need for robust energy efficiency programmes and policies at all levels. In response to the global environmental concerns and the quest to attain a minimum level of CO_2 and other related emissions, the energy production and consumption chains across different sectors must utilize sustainable and energy efficient approach and technologies in their operations.

Different countries in attempting to intervene and save the environment have adopted certain legislations all aimed at ensuring the attainment of an eco-friendly energy system. On a global scale, the energy consumption profiles of various sectors have been examined to critically assess either their energy consumption or contribution to greenhouse gas emissions. Lighting is noted by the International Energy Agency (IEA) to be responsible for about 19% of global electricity use and around 6% of global greenhouse gas emissions [21]. Furthermore, it was observed by [20, 22, 23] that public lighting constitutes a non-negligible source of CO_2 emission and accounts for about 12% of electricity consumption according to the Italian research institute on energy consumption for lighting in public sector. The percentage energy consumption of public lighting has highlighted the fact that lighting

has the tendency to alter the energy and economic balance of major cities [22].

Besides public lighting, recent statistics have indicated that residential energy use intensity has continued to increase across the globe. For instance, in Europe, [24] reported that the percentage residential energy use in France, Germany, Spain and the UK was 25%, 25%, 19% and 26% respectively. In Nigeria, Bangladesh, Brazil, Indonesia and South Africa, the energy consumption by residential sector is noted to be 77.9%, 51.0%, 10.6%, 37.0% and 23.2% respectively while in the US, 55% of energy used in buildings is attributed to households [25-27]. With such high level of energy consumption in residential sectors especially in Nigeria, presents the need for introducing energy efficiency measures.

Increasing energy demands in all sectors has driven new and innovative solutions to tackle the emerging energy challenges. These solutions which are multi-pronged are geared towards not only ensuring energy sustainability but also mitigating the climate change and related environmental challenges. As opined by [28], in the development and operation of any energy system, the environmental concerns, markets, users and other factors besides technology are some of the key areas for considerations. According to [29-32], tackling the issue of energy efficiency requires a conscious effort of developing renewable energy sources and building energy efficient infrastructures while also impressing on efficient energy use.

Energy efficiency implies the use of technology which is not energy intensive to carry out a similar task [33]. Such energy efficient measures have been described by The International Energy Agency [34] as not just being cost

effective, but also an effective approach to improve energy security and access especially to areas with vulnerable population. According to the IEA 2018 reports [35], energy efficiency improvements in all sectors of energy use have yielded significant results globally. The report observed the remarkable energy savings achieved as a result of energy efficient appliances use. This would enhance the achievement of the sustainable development goals if this is adopted and implemented as an action plan by policy makers and administrators. This is particularly important for most developing countries where energy access rate is still a recurring challenge.

2.2 Residential Energy Use

The residential sector has been described by [36] as the sector which consumes secondary energy and is majorly an undefined energy sink because of the following reasons:

- The sector encircles several types of structure sizes, geometries, and thermal envelope materials.
- The behaviour of the occupants is completely different and has a potential of impacting energy consumption up to 100% for a given residence [37].
- Privacy concerns hinder to a great extent individual's household energy data collection.
- Detailed sub-metering of residence end-uses has restrictive cost.

Despite the prevalence of energy use in the residential sector as noted in [38, 39], many energy users are either unaware or take for granted the energy efficiency procedures which has the potential to reduce energy bills, improve quality of life and help promote a sustainable environment. For

example, in most developing countries where electricity access rate is low, [40] asserts that energy efficiency awareness programmes is one good way to educate and encourage energy users to adopt energy efficient behaviour.

The urban areas, with about 67% of the global energy consumption has been identified as the energy consumption hub [41], having nearly a half of the world's population residing in these areas [42]. Interestingly, according to [25], a 73% increase in energy consumption has been projected by 2030. In some developed countries like UK, USA, Canada and China, the government takes the responsibility of publishing the initial residential sector energy consumption predictions indicating the gross energy values as declared by the various energy service providers [43-46]. No doubts these estimates may not be error free as argued in [36] due to unreported energy or on-site generation which may not have been duly accounted for. However, making available such information gives an insight into the sectoral energy consumption. Regrettably, having similar energy consumption information in some developing countries may prove to be a challenge. **Filling this knowledge gap in energy consumption in Nigeria is one of the objectives of this study**.

2.3 Review of Building Energy Modeling Approach

In a review of the various modelling techniques, [36] describes energy consumption modelling as that which try to quantify energy requirements as a function of input parameters. Whereas modelling is carried out for various reasons, the authors noted that the two most common reasons were; macro-scale: - involving the national or regional energy supply determination and the micro-scale: - which involves the changes in specific residential energy consumption resulting from technological upgrade.

Regardless of the reasons for modelling, the authors concluded that the modeling outcome could be a useful tool that is capable of influencing residential housing policies. In a related study, [47] performed a review on the prediction of building energy consumption. The authors reviewed newly developed models for tackling building energy consumption predictions which they admitted was complex and difficult to accurately predict. Some of the models reviewed in [47] are the elaborate and simplified engineering methods, the statistical methods and the artificial intelligence methods.

Using the statistical method, the modelling of household occupant behaviour to simulate residential energy consumption was performed by [48]. The main aim was to show the interaction of occupants with the main residential energy consuming loads throughout the day. The developed occupant's model together with the residential load models are utilised to create a high-resolution energy consumption profile. The top-down and bottom-up approaches for building energy modelling was described by [36, 49]. In the top-down approach, the building consumption prediction is obtained at the regional or district level with no consideration to the differences at the individual user end. This approach has been widely used to estimate urban energy consumption due to its simplicity. Some of the works adopting this method are well documented in [50-53]. The various authors used an econometric regression model with the application of socio-economic variables to estimate household energy consumption. On the contrary, the bottom-up approach focuses on modeling of individual end-use energy consumption within the building which can be summed up and extrapolated to obtain the regional estimates [36, 49]. Further classification of the bottom-up method into two categories namely: the statistical method and the physics-based method were described by [36]. Whereas the former method is similar to the top-down approach, the latter is not. The latter

neither requires historical data nor socio-economic factors but relies on the physical characteristic of the subject to simulate the building energy usage. Many literatures have documented in details studies carried out using these models [54-56].

Residential energy consumption modelling using energy measurements data from smart meters, electricity utility bills, organized national or regional survey information, questionnaires, and other such related tools or a combination of tools have been well researched and reported [57-62]. However, very few literatures exist on energy consumption prediction in areas where most of the aforementioned tools are either lacking or scarcely available. For example, while [63] used household survey alongside both online sales data of electrical appliances and household-reported energy expenditure to estimate household electricity consumption in Nigeria, [64] assessed the energy usage and intensity of buildings as-built and when retrofitted with green features using measured data from an analogue meter.

What other tools can be deployed and how are energy consumption predictions done in countries like Nigeria with estimated billing systems and 55% of electricity consumers without metering devices [65]? **One of the methods to address some of these issues is the focus of this research**.

2.4 Energy Use in Public Lighting

The global impact of lighting in general and public lighting in particular and its contribution to emissions have been highlighted in [20-23]. Resulting from such studies, new methods and lighting schemes aimed at reducing

energy cost while achieving high-quality design with minimal maintenance are continuously being explored [66]. The outcome of such effort leading to the improved energy savings and efficiency was acknowledged in the IEA 2018 reports [35]. The adoption and sustenance of such action plan would no doubts enhance the achievement of the sustainable development goals.

The energy and economic balance of many cities can be largely impacted by the energy consumption of streetlights as observed by [22]. In view of this, many municipal authorities have taken proactive measures such as switching to more energy efficient and sustainable lighting options with dimmer control technologies. However, in some developing countries, very little or no attention is paid to some of these energy efficient measures which can as well impact on the energy access rate which has remained a recurrent challenge.

Nigeria for instance is one of such developing countries with huge renewable energy potentials [67] but with poor electricity access rate. The gap between power generation and demand continues to widen resulting from an increasing population. Due to the non-availability of a reliable electricity supply, many households and institutions have resorted to dependence on self-generated power. According to a study by [68], most household own and operate a petrol or diesel generator and statistically, Nigeria is the world's highest importer of generator [69]. As reported in [70], some municipal streetlights are powered using standby generators. Although this approach seems to be a pragmatic response to the challenges of providing good illumination at night, [70] observed that this is done with a significant environmental and huge financial cost because of the diseconomies of scale in electricity generation.

With such high numbers of petrol or diesel operated generators by both individual and public institutions in Nigeria, the environmental and public health hazards are significant. Regrettably, such hazards are under reported as in the cases noted in [71-73]. Considering the importance of energy efficiency and the need to mitigate both the environmental hazards and risk associated with some of the unsustainable energy use highlighted in the literature, the need for a sustainable and energy efficient options for powering public lighting becomes imperative. Also, since lighting is one of the basic end-uses of electricity, its carbon footprint is expectedly significant. **Understanding the energy cost dynamics and estimating the carbon footprint of cities resulting from the use of several stand-alone diesel generator is one of the objectives of this thesis**.

2.5 Review of Lighting Carbon Footprint of Related Studies

To understand the diverse approach that may be employed in estimating the carbon footprints of different socio-economic activities such as; lighting systems, airport carbon emissions, transportation, household land use or students' behavior, [74-79] examined several case studies. For instance, using the Bologna International Airport (Italy) as a case study, [74] employed the transport carbon footprint methodology to examine airport carbon emissions. To achieve this, the total airport emissions namely;- landside emissions and airport airside emissions was separated into two units. Furthermore, the various components of the two units were disaggregated to cover several activities in and around the airport and the unit carbon footprint was estimated based on these activities. In a transport related study, the carbon footprint resulting from household use of public transport in Kolkata City of India was estimated by [75]. Using a sampling

survey of 500 households across different income classes, the data on the means of transport of the households alongside other variables that may affect choice of means of transportation was obtained. The carbon footprint was estimated based on the data obtained.

Similarly, [76] adopted diverse analytical models in conjunction with several conversion factors to estimate the carbon footprints of students in a University in China. The data on students' behavior vis-à-vis energy consumption activities were obtained using a survey. The survey which was grouped into three major categories covered daily activities of students for example daily life, academics life, transportation, and 17 other different subcategories. The carbon footprints of the students with respect to each activity, and the carbon footprints of all the students were estimated. Using a life-cycle approach the effect of urban heat island on outdoor lighting systems was examined by [79]. This method enables researchers to assess the environmental impact of goods/services by quantifying the use of resources (e.g. energy, water) in the production of the goods/services and the emissions arising from the use of the goods/services throughout the lifecycle of the goods/services.

2.6 Future Power Network

The gradual and subtle integration of more renewable energy resources into the power generation mix has redefined the future of the power generation and distribution networks. Most existing power system structures were designed for the traditional unidirectional flow of electricity, i.e. from the bulk power generation to the end users [12].

In the conventional or traditional structure, most bulk power generation stations are situated far from city centers with generation capacities ranging from hundreds to thousands of MW. The generated power is transformed and transmitted through the transmission lines which are usually overhead conductors operating at very high voltage levels. In Nigeria, power generation is managed by the Generation Companies (GenCos). This sector currently has about 26 grid-connected generating plants in operation with a total installed capacity of 12,946.4 MW and generation capacity of 8,243.5 MW. Out of this number, hydropower from three major plants accounts for 1,938.4 MW of the total installed capacity with 1,355 MW as available capacity which forms about 21 % of the total generating capacity. The thermal based installed capacity is about 11,008 MW with available capacity of 6,888.5 MW [13, 80].

The transmission company of Nigeria (TCN) which comprised of two departments, System Operator and Market Operator is responsible for the management of the radial transmission network which consists of 5,523.8 km of 330 kV and 6,801.49 km of 132 kV lines connecting 32 substations of 330 kV and 105 substations of 132 kV substations [13, 80]. The main duties of the transmission companies are the management of electricity transmission assets, system operation and electricity trading. From the Nigerian Electricity Regulatory Commission (NERC), Nigeria's transmission network consists of high voltage substations with a total (theoretical) transmission wheeling capacity of 7,500 MW. Currently, transmission wheeling capacity (5,300 MW) is higher than average operational generation capacity of 3,879 MW but it is far below the total installed generation capacity of 12,946.4 MW. The Nigerian transmission voltage levels are 330 kV for the grid transmission; 132 kV for the sub-transmission lines, while

the 33 kV, 11 kV and lower voltages constitute the distribution networks [13, 80].

The power distribution network provides the main interface between the transmission networks and delivers electricity to the industrial, commercial and residential end customers. The distribution network comprises of 33 kV, 11 kV and low voltage circuits (230 V). Power utilisation at this level brings the power supply chain to a full cycle. In Nigeria, this sector is being managed by the Distribution Companies (DisCos) and seems to be the worst affected part of the power system as a result of the numerous challenges it encounters daily. Some of these challenges includes transformer overloading, dilapidated feeder pillars in transformer substations, lack of or the use of inappropriate protective equipment, electricity theft, phase over loading, poor billing system, frequent outages, low voltage profile due to losses in the Transmission and Distribution (T&D) lines, broken poles & cross arms and other forms of vandalism.

In Nigeria, most power outages and interruptions occur at the distribution level and in most cases without any prior notification to the consumers. Also, because most consumers either have outdated metering systems or do not have metering devices at all, there appear to be no energy management at the distribution level, no reliable real-time data indicating the state of the distribution system, and lacks a properly automated and coordinated controls to take immediate and decisive action against failure events. As observed by [81], such action exposes the distribution transformer to frequent breakdown resulting from lack of information to indicate the loading and current status of the transformers and associated feeders at the sub-station.

The quest for a more sustainable means of power generation and consumption resulting from global environmental concerns has and would continue to impact on the future power network. The existing power structures of most countries were not designed to meet the needs of increased deployment of DERs. However, with the gradual energy transitioning, the future power network must be designed to accommodate and enhance the integration of DERs.

2.7 Renewable Energy Technologies Application

The future power systems would be predominately driven by DERs technologies. Around the world, there is sustained outcry as a result of the biting effects of climate change which has resulted in many extreme weather events. Besides this, another compelling influencing factor that has necessitated the widespread promotion and adoption of renewable energy technologies is the market liberalisation and energy dependency. The global level of renewable energy (RE) penetration has continued to increase [82] and with the various energy transition timelines set, the trend is likely to increase exponentially. The current level of renewable energy penetration and the capacity was discussed in detail in chapter 1.

2.8 Renewable Energy Technology in Nigeria

Nigeria is one of the countries that are significantly endowed with renewable energy resource (RES) potentials. However, the country's current energy mix (Fig. 2.1) is mainly comprised of thermal and hydro power sources. The Energy Commission of Nigeria (ECN), in the second draft of the Renewable Energy Master Plan (REMP) had proposed to increase the supply of

renewable electricity from 13% of total electricity generation in 2015 to 23% and 36% by 2025 and 2030 respectively [83].

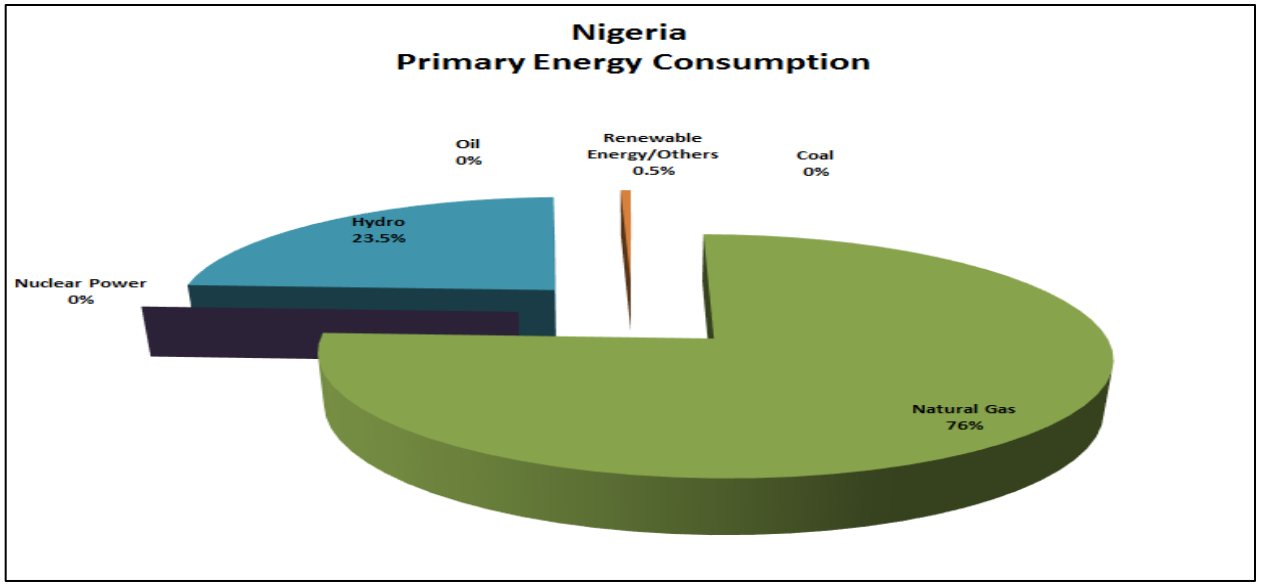

Fig. 2.1. Nigeria's primary energy mix [13] [83].

Table 2.1. Nigeria's renewable energy potential as contained in the REMP [83].

Resource	**Potential**	**Current Utilisation and further remarks**
Large Hydropower	11,250MW	1,900MW exploited
Small Hydropower	3,500MW	64.2MW exploited
Solar	4.0kWh/m2/day – 6.5 kWh/m2/day	15MW dispersed solar PV installations (estimated)
Wind	2-4m/s@10m height mainland	Electronic wind information system (WIS) available
Biomass (non-fossil organic matter	Municipal waste	18.5 million tonnes produced in 2005 and now estimated at 0.5kg/capita/day
	Fuel wood	43.4 million tonnes/yr. fuel wood consumption
	Animal waste	245 million assorted animals in 2001

Agricultural residues	91.4 million tonnes/yr. produced
Energy crops	28.2 million hectares of arable land; 8.5% cultivated

Like most other sectors in Nigeria, the policy makers have crafted a well-structured REMP and other related policies which aim at transitioning the nation's energy sector by the integration of more renewable energy into the countries' energy mix and implementation of energy efficient and environmentally friendly technologies. However, previous experience has shown that most times, the transition periods are never met.

2.9 Electric Vehicle and Electric Vehicle Charging

Electric vehicles (EV) although first developed in 1914 [84], are in recent times becoming a major talking point both in the automobile and power industry. This so because of the rising concerns of emissions and other environmental concerns associated with fossil fuel powered vehicles. The transportation sector accounts for 25% and 20% of the global greenhouse gas emissions and global primary energy consumption, respectively [85, 86]. Besides this, the decarbonisation of the transport sector through electrification and the role of EV in the demand side management of the electricity systems have evoked renewed global interest. The improvements in battery technology along with the advances in the EV charging technologies had greatly influenced the widespread global embrace and purchase of EVs. For instance, in 2021, more than 16.5 million EVs were on the road, tripling the 2019 figure [82, 87]. Also, as depicted in Fig. 2.2, the global electric car stock has steadily been on the increase and this trend is likely to accelerate over the next couple of years as a result of approaching 2030 and 2035 deadline on ban of new petrol and diesel cars in some countries.

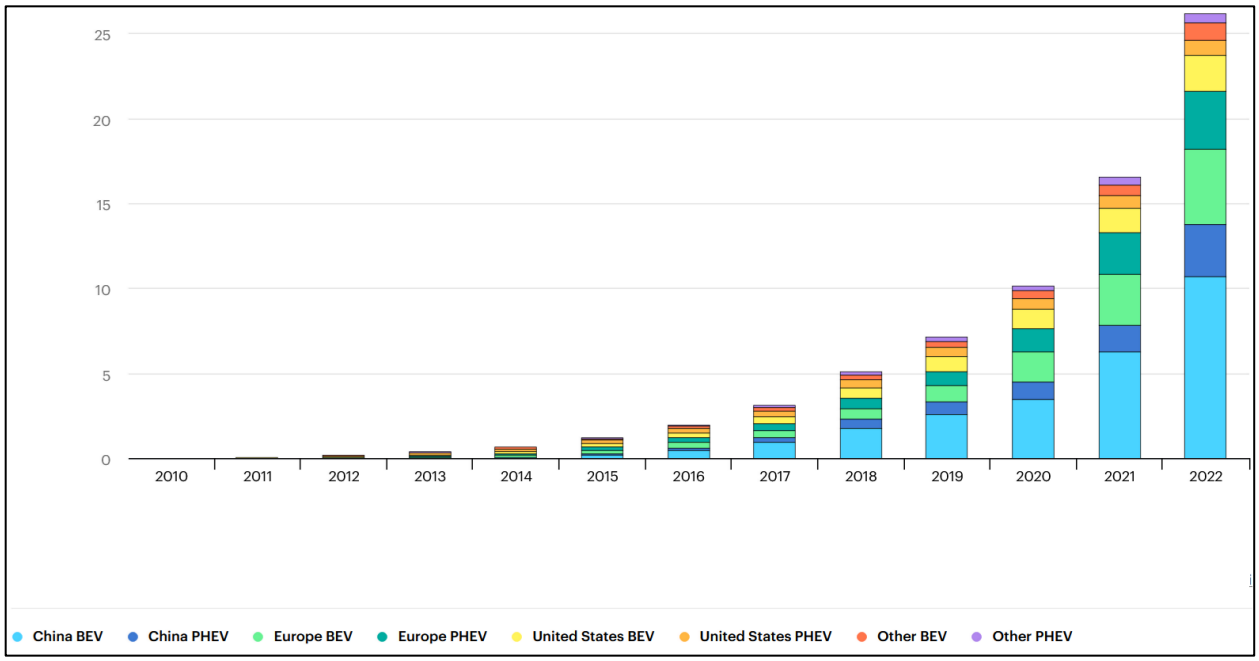

Fig. 2.2. Global electric car stock 2010-2022 [86].

Besides the environmental concerns, the economic opportunities and enticing revenue streams offered by EVs are another driver for the EV market. Depending on its usage, EVs can operate in the following capacities;- a supplier of electricity to the grid, an energy storage device or a load to the grid. From the perspective of the electricity networks, [12, 88] EVs can be further seen as:

- Energy storage systems – the battery packs of idle or stationary EVs can be leveraged to send power back to the grid during periods of high demand while also recharging during periods of low demand. The vehicle to grid (V2G) application of EVs has the potential to buffer the uneven effects likely to result from RE penetration by providing voltage and frequency support, thus enhancing the grid stability.
- Controllable loads – as a flexible or controllable load, EVs charging offers the opportunity to provide balance to the power system. The

charging schedule of the EVs can be managed in accordance with the market players or system operators' needs. Fig. 2.3 [89] illustrates how managed EV charging can be used to meet the grid needs.

- Dumb loads – Just like most other residential, commercial or industrial electrical loads, EVs can be charged without any form of load control.

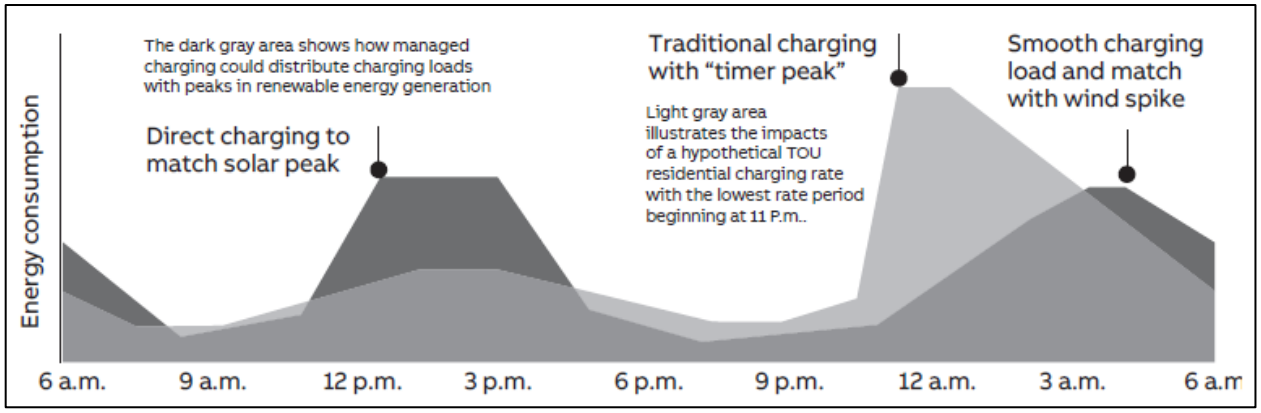

Fig. 2.3. Opportunity of EV smart charging to meet grid needs [89].

With the evolution of the various DERs and their subsequent integration into the grid, there is a growing concern that the power system may be put under pressure. As noted previously, the traditional grids comprised mostly of coal-fired power plant and combined-cycle gas-turbine which were designed to continuously operate with very little or no flexibility. The emerging RES are mostly variable in nature with little dispatchability. The management of the electricity grid involves load forecasting and dispatching of generation to meet the required demand. These demands are met either by using one or a combination of the following:

- Using storage to discharge at peak demand.
- Adopting demand side response strategy.

With more EVs and their charging infrastructures introduced into the power system, the future grid is likely to benefit during periods of peak demand by the application of V2G by managing charging to shift the load. As illustrated in Fig. 2.3, a systematic load management can be planned based on the power system load profile to reduce or balance the peak requirement. Achieving this would require the careful coordination of the power system.

2.10 Distributed Energy Resources Management

With the integration of DERs into the power network, the management and control of the energy flow would require advanced communication capabilities. To achieve this, the distribution networks must be subjected to advanced control, monitoring and management. As observed by [90], one of the benefits of active distribution network management is the opportunity to maximise the existing network infrastructures while still taking full advantage of the various DERs in a coordinated manner. According to [91], DER management systems (DERMS) as an emerging control solution, has the potential to increase the grid reliability, flexibility and hosting capacity [92].

Different management strategies have been proposed and a clear demonstration of the application of DERMS in the coordination of DERs across various levels of the electric system was carried out in [92]. The Advanced Distribution Management Systems (ADMS) is described by [93] as the control unit of the distribution network which supports network operating decisions. According to [94], the role of the DERMS is to monitor and manage DERs to address the grid constraints determined by the ADMS. This fits within the framework of an ADMS software platform since the ADMS enhances the performance of the distribution grid [94, 95].

2.11 Review of Distribution Networks with DERs Integration

The high penetration of DERs proliferation at different levels in the distribution networks would require continuous research to examine the performance of the systems.

The integration of EVs in a microgrid with DGs was investigated in [96]. With different levels of penetration assumed, the voltage profiles over a 24-hour period was evaluated for both the winter and summer seasons. The results indicated that the voltage drops were less significant for the dual-tariff EV charging regime with increased levels of DG penetration. Using the Great Britain (GB) power distribution network, [97, 98] carried out different but related studies. While [97] investigated the impact of EV on the distribution network, [98] performed a similar analysis but with EVs and other storage systems. Reference [99] investigated the impact of optimised DERs on local grid constraints. The studies having considered various simulated scenarios of optimised DERs concluded that their adopted method was capable of benefiting communities looking to optimise investment decisions in low carbon technologies.

A systematic valuation process was proposed and adopted by [100] to quantify the value of DERs in active distribution network (ADNs). The aim of the proposed valuation scheme was to monetise the DERs contributions to ADN and the society in both short and long term horizon presenting a methodology for comparing and priortising a range of DERs portfolios. The deployment of transactive energy (TE) in the future distribution networks was proposed by [101]. They argued that transactive energy would not only increase the convenience for consumers but would also improve the system reliability index.

The role of EVs in the future distribution networks has been succinctly described in [102, 103]. Besides its considerable sustainability benefits, EVs has the potential to assist in emissions reduction, promote the global shift toward cleaner growth, provide grid services, encourage the use of home storage, and support the 'future of electric mobility'. The role of EVs in unlocking distribution network flexibility by the provision of demand response services has been investigated by [104-106]. Resulting from the reviewed studies, it is obvious that DERs as an emerging technology would sustainably enhance future grid applications, **hence DERs consideration in the provision of black start service which is one of the objectives of this research**.

2.12 Black Start Application in Distribution Network Using DERs

Power systems are complex infrastructures designed with the aim to withstand system disturbances. However, during extreme weather events such as hurricanes, super storms, wildfire or severe flooding, the robustness of the power system designed to meet "N-1 or N-2" criteria is usually threatened, often resulting in a partial or total system collapse. A blackout usually occurs when there is a partial or complete loss of power in the electricity grid. The process of grid reenergization by the provision of power to a power system unit to enhance the grid restoration process is called black start [107].

Although blackouts events do not occur frequently [108], yet the rapidly and constantly changing extreme weather events driven by climate change has resulted in frequent weather-related outages [109]. The economic, and social impacts of such occurrence are significant and hence require an

efficient restoration scheme alongside a decision support system [4]. For instance, according to [110], the annual inflation adjusted cost of weather-related outages is estimated to be between $25 billion and $70 billion.

Besides weather-related outages, a more recent threat capable of causing and inflicting great harm to the power system is the cyber-physical and terrorism related attacks [111, 112]. With the increase in terrorism related activities and cyber hacking, recent advances and digitalization of the power system aimed at enhancing a bidirectional flow of communication between power consumers and power providers has further exposed the system to certain cyber risks.

Regrettably, since the occurrence of extreme weather events cannot be out rightly avoided, reinforcing the power system to improve its resilience to such events becomes the only credible alternative. Reducing the power outage time to the barest minimum by deploying advanced restoration tools such as System Restoration Navigator (SRN) developed by [113] and Optimal Black start Capability deployed by [114] are some of the unique approaches so far adopted to enhance the system resilience.

Besides weather-related outages, other scheduled and unscheduled events such as;- (system maintenance, new installations, equipment failure, fallen trees, aging infrastructures) are also some of the other causes of power outages [115]. Regardless of the causes, when there is a power outage, both the transmission and distribution systems are de-energised culminating to a loss of supply at the consumer end. For scheduled events, the outage period may only last hours. However, for unscheduled events, this may last days, weeks or even months depending on the severity of the event and the extent of damage caused.

2.13 Review of Blackout Events in the World

In addition to the existing body of knowledge in this area, this section aims to provide recent update on blackout events around the world with particular emphasis on the events with the most significant impacts.

Several studies [116-120] have examined and reviewed most of the major blackout events around the world. These studies are quite useful in understanding the trends, the causes (technical and non-technical), the economic and social impact, the outage duration, the restoration approach and the possible ways to ameliorate the associated impacts. For example, using information from previous blackout events in the world, [116] statistically analysed the characteristics and main causes of power system failures and the effect on the power system. Atmospheric phenomena, technical, human factor and lack of data were identified as the leading main causes of failures in power systems.

Using publicly available data on different blackout events around the world for a period spanning from 1965 to 2015, [117] studied the blackout trends and developed a dataset. Using information from the dataset, a formula was applied to determine the largest blackout event by comparing the total number of people affected and the restoration time. Based on trend outlined in the study, future improvements on the power system could be achieved. Similarly, [118] carried out a review of the power system blackout and highlighted on the impact and lessons learnt from major blackout events.

The analysis and classification of major blackout events between 2003 and 2015 was conducted by [119]. Within this 13-year period, 14 major blackout incidents occurred. Using five significant indices namely: affected number of people, total load lost (MW), outage duration, affected population

(percentage), and severity (in system-minutes) the classification was done. From this analysis, it was found that, the 2012 Indian, 2006 Pakistanian and 2015 Turkish blackout events affected the largest number of people. The 2003 blackout event in North America was noted to be the event with the longest outage duration and largest amount of load lost followed by Indian and Turkish blackout event. The 2003 London blackout event had the least consequences.

The authors in [120] critically reviewed previous blackout events in the world with a view to draw lessons for China's power industry. Their approach was to analyse the sphere of influence, weigh the scale of effects, and examine the restoration measures along with the various causes. The study identified commonalities of previous blackout incidents for example: the wide scope of influence of blackout events and the significant economic losses associated with such incidents. Resulting from the study, recommendations capable of maximizing the ability to prevent large-scale blackouts in China were made.

Some of the literatures reviewed above have captured most of the major blackout events around the world. However, recent blackout incidences have not been reported. For example, the blackout event of August 2020 in Sri Lanka affected about 21 million people. The event which was attributed to technical issues lasted for about seven hours [121]. Similarly, the blackout event of June 2019 in Argentina, Paraguay and Uruguay affected about 48 million people. This event which was technical related was attributed to a failure to correctly reprogram the electricity system after a new bypass was installed on one of the transmission lines [122]. Also, in 2019, Venezuela experienced a series of blackout events with the first being that of March 2019. About 30 million people were affected. The failure of the main Bolivar

Hydroelectric Plant was noted to have caused the incident. Similar blackout events occurred in April and July 2019, leaving more than half of the country without power [122].

In August 2019, about 1 million customers in the United Kingdom lost power resulting from loss of generation which led to frequency drop. However, the system was restored back to normal in about 45 minutes [123]. A deadly storm in 2017 (Hurricane Maria) hit Puerto Rico and caused a total blackout event which left 1.5 million people in complete darkness. Unfortunately, due to the extent of damage, about 1.5 million people were still without electricity for more than three months after the blackout events [122].

2.14 Review of Blackout and Black Start Concept and Terms

In this section, some of the terms and concept associated with blackout and black start are either defined or reviewed. During an unscheduled event, the power system which is usually designed to meet the "N-1" or "N-2" criteria is compromised leading to a total or complete power outage. To reenergise the grid, a series of complex procedures are observed. The entirety of this process is known as power system restoration. Hence the development of an efficient restoration strategy is important to the improvement of the power system resilience.

2.14.1 Power system restoration

Power system restoration is the key needed to overcome power system blackout. [124] describes power system restoration as a multi-objective, multi-stage, multi-variable and multi-constraint optimisation issue which is full of non-linearity and uncertainty. Furthermore, it is viewed to be a typical

semi-structured decision-making but without complete solution process [124]. However, the primary objective of power system restoration as opined by [125] is to enable the immediate return of normality of the entire network with minimal loss and impacts to power consumers.

During a total grid failure or blackout and without support from neighboring interconnecting systems, the first objective is to engage the black-start procedures. This involves activating power plant or black-start units [126, 127] capable of providing the required power which would be used to activate other thermal plants. This method of service restoration is called the bottom-up approach.

The three major phases of power system restoration following a blackout event is succinctly described in [128] as: preparation, network restoration and load restoration (see Fig. 2.4). During the preparation phase, all the necessary information is gathered using the outage management system (OMS) described by [129]. Data such as the customer information system (CIS), interactive voice response (IVR), and advanced metering infrastructure (AMI) alongside field measurements obtained from the use of supervisory control and data acquisition (SCADA) system is used to examine the grid structure. Resulting from the assessment of the control center, maintenance crews are deployed to troubleshoot and replace the faulty components or isolates failed units. With this satisfactorily achieved, the restoration procedure is initiated.

System restoration following a total blackout begins with the activation of the black-start unit. The black-start provides cranking power to thermal power plants. The thermal plants gain inertia and resynchronization with other units is achieved. However, since the system restoration process may

not be a strait jacket process, and might fail for certain reasons, a repeat of the restoration sequence maybe necessary. The last phase of the restoration process is triggered following the success of the restoration phase.

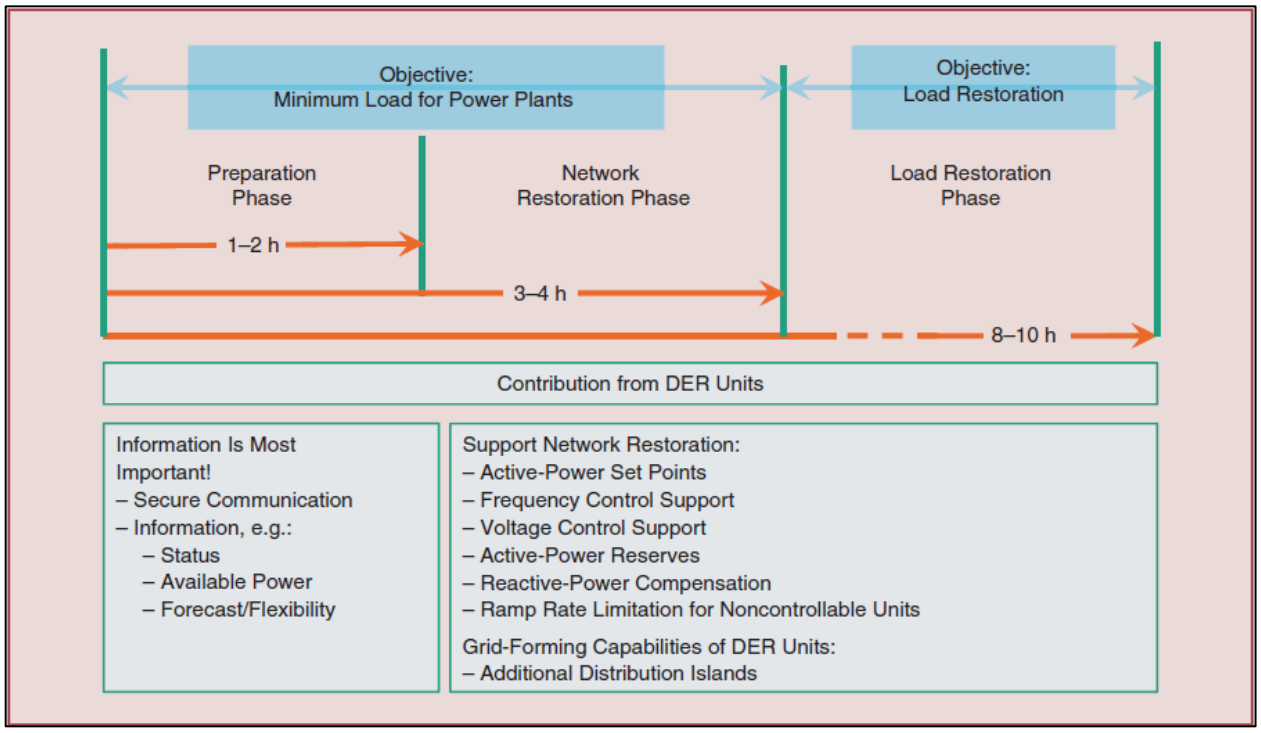

Fig. 2.4. The power system restoration phases and the contribution from DER units [128].

Load restoration is achieved following the success of the preparation and network restoration phases. The main consideration during this phase is to restore supply to network and connect consumers to the grid. While achieving the aim of this phase, critical attention is always given to issues of cold load pick up (CLPU) arising from prolonged outages. A simple case of service restoration using reconfiguration is described by [130].

Fig. 2.5 [130], captures a simple restoration procedure for a typical radially operated distribution system. The first plot indicates the state of the system without any disturbance. The six aggregated loads operating normally are

energised by the red and green feeders. The loads in each of the feeders are energised by their respective sub-stations and the tie switch between each feeder remains in the normally open position. In the second plot, during the occurrence of a fault on the green feeder, the protective relay trips thus de-energising the entire feeder leading to loss of supply for consumers on that feeder. Using the sectionalising switch located in the middle of the green feeder, the faulty section of the feeder close to the substation is isolated from the healthy section by opening the switch as captured in the third plot. With that sequence performed, the tie switch situated on the red feeder is closed, thus transferring power to the healthy section of the green feeder. This ensures that only a limited section is left without power while the maintenance and restoration work is ongoing at the affected side of the feeder. With the faults cleared on the green feeder, the tie switch is opened, and the sectionalizing switch closed, thus restoring supply to the green feeder as seen in the fourth section.

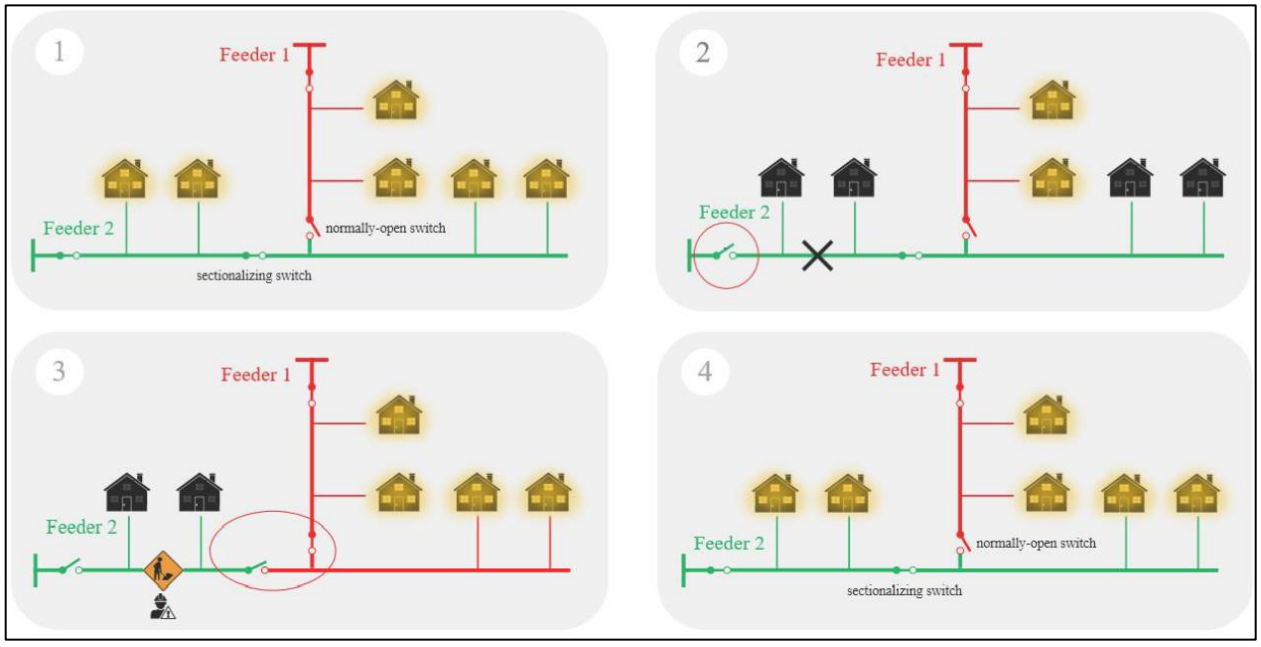

Fig. 2.5. A simple case of service restoration using reconfiguration [130].

2.14.2 Cold Load Pick Up

CLPU is a phenomenon which occurs following a prolonged period of blackout event. During service restoration, the residual load tends to be higher than the normal or pre-outage demand level resulting from thermostatically controlled loads, refrigerators, heating/cooling, pressing irons starting simultaneously [128, 131]. Due to these unpredictable uncertainties, appropriate reserves must be made available when carrying on with load restoration.

For grid with distributed generators, another phenomenon occurs when values of the pre-blackout power are not fed in immediately upon system restoration but begin to slowly increase their active power after monitoring the grid for certain duration [128]. As noted in [128], the current German code specifies that the grid must be energised and observed for 60 seconds before limiting the ramp rate of the active power to 10% of P_{nom}/min.

In Fig. 2.6, using an illustrative feeder configuration with a 1-MW nominal load, 600 kW of distributed generation, and a CLPU with 100% overshoot and a 15-min decay time, the simplified modeled load, generation, and residual load behaviour of the CLPU is demonstrated [128]. As shown in the Figure, there is need for generation reserve to provide for the overshoots after feeder connection. Also, it is seen that the simultaneous increase in load decay and generation culminates to an even steeper gradient of the residential load.

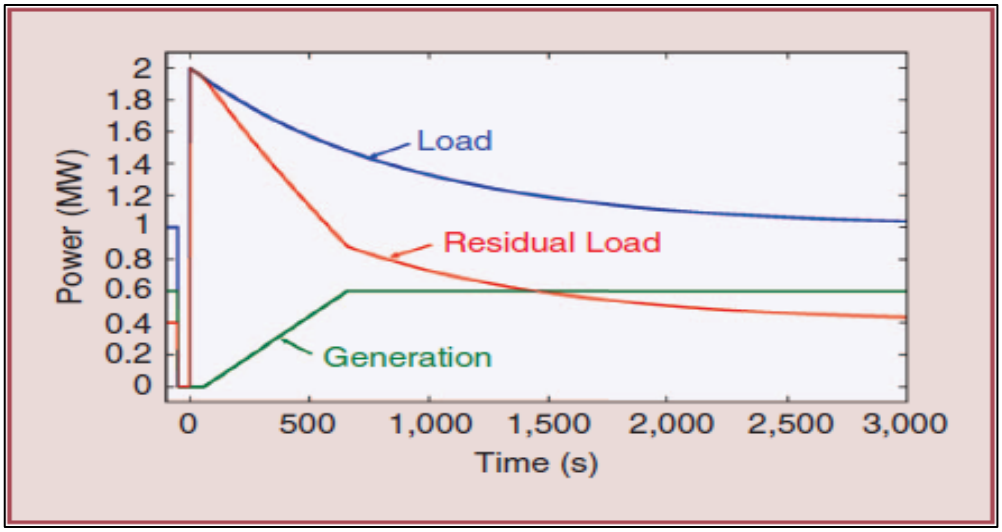

Fig. 2.6. CLPU: the load, generation, and residual load behaviour after feeder reconnection [128].

2.14.3 Power System Resilience

Resilience is defined by [132] as "*the ability to withstand and reduce the magnitude and/or duration of disruptive events, which includes the capability to anticipate, absorb, adapt to, and/or rapidly recover from such events*". In Fig. 2.7, the concept of resilience is further described by the Electric Power Research Institute (EPRI) [133]. Three key terms prevention, recovery and survivability have been used to summarily explain the concept of resilience.

Prevention is described as the necessary steps and precautions taken to avoid unexpected occurrences. Prior to such occurrences, the power system can be reinforced by the prompt replacement of aging infrastructures and continuous performance of routine preventive maintenance checks. Recovery is the actual state of readiness in preparation for such events. These could be in terms of the restoration strategy, the damage prediction, crew readiness and resource allotment. The last element is survivability. During blackout events, some critical facilities like hospitals,

telecommunication infrastructures, traffic systems, must still operate. The adoption of alternative proven technologies to ensure the continuous safe operation of such critical facilities throughout the blackout duration is described as survivability.

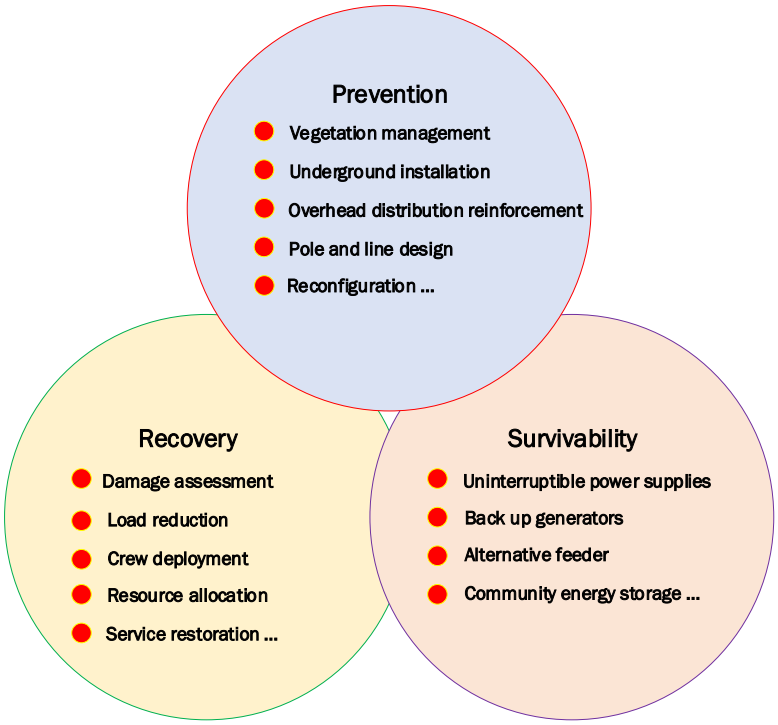

Fig. 2.7. The 3 elements of resilience identified by EPRI [133].

To achieve a high degree of power system resilience, a combination of the three elements must be fully operational. A well thought out and carefully designed restoration strategy must be put in place prior to the occurrence of an extreme weather events. Field trial drills must be carried out from time to time as a way of mimicking the real scenario. Technologies that can be used to forecast extreme weather events must be adopted and updated regularly. In the prevention phase, the deployments of sectionalising switches at strategy locations along the lines can help not only prevent a total power loss, but also enable a speedy recovery.

The adoption of RES alongside with battery storage have equally proven to be useful especially as these technologies are receiving increased worldwide deployment. As demonstrated by [134, 135], photovoltaic battery backup and energy storage systems are already being used as backup sources during system blackouts. To further improve on survivability and the overall resilience of the power system, an improvement on these technologies and ways of integrating them into the restoration plans is a subject of ongoing research.

A conceptual resilience curve (see Fig. 2.8) is used in [136] to describe typical system resilience characteristics before, during and after an extreme event. The vertical and horizontal axis of the plot represents the resilience level and time respectively. At the inception before the occurrence of any extreme weather events, the power system designed to meet the 'N-1' or 'N-2' criteria is denoted to have a resilience status of R_o corresponding to time t_o to t_e. The resilience status of the power system at this time instance is described as robust. This is called the pre-event state.

During the pre-event state, the EPRI element of resilience corresponding to the current system status is assumed to be fully operational. Following the forecast of an extreme weather event, the crew and resource deployment is heightened. At the occurrence of an extreme weather event, the system resilience falls from R_o to R_{pe} at time t_e to t_{pe} and last till time t_r. This period is described as the post-event degraded state. The duration of the post-event degraded state is dependent of the level of damaged resulting from the extreme weather event. Following the second component of the EPRI resilience element, crew deployment, damage assessment, and restoration effort is carried out. With significant recovery and restoration efforts made, the system resilience is improved from R_{pe} to R_{pr} at time t_r to t_{pr}. At time t_{pr}

to t_{ir}, the system resilience is maintained at R_{pr} with the remaining restoration effort still progressing. This phase is described as the post-restoration state. Although the power system resilience is yet to reach its pre-event status, the system is still described as having achieved robust status.

Following a complete infrastructure and system recovery, the system resilience is restored from R_{pr} to R_o at time t_{ir} to t_{pir}. Also, during the post-event degraded and post-restoration state, the survivability component of the EPRI element was triggered to ensure that critical facilities were not without power. In practice, the timing of the various stages of recovery is fully dependent on the severity of the associated event and the speed of the ground team effecting the necessary repairs. The effective coordination of the entire process is largely dependent on the nature and type of the outage management service being deployed.

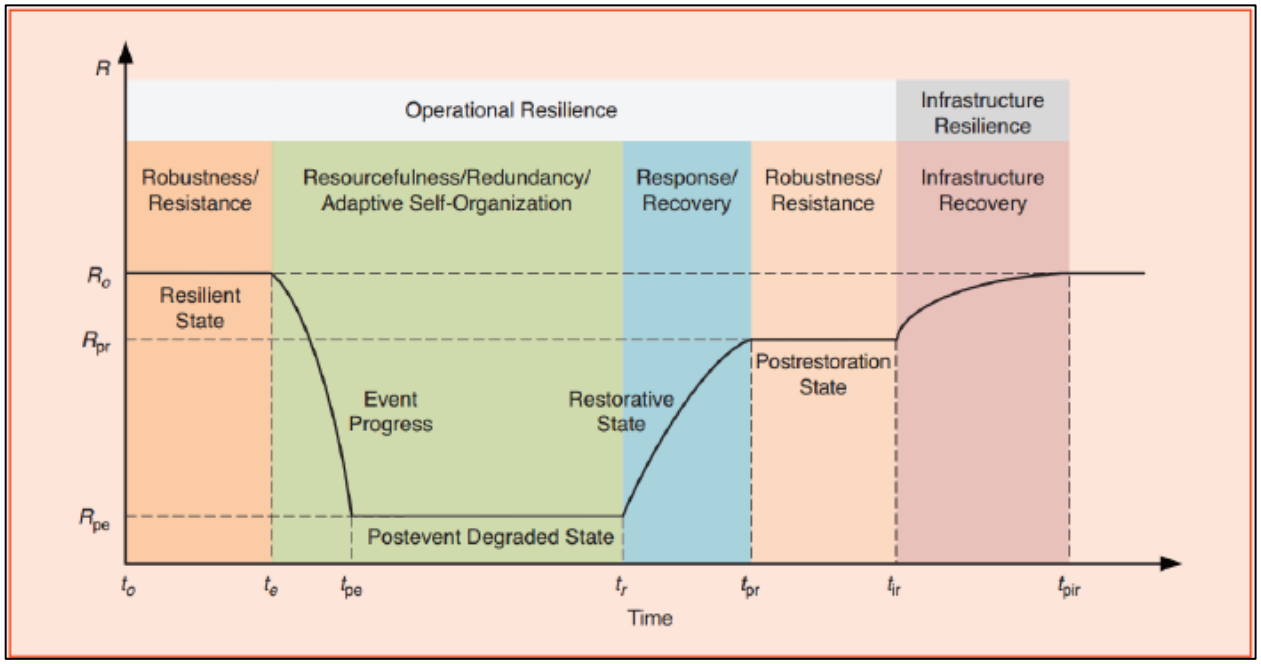

Fig. 2.8. A conceptual resilience curve before, during and after an extreme event [136].

In a more revolutionary approach to enhance the power system resilience, the UK National Grid Electricity System Operators (ESO) in partnership with SP Energy Networks (SPEN) and TNEI (a specialist energy consultancy) did explore a radical approach to system restoration by using DERs. The Distributed ReStart project is proposing the use of a Distributed ReStart Zone (see Fig. 2.9) which contains all assets and DERs located within a predefined distribution network area and includes transmission network synchronization point(s) [137, 138].

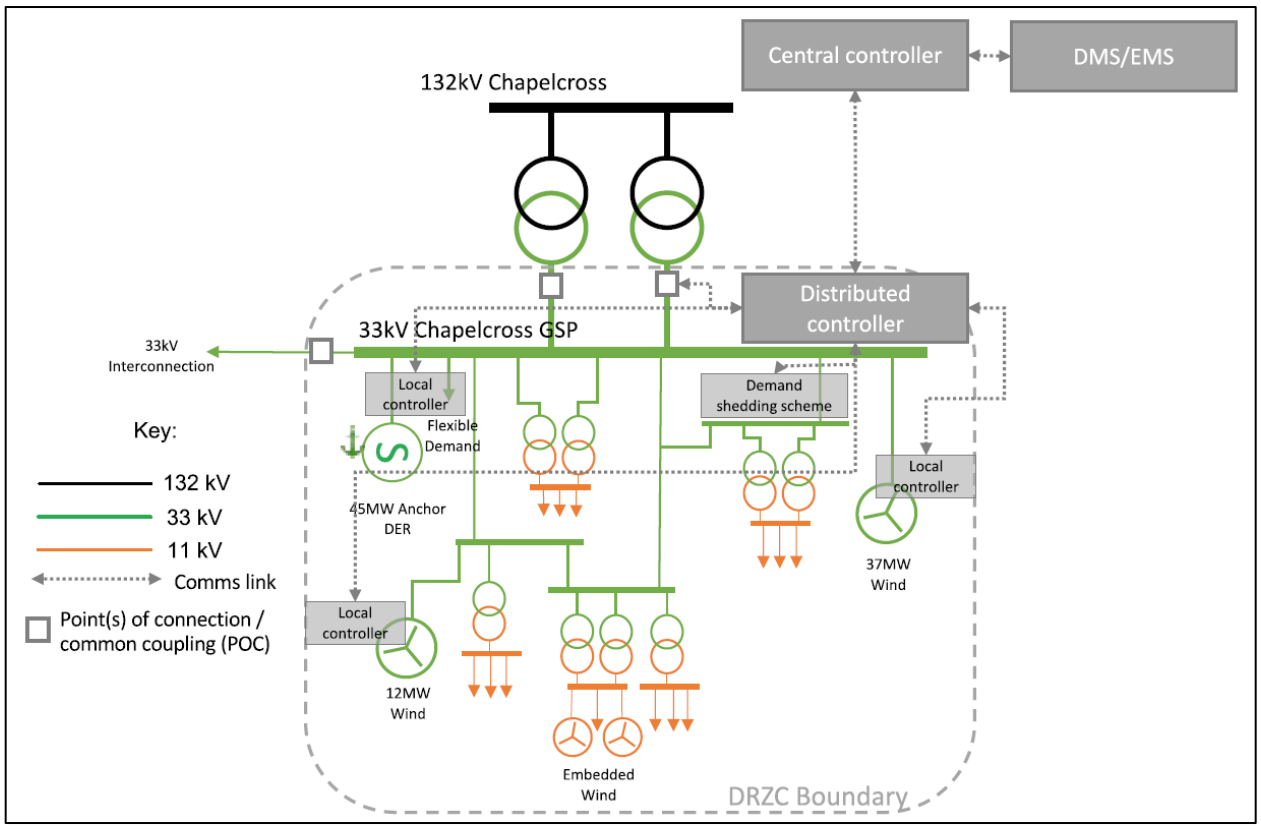

Fig. 2.9. Distributed ReStart Zone with indicative Distributed ReStart Zone controller (DRZC) system hierarchy [137, 138].

The Distributed ReStart project is expected to monitor the frequency and voltage stability and power island capability to resynchronise to the transmission system during the restoration process. Besides having the

capacity to display the response of the connected energy and network resources, the proposed system would provide operators with a view of the current DRZC progress within the restoration plan. Some other additional advance capabilities proposed to be included in the design include the real-time monitoring of the DRZC well ahead of the black start event and the calculation and display of the export capability of the power island at the point of connection (POC) [137, 138].

2.15 Outage Management System in Distribution Network

A tool deployed by utilities in grid management and power restoration resulting from service disruption is called outage management system (Fig. 2.10) [95]. To improve the resilience of the power system, a robust OMS plays a significant role. The OMS, as a major component of the resilience element, is used in the normal daily outage prediction and analysis of the location and extent of damage resulting from the grid disruption. The timely dispatch of crew and maintenance personnel to the affected troubled locations is dependent on the information provided by the OMS.

The operation of the conventional OMS is described in [129, 139]. During disruption of power supply, the Supervisory Control and Data Acquisition, smart meters through Advanced Metering Infrastructure, Customer Information System, Interactive Voice Response, other applications in Distribution Management System (DMS) and maintenance crew sends information to the OMS. Using all the information obtained, damage assessment is carried out while real time monitoring and evaluation of the grid operating conditions is ongoing. Based on the damage report, a set of restoration strategies is generated, and the restoration protocol triggered.

Depending on the nature of damage, restoration can be performed either by crew or RCSs deployment.

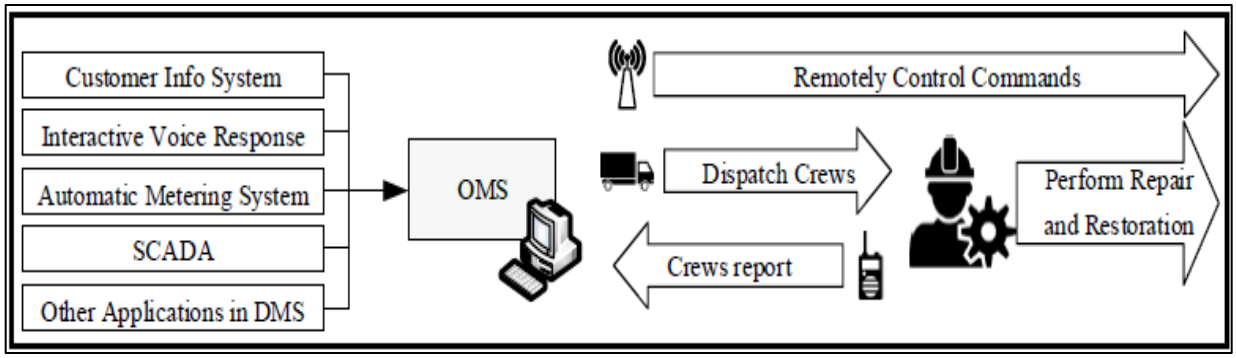

Fig. 2.10. Outage management system for distribution systems [95].

Outage management system alone may not be quite efficient during extreme weather events due to the dynamic nature of the distribution systems. In practice, the distribution system undergoes several changes resulting from operational configuration, network additions, routine switching for maintenance reasons and growth [95]. A combination of damage prediction and crew staging mechanisms along with real-time tools such as SCADA, DSM and OMS has been noted to improve the overall system functionality. This new system is called Advanced Distribution Management Systems (ADMS) [95].

The ADMS (Fig. 2.11) is described as the central controller of the distribution network which supports network operating decisions [93]. It harmonises and optimise the functionality of all the other systems which enables the streaming of decision making thereby enhancing the performance of the emergency response. By leveraging on the Geographic Information System (GIS) as built network model, the ADMS integrates with other tools to create a real-time network model and provides a unified platform for control and

dispatch with a comprehensive view of the distribution system during an outage [93, 95].

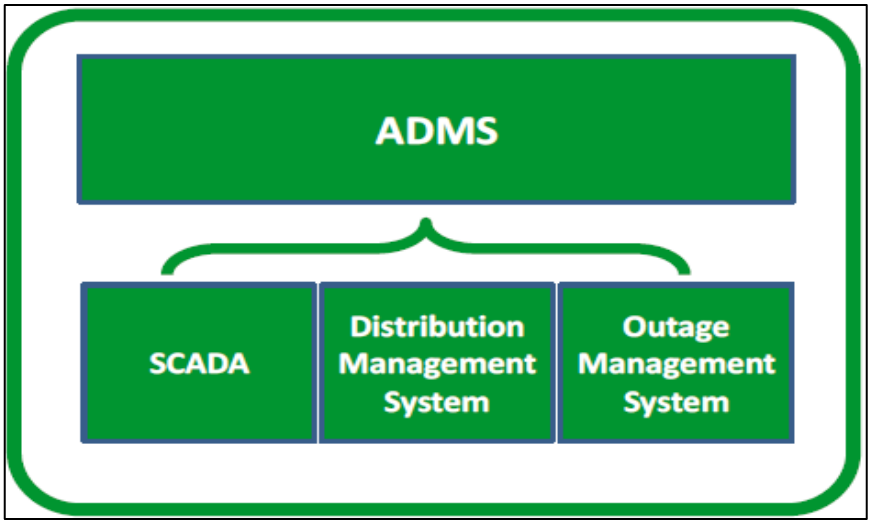

Fig. 2.11. Structure of the ADMS [95].

According to [93], the three operating approaches offered by an ideal ADMS to best meet reliability and efficiency goals are:

- "Provide users with the solution's advanced tools and visual context".
- "Prompt users with recommended switching operations".
- "Fully automate network management with closed loop control functionality".

Additionally, the information needed across the utility enterprise is delivered by the ADMS model for the following reasons:

- "Monitoring, analysis and control of network operations".
- "Managing, analysis and control of network operations".
- "Planning analysis: online to evaluate 'what if' scenarios and offline to assess historical activity and plan for future network enhancements".

- "Preparing for effective and secure deployment of DER, including storage and microgrids".

The overall outage duration can significantly impact on the power system resilience. Deploying advanced tools and well thought out restoration strategies are some of the ways in which power system resilience can be improved. Again, the method adopted in the provision of black start services also determines the grid restoration time. **This thesis work aims among other objectives to develop a black start restoration method based on DER**. The next section reviews some of the existing black start methodologies. Also, some of the research questions are highlighted.

2.16 Black Start Restoration Methodology

Several studies on black start restoration methods have been carried out with different restoration methods or a combination of methods: heuristics, meta-heuristics, expert systems, mathematical programming, and multi-agent suggested [140-151]. These studies provide useful insights of the advantages and disadvantages of some of the restoration approaches. Some of such suggested methods would be briefly reviewed in this section.

Using heuristic method, [140, 141] proposed a restoration scheme to enhance minimum feeder loss while promoting a faster service restoration. The proposed method relied on branch power flow unlike previous methods which relied on current flow. The result from this method indicated that optimal configuration and reduced computational burden resulted in better restoration plan. One of the objectives of the meta-heuristics approach as opined by [142-144], is to minimise the out of service areas and the number of manually and automated controlled switch operations and losses. The

approach used by the authors involves a combination of particle swarm optimisation, neural network, simulated annealing, fuzzy theory, genetic algorithm, tabu searching and ant colonies. However, when applied to practical distribution systems, this approach requires extensive computational time which has been noted to be one of the drawbacks of this method.

The expert system is designed in such a manner to activate a restoration plan with appropriate switching sequence. The approach is based on the knowledge-based techniques which involves the representation of expert knowledge as rules by the application of (IF-THEN statements) and the use of inference engine to infer from such rules [145, 146]. Although this approach has been considered to be quite effective in-service restoration problem, however, the high cost associated with the maintenance of large expert system is a disadvantage. Using the mathematical programming approach, [147-149] formulated the service restoration problem as a mixed integer non-linear problem (MINLP). This method of service restoration approach can be applied to obtain optimal solutions. However due to the expansion problem, the computational time normally exceeds the practically allotted time. However, [150, 151] proposed using a multi-agent system which was capable of addressing the shortfall of the mathematical programming approach. A critical review of the various restoration methodologies with highlights on the state of the arts along with the merits and demerits of the various approaches has been well articulated in [150].

2.17 Black Start with DER

The era of global over dependence on oil for energy related services is slowly coming to a halt. The burning effect of climate change resulting from

greenhouse gas emission and other such pollutions has continued to impact negatively on the environment. Developments in the field of renewable energy technologies has continued to transform the energy sector even as the cost of energy from these sources is increasingly becoming competitive with that of the fossil-based power plants. As a result of this, the use of DERs as an alternative energy source or in conjunction with conventional energy sources is increasingly becoming popular. For example, during blackout scenarios, some DERs are used in the provision of power to support critical facilities. With such capacity and reliability comes the quest to integrate DERs in the provision of black start services during power system restoration. This section aims to review DERs as a potential resource to be adopted in black start service restoration.

The definition of DERs varies depending on the context of usage. However, [17] describes it as "*electricity-producing resources and controllable loads that are connected to a local distribution system or connected to a host facility within the local distribution system*". Such technologies could be either renewable or non-renewable, and include but not limited to:- wind turbines, solar panels, small hydro power plant, diesel generators, combine heat and power (CHP) plants, small natural gas fuelled generators (SNGFG), steam turbine generator (STG), electricity storage systems, electric vehicles and controllable loads, such as HVAC systems and electric water heaters. With this broad range of technologies comes the concept of Distributed Generation (DG) which is defined by [18] as "*relatively small-scale generators that produce several kilowatts (kW) to tens of megawatts (MW) of power and are generally connected to the grid at the distribution or substation levels*". The theoretical benefit of DG as highlighted in [152, 153] is presented in Table 2.2.

Table 2.2. The theoretical benefits of distributed generation [152, 153].

Reliability and Security Benefits	**Economic Benefits**	**Emission Benefits**	**Power Quality Benefits**
Increased security for critical loads Relieved transmission and distribution congestion Reduced impacts from physical or cyber attacks Increased generation diversity	Reduced costs associated with power losses Deferred investments for generation, transmission, or distribution upgrades Lower operating costs due to peak shaving Reduced fuel costs due to increased overall efficiency Reduced land use for generation	Reduced line losses Reduced pollutant emissions	Voltage profile improvement Reduced flicker Reduced harmonic distortion

According to [130], DERs can be further classified according to their roles in the provision of black start restoration services as: black start DGs, non-black start DGs, energy storage and controllable loads. Although controllable loads do not provide power, they can however be deployed in demand side response (DR) schemes for load management by either shedding or re-connecting, hence it is classified as a special type of DER. The various classifications of DERs are presented in Table 2.3.

As indicted in Table 2.3, some DERs have been classified as black start and non-black start DGs. This classification is based on the uncertainties surrounding some of the DGs output. The variability of some of the RE sources has been the main challenge hindering the incorporation of these REs in the black start restoration plan. For instance, the intermittent nature of renewable energy sources like wind and solar energy makes them classified as not being suitable for black start service restoration. However,

[154] noted that the effect of renewable energy resources associated with restoration problem has not been widely researched as only very few literatures have discussed this.

Table 2.3. Classifications of DERs according to role in black start restoration [130].

DER Type	Black start Capability	Dispatchable?	Examples
Black start DG	Yes	Yes	Diesel Generator, CHP, SNGFG, STG, Micro Turbine, Fuel Cell
Non-Black start DG	No	Yes	Micro Turbine, Small-Hydro
		No	Wind Generators, Photovoltaic
Energy Storage	Yes, when discharging	Yes	Battery, PHEV, Flywheel
Controllable Loads	No	Yes	Emergency DR, Load (Direct Load Control), Economic DR Load

The conventional service restoration is carried out using black start DGs. According to [155], a resource that is capable of performing self-start with voltage and frequency regulation is described as black start DG. A non-black start DG on the other hand is described as a resource which requires external cranking power (e.g. battery, small diesel generators, and other source of external power) to kick start [18]. A non-black start DG whose output power is both active and reactive at any given set points is described as dispatchable. For non-dispatchable DGs, their power generation is uncontrollable due to their variability.

Improvements in EVs technologies has been made possible largely due to the significant developments and ongoing research in the energy storage technologies. The development of smaller but effective battery storage

technology has been a major boost to further advancement of RES like solar and wind. As noted in [156], PVBBSs and ESSs are being used in the provision of backup power for critical loads and as a result of its fast response are capable of significantly enhancing transient stability if chosen to regulate voltage and frequency. Research in the use of PHEV in black start restoration is still at infancy stage but with very promising potential due to the advanced storage technologies currently in use and their contribution in the electric distribution system. Example of such contribution is the use of electric buses as a means of proving resilience in the distribution system reported in [157]. Flywheels and other storage technologies are being explored as a means of providing ancillary services capable of improving grid reliability and efficiency [17].

New and innovative approaches are being adopted to conserve, manage, and optimise the ways in which energy is being utilised. For instance, [17] noted the adoption of DR to provide services as alternative to meet a local-area capacity. Controllable loads such as Heating Ventilation and Air Conditioning Systems (HVAC), electric water heaters, heat pumps can be controlled in order to maintain system stability. The application of advanced and smart technologies can be used to control these loads, thus allowing for frequency, and spinning reserve management.

2.18 DERs in Microgrids

The evolution in the electrical engineering field has brought with it new concept and terms. Microgrids is one of such emerging concept and is defined by the US Department of Energy (Microgrid Exchange Group) as "*a group of distributed energy resources and interconnected loads within a given electrical territory, which behaves as a single controllable entity with*

respect to the main network, to which it can connect and disconnect to 'island'" [158, 159]. Similarly, the CIGRE C6.22 working group (Microgrid Evolution Roadmap) describes it as "*an electrical distribution system consisting of diffuse loads and sources of energy (distributed generators, storage devices or controllable loads) that can be operated in a coordinated way*" [159, 160]. The commonality of both definitions is the inclusion of DERs, controllable entity or load and coordination of the entire system in a specific manner. Since DERs are integral components of microgrids, it implies therefore that microgrids can as well be seen as a potential black start restoration unit.

2.19 Black start Restoration Method using DERs

The contributions of DERs both renewable and non-renewable in the provision of alternative source of power or in grid/off grid applications especially at the LV distribution level cannot be over emphasized. As mentioned earlier, studies in [134, 135, 156] observed that recent technological research have shown the potential of employing DERs along with RCSs in the provision of black start services. Furthermore, other studies also reported the progress made in the deployment of electric buses in the distribution system to facilitate and enhance the system resilience [157]. All of these measures are strong indications pointing to the possibility of DERs deployment in the provision of black start services. Hence this section aims at reviewing some of the existing DERs black start restoration methods.

Using a microgrid structure, [161] proposed a method of grid restoration for critical load on the distribution feeder. The procedure adopted was a four-step approach namely: restoration tree construction, load group formation, solving the critical load restoration problem as a maximum coverage

problem and lastly determining the restoration action. The maximum coverage problem which is a linear integer program (LIP) was solved and the restoration method was applied to a practical distribution system. By choosing the best possible arrangement of power network configuration, a service restoration problem in a microgrid was solved by [162]. This was achieved by the application of Lagrangian technique and dynamic programming to give an analytical sub-optimal but efficient solution to the problem. The simulated results indicated that both approaches proved to be useful in providing solutions very close to the optima.

By modelling a critical load problem as a chance-constrained stochastic program, [163] developed a two-stage heuristic method that was used in addressing the critical load restoration problem. The restoration sequence used was to first create a strategy table and then solve the linear integer optimization problem to obtain the restoration strategy. Although this approach seems interesting, however the authors were yet to apply it to a practical system to test its effectiveness. By first establishing a feasible restoration tree from microgrid to critical loads, followed by the incorporation of the reserve capacity as constraints of the restoration problem and lastly using emergency power supply vehicles, a three-stage service restoration approach was proposed by [164]. Using this method, the system resilience was evaluated by the non-parametric kernel density estimation and numerical simulations conducted to demonstrate the effectiveness of this approach. [165] in their research proposed a look-ahead service restoration method based on DGs to serve critical loads in a secondary network distribution system. Their assumption was based on the availability of a hierarchical control infrastructure, DGs and load which can be centrally controlled. A heuristic method aimed at obtaining the allocation plan by solving a mixed-integer linear program was proposed by [157]. The

method was validated by numerical simulations performed on the IEE 123-node feeder system using different scenarios. Electric buses were considered as a kind of resource by the authors.

Considering the application of recent technology such as the deployment of DERs along with RCSs and ESS in the provision of black start services, [166] proposed a multi-time step service restoration method aimed at generating an optimal control sequence for RCs, ESS and dispatchable DGs. This was necessary to help the DSO in their decision making. Their methodology was based on the formulation of a mixed-integer linear programming model which was tested on the modified IEEE 13-node and IEEE 123-node test feeders. Similarly, [167] used a mixed-integer linear programming model to formulate a sequential service restoration (SSR) framework to generate restoration solutions for distribution systems and microgrids. The control actions in the sequence were such as to systematically control the switches, distributed generators, and switchable loads to form multiple microgrids.
Using the modified IEEE 123 node test feeder, the effectiveness of the model was examined. In an attempt to improve upon existing studies, [168] considered the effect of energy optimization and dynamic stability which they observed was lacking in existing methods examined in various literatures. Their sequence restoration method which placed emphasis on achieving optimal switching time was on multi-objective optimization. The IEEE 123 node test feeder was used for the simulation performed in PSCAD. The advanced feeder restoration approach was proposed in [169] for the restoration of critical loads using DERs. Using a mixed-integer linear program the model was developed and tested on the IEEE 123-node test feeder and IEEE 906-bus feeder. The results of the simulation showed that both network failure probability and the availability of DERs was taken into consideration in the determination of the restoration plan. Besides being

able to carry out a damage assessment of the distribution feeder, the approach also demonstrated the potential to restore maximum number of critical loads. Using microgrids as black start resources for power system restoration, [170] proposed a model predictive control (MPC) based generator start-up optimisation strategy. The mixed integer linear programming was applied in the optimisation of the generator start-up sequence. By discretising the probability distribution of the forecast errors, the uncertainties of black start resources were modeled. The modified IEEE 118-bus system was utilized for the numerical simulations and the restoration strategy verified by the Zhejiang provincial power system as being successful in restoring the power system. The transient behaviour of the microgrid was however not verified.

To restore critical loads due to power loss resulting from power outage in the distribution system, [135] proposed a novel restoration approach. The approach was based on the use of a mixed-integer linear program formulated to maximise the total prioritised loads restored while at the same time ensuring operation constraints of the participating microgrid and satisfying self-adequacy. The authors employed a multiagent coordination scheme aimed at achieving global information through only communications. To validate their proposed scheme, the modified IEEE distribution test system was used with the numerical results being satisfactory. Using the multi-agent based technique, [171] proposed a system that could be deployed to locate fault, isolate affected area and aid in service restoration in microgrids. A spanning tree search algorithms was adopted by [172] in developing a restoration strategy for distribution system. Using this method, the microgrids are modeled as virtual feeders in the distribution system and the radial structure of the distribution network by a spanning tree. The primary objectives of the proposed algorithm are to

minimise the switching operations during restoration while maximising the out-of-service load to be restored. The model was tested on the modified IEEE 37-node system and the simulated results proved to be effective.

By using microgrid as a resilience resource, [173] using a combination of reconfiguration approach and microgrid applications developed a restoration strategy based on spanning tree search strategy. To reduce the computational complexity, the authors proposed the use of heuristic method to simplify the graph. Using this method, the distribution network is reduced to connected graphs with the load zones modeled as vertices and feeder line sections as edges. The problem is defined as optimisation problem with the objective function as minimizing the number of switching operations. Using the four-feeder 1069-bus test system, the proposed method was simulated. The results when compared to other results from literature showed a significant improvement in load restoration. The critical load restoration problem was solved by a two-stage method proposed by [174]. To determine the optimal restoration strategy, the authors proposed a decision-making method with the objective of maximising the number of loads restored weighted by their priority. The approach used involved the problem formulation as a mixed-integer semidefinite program (SDP) with an iterative algorithm proposed to deal with integer variables. The method was validated by numerical simulation using the modified IEEE 13-node test feeder. The results showed an efficient restoration strategy.

2.20 Chapter summary

Achieving a sustainable future is solely dependent on the energy choices energy user's make. Even though the quest for energy transition from conventional to non-conventional and renewable appears to be slow,

however the trend from the various literature shows that significant progress has been made. The rate of DERs deployment at every level of the power system has continued to increase especially with different looming datelines of petrol and diesel car bans. From the review of the literature, different research gaps have been identified in the state of art and would be addressed in this thesis.

Without doubts, considerable research has been carried out in the areas of DERs applications in distribution networks as well as for microgrid restoration. However, at present there seems to be a dearth of sufficient information about decarbonising some aspects of power system operations unlike other sectors like the transport sector. As observed by [130], specific research in the area of black start from distribution systems and microgrids is quite limited. This study therefore fills that knowledge gap by aiming to implement different impact studies considering an increase in the load and addition of distributed-generation sources using data from a real low voltage (LV) distribution network in Nigeria. Over and above that, a unique BSR sequence capable of improving the resilience of the power grid in the unlikely events of a blackout would be developed to incorporate DERs and implemented using the Nigerian 330 kV 48-bus system.

CHAPTER 3

3.0 ENERGY EFFICIENCY, LOAD DEMAND ESTIMATION AND EMISSION ANALYSIS

3.1 Introduction

The need for energy efficiency consideration in the residential electricity market and the dynamic change in residential power demand is presented in this chapter. The availability of residential or sectorial energy consumption information in Nigeria have continued to be a challenge owing to the continued reliance on estimated billing systems and the lack of electricity meters by 55% of electricity consumers [65]. This study investigates the impact of the residential energy consumption in Nigeria leading to the development of a high-resolution energy consumption profile and discusses its potential for its application in demand response.

Also, as observed by [68], in Nigeria, most household own and operate a petrol or diesel generator due to the non-availability of a reliable electricity supply. According to [70], municipal streetlights are being powered by dedicated diesel generators in some states. To highlight the energy cost dynamics and estimate the carbon footprint of a city resulting from the use of several stand-alone diesel generator to power streetlights, several case studies were conducted. The outcome of the study showed how to optimise energy consumption and improve energy efficiency.

Lastly, a techno-economic analysis of energy cost of municipal street lighting system using different metrics such as Life Cycle Cost (LCC), Annualized Life Cycle Cost (ALCC), Net Present Cost (NPC), Cost of Energy (COE), and Return on Investment (ROI) were performed. The carbon

footprint of municipal street lighting was estimated, and the economic viability of other options considered. The results of this study have been peer reviewed and publish in [70, 175].

Obtaining the energy use data is required in the development of building energy models. Deployment of smart meters is one of the ways to achieve this. However, in areas without smart meters, the bottom-up modeling approach involving the modeling of individual residential loads becomes imperative. The aim of the work in this chapter is to adopt this approach to second-guess the daily consumption of individual appliances for different classes of residential energy users. This is done using a simple excel-based algorithm based on a typical Nigerian urban household energy use data for rainy and dry seasons periods across the various residential categories considered in this study. Using this model, a high-resolution energy consumption load profile is developed and can be used as an input in the long-term energy demand prediction.

3.2 Residential Energy Use Optimisation

3.2.1 Building modelling method

Many tools have been developed and deployed by various researchers to accomplish building energy consumption prediction and modeling. One of such approach is the bottom-up approach which takes into consideration individual end-uses energy consumption of the respective individual housing types. The result obtained at the individual level is further extrapolated to give regional energy consumption depending on the representative weight of the modeled sample. This is achieved using either the statistical methods (SM) or the Engineering method (EM). In the SM, residential energy consumption is assigned to end-users based on types of regression analysis

and historical information. Once this is done, the model can be used to make an estimate of the energy consumption of dwellings representative of the residential stock. On the contrary, the EM utilizes the knowledge of the end user appliance power ratings to distinctly estimate the dwelling energy consumption [36]. The advantage of using the EM modelling approach is its non-reliance on historical data for the determination of residential total energy consumption which is a peculiar characteristic of the chosen case study location in this research.

Using a combination of the distribution and archetypes EM techniques, the model for this study was developed. To calculate the energy consumption of each end-use, the distribution technique uses distribution of appliance ownership and use with common appliance ratings, while archetypes is used to broadly classify the housing stock according to vintage, size, house type [36]. Different classes of residential types usually referred to as "archetypes" exist and some of the typical Nigerian residential types was taken into account during the EM modelling.

3.2.2 Residential types, household size and scenario description

Different types of residential housing exist in Nigeria. However, for the purpose of this study, the following type of housing schemes which is common in any part of the country was considered. The various buildings layout schematics is presented in **Appendix A**.

- Four bedrooms flat with an average family size of seven.
- Three bedrooms flat with an average family size of five.
- Double room self-contained with an average family size of three.
- Single room self-contained with an average family size of two.
- Two bedrooms apartment with an average family size of four.

- One bedroom apartment with an average family size of two.

The typical occupancy pattern predominant in Nigeria has been described in [70, 175]. Hence, the three different scenarios proposed by the study is adopted in this research.

Scenario 1:

The house's occupants are fully engaged at work or school and thus mostly have a period of inactivity in the house between the hours of 09.00 to 16.00. They return from their various engagements at around 16:00 and resume their regular house activities and the cycle continues the next day.

Scenario 2:

Some house's occupants are engaged in a job or activity that averagely ends by 14.00. They either return home with the kids or the kids are dropped off at home. In any case, their average unoccupied period is from 09.00 to 14.00. It is assumed that someone would always be home at this time to take care of the kids. The same cycle resumes the next day.

Scenario 3:

Some family members are not engaged in any external activities. Hence, there's no period of inactivity in the house. At any time, there must always be somebody at home. The underlining assumption in all scenarios is that there is a constant power supply.

3.2.3 Occupants' energy use routine

The daily routine of residential energy users is unpredictable and is influenced by so many factors such as household size, cultural background, financial status, season, weather and other undefined factors. However, as residential occupants' behaviour and energy use varies widely, these must be assumed across the various types of residence. The period of energy usage and non-usage is related to the active and inactive or occupied and unoccupied periods respectively.

3.3 Domestic Residential Load Profile Determination

To model the appliance energy-consumption profile for a typical household, the information relating to the daily appliance usage is obtained [176]. The information include: the daily energy-consumption of each appliance, the occupied or usage period and the ownership of each appliance. The product of the power rating of each appliance, the duration of use and the number of appliances is used to determine the level of household electricity consumption. Hence, for a household with n number of appliances, the electricity consumption is estimated using equation (3.1).

$$E_{ha} = \sum_{i=1}^{n} (Ri \times Hi \times Qi)/1000 \tag{3.1}$$

Where:

E_{ha} is the total electricity consumed by a household (kWh).

R is the power rating of an appliance (W).

H is the duration of operation of an appliance (h).

Q is the unit quantity of the appliance, i the daily data is further extrapolated to arrive at a monthly figure assuming a 30-day month.

In order to determine the daily consumption of the various dwelling and for all the scenarios, an energy audit was conducted, relying on the hourly time step recording of individual appliance usage. The energy audit survey template had a Table indicating all possible appliances with an hourly time step. This template was then distributed to the occupants of the various residential types to mark when an appliance was in use and in which time step it was used. This was done to reflect the rainy and dry season period of the country.

Using a simple excel-based algorithm developed, the recorded electrical consumption of each appliance was used to quantify the amount of electricity used during each hourly time step. Energy demand analysis is carried out for each activity: lighting, television, DVD/DVR, home theatre, cable decoder, fan, laptop & mobile phone charger, air conditioner, refrigerator/freezer, microwave, blender, washing machine, water heater, iron and water pump.

At the end of each time step the sum of consumption is obtained. By adding the hourly consumptions together, the total daily consumption was reached. The highest electrical consuming day of the week was used in computing the daily consumption. The typical daily load profile of energy consumption for different building types, representative of the typical residential sector buildings in an urban area of Nigeria was developed and presented in **Appendix B**. The typical average urban rainy and dry seasons load profiles are shown in Fig. 3.1 and Fig. 3.2 respectively while the aggregated load profile is shown in Fig. 3.3. A similar trend is observed across the three load profiles with a morning and evening peaks occurring at 07:00 and 20:00 hours respectively while the off-peak occurs at 10:00 hours.

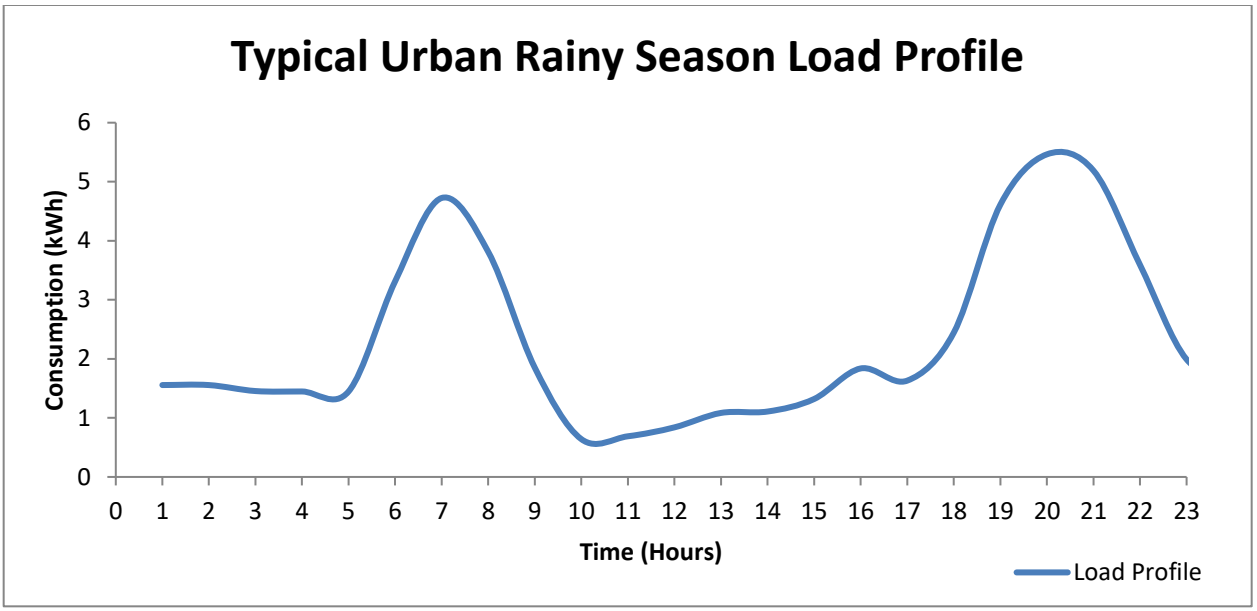

Fig. 3.1. Typical average urban rainy season load profile.

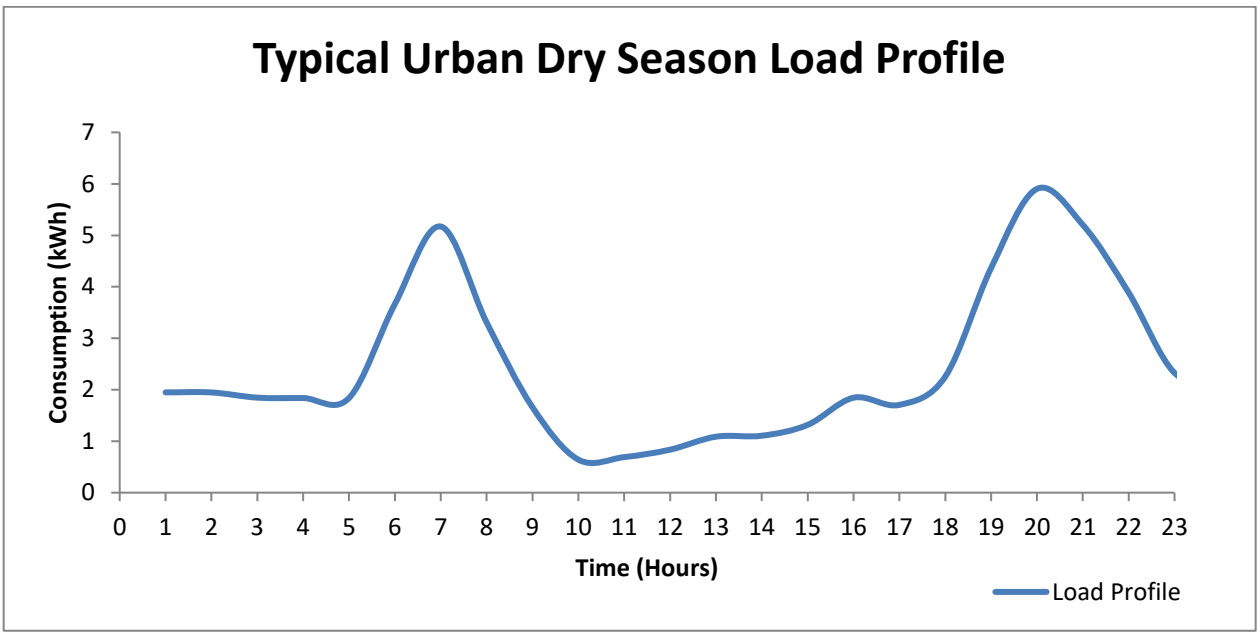

Fig. 3.2. Typical average urban dry season load profile.

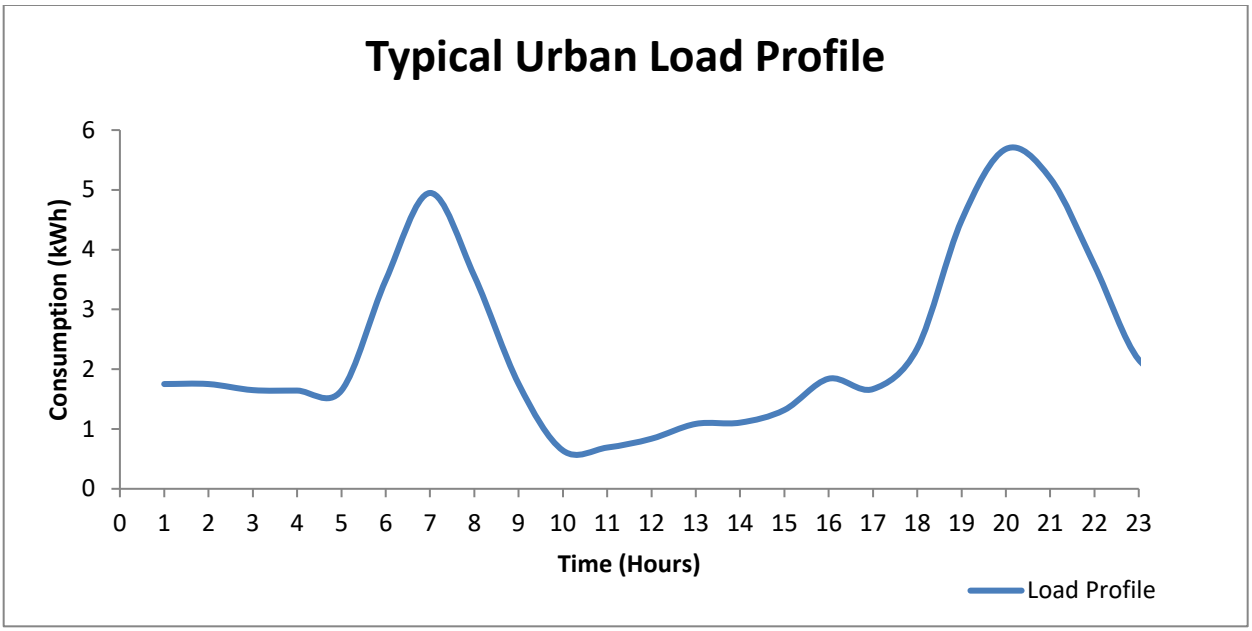

Fig. 3.3. Typical urban load profile.

Using equations (3.2) to (3.5), the average demand, load factor, demand factor and unit power density of the various residential types were determined (**Appendix C**). Table indicating the assumed wattages of the various appliances is presented in **Appendix D**.

$$\text{Average Demand} = \text{Total Energy/Hours} \tag{3.2}$$

$$\text{Load Factor} = \text{Average Hourly Demand/Maximum Hourly Demand} \tag{3.3}$$

$$\text{Demand Factor} = \text{Maximum Demand/Total Connected Load} \tag{3.4}$$

$$\text{Unit Power Density} = \text{Average Power Requirement/Square Footage of Building} \tag{3.5}$$

3.4 Energy Use Optimisation in Municipal Lighting Case Study

The objective of this study is to examine the carbon footprints of using the standalone diesel generators for street lighting in the city of Uyo, Southern Nigeria and the alternatives to reducing the carbon footprints. It was observed that existing literature had mostly focused on domestic and telecommunication base station usage of generator for energy provision. This study aims to fill this knowledge gap by assessing not only the use of generator for municipal lighting but also the associated environmental impacts of this kind of activity and the techno-economic analysis of the various alternatives.

In examining the energy use of municipal street lighting along with its carbon footprint, a Life Cycle Assessment approach (LCA) [79, 177] was adopted. This method involves the quantification of the environmental impacts and Greenhouse Gas (GHG) emissions resulting from pre-defined activities whether directly or indirectly. Data collection for such activities is achieved either through direct onsite real-time measurements or estimations based on emission factors and models. In this research, the emission factor and model which is the most preferred method in many literatures was adopted.

The three different methodologies used in quantifying the GHGs according to the International Standards Organization (ISO) [178] includes: measurement, calculation and a combination of both. Using the calculation method along with the British Standards Institution (BSI, 2008) [179] and Carbon Trust and Crown (CTC, 2008) [180] LCA approach, the CO_2 emission (eqn. 3.6) for the municipal lighting was determined.

$$CO_2 \text{ emission} = \text{Activity data (kg/km/liters)} \times \text{Emission factor } (CO_2 \text{ per unit}) \quad (3.6)$$

3.4.1 Activity data collection

The activity data related to this study involves the quantity of diesel in liters (L) used in running the various generators involved in municipal street lighting. This requires the direct measurements within the life cycle (LC) of a specific product and provides information on the activities which resulted in the emission. In order to estimate this, secondary data on the number of diesel generators, generator ratings and streetlights within the study area is obtained. This information was provided by the street lighting monitoring unit of the state Ministry of Works and the various road names were anonymised at the point of data collection. Only four major roads were purposively selected for this study. The selections were done taking into consideration certain features, for example the road length or, the traffic density. The summary of the activity data is presented in Table 3.1.

Table 3.1. Summary of Activity Data.

Roads	No. of Poles	Lamp Wattage per Pole (W)	Total Load for the Road (kW)	No. of Generators per Road	Average Monthly Fuel Consumption per Generator (L)
Road 1	575	500	287.5	6	5,611
Road 2	300	500	150.0	7	6,705
Road 3	150	500	75.0	3	4,546
Road 4	192	500	96.0	4	3,702

To determine an activity data and convert it to resultant CO_2 emissions, emission factors are applied. Also, for the emissions to be calculated, the carbon footprint boundary is set in order to categorise the various components of the carbon footprint for the analysis. This is achieved using

standard methods for the determination of GHG emission factors in the evaluation of fuel combustion. For this study, the secondary data on emissions factor were obtained from [180] (see Table 3.2). Also, the estimated values of the carbon footprint of various fuel types and energy sources for the production of 1 kWh of electricity used in this study is presented in Table 3.3 [181].

Table 3.2. Carbon Footprint Measurement Formula [180].

Variable	**Carbon Footprint Formula**	**Notes**
Fuel	$\mathrm{CO}_2 = \mathrm{AMF} \times \mathrm{FEF}$	AMF: Average Monthly Fuel in liters used FEF: Fuel Emission Factor (CO_2e/Liters) Every liter of diesel releases 2.8 kg of CO_2, 10.7 kWh of electric energy, "contains 38 MJ of energy [79, 182, 183]"
Electricity	$\mathrm{CO}_2 = \mathrm{AME} \times \mathrm{EEF}$	AME: Average Monthly Electricity used (kWh) EEF: Electricity Emission Factor (CO_2e/kWh) The EEF is (0.585 CO_2e/mWh)

Table 3.3. Carbon Footprint of Various Fossil Fuels and Renewable Energy Sources for the Production of 1 kWh of Electric Energy [181].

Fossil Fuel	
Fuel Type	CO_2 Footprint (lb)
Wood	3.306
Coal-fired plant	2.117
Gas-fired plant	1.915
Oil-fired plant	1.314
Combined-cycle gas	0.992
Green and Renewable Sources	
Hydroelectric	0.0088
Photovoltaic	0.2204
Wind	0.03306

3.4.2 Analysis of results

The carbon (CO_2) footprint, the energy cost and potential cost savings of the municipal lighting is determined using the given parameters and other secondary sources. The related economic analysis is also performed using the results obtained from this study.

3.4.3 Energy consumption cost and carbon footprint considerations

In performing the energy consumption cost and emissions analysis, the study assumes the usage of the minimum average monthly liters of diesel (Table 3.1) as the benchmark for all the analysis. Thus, for the 20 generators with average ratings of 100 kVA, 74,040 liters and 888, 480 liters of diesel are consumed monthly and yearly respectively. The study also assumes the prevailing cost per liter of diesel in Nigeria of ₦210 ($0.58) and exchange rate in December 2018 of US$1 = ₦ 362 respectively. Hence, the annual cost of diesel is estimated to be ₦186,580,800 ($515,417). With reference to Table 3.2, and using the yearly diesel consumption figures, the estimated annual energy generated by the diesel generators is 9,378,400 kWh since 1 kWh equals 3.6 MJ of energy.

The annual CO_2 footprint emitted by the 20 diesel generators is determined using equation (3.6) to be 2,487,744 kg of CO_2. The daily energy consumption assuming 12 hours of usage is determined from equation (3.7) and the results are presented in Table 3.4. A comparative energy consumption analysis of using equivalent 120 W Light Emitting Diode (LED) lamp fittings instead of the existing 250 W High Pressure Sodium (HPS) lamp fittings is also carried out and presented in Table 3.4. According to [79, 182, 183], the luminance of a 250 W lamp fittings is comparatively similar to that

of an equivalent 120 W LED lamp fitting hence its choice as the replacement fittings. The daily and annual energy savings if an equivalent 120 W LED lamp fittings were used as a replacement is given as 3,797 kWh and 1,385,920 kWh respectively.

$$\text{Energy Consumption/day} = \text{Total Wattage} \times \text{Hours of usage} \tag{3.7}$$

Table 3.4. Lighting energy consumption results.

S/N	Luminary Type	Daily Consumption (kWh)	Annual Consumption (kWh)
1.	HPS	7,302	2,665,230
2.	LED	3,505	1,279,310.4

The carbon footprint is determined from equation (3.8) using the energy consumption results presented in Table 3.4. The carbon footprint results are presented in Table 3.5.

$$\text{Carbon Footprint} = \text{Energy Consumption} \times CO_2 \text{ Footprint of Fuel Type} \tag{3.8}$$

Table 3.5. Carbon footprint results.

S/N	Luminary Type	Daily Carbon Footprint (kg CO_2)	Annual Carbon Footprint (kg CO_2)
1.	HPS	4,347	1,586,457
2.	LED	2,087	761,427

The energy cost is determined from equation (3.9) and the underlying assumption is that the lighting system is powered from a grid connected source.

$$\text{Energy Cost} = Wattage \times Hours \times \lambda \tag{3.9}$$

Where:

λ represents the kWh rate of electric energy.

The prevailing rate of ₦26.41 ($0.073) per kWh of electricity in Nigeria as of December 2018 was adopted in this study. The energy cost results are presented in Table 3.6.

Table 3.6. Energy cost.

S/N	Luminary Type	Daily Energy Cost (₦)	Annual Energy Cost (₦)
1.	HPS	192,845.82	70,388,724.3 ($194,444)
2.	LED	92,567.05	33,786,587.7 ($93,333)

3.4.4 Techno-economic assessment case study

A techno-economic assessment of the municipal lighting considering the generator-connected, grid-connected, and a solar-connected system was carried out. The method is applied to estimate the Life Cycle Cost, Annualized Life Cycle Cost, Cost of Energy, the Net Present Cost and the CO_2 emissions resulting from the use of the various energy sources.

3.4.4.1 Scenario 1 – Generator-connected municipal lighting LCA

According to [184, 185], estimating the LCC involves determining the cost of owning, maintaining and operating the project over its lifetime in today's money. To achieve this, all future cost are brought to present values and compared with the base case. In this study, it is assumed that no generator replacement would be carried-out throughout the 25 years duration which is equivalent to the life cycle of a PV panel. The 2018 Central bank of Nigeria (CBN) interest (*ir*) and inflation (*if*) rates of 14% and 11% respectively are used throughout this study [185]. Equations (3.10) to (3.34) [184, 185],

are used to determine the life cycle cost (LCC_{HPSGEN}) of a generator connected HPS lamp street lighting system. All the abbreviations used in these equations and subsequent ones are contained in the remarks column in Tables E.1 to E.3 (**Appendix E**).

The sum of the generator cost (C_{GEN}), HPS fittings cost ($C_{HPSFGEN}$), HPS lamp cost ($C_{HPSLGEN}$), armored cable cost ($C_{ACABHPSGEN}$), pole cost ($C_{POLEHPSGEN}$), installation cost ($C_{INSTALLHPSGEN}$), labour cost ($C_{LABHPSGEN}$), concrete reinforcement cost ($C_{REINFORCEMENTHPSGEN}$) and cable cost ($C_{CABHPSGEN}$) is the initial investment capital cost (ICC_{HPSGEN}) expressed in equation (3.10).

$$\mathrm{ICC_{HPSGEN}} = C_{GEN} + C_{\mathrm{HPSFGEN}} + C_{\mathrm{HPSLGEN}} + C_{\mathrm{ACABHPSGEN}} + C_{\mathrm{POLEHPSGEN}} + C_{\mathrm{INSTALLHPSGEN}} + C_{\mathrm{LABHPSGEN}} + C_{\mathrm{REINFORCEMENTHPSGEN}} + C_{\mathrm{CABHPSGEN}} \quad (3.10)$$

The first, second, third and fourth present worth of the cost of oil and filter change is determined using equations (3.11) to (3.14) while equation (3.15) is used in determining the total present worth of oil and filter (C_{PWOFC}) change. Information on the frequency of diesel generator maintenance is well documented in [186, 187] and has been adopted for this study.

$$C_{\mathrm{OFC1PW}} = \mathrm{C_{OFC}}\left(\frac{1+\mathrm{if}}{1+\mathrm{ir}}\right)^{5} \quad (3.11)$$

$$C_{\mathrm{OFC2PW}} = \mathrm{C_{OFC}}\left(\frac{1+\mathrm{if}}{1+\mathrm{ir}}\right)^{10} \quad (3.12)$$

$$C_{\mathrm{OFC3PW}} = \mathrm{C_{OFC}}\left(\frac{1+\mathrm{if}}{1+\mathrm{ir}}\right)^{15} \quad (3.13)$$

$$C_{\mathrm{OFC4PW}} = \mathrm{C_{OFC}}\left(\frac{1+\mathrm{if}}{1+\mathrm{ir}}\right)^{20} \quad (3.14)$$

$$C_{PWOFC} = C_{OFC1PW} + C_{OFC2PW} + C_{OFC3PW} + C_{OFC4PW} \quad (3.15)$$

Using equations (3.16) to (3.19), the first to fourth present worth of decarbonising the generator ($C_{GENDECARBONPW}$) is determined. The sum of the present worth of all the decarbonisation is expressed using equation (3.20).

$$C_{GENDECARBON1PW} = C_{GENDECARBON}\left(\frac{1+if}{1+ir}\right)^{5} \quad (3.16)$$

$$C_{GENDECARBON2PW} = C_{GENDECARBON}\left(\frac{1+if}{1+ir}\right)^{10} \quad (3.17)$$

$$C_{GENDECARBON3PW} = C_{GENDECARBON}\left(\frac{1+if}{1+ir}\right)^{15} \quad (3.18)$$

$$C_{GENDECARBON4PW} = C_{GENDECARBON}\left(\frac{1+if}{1+ir}\right)^{20} \quad (3.19)$$

$$C_{PWGENDECARBON} = C_{GENDECARBON1PW} + C_{GENDECARBON2PW} + C_{GENDECARBON3PW} + C_{GENDECARBON4PW} \quad (3.20)$$

In equations (3.21) to (3.24), the first to fourth present worth cost of the engine overhauling is determined while equation (3.25) is used to determine the summation of the total cost of present worth of engine overhauling.

$$C_{ENGOH1PW} = C_{ENGOH}\left(\frac{1+if}{1+ir}\right)^{5} \quad (3.21)$$

$$C_{ENGOH2PW} = C_{ENGOH}\left(\frac{1+if}{1+ir}\right)^{10} \quad (3.22)$$

$$C_{ENGOH3PW} = C_{ENGOH}\left(\frac{1+if}{1+ir}\right)^{15} \quad (3.23)$$

$$C_{\text{ENGOH4PW}} = \text{C}_{\text{ENGOH}} \left(\frac{1+\text{if}}{1+\text{ir}}\right)^{20} \quad (3.24)$$

$$\text{C}_{\text{PWENGOH}} = C_{\text{ENGOH1PW}} + C_{\text{ENGOH2PW}} + C_{\text{ENGOH3PW}} + C_{\text{ENGOH4PW}} \quad (3.25)$$

According to [70], the hour life of the HPS lamp considering 12 hours of daily usage is approximately 5 years. The cost of the first to fourth present worth of the HPS lamp ($\text{C}_{\text{HPSLGENPW}}$) is determined using equations (3.26) to (3.29). The sum of all the present worth of the HPS lamp is computed from equation (3.30).

$$C_{\text{HPSLGEN1PW}} = \text{C}_{\text{HPSLGEN}} \left(\frac{1+\text{if}}{1+\text{ir}}\right)^{5} \quad (3.26)$$

$$C_{\text{HPSLGEN2PW}} = \text{C}_{\text{HPSLGEN}} \left(\frac{1+\text{if}}{1+\text{ir}}\right)^{10} \quad (3.27)$$

$$C_{\text{HPSLGEN3PW}} = \text{C}_{\text{HPSLGEN}} \left(\frac{1+\text{if}}{1+\text{ir}}\right)^{15} \quad (3.28)$$

$$C_{\text{HPSLGEN4PW}} = \text{C}_{\text{HPSLGEN}} \left(\frac{1+\text{if}}{1+\text{ir}}\right)^{20} \quad (3.29)$$

$$\text{C}_{\text{PWHPSLGEN}} = C_{\text{HPSLGEN1PW}} + C_{\text{HPSLGEN2PW}} + C_{\text{HSPLGEN3PW}} + C_{\text{HPSLGEN4PW}} \quad (3.30)$$

The present worth of workers' wages for lamp replacement is determined using equation (3.31).

$$C_{\text{PWHPSGENWW}} = \sum_{\text{n}=1}^{25} C_{\text{HPSGENWW}} \left(\frac{1+\text{if}}{1+\text{ir}}\right)^{n} \quad (3.31)$$

The overall cost of operation and maintenance of the generator-powered HPS street lighting system is determined using equations (3.32).

$$C_{\mathrm{OMHPSGEN}} = C_{\mathrm{PWHPSLGEN}} + C_{\mathrm{PWHPSGENWW}} + C_{\mathrm{PWOFC}} + C_{\mathrm{PWGENDECARBON}} + C_{\mathrm{PWENGOH}} \quad (3.32)$$

The present worth of the cost of running generator using diesel is determined using equation (3.33), while the life cycle cost of HPS street lighting system using a diesel-powered generator is computed using equation (3.34). $C_{\mathrm{ENERGYCOSTHPSGEN}}$ is the annual diesel cost obtained from [70].

$$C_{\mathrm{PWENERGYCOSTHPSGEN}} = \sum_{\mathrm{n}=1}^{25} C_{\mathrm{ENERGYCOSTHPSGEN}} \left(\frac{1+\mathrm{if}}{1+\mathrm{ir}}\right)^{n} \quad (3.33)$$

$$\text{Life Cycle Cost } (\mathrm{LCC_{HPSGEN}}) = ICC_{\mathrm{HPSGEN}} + C_{\mathrm{OMHPSGEN}} + C_{\mathrm{PWENERGYCOSTHPSGEN}} \quad (3.34)$$

The annualized life cycle cost $(\mathrm{ALCC_{HPSGEN}})$ and the cost of energy (COE_{HPSGEN}) using a diesel-powered generator is calculated using equations (3.35) and (3.36) respectively [188, 189]. D_L is the daily energy demand [70].

$$\mathrm{ALCC_{HPSGEN}} = \mathrm{LCC_{HPSGEN}} \left[\frac{\mathbf{1}-\left(\frac{\mathbf{1}+\mathrm{if}}{1+\mathrm{ir}}\right)}{\mathbf{1}-\left(\frac{\mathbf{1}+\mathrm{if}}{1+\mathrm{ir}}\right)^{\boldsymbol{N}}}\right] \quad (3.35)$$

$$\mathrm{COE_{HPSGEN}} = \frac{\mathrm{ALCC_{HPSGEN}}}{365 \times D_{L(HPS)}} \quad (3.36)$$

3.4.4.2 Scenario 2 – Grid-connected municipal lighting LCA

The cost associated with grid-connected street lighting system using HPS bulbs is considered in this scenario. The study assumes an average life expectancy of a transformer to be 25 years. The sum of the transformer

cost (C_{TRANS}), HPS fittings cost ($C_{HPSFGRID}$), HPS lamp cost ($C_{HPSLGRID}$), armored cable cost ($C_{ACABHPSGRID}$), pole cost ($C_{POLEHPSGRID}$), installation cost ($C_{INSTALLHPSGRID}$), labour cost ($C_{LABHPSGRID}$), concrete reinforcement cost ($C_{REINFORCEMENTHPSGRID}$), materials for transformer installation cost ($C_{MATERIALINSTALLTRANS}$) and cable cost ($C_{CABHPSGRID}$) is the initial investment capital cost ($ICC_{HPSGRID}$) expressed in equation (3.37). Equations (3.37) to (3.47), [184, 190] are used to determine the life cycle cost ($LCC_{HPSGRID}$) of an equivalent grid-connected HPS lamp street lighting system.

$$\mathrm{ICC_{HPSGRID}} = C_{\mathrm{TRANS}} + C_{\mathrm{HPSFGRID}} + C_{\mathrm{HPSLGRID}} + C_{\mathrm{ACABHPSGRID}} + C_{\mathrm{POLEHPSGRID}} + C_{\mathrm{INSTALLHPSGRID}} + C_{\mathrm{LABHPSGRID}} + C_{\mathrm{REINFORCEMENTHPSGRID}} + C_{\mathrm{MATERIALINSTALLTRANS}} + C_{\mathrm{CABHPSGRID}} \quad (3.37)$$

The cost of the first to fourth present worth ($C_{\mathrm{HPSLGRIDPW}}$) of replacing the HPS lamp is determined from equations (3.38) to (3.41), while equation (3.42) is the summation of all the present worth of the HPS lamp ($C_{\mathrm{PWHPSLGRID}}$).

$$C_{\mathrm{HPSLGRID1PW}} = \mathrm{C_{HPSLGRID}} \left(\frac{1+\mathrm{if}}{1+\mathrm{ir}}\right)^{5} \quad (3.38)$$

$$C_{\mathrm{HPSLGRID2PW}} = \mathrm{C_{HPSLGRID}} \left(\frac{1+\mathrm{if}}{1+\mathrm{ir}}\right)^{10} \quad (3.39)$$

$$C_{\mathrm{HPSLGRID3PW}} = \mathrm{C_{HPSLGRID}} \left(\frac{1+\mathrm{if}}{1+\mathrm{ir}}\right)^{15} \quad (3.40)$$

$$C_{\mathrm{HPSLGRID4PW}} = \mathrm{C_{HPSLGRID}} \left(\frac{1+\mathrm{if}}{1+\mathrm{ir}}\right)^{20} \quad (3.41)$$

$$\mathrm{C_{PWHPSLGRID}} = C_{\mathrm{HPSLGRID1PW}} + C_{\mathrm{HPSLGRID2PW}} + C_{\mathrm{HSPLGRID3PW}} + C_{\mathrm{HPSLGRID4PW}} \quad (3.42)$$

Using equation (3.43), the present worth of workers' wages for lamp replacement is determined. The sum of equations (3.42) and (3.43) gives the cost of operation and maintenance ($C_{\mathrm{OMHPSGRID}}$) of the grid powered HPS system equation (3.44).

$$C_{\mathrm{PWHPSGRIDWW}} = \sum_{\mathrm{n}=1}^{25} C_{\mathrm{HPSGRIDWW}} \left(\frac{1+\mathrm{if}}{1+\mathrm{ir}}\right)^{n} \tag{3.43}$$

$$\mathrm{C}_{\mathrm{OMHPSGRID}} = C_{\mathrm{PWHPSLGRID}} + C_{\mathrm{PWHPSGRIDWW}} \tag{3.44}$$

Using equation (3.45), the present worth of energy consumption cost is determined. $C_{\mathrm{ENERGYCOSTHPSGRID}}$ is the annual energy consumption of HPS system in kWh [70] multiplied by the current cost per kWh of electricity. The losses at the rated voltage for an 11kV transformer class of rating 200kVA are documented in [191, 192]. The present worth of transformer losses are determined from equation (3.46) using the values of the no load and load losses in watts. $C_{\mathrm{TRANSLOSSCOSTHPSGRID}}$ is the summation of the present worth (PW) of no-load losses and load losses.

$$C_{\mathrm{PWENERGYCOSTHPSGRID}} = \sum_{\mathrm{n}=1}^{25} C_{\mathrm{ENERGYCOSTHPSGRID}} \left(\frac{1+\mathrm{if}}{1+\mathrm{ir}}\right)^{n} \tag{3.45}$$

$$C_{\mathrm{PWTRANSLOSSCOSTHPSGRID}} = \sum_{\mathrm{n}=1}^{25} C_{\mathrm{TRANSLOSSCOSTHPSGRID}} \left(\frac{1+\mathrm{if}}{1+\mathrm{ir}}\right)^{n} \tag{3.46}$$

Using a grid-connected system, the life cycle cost ($\mathrm{LCC}_{\mathrm{HPSGRID}}$), the annualized life cycle cost ($\mathrm{ALCC}_{\mathrm{HPSGRID}}$) and the cost of energy ($\mathrm{COE}_{\mathrm{HPSGRID}}$) is calculated using equations (3.47), (3.48) and (3.49) respectively [188, 189].

$$\text{Life Cycle Cost } (\text{LCC}_{\text{HPSGRID}}) = ICC_{\text{HPSGRID}} + C_{\text{OMHPSGRID}} + C_{\text{PWENERGYCOSTHPSGRID}} + C_{\text{PWTRANSLOSSCOSTHPSGRID}} \quad (3.47)$$

$$\text{ALCC}_{\text{HPSGRID}} = \text{LCC}_{\text{HPSGRID}} \left[\frac{\mathbf{1}-\left(\frac{\mathbf{1}+\text{if}}{1+\text{ir}}\right)}{\mathbf{1}-\left(\frac{\mathbf{1}+\text{if}}{1+\text{ir}}\right)^{N}} \right] \quad (3.48)$$

$$\text{COE}_{\text{HPSGRID}} = \frac{\text{ALCC}_{\text{HPSGRID}}}{365 \times D_{L(\text{HPS})}} \quad (3.49)$$

3.4.4.3 Scenario 3 – Solar-connected municipal lighting LCA

In the third scenario, an equivalent solar PV powered street lighting system using LED fittings is considered. The average PV life span of 25 years is assumed in this study. The life cycle cost (LCC_{SPV}) of an equivalent solar powered LED lamp street lighting system is computed using equations (3.50) to (3.60) [184, 190]. The initial investment capital cost (ICC_{SPV}) expressed in equation (3.50), is the sum of the solar PV module cost (C_{SPV}), LED fittings cost (C_{LED}), battery cost (C_{BAT}), charge controller cost ($C_{CONTROLLER}$), cable cost (C_{CABSPV}), battery box cost (C_{BOX}), solar rack cost (C_{SRK}), concrete reinforcement cost ($C_{REINFORCEMENT}$), pole cost ($C_{POLESPV}$), labour cost (C_{LABSPV}) and installation cost ($C_{INSTALL}$).

$$\text{ICC}_{\text{SPV}} = C_{\text{SPV}} + C_{\text{LED}} + C_{\text{BAT}} + C_{\text{CONTROLLER}} + C_{\text{CABSPV}} + C_{\text{BOX}} + C_{\text{SRK}} + C_{\text{REINFORCEMENT}} + C_{\text{POLESPV}} + C_{\text{LABSPV}} + C_{\text{INSTALL}} \quad (3.50)$$

The cost of the first to fourth present worth (C_{BATPW}) of replacing the battery is determined using equations (3.51) to (3.54). Equation (3.55) is the sum total of all the present worth of battery replacement cost (C_{PWBAT}).

$$C_{\text{BAT1PW}} = \text{C}_{\text{BAT}} \left(\frac{1+\text{if}}{1+\text{ir}}\right)^{5} \quad (3.51)$$

$$C_{\mathrm{BAT2PW}} = \mathrm{C_{BAT}}\left(\frac{1+\mathrm{if}}{1+\mathrm{ir}}\right)^{10} \quad (3.52)$$

$$C_{\mathrm{BAT3PW}} = \mathrm{C_{BAT}}\left(\frac{1+\mathrm{if}}{1+\mathrm{ir}}\right)^{15} \quad (3.53)$$

$$C_{\mathrm{BAT4PW}} = \mathrm{C_{BAT}}\left(\frac{1+\mathrm{if}}{1+\mathrm{ir}}\right)^{20} \quad (3.54)$$

$$\mathrm{C_{PWBAT}} = C_{\mathrm{BAT1PW}} + C_{\mathrm{BAT2PW}} + C_{\mathrm{BAT3PW}} + C_{\mathrm{BAT4PW}} \quad (3.55)$$

The cost of the present worth of LED fittings replacement, the present worth of charge controller replacement, and the present worth of maintenance is computed using equations (3.56), (3.57) and (3.58) respectively. The PW of maintenance cost is determined using the ratio of maintenance per year (M/Yr) which is assumed to be 2% of the total PV cost.

$$C_{\mathrm{PWLED}} = C_{\mathrm{LED}}\left(\frac{1+\mathrm{if}}{1+\mathrm{ir}}\right)^{13} \quad (3.56)$$

$$C_{\mathrm{PWCONTROLLER}} = C_{\mathrm{CONTROLLER}}\left(\frac{1+\mathrm{if}}{1+\mathrm{ir}}\right)^{12} \quad (3.57)$$

$$C_{\mathrm{PWM}} = \frac{M}{\mathrm{yr}}\left(\frac{1+\mathrm{if}}{1+\mathrm{ir}}\right)\left[\frac{1-\left(\frac{1+\mathrm{if}}{1+\mathrm{ir}}\right)^{N}}{1-\left(\frac{1+\mathrm{if}}{1+\mathrm{ir}}\right)}\right] \quad (3.58)$$

The cost of operation and maintenance of the solar PV street lighting system and the total life cycle cost is determined from equations (3.59) and (3.60) respectively [188, 189].

$$\mathrm{C_{OMSPV}} = C_{\mathrm{PWBAT}} + C_{\mathrm{PWLED}} + C_{\mathrm{PWCONTROLLER}} + C_{\mathrm{PWM}} \quad (3.59)$$

$$\text{Life Cycle Cost } (\mathrm{LCC_{SPV}}) = ICC_{\mathrm{SPV}} + C_{\mathrm{OMSPV}} \quad (3.60)$$

The annualized life cycle cost ($ALCC_{SPV}$) and the cost of energy (COE_{SPV}) using a solar powered PV LED street lighting system is obtained from equations (3.61) and (3.62) respectively [188, 189].

$$\mathrm{ALCC_{SPV}} = \mathrm{LCC_{SPV}} \left[\frac{\mathbf{1}-\left(\frac{\mathbf{1}+\mathrm{if}}{1+\mathrm{ir}}\right)}{\mathbf{1}-\left(\frac{\mathbf{1}+\mathrm{if}}{1+\mathrm{ir}}\right)^{\boldsymbol{N}}} \right] \tag{3.61}$$

$$\mathrm{COE_{SPV}} = \frac{\mathrm{ALCC_{SPV}}}{365 \times D_{L(LED)}} \tag{3.62}$$

3.4.5 Analysis of scenario results

The initial capital cost of investments, the operation and maintenance cost, the energy cost, the life cycle cost and the annualized life cycle cost for the three scenarios are compared in Fig. 3.4.

In Table 3.7, the ICC, LCC, ALCC, O/M and COE of the different scenarios are compared. The major index used in the economic assessment of a project's viability is the LCC. Although the SPV system has a higher ICC cost, however, its LCC and ALCC cost are the lowest, hence making it the most economically viable option. The grid-connected system had both the highest LCC and ALCC respectively.

The operations and maintenance (O/M) cost of the three systems is further broken down and described in detail in Figs. 3.5 to 3.9. However, by inspection from Fig. 3.4 and Table 3.7, it can be observed that the cost of O/M of the generator-connected system is much higher compared to the other two.

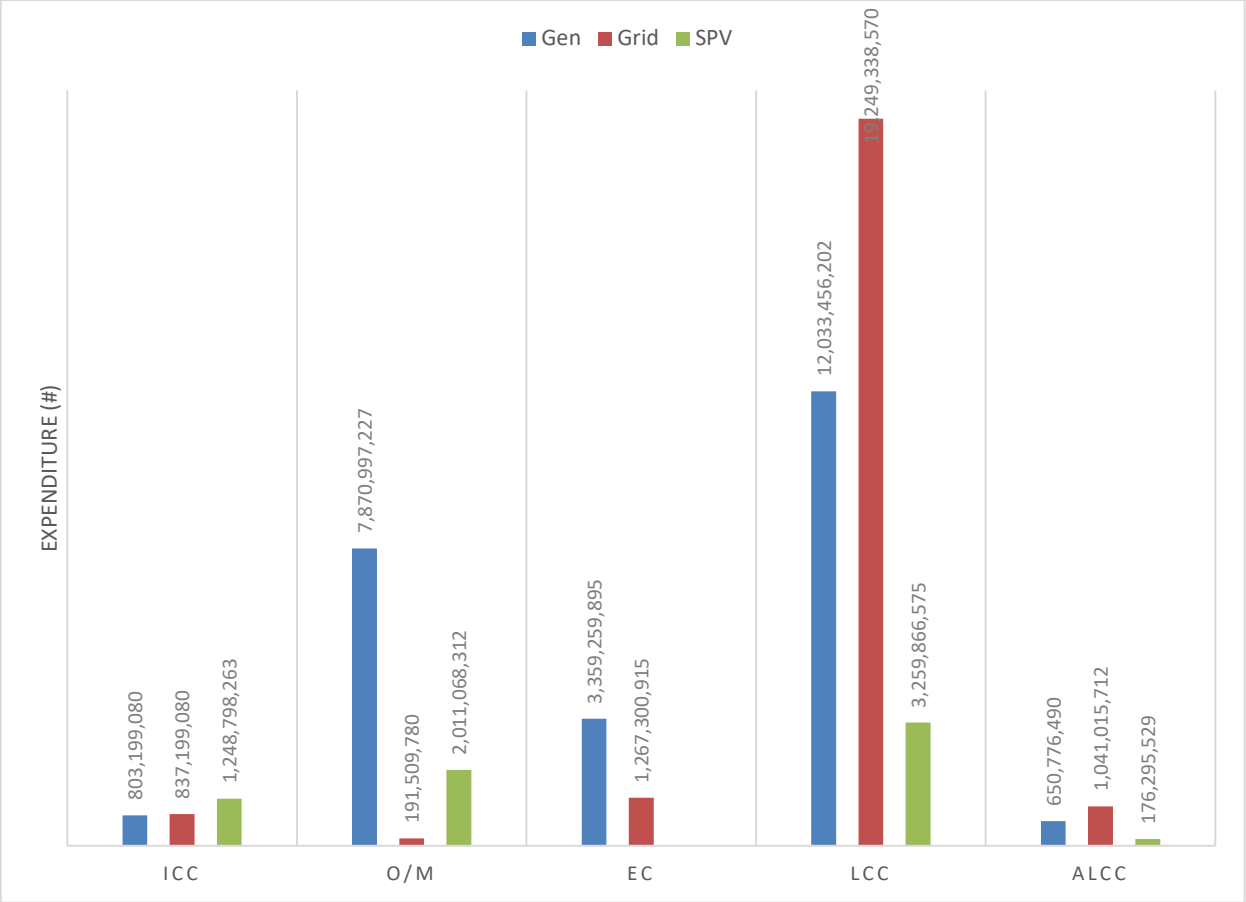

Fig. 3.4. Economic performance analysis of the three scenarios.

Table 3.7. Scenarios cost summary based on different indices.

Scenarios Indices	**Generator-powered Cost (₦ and $)**	**Grid-powered Cost (₦ and $)**	**Solar PV-powered Cost (₦ and $)**
ICC	803,199,080	837,199,080	1,248,798,263
	(2,218,782)	(2,312,701)	3,449,719)
LCC	12,033,456,202	19,249,338,570	3,259,866,575
	(33,241,592)	(53,282,128)	(9,005,156)
ALCC	650,776,489	1,041,015,712	176,295,529
	(1,797,725)	(2,881,529)	(487,004)
O/M	7,870,997,227	191,509,780	2,011,068,312
	(21,743,086)	(529,033)	(5,555,437)
COE	244.17	390.59	137.80
	(0.675)	(1.08)	(0.38)

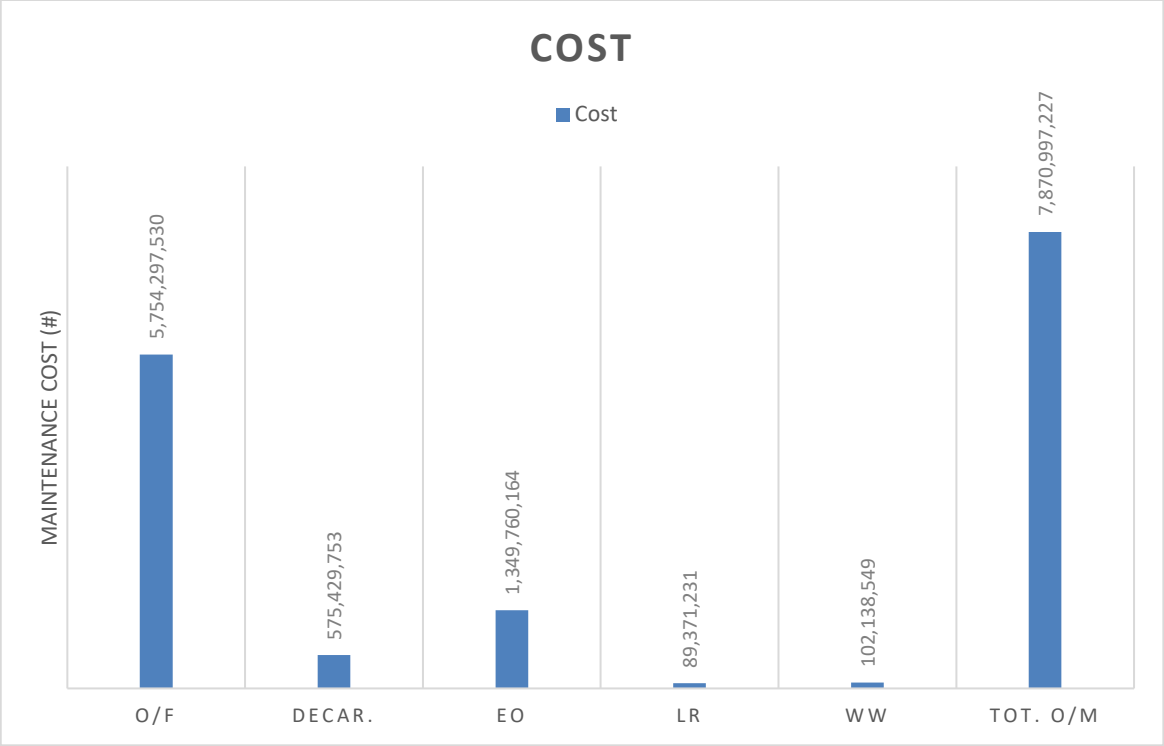

Fig. 3.5. The O/M cost of the generator-powered system.

The breakdown of the various maintenance cost of the generator-connected system is presented in Fig. 3.5. Noticeably, oil and filter (O/F) and engine overhauling (EO) takes the greatest chunk of the total maintenance cost having 73% and 17% respectively. According to [186, 187], after every 300 hours of generator operation, oil and filter replacement should be carried out. Using the assumed 12 hours of generator usage for this study, this would translate to oil and filter replacement for about 365 times throughout the 25 years lifespan of the generator. Likewise, the engine overhauling which is carried out after every 6000 hours of generator operation [186, 187]. This would amount to overhauling the engine for 17 times throughout the 25 years lifespan of the system. The percentage distribution of the various O/M cost components is presented in Fig. 3.6.

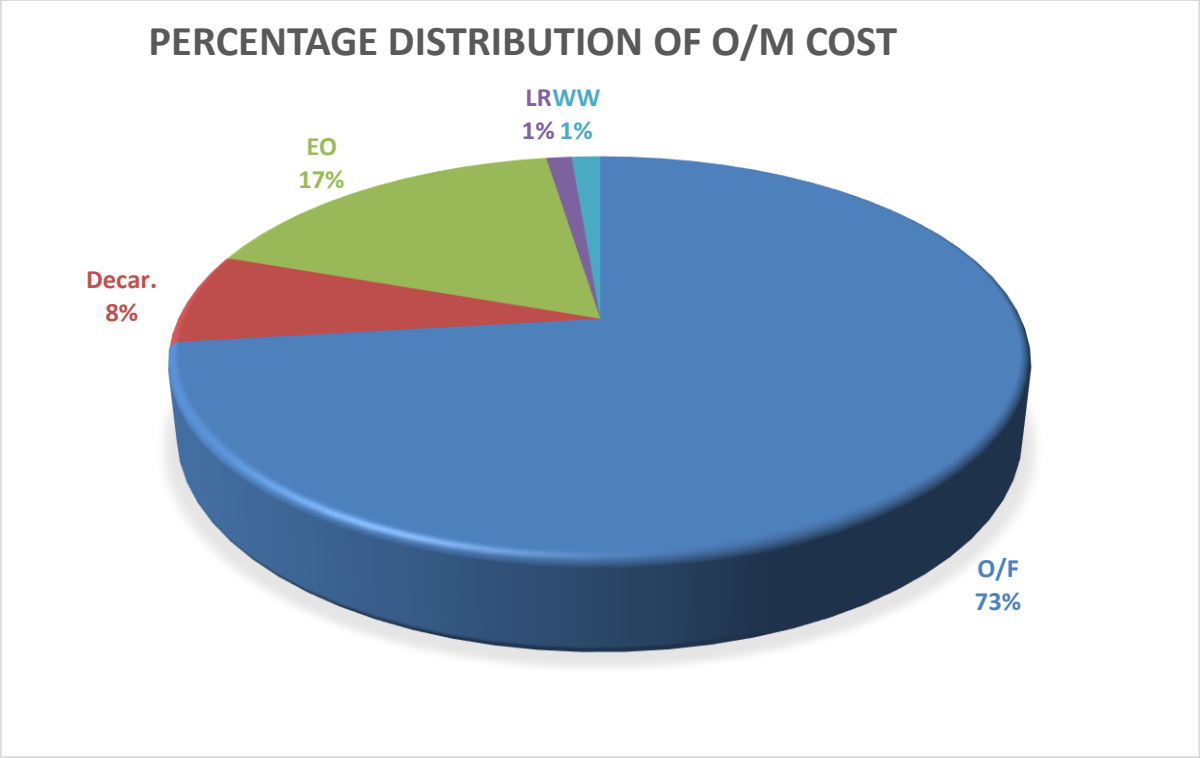

Fig. 3.6. Percentage distribution of O/M cost of the generator-powered system.

According to [186, 187], the process of decarbonising the generator is usually carried out after 1500 hours of generator operation. Again, for the 25 years lifespan of the system, this process would be done for 73 times, and this constitute 8% of the total operation and maintenance cost. The lamp replacement (LR) and workers' wages (WW) are the least cost components having only 1% of the total operation and maintenance cost.

For the grid-connected system, Fig. 3.7 and Fig. 3.8 capture the O/M cost and the percentage distribution of the cost components respectively. Only two components constitute the O/M cost for the grid connected system. The WW constitutes 53% of the total O/M cost while the lamp replacement takes the remaining 47%.

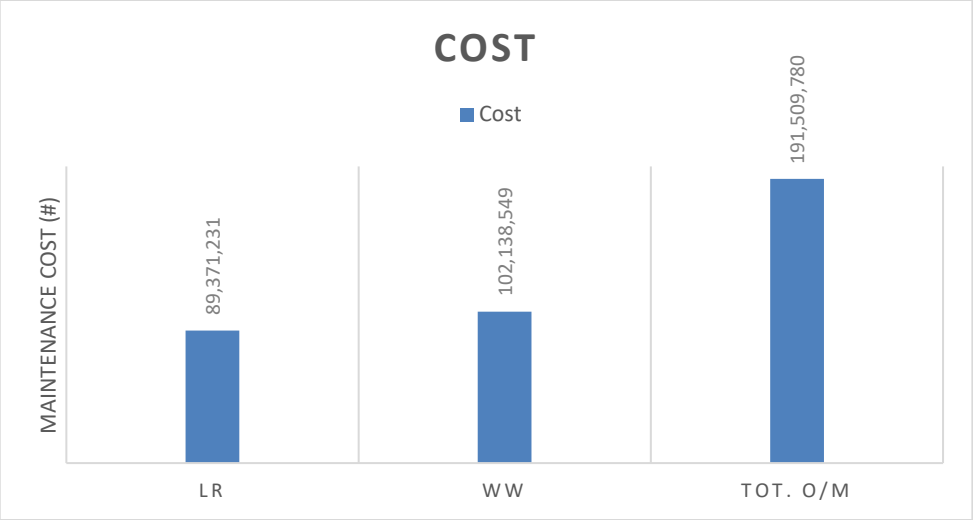

Fig. 3.7. The O/M cost of the grid-connected system.

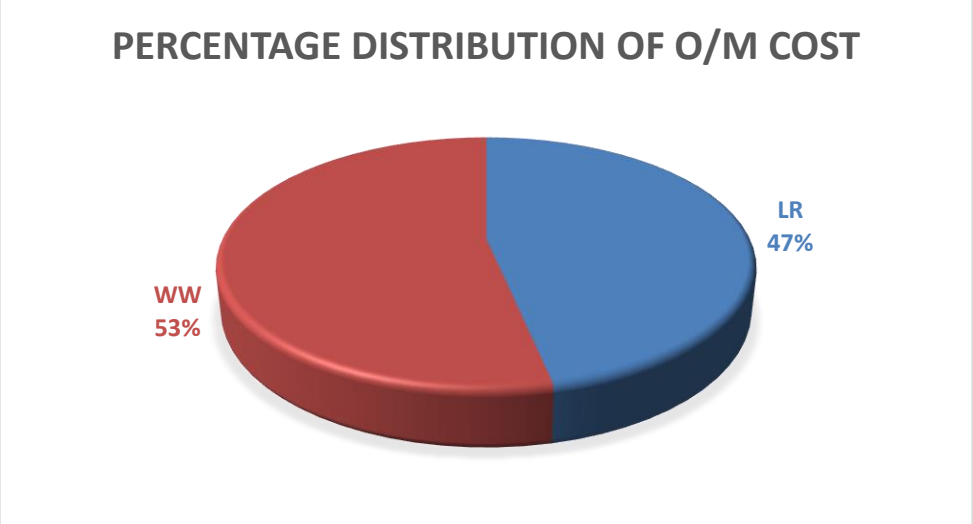

Fig. 3.8. Percentage distribution of O/M cost of the grid-connected system.

In Fig. 3.9 and Fig. 3.10, the major components that constitute the O/M cost for the SPV system are the battery replacement (BR) cost, lamp replacement (LR) cost, charge controller replacement (CCR) and the present worth of maintenance cost (PWM). The BR constitutes 70% of the total O/M cost while the PWM constitute 20% of the O/M cost. The LR and CCR constitutes 7% and 3% respectively.

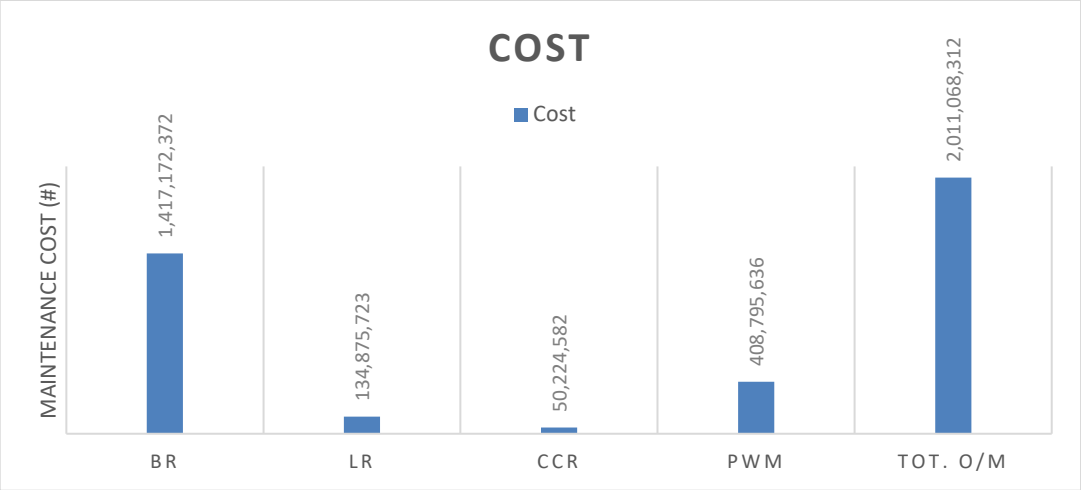

Fig. 3.9. The O/M cost of the SPV system.

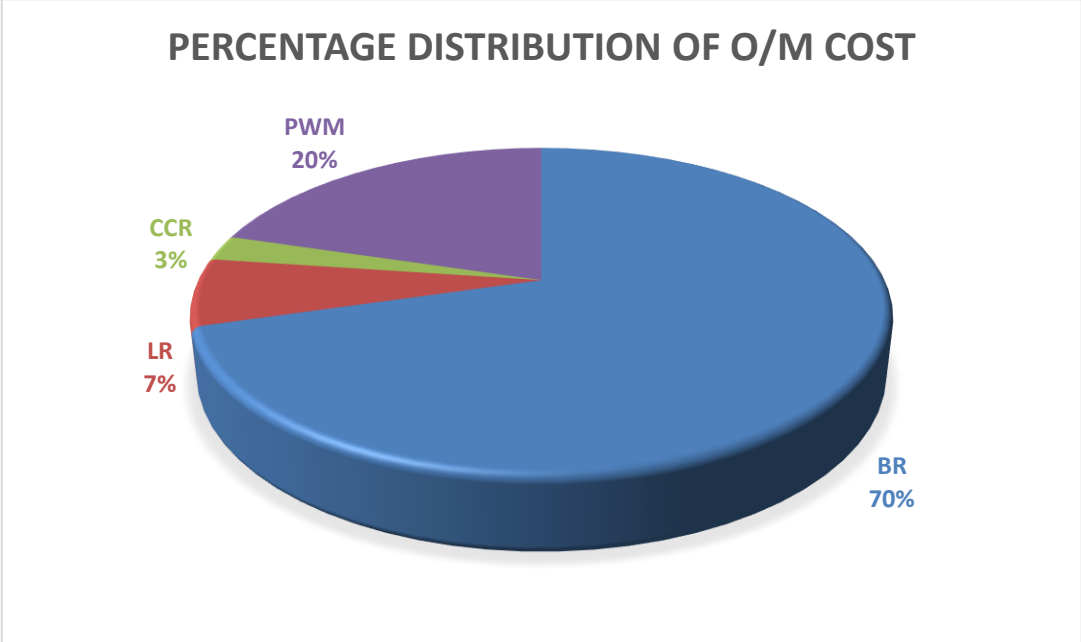

Fig. 3.10. Percentage distribution of O/M cost of the SPV system.

3.5 Modelling and Results Validation

Hybrid Optimisation Model for Multiple Energy Resources (HOMER) is a software application originally developed at the National Renewable Energy Laboratory for the design, technical and financial evaluation of off-grid and on-grid power systems. HOMER Pro 3.13.1 software is used in this study to

simulate the generator connected and the solar PV connected street lighting systems. The grid connected system was exempted due to the software design constraint as only the cost of electricity is allowed as input for the grid-connected system.

In conducting the analysis, HOMER relies on specific information with respect to the major components of the various systems namely: size of diesel generator, solar PV, batteries, and converters. The simulation is performed once the required parameters capital cost, operation cost, maintenance cost, replacement cost, diesel cost, system size, quantity, hours of operation, system lifetime, load type, discount and inflation rates have been inputted. The total NPC, and the Levelised Cost of Energy (LCOE) is determined and a sensitivity analysis to justify the sensitivity of the system to certain factors such as component resource cost or availability is conducted.

3.5.1 Modelling of the component in HOMER

The availability of the required renewable energy resources is the first step required to building the schematic of the various models. For the study location, the solar resources from NASA surface meteorology which provides the average solar radiation and clearness index was download and entered in HOMER Pro from the resource window as shown in Fig. 3.11.

The schematic diagram of the simulated generator-connected and SPV streetlight systems are shown in Fig. 3.12 and Fig. 3.13 respectively. The basic compositions of the two systems are the diesel generator, the PV module, batteries, converter, and the streetlight load. According to [70], the streetlights in the study area are partitioned into sections. Each section is

being powered by one generator. Due to design constraints in HOMER, only one section was considered for the simulated analysis.

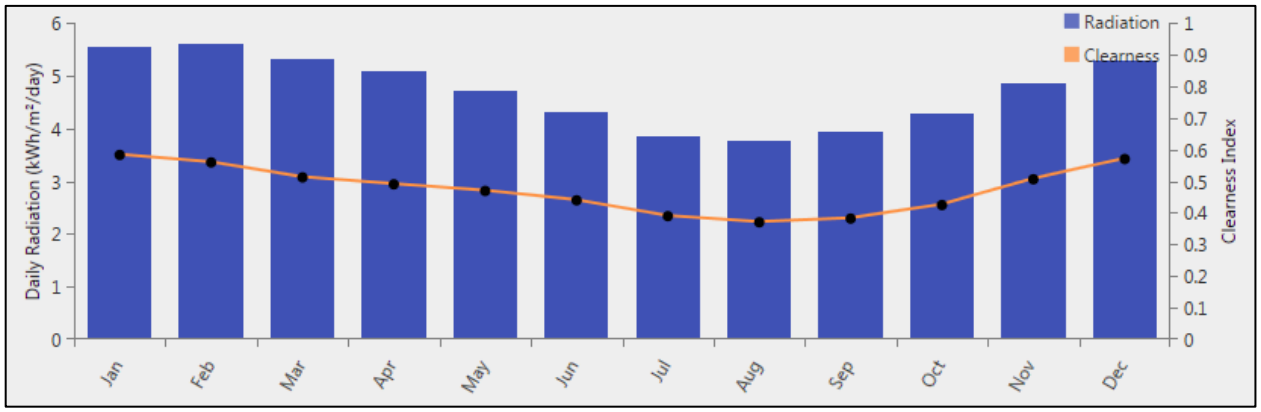

Fig. 3.11. Monthly average solar radiation and clearness index of study location.

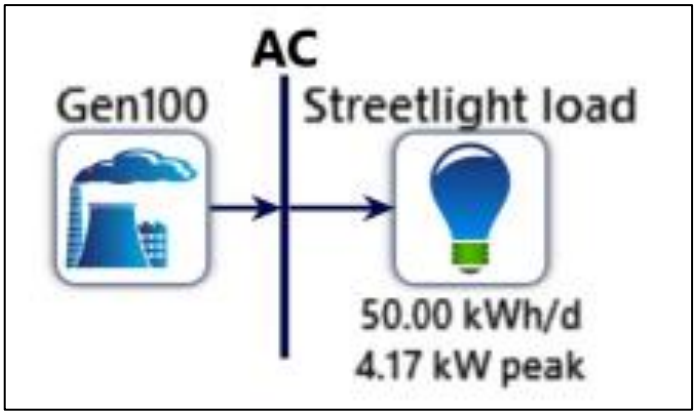

Fig. 3.12. Schematic diagram of the generator simulated system.

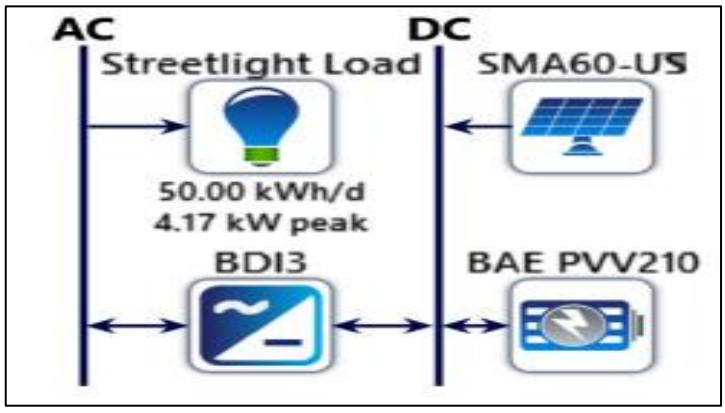

Fig. 3.13. Schematic diagram of the PV simulated system.

From the schematic diagram of the generator simulated system (Fig. 3.12), the AC power generated from the diesel generator is directly used to power the lighting system through the AC bus (Fig. 3.14). In the case of the PV system (Fig. 3.13), during the day, the solar energy obtained from the PV arrays is used for charging the battery. The stored energy in the battery is then converted using the converter to provide power for the street light load during the night and the cycle continues.

Fig. 3.14. Diesel generator output to AC Panel used for municipal street lighting.

The simulated study is used to determine the NPC and the LCOE for the generator-connected and SPV systems as well as the emissions from the generator-connected system. To determine the NPC, HOMER employs the total NPC to signify the life-cycle cost of the entire system with due consideration to the annual real interest rates. It also takes a linear depreciation component, implying that the salvage value is directly proportional to the remaining life. This cost was determined for the generator and SPV systems to be ₦95,004,764 ($262,444) and ₦61,401,282 ($169,617) respectively for the chosen section.

The LCOE represents the average minimum cost at which the electricity produced by an asset is required to be sold in order to offset the total cost of production over its lifetime. This cost accounts for the expected power

costs, which includes but not limited to capital costs, operation and maintenance cost, the debt servicing and return on equity invested (weighted average cost of capital), fuel cost and cost associated with CO_2 and other emissions as well as decommissioning cost. This cost was determined to be ₦289 ($0.8) and ₦187 ($0.5) for the generator and SPV powered systems respectively. As the SPV system do not have emissions, the emissions associated with the generator powered system for just a streetlight cluster considered in the simulation is presented in Table 3.8.

Table 3.8. Emissions of a section of the generator-connected street lighting system.

Pollutant	**Quantity (kg/yr)**
Carbon Dioxide	83,631
Carbon Monoxide	569
Unburned Hydrocarbons	23.0
Particulate Matter	2.28
Sulfur Dioxide	205
Nitrogen Oxides	45.5

3.6 Conclusion

An excel-based algorithm was developed and used to estimate the urban residential energy use of different residential types in the absence of smart meters or historical data. Using the predicted results based on the appliance energy end use methodology, a load profile indicative of a typical urban residential energy demand was developed.

The performance analysis of grid-connected, standalone diesel generator-connected and photovoltaic powered street lighting systems in the city of Uyo, Southern Nigeria was presented in this chapter. A simple economic analysis using indices such as LCC, ALCC, NPV and ROI were performed. The

techno-economic analysis of the three lighting options performed provided a clear indication of the economic viability and technical feasibility of the various options. Besides this, the environmental concerns and carbon footprint associated with the various lighting options makes the PV system a preferred alternative.

HOMER Pro 3.13.1 software was used in this study to simulate the generator connected and the solar PV connected street lighting systems. The HOMER simulated NPC cost was determined for the generator and SPV systems. The LCOE which represents the cost of unit of electricity produced per kilowatt-hour was also determined. Lastly, the emissions resulting from the generator powered lighting system was also estimated.

The major contributions of this chapter are:

- An excel-based algorithm was developed and used in the absence of smart meters or historical data to estimate the urban residential energy use of different residential types in Nigeria.
- Models of different residential housing types were developed and the appliance energy end use methodology adopted to produce a load profile indicative of a typical urban residential.
- A techno-economic analysis of the three lighting options, (generator-connected, grid-connected, and solar-connected) was performed and simulated in HOMER Pro software to determine its economic viability and technical feasibility.
- Recommendations with respect to options available for municipal authorities to sustainably provide public lighting with minimal environmental and economic concerns were made.

CHAPTER 4

4.0 DISTRIBUTION NETWORK MODELLING, OPTIMISATION AND ANALYSIS

4.1 Introduction

The performance of the distribution network with and without the integration of distributed generation and electric vehicles is presented in this chapter. Several case studies involving both fixed and variable load profiles were carried out. The impact of DERs integration on the voltage profile of a typical low voltage distribution network in Nigeria was examined under different scenarios. Also, following the integration of PV systems in the network, Volt-VAr optimisation (VVO) was performed to enable the inverter-based PV systems participate actively in voltage regulation by the provision of flexible reactive power support. The results of this study have been peer reviewed and publish in [193-195].

The technical capabilities of a typical low voltage (LV) distribution network (DN) in Nigeria to absorb the integration of small-scale distributed generators, electric vehicles and their associated charging infrastructures is assessed. Also, the dynamic behavior of the distribution network with power electronic interface is investigated and the voltage concerns addressed by the implementation of a distribution grid optimal power flow (DOPF) optimisation. To the best of the researcher's knowledge, there's no existing technical and in-depth literature assessing the Nigerian low voltage distribution network for DG, EV, slow and fast charging infrastructures. Hence this study aims to fill this knowledge gap by presenting a simulation analysis of the distribution network considering different scenarios and loading profiles. In addition to this, the research aimed to address the

question regarding the readiness of the Nigerian grid for DG and EV integration and the options available for distribution network operators to maintain a secure and safe network operation at all times with additional loads introduced into the network.

4.2 Power System Structure

The power system is a complex interconnections of various components linked together in a coordinated manner so as to provide power to the end user. The various structures which constitute the power system could be categorized into the following major units namely: generation, transmission, sub-transmission, distribution, and end users. This major unit with the various voltage transition levels is represented diagrammatically in Fig. 4.1 using a single line diagram.

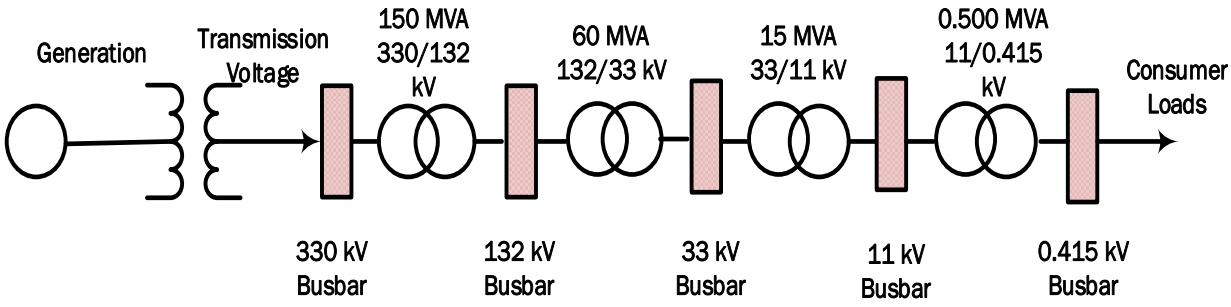

Fig. 4.1. Line diagram indicating voltage transformation in a Nigerian power network.

4.3 Distribution Network Structure

Typically, the distribution system begins with the voltage transformation from the transformer high voltage side to the low voltage side using a step-down transformer at a distribution substation. Different countries operate at different distribution voltage levels and in some instances, the distribution

substation is fed directly from the high voltage transmission line depending on the need of the end users. In Nigeria for instance, most domestic and some commercial customers are connected to the power distribution via 11 KV overhead lines and the voltage is further transformed to 0.415 KV phase to phase using a 0.5 MVA, 0.3 MVA or 0.2 MVA step down transformer depending on the customers size and load profile assessments of the end users. Each distribution substation serves about one to four primary feeders. In Nigeria, the distribution is done mostly with overhead conductors and the feeders are radial implying that there is only a unidirectional flow of power from the distribution substation to the end user.

4.3.1 Distribution substation

The distribution substation is the last level in the series of voltage transformation. Its primary role is that of transforming a higher voltage level to a lower and distribution voltage level. The voltage transformation is accomplished by the use of a step-down transformer. The transformer could be one or more, three-phase or three single-phase units depending on the design. In Nigeria, a typical distribution substation has only one three-phase unit transformer and the voltage is distributed at 415 V phase to phase or 240 V phase to neutral. There are series of protection schemes installed depending on the complexity of the substation to forestall the occurrence of short circuits. There are also metering devices to capture the substation parameters like, voltage, current, power, and other addidtional data. The structure of a typical Nigerian distribution substation with the major component is shown in Fig. 4.2.

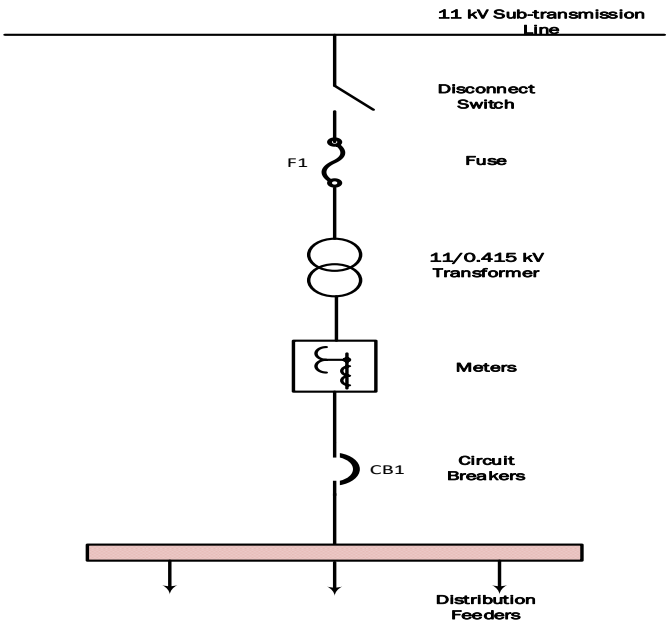

Fig. 4.2. Line diagram indicating voltage transformation in a typical distribution network.

4.3.2 Feeder characteristics

Most distribution feeders in Nigeria are radial and are characterized by uni-directional power flow (from the distribution sub-station to individual end-users). Just like in most distribution systems, the variation in loads of different consumers alongside the un-equal spacing of the overhead conductors and lack of phase balancing in a typical Nigerian system culminates to the inherent severe unbalanced loading of the distribution feeder.

4.3.3 Distribution feeder

For determining the existing operating conditions of a feeder and also predict short, medium and long-term scenarios, a critical analysis of the distribution feeder is important. For this analysis, a detail layout of the feeder distribution map such as that described by [196] is considered. A

model of a typical LV distribution network and load distribution schematic used in this study is shown in Fig. 4.3 and Fig. 4.4 respectively.

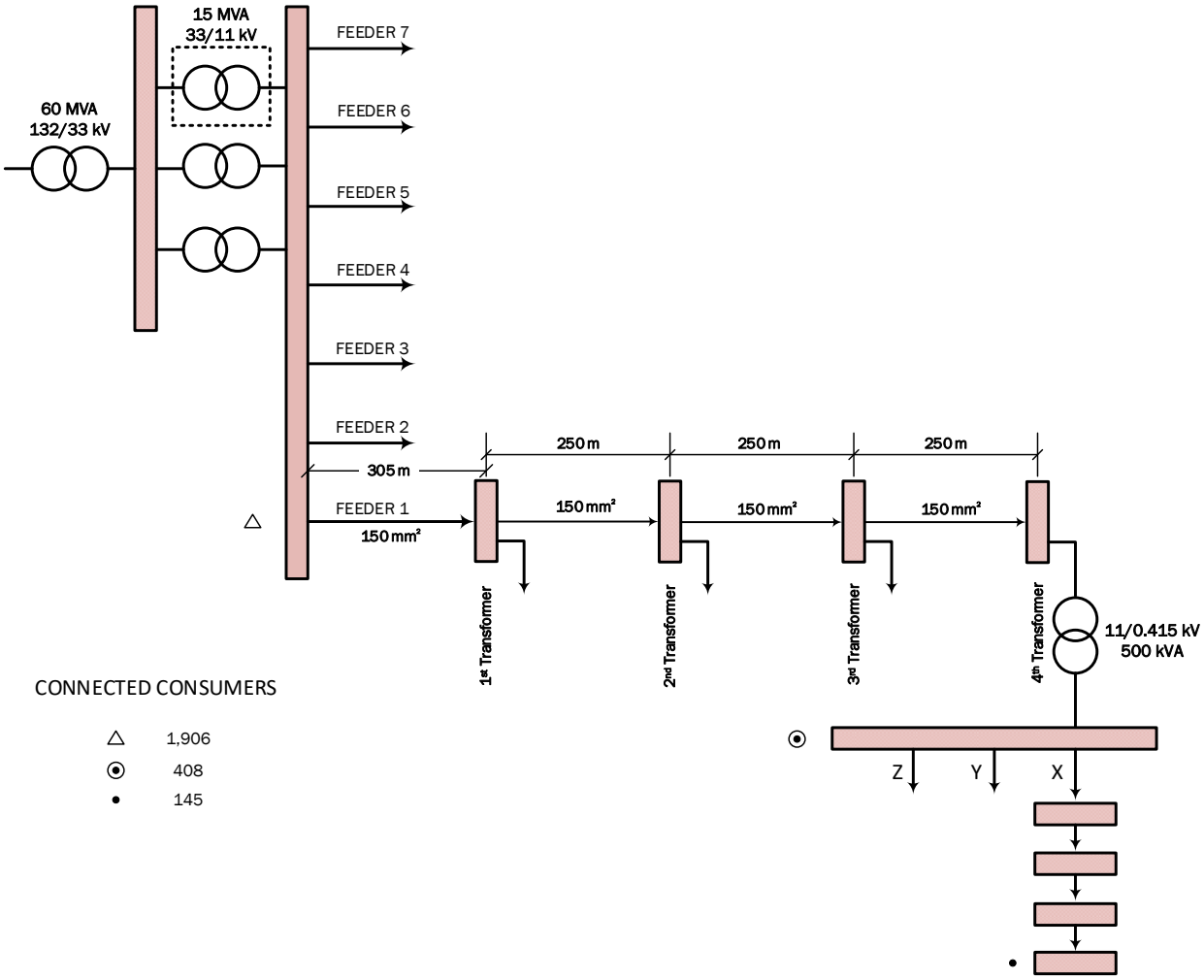

Fig. 4.3. Model of a typical low voltage distribution network in Nigeria.

A model of a typical distribution system in Nigeria consists of a 60 MVA 3-phase 33 kV ideal voltage source, connected to 15 MVA, 33/11 kV YY0 transformers, and seven 11 kV outgoing feeder's substation. Each 11 kV feeder serves a certain number of 11/0.415 kV substations. The substation serves a certain number of consumers depending on the transformer rating and customers' size of a particular area. The distribution is done mostly

using overhead conductors. The loading of the various low voltage feeder circuits or uprisers is schematically represented in Fig. 4.4.

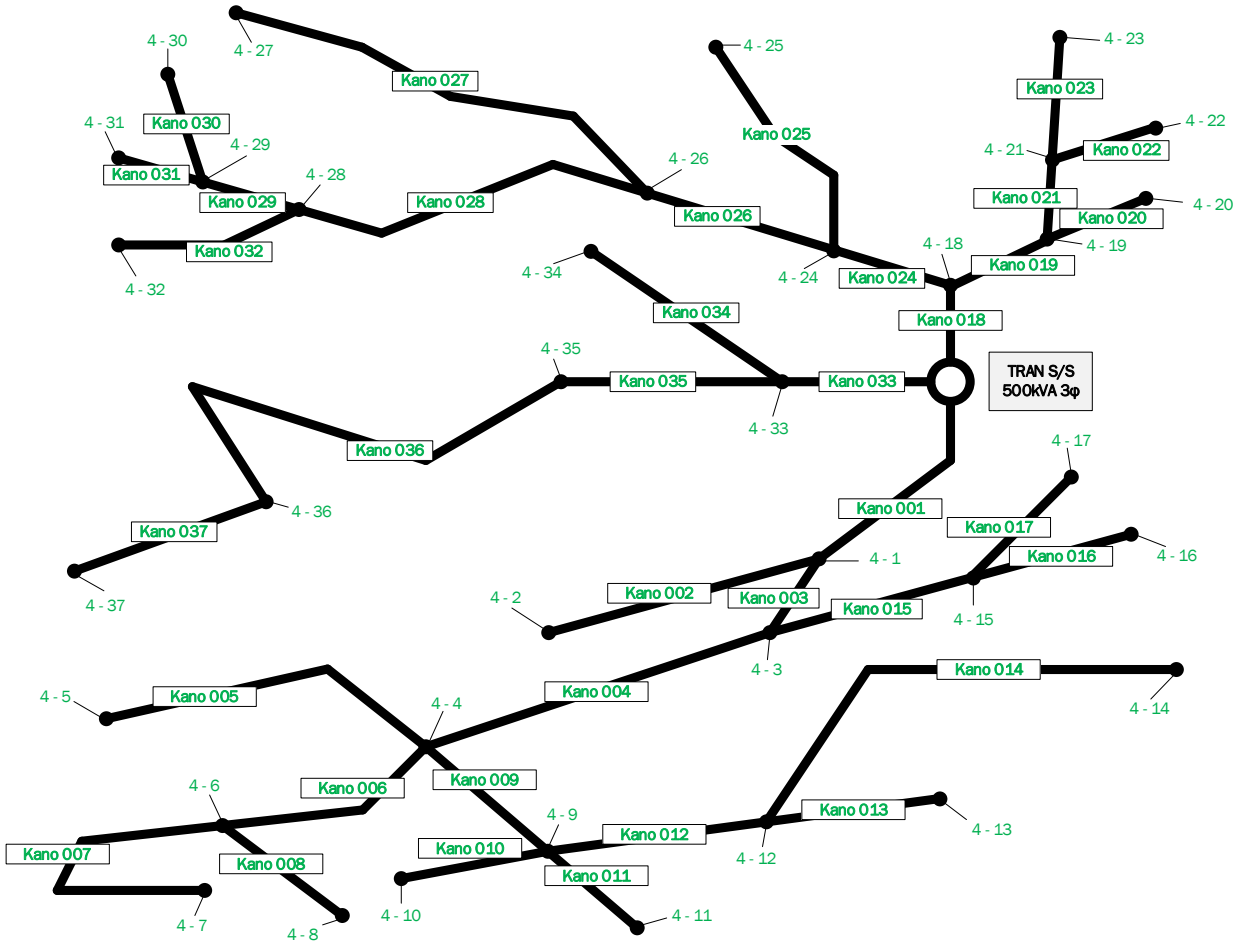

Fig. 4.4. Schematic of a load distribution diagram in a LV network in Nigeria.

4.4 Distribution Network with EV and DG Analysis

In response to the changing dynamics of the future power system, it is evident that the distribution network would be the host of the various technologies and as such the need for its assessment cannot be overemphasized. Determining the operating conditions of the network to predict the short-, medium-, and long-term scenarios is critical to the integration of DERs hence this research.

This work models a real Nigerian distribution network and investigates the challenges resulting from the connection and penetration of different EV types and their associated charging technologies. A typical DG energy source is modelled and implemented with the intention to facilitate the connection of large EV loads mitigating the impact on the grid especially during times when the network is heavily congested.

4.4.1 Case study

A typical Nigerian low voltage network (Fig. 4.3) was considered as the case study in this research. The network model, which is representative of a typical distribution system in Nigeria consisting of a 60 MVA 3-phase 33 kV ideal voltage source, connected to a 15 MVA, 33/11 kV YY0 transformers, and seven 11 kV outgoing feeder's substation was analysed. PSCAD/ EMTDC dynamic power system analysis software was used to simulate different case studies for various levels of EV and DG integration. The developed model was built with the intent to perform some dynamic analysis using variable load profiles as demonstrated in subsequent case studies.

4.4.2 Nodal representation of the network

Fig. 4.4 is the schematic representation of the load distribution diagram in the LV network considered in this case study. A total of about 408 consumers are connected to the 0.500 MVA transformer sub-station. The average distance between each LV pole span is 45 m. The feeder analysis indicates that the feeder's load density could be averagely estimated to be about 10 buildings per 135 m length of overhead distribution line. The loads across the various LV feeder circuits are not uniformly or evenly distributed. The number of consumers on feeder circuits X, Y and Z are 145, 138 and 125, respectively (see Fig. 4.3). The average length for feeder circuits X, Y & Z

are 2,295 m, 1,620 m and 990 m, respectively. Using this schematic diagram, the nodal representation of the network is developed (Fig. 4.5).

Feeder circuit X with 145 consumers is represented in Fig. 4.5. The first or starting node after the substation node is labeled as 4-1 while the last node is labeled as 4-17. For ease of tabulation, the alphabetical representation of node 4-1 is A, and node 4-17 is Q in that order. Between each node, a number of consumers living in different house types with different load profiles are connected. Different consumers are classified into different housing types described in chapter 3 namely: type 1 to type 4, with the annual energy consumption 8,141 kWh, 20,823 kWh, 33,688 kWh and 37,766 kWh respectively.

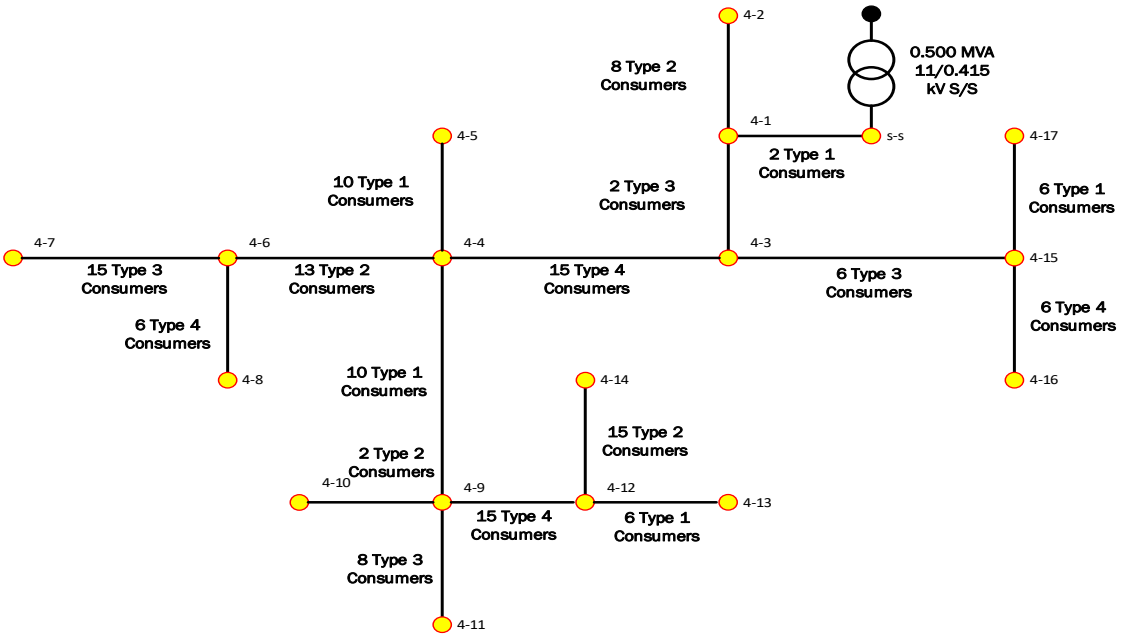

Fig. 4.5. Nodal representation of one arm (circuit X) of the LV network under consideration.

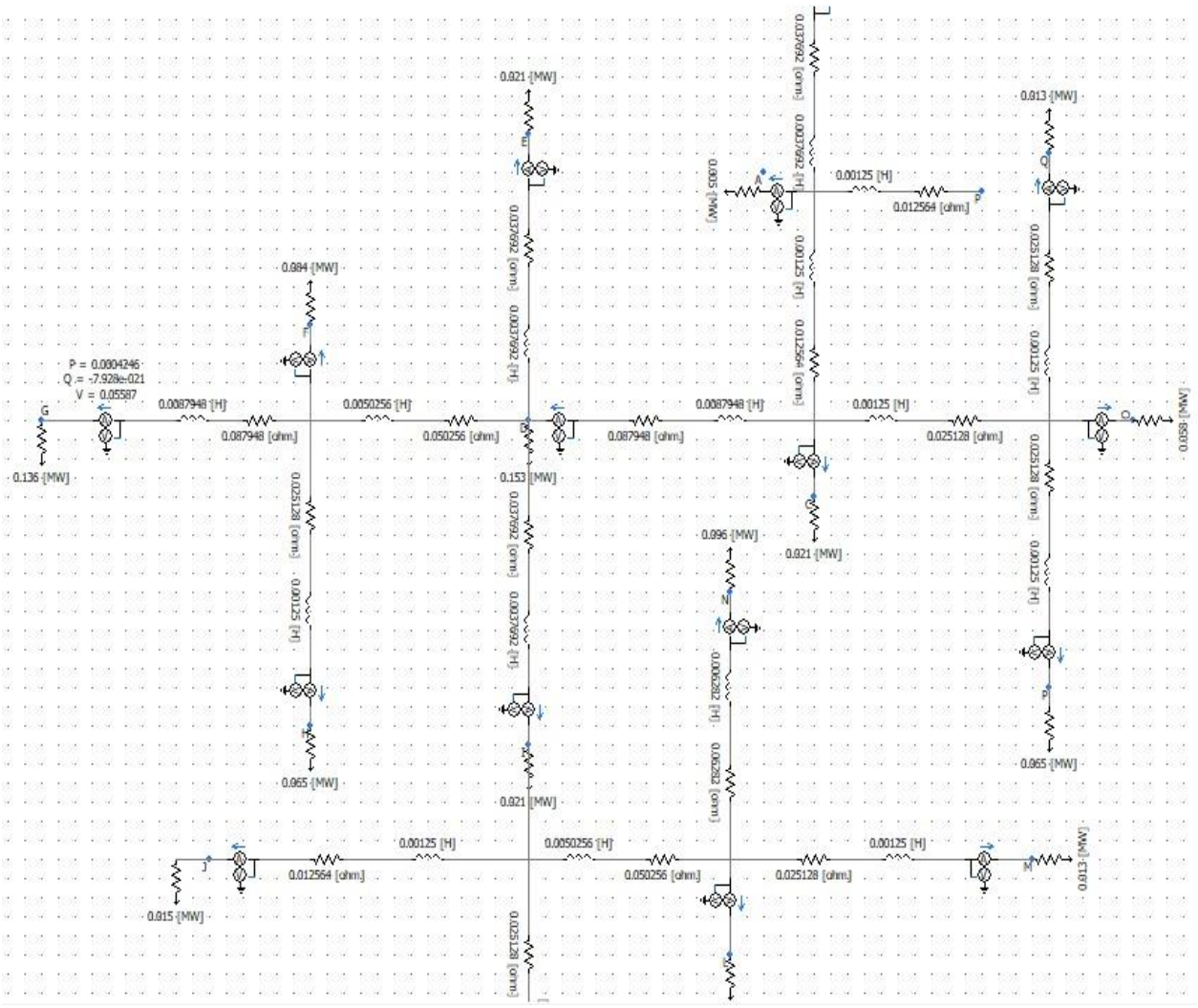

Fig. 4.6. PSCAD/ EMTDC model of the nodal representation of one arm (circuit X) of the LV network under consideration.

4.5 Distribution Network Modelling

For the first case study, the loads were modelled using the 'lumped load model'. In this method, a lumped load placed at the end of the line is considered while the exact equivalent demand for lumped loads is determined by taking into consideration a diversity factor. Each of the equivalent lumped load for aggregated or group of consumers was modelled as a fixed PQ load. Ideally, using the hourly load profile of the various consumers would have been appropriate; however this information was not

available at this research stage. Using equation (4.1) [104-106], along with relevant parameters, the equivalent lumped load demand for the various segments of the network under minimum and average loading conditions were determined, respectively.

$$PN + Q\sqrt{N} = LD \tag{4.1}$$

Where:

P represent active power.

N represent total number of consumers in a segment.

Q is the reactive power.

LD is the minimum and average lumped demands.

The values of LD are calculated using minimum and average network demand. The results of the calculated equivalent lumped demand at minimum and average load are shown in Table 4.1. Applying this method, the different customer loads were distributed amongst the lines across each feeder based on the ratio of the number of buildings per line segment and feeder, respectively.

Table 4.1. Calculated equivalent lumped demand at minimum and average load.

Nodes	**Number of Consumers (N)**	**Types**	**Min. P and Q Avg. P and Q**	**Min. LD (kW)**	**Avg. LD (kW)**
S/S – 4-1	2	1	0.41 and 0.19 1.15 and 0.55	1.09	3.08
4-1 – 4-2	8	2	0.6 and 0.29 3.15 and 1.52	5.62	29.50
4-1 – 4-3	2	3	0.9 and 0.43 4.5 and 2.17	2.41	12.07
4-3 – 4-4	15	4	0.9 and 0.43 5.0 and 2.42	15.17	84.37

4-4 – 4-5	10	1	0.41 and 0.19 1.15 and 0.55	4.70	13.24
4-4 – 4-6	13	2	0.6 and 0.29 3.15 and 1.52	8.85	46.43
4-6 – 4-7	15	3	0.9 and 0.43 4.5 and 2.17	15.17	75.90
4-6 – 4-8	6	4	0.9 and 0.43 5.0 and 2.42	6.45	35.93
4-4 – 4-9	10	1	0.41 and 0.19 1.15 and 0.55	4.70	13.24
4-9 – 4-10	2	2	0.6 and 0.29 3.15 and 1.52	1.61	8.45
4-9 – 4-11	8	3	0.9 and 0.43 4.5 and 2.17	4.41	42.14
4-9 – 4-12	15	4	0.9 and 0.43 5.0 and 2.42	15.16	84.37
4-12 – 4-13	6	1	0.41 and 0.19 1.15 and 0.55	2.93	8.25
4-12 – 4-14	15	2	0.6 and 0.29 3.15 and 1.52	10.12	53.14
4-3 – 4-15	6	3	0.9 and 0.43 4.5 and 2.17	6.45	32.32
4-15 – 4-16	6	4	0.9 and 0.43 5.0 and 2.42	6.45	35.49
4-15 – 4-17	6	1	0.41 and 0.19 1.15 and 0.55	2.93	8.25

4.6 Analysis of Results

4.6.1 Voltage profile analysis without DG and EV integration

The result of the LV network simulation is analysed during the minimum and average loading conditions, respectively. For each of these loading conditions, two scenarios are considered and discussed. The first scenario is the basic or normal scenario. In this scenario, the simulation of the LV network is carried out using the existing network parameters. The network parameters such as the overhead conductor sizes, line impedances and the load spread across the network have not been altered. In the second scenario (reinforced scenario), the LV network is reinforced, hence the impedance value of the various branches of the LV network is recalculated as an improvement for all the voltage profiles where the consumers are connected. The result of this improvement at minimum loading conditions is presented in Table 4.2 with the values highlighted in red indicating violations of the acceptable voltage limits.

Table 4.2. Per unit voltage values of both scenarios in minimum loading of the network – red highlighted values indicate violations.

Node Connection Points	**Basic Scenario Voltage Profiles (p.u.)**	**Reinforced Scenario Voltage Profiles (p.u.)**
A	1	1.04
B	0.99	1.01
C	0.98	0.99
D	0.94	0.96
E	0.93	0.96
F	0.92	0.95
G	0.92	0.91
H	0.94	0.95
I	0.93	0.95
J	0.93	0.95
K	0.93	0.95
L	0.92	0.95
M	0.92	0.95
N	0.91	0.94

O	0.98	0.99
P	0.98	0.99
Q	0.98	0.99

The per unit voltage value across each node using the existing and recalculated impedance value at minimum loading conditions indicates that there is violation of the acceptable voltage limits of 1.06 p.u. (+6%) and 0.94 p.u. (-6%) of the declared nominal voltage in Nigeria. In the basic (normal) scenario, nodes E, F, G, I, J, K, L, M and N are in violation of the voltage limits whereas only node G (Node 4-6 – 4-7 in Table 4.1) is in violation of the voltage limits in the reinforced scenario.

The behaviour of the network voltage across the various nodes assuming an average daily load profile of all consumers is shown in Fig. 4.7 and Fig. 4.8. This network profile is without the connection of EVs and DGs. The upper voltage limit of 1.06 p.u. is not reached for the scenarios considered in this study. In the voltage results, only the lower operating voltage limit of 0.94 p.u. is shown on the labels.

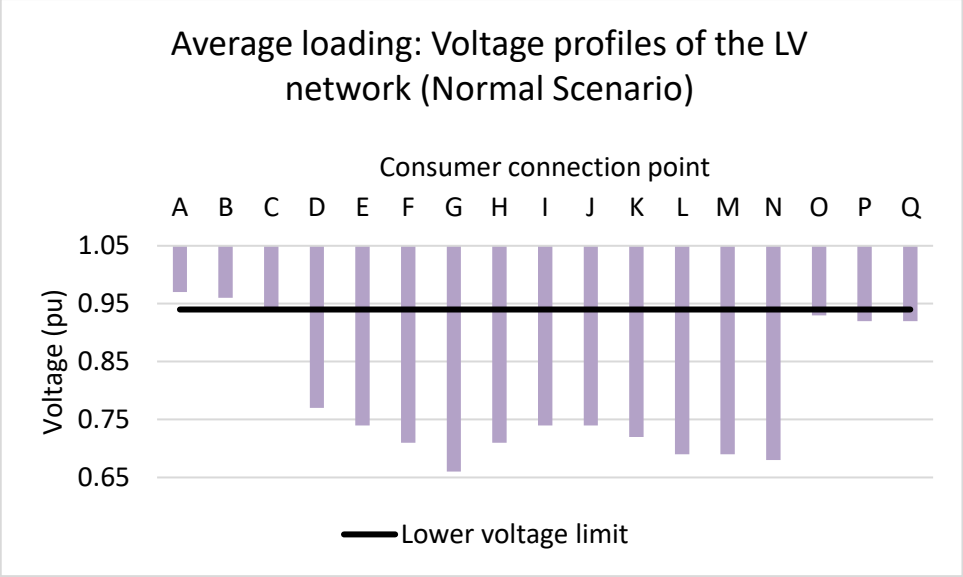

Fig. 4.7. Basic scenario average loading voltage profile.

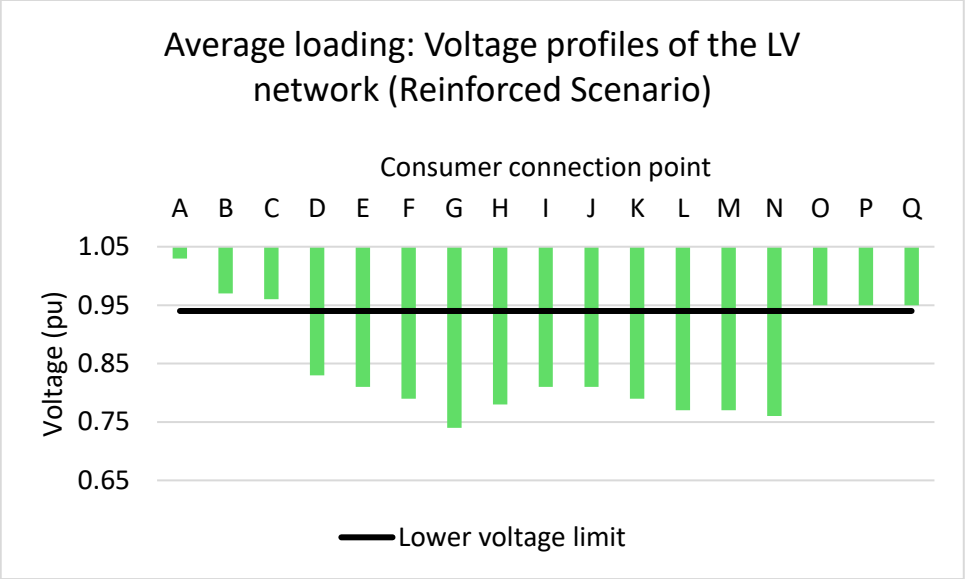

Fig. 4.8. Reinforced scenario average loading voltage profile.

For both scenarios, without EV integration in the network, the average loading results indicate that voltage profiles at points D to Q and D to N exceeded the acceptable threshold range for basic and reinforced scenario respectively. The obtained voltage profile is however typical for some LV networks in Nigeria due to network overloading and other such challenges previously highlighted in section 4.3.2.

In Fig. 4.7, with the original network impedance in the LV network, the maximum voltage drop occurs at points G, L and N corresponding to nodes (4-6 – 4-7, 4-9 – 4- 12, & 4 -12 – 4- 14) respectively due to large number of consumers and hence large consumption (see Table 4.1), and also due to the proximity of these points to the distribution substation transformer. For instance, point "G" (node 4-6 – 4-7) experienced a voltage drop of up to 35%. In Fig. 4.8, resulting from the modification of the cable impedance, a voltage improvement of up to 10% at these critical loaded points was recorded. Also, points A, B, C, O, P and Q were observed to operate within the acceptable voltage limits. Arguably, these load connection points are

located closer to the distribution substation transformer and also have the smallest number of consumers in the entire network with minimal consumption, as can be observed in Table 4.1.

As was observed by [81], power outages and interruptions are a frequent occurrence in Nigeria especially at the distribution level. Also, resulting from insufficient power generation capacity and electricity access rate, some parts of the country engage in frequent load shedding arrangements. In view of this peculiar Nigerian situation, the LV network is modified to reflect a more likely scenario where each consumer operates at a minimum loading. Fig. 4.9 and Fig. 4.10 displays how the various connection points are affected when each consumer has minimal demand in the LV network. To highlight the obvious improvements recorded, voltage results of each node during the existing (basic or normal) and reinforced scenarios when each consumer follows their minimum fixed demand are also presented in Table 4.2.

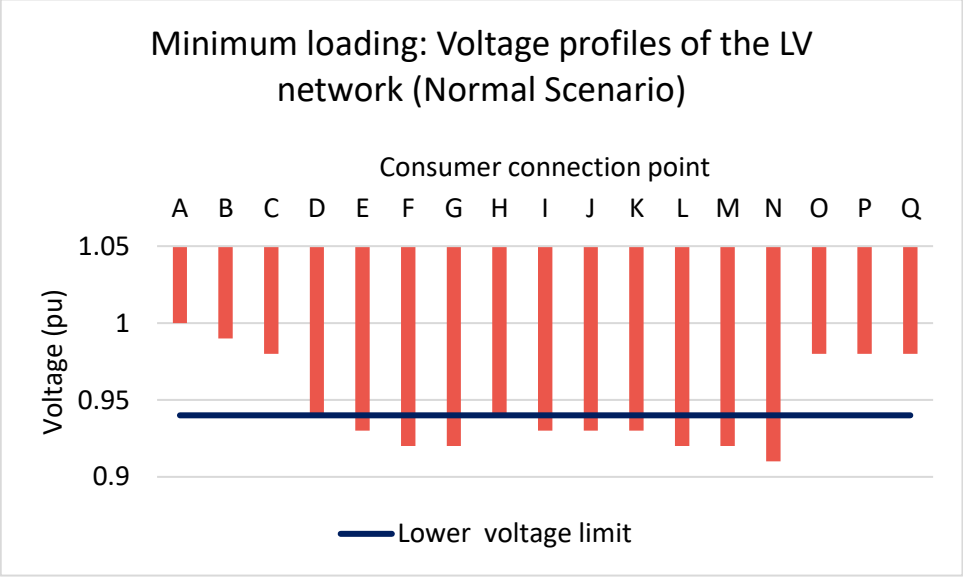

Fig. 4.9. Basic scenario minimum loading voltage profile.

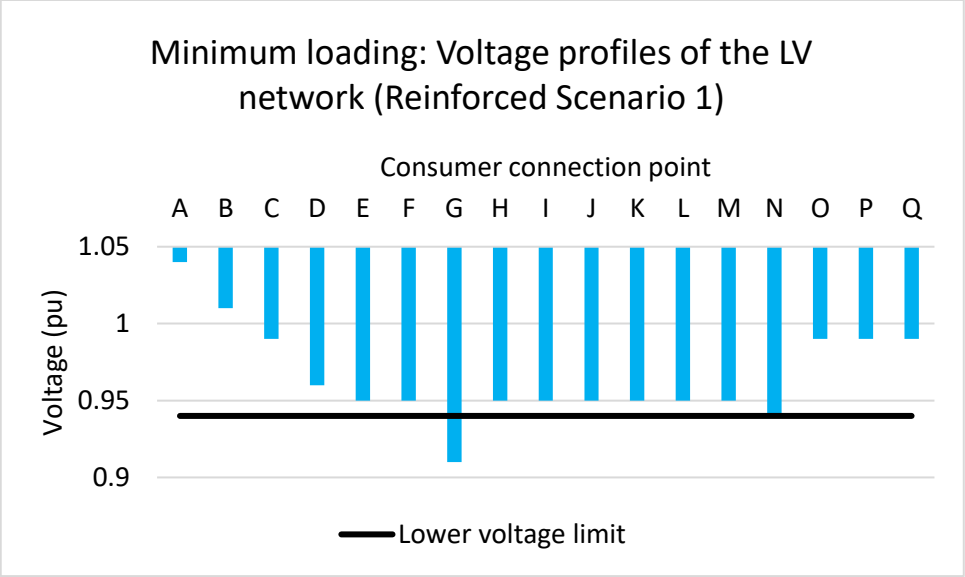

Fig. 4.10. Reinforced scenario minimum loading voltage profile.

The results in Fig. 4.9 illustrate that although there is still violation of the acceptable limits, however, some node connection points in the LV network remained within acceptable operating voltage. In Fig. 4.10, besides node G, all the other points are well within the acceptable limits with most of the points showing an improvement of up to 2-4%. With the optimised cable impedances, the simulation results show that voltage profiles are more stable.

A more general assessment of the results from the reinforced scenario minimum network loading indicates that the voltage profiles across all points are relatively stable and within the acceptable voltage limits except for point G. The reason for this exception is due to the distance of this connection point from the substation besides the large number of consumers connected to that node point. Therefore, the simulation results obtained suggest that with the connection of small-scale domestic wind turbines as a DG, local

voltage control measures can be provided across the LV network as a further improvement.

Studies [197, 198] demonstrated that EV charging stations can be supported with either wind, PV or a combination of both generations in the HV/MV side of the network. Such units act as backup units to balance the generation and supply at the point of EV charging. In this study, charging of EVs from renewables was considered and a small-scale wind turbine (SSWT) was considered. Using parameters of a commercially available SSWT designed for an urban environment, the wind turbines are modelled and implemented in PSCAD/EMTDC. The SSWT are positioned close to the charging points to provide local voltage mitigation measures and facilitate EV and charger unit connection near the congested and critical busbars points in the LV network. Although SSWT are modelled and connected near the busbars where the EV charging units are connected, however, to provide additional generation to offset the energy use resulting from EVs charging, a larger DG unit can also be connected near the main substation.

4.6.2 Impact of DG and EV integration on the steady state voltage

In this section, the results of integrating a DG unit along with two different EV charging modes and two categories of EV users' types are presented. The network voltage profile with the improved and optimised cable impedances (reinforced scenario) is used. The objective is to see how the network feasibility changes under different network conditions. Table 4.3 shows the EV charging modes and categories of EV users considered in this study.

Table 4.3. Electric vehicle parameters used in the network.

Type of EV Users	**EV User Type 1**	**EV User Type 2**
Type of charger	Slow speed chargers	Fast speed chargers
Charging power	2 kW at each station	10 kW at each station
Connection point	C, I and O	A and Q

As captured in Table 4.3, two categories of EVs users and two types of chargers are simulated in the LV network. The first category of EV users (user type 1) represents residential consumers who are using slow charging located at their residential outlets or public slow charging outlets at points C, I and O. The second category of EV users (user type 2) represents commercial fleet charging outlets that require fast speed charging due to their busy daily routines. The second type of chargers are connected at outlet points A and Q. The EV loads are modelled as a constant PQ load in the network.

The underlining assumptions used in this study is that there are five vehicles at each of the various charging outlets (C, I, O, A and Q). Considering this assumption, there are a total of 15 cars at connection points (C, I and O) and 10 cars at connection points (A and Q) respectively. Using the charging power per vehicle of 2 kW and 10 kW for the slow speed chargers and fast speed chargers respectively, the charging demand exerted at points (C, I and O) and points (A and Q) are 30 kW and 100 kW respectively. The total number of cars connected to the network and the cumulative load exerted on the network are 25 and 130 kW respectively. With this considerations, local mitigation measures by means of connecting a small-scale domestic wind turbines into the network near the charging stations to support and facilitate the connection of EVs is simulated. The results are illustrated and discussed in Fig. 4.11 and Fig. 4.12 respectively.

The results of the voltage profiles after the addition of two different EV charger types and a 2.5 kW, 3 bladed horizontal axis SSWT unit in the network are compared. Points C, I and O had an additional total demand of 30 kW due to simultaneous charging of 15 vehicles altogether, whereas points A and Q had an additional total demand of 100 kW due to the charging of 10 vehicles simultaneously. These charging demands were exerted onto the base demand of the LV network.

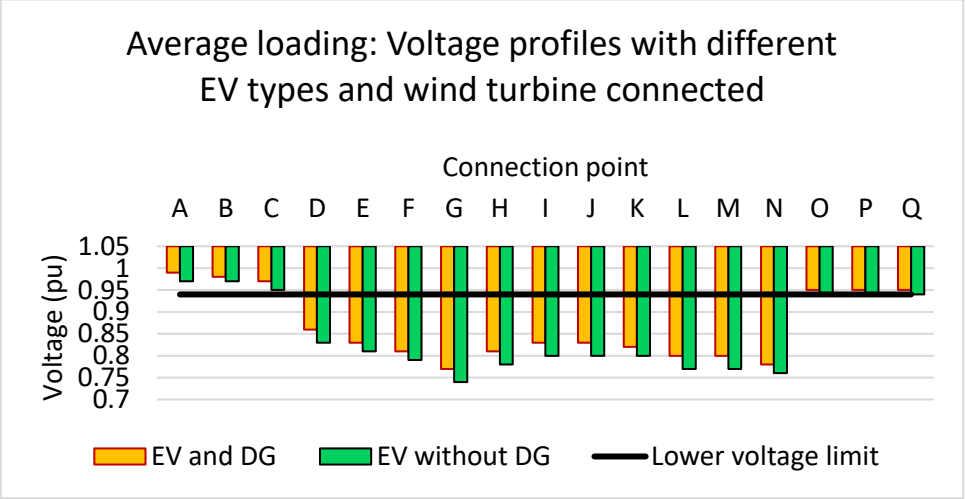

Fig. 4.11. Reinforced scenario average loading voltage profile with EV types and wind turbine connected.

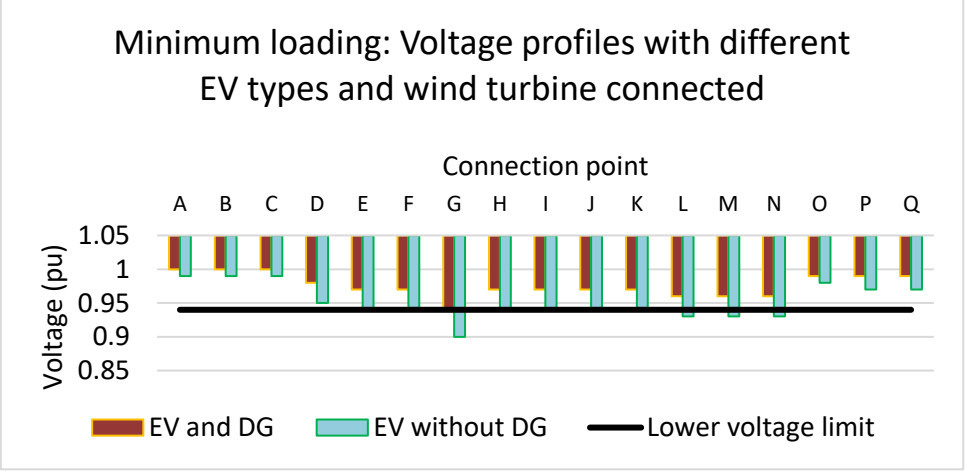

Fig. 4.12. Reinforced scenario minimum loading voltage profile with EV types and wind turbine connected.

In Fig. 4.11, the integration of EVs and DGs into the LV network during average loading conditions is presented. The results indicate that nodes D to N exceeded the acceptable voltage limits, therefore charging EVs during peak demand or average load demand is not practicable. However, EVs can be charged in the network during off-peak hours. In Fig. 4.12, the voltage profile result during period of minimum loading is illustrated. Clearly, besides node point G, L, M and N, all the other node points are within the acceptable limits when EVs are charged. However, with EVs and DGs connected, only node point G is in violation of the acceptable limit. This violation as previously explained is as a result of the long distance of this point from the substation.

It can be seen from Fig. 4.12 that EV charging stations with local DG units facilitate the charging of EVs and improve the stability of the system by keeping the connection points within the acceptable operating limits, with the exception of one node. A further analysis showed that at minimum network loading condition, the highest improvement in the voltage profile was observed at point G. Here the voltage was improved by up to 4% after the connection of a 10-kW small-scale domestic wind turbine. The DG units were connected at points C, I, O, A, Q and G, with 5 of these points indicating where the EVs were charged, whereas the 6^{th} point (G) was chosen since the previous results (see Fig. 4.8 and Fig. 4.10) showed that voltage violation occurs due to high consumption of electricity by many consumers in that point.

In summary, the results presented show how the voltages profiles of a typical Nigerian LV network are affected at minimum and average loading conditions with and without the integration of EVs and DGs. Furthermore, the results emphasized the importance of connecting small-scale DG units at the points where the demand associated with the charging of EVs is higher

than the base network demand. It can also be concluded that increasing the sizing and capacity of these wind turbines will allow for a further voltage improvement; however, with recent technological improvements in PVs, these could be more suitable to be connected as an alternative to wind turbines.

4.6.3 Voltage and harmonic modelling study using variable load profiles

In this section, using the variable load profiles of different consumers, the voltage and harmonic analysis with EVs integrated into the network is performed.

The loads on feeder Z (Fig. 4.3) were modelled using the 'lumped load PQ model' in PSCAD/EMTDC tool and the node points represented by the symbol 'N'. Each connection node on the nodal diagram (Fig. 4.13) serves a different number of consumers. Residential consumers are connected on nodes 1 to 14, while commercial consumers are connected on nodes 15 and 16. In total, 125 consumers are connected to feeder Z. The number of consumers and the various connection nodes are presented in Table 4.4 while the consumers daily load profiles is presented in Fig. 4.14.

An analysis of both Table 4.4 and Fig. 4.14 indicates that node connection points N2, N7, N11 and N13 have larger number of residential properties hence, resulting in the equivalent aggregated lumped demand being higher. The peak and the minimum demand for both residential and commercial buildings is experienced between 18:00 and 19:00, and between 03:00 and 06:00, respectively. To further reduce the complexity of the EV scenario analysis, the 24-hour load profiles was broken into six different 4-hour

intervals. For instance, the average of the aggregated demand between 00:00 and 04:00 is calculated and shown as the demand between 00–04h.

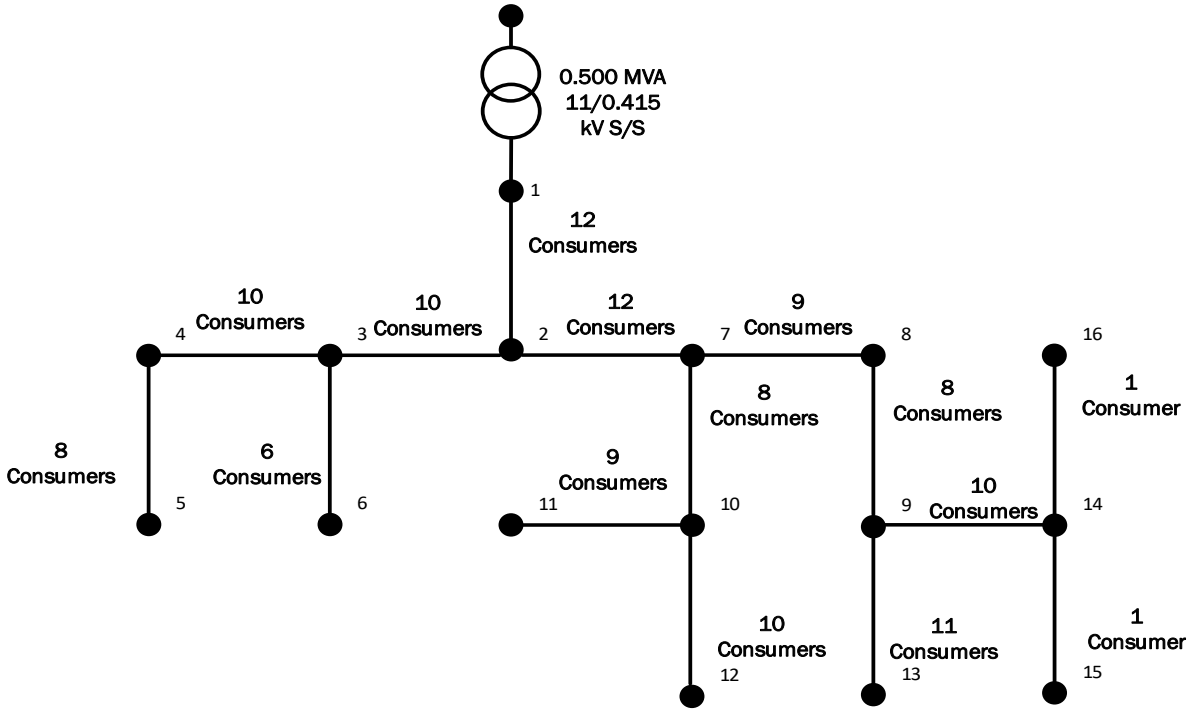

Fig. 4.13. Nodal representation of feeder circuit Z.

Table 4.4. Feeder circuit Z topology.

Nodes (N)	Number of Consumers	Connection Node
N1–N2	12	2
N2–N3	10	3
N3–N4	10	4
N4–N5	8	5
N3–N6	6	6
N2–N7	12	7
N7–N8	9	8
N8–N9	8	9
N7–N10	8	10
N10 –N11	9	11
N10–N12	10	12

N9–N13	11	13
N9–N14	10	14
N14–N15	1	15
N14–N16	1	16

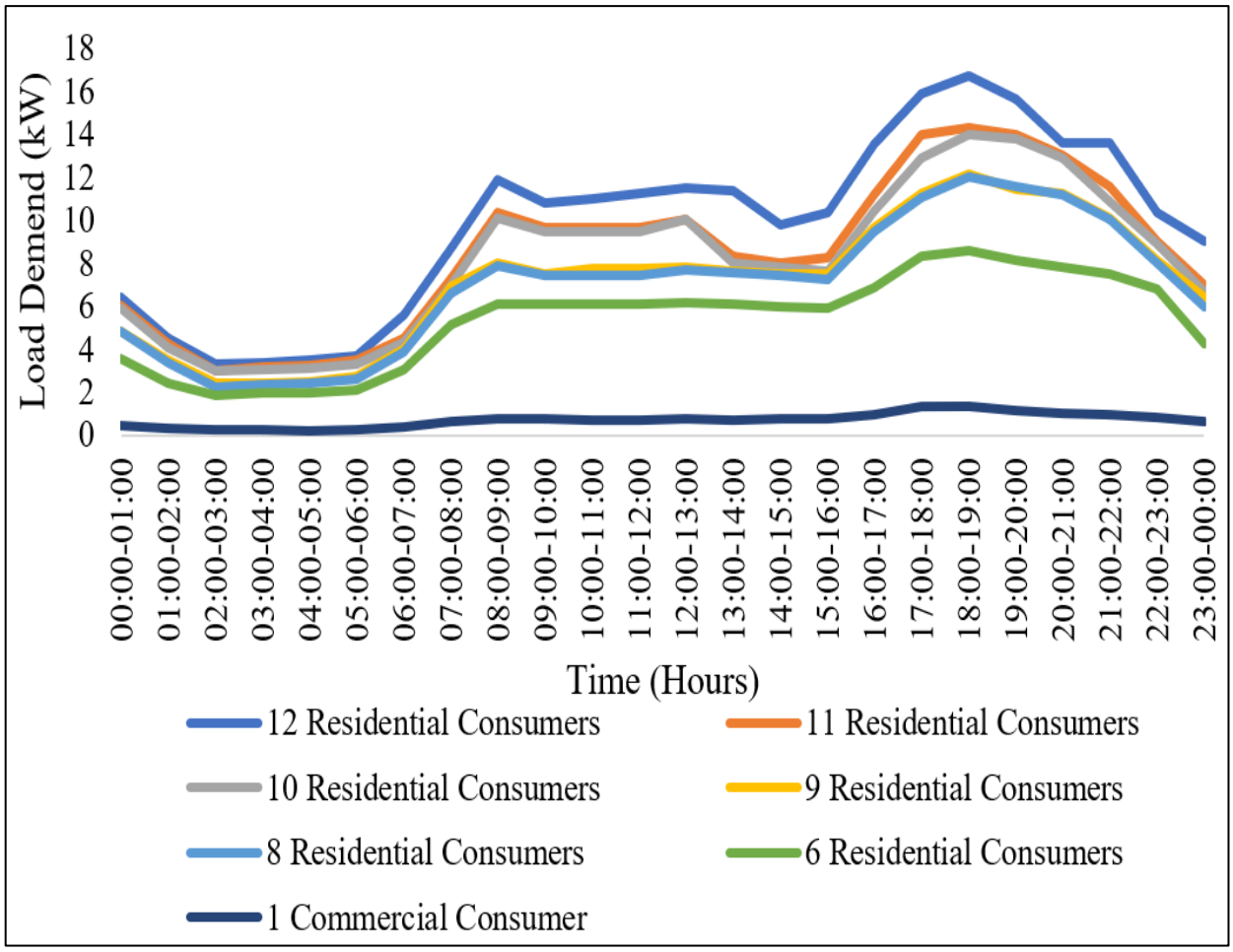

Fig. 4.14. Daily load profiles of the aggregated distribution feeder circuit Z consumers.

4.6.3.1 Scenario description with EV chargers

Different charging scenarios are implemented at various time intervals into different parts of the network as shown in Table 4.5. To illustrate a more realistic outcome, mixed EV-charging activities was adopted to cater for the

diverse needs of motorists. The location of the charge points was determined by their proximity to the transformers and the type of consumers. For example, slow-speed domestic chargers were provided for EV charging in most residential node points, while for commercial node points, fast and rapid chargers were equally provided. The study assumes in the second column of Table 4.5 that the numbers of EVs corresponds to the number of charging points and charging is at maximum power.

The charging hours are determined based on the charging durations and charging frequency of customers. The impact of these charging activities is compared to the baseload of the network (without EVs) and a detailed analysis focusing on the network voltages and harmonics is presented in the next section.

Table 4.5. Charging connection scenarios.

Charger Point	Charger Speed	Justification	Time of Day
N2	2 x Slow 1 x Fast	Mixed charging activities after work hours	20:00–00:00
N3	2 x Slow	Overnight residential charging	00:00–08:00
N6	1 x Slow	Mostly residential area	16:00–20:00
N8	2 x Slow	Proximity to commercial area	20:00–00:00
N9	1 x Fast	Commercial charging during early work hours	08:00–12:00
N10	2 x Slow	Overnight residential charging	00:00–04:00
N11	1 x Slow	Residential charging	12:00–16:00
N13	1 x Slow	Residential charging	16:00–20:00
N14	2 x Fast 1 x Fast	Proximity to commercial activities	08:00–12:00 20:00–00:00
N15	1 x Fast 1 x Rapid	Hub of commercial activities	12:00–16:00 16:00–20:00
N16	1 x Fast 1 x Rapid	Hub of commercial activities	12:00–16:00 16:00–20:00

4.6.4 Voltage profile analysis with and without EV integration

Fig. 4.15 to Fig. 4.17 shows the simulation results indicating the daily voltage fluctuations with and without EVs. The nodal voltages between 00:00 and 08:00 are studied in Fig. 4.15. The voltage loss caused as a result of EV connection to the network is negligible. This is evidently due to the minimal network demand and the presence of a 3-kW slow-speed chargers only.

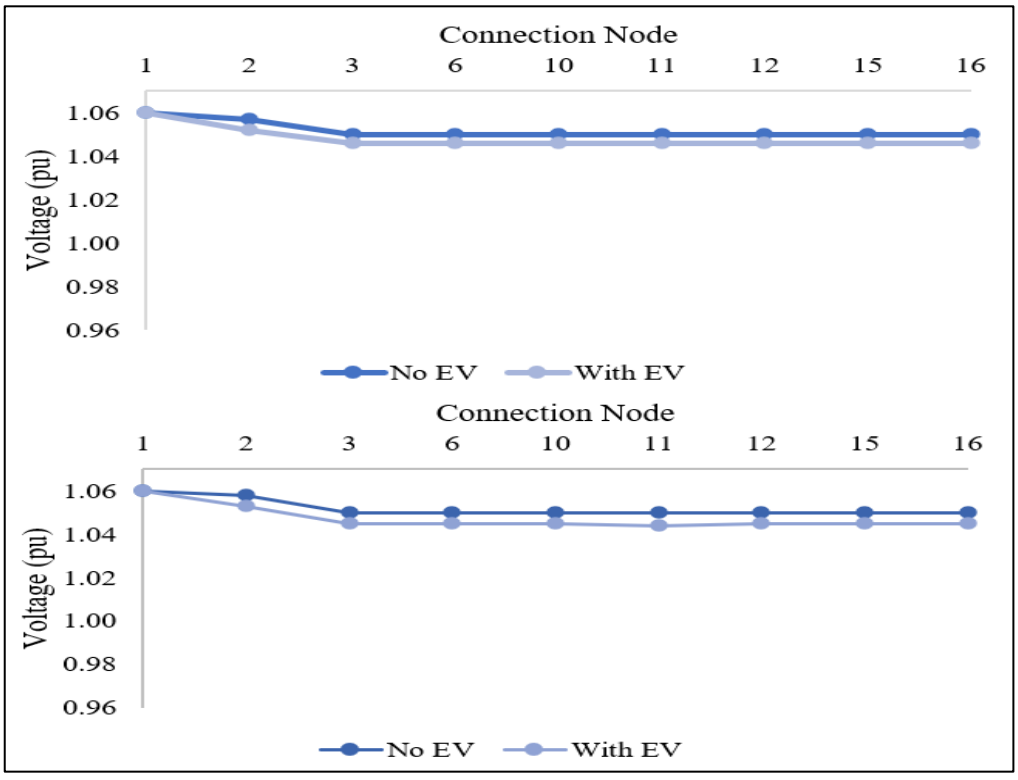

Fig. 4.15. Nodal voltage profiles between 00–04h (top) and 04–08h (bottom).

In Fig. 4.16 and Fig. 4.17, the nodal voltages between other intervals of the day are captured. Expectedly, due to higher feeder demand and the presence of high-powered EV chargers, larger voltage fluctuations is experienced. Also, following the connection of the various charging

scenarios, the minimum voltage is 0.99 p.u. and 0.96 p.u. near the commercial nodes (N14–N16) between 08:00–12:00 and 16:00–20:00, respectively. However, it's worth mentioning that the voltage violations limits are not reached in the feeder.

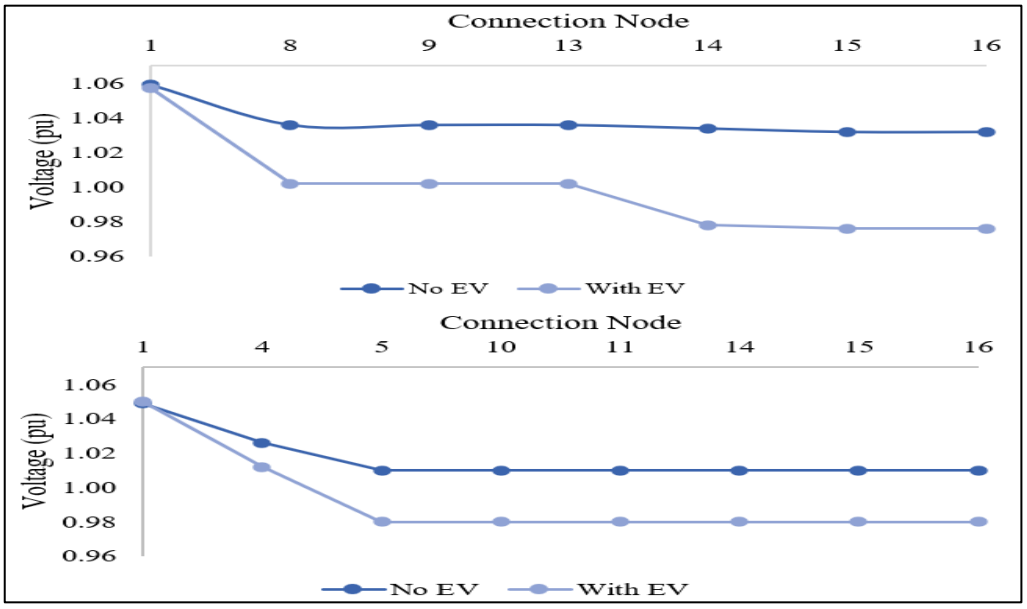

Fig. 4.16. Nodal voltage profiles between 08–12h (top) and 12–16h (bottom).

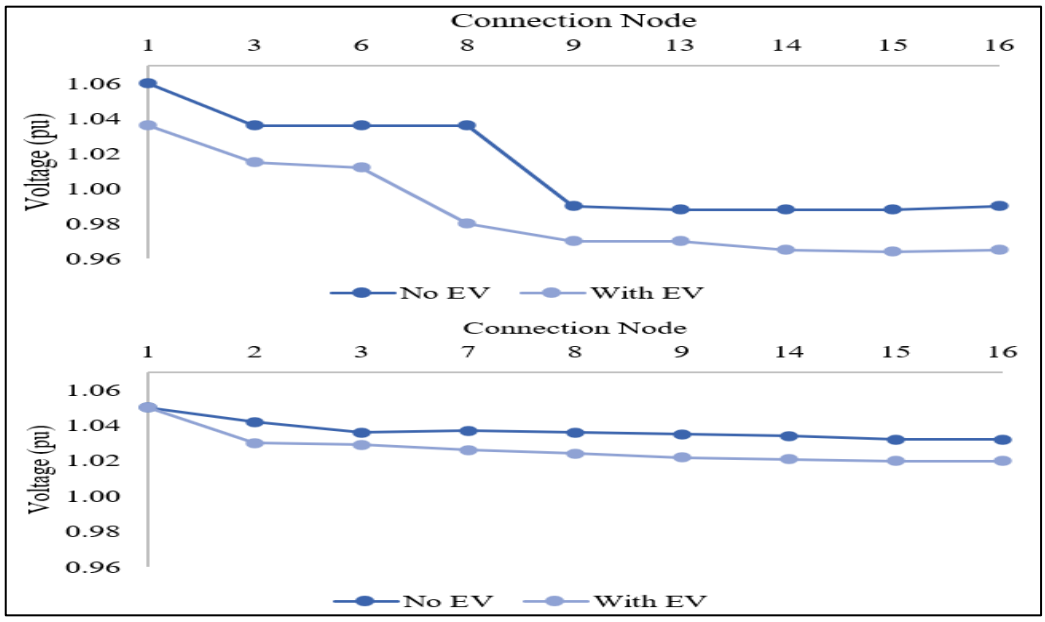

Fig. 4.17. Nodal voltage profiles between 16–20h (top) and 20–00h (bottom).

4.6.5 Voltage drop with a slow-speed single-phase charger

The voltage drops after a single-phase battery charger is connected between nodes N3–N6 is analysed in Fig. 4.18. The voltage drop is negligibly small — represented by the green line.

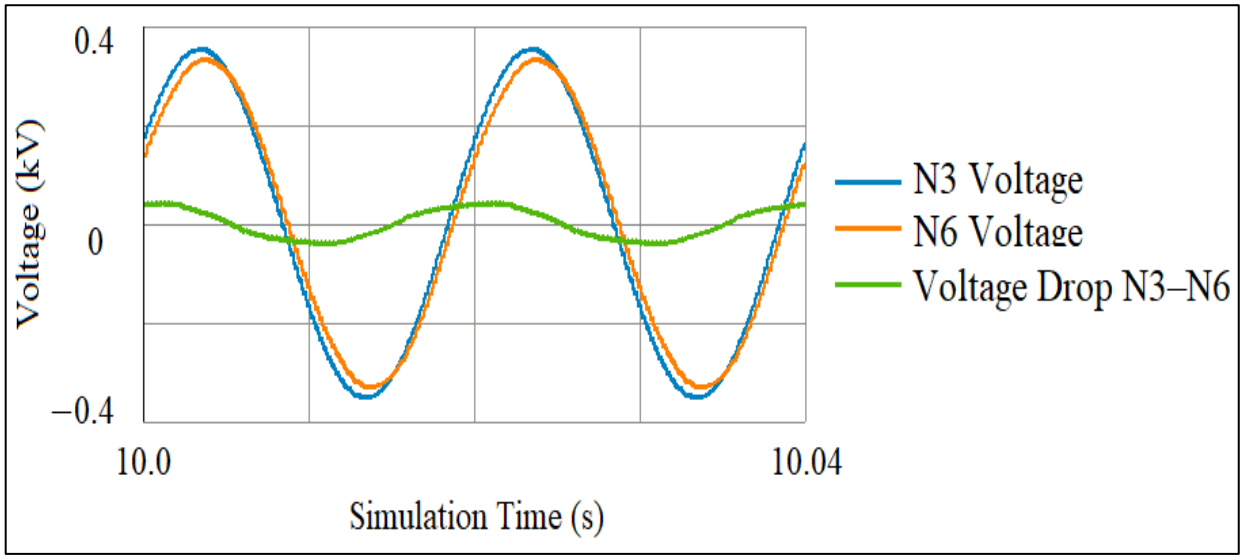

Fig. 4.18. Voltage drop along the line with the slow-speed battery charger.

4.6.6 Harmonic and transient analysis

Harmonics are distortions in the nominal voltage and current waveforms conveyed by nonlinear loads that may compromise the power quality and efficiency of the system. Recognising and monitoring of harmonics in order to avoid distribution network operating concerns and equipment deterioration is important [199]. The summation of all higher order harmonics determines the degree of Total Harmonic Distortion (THD), as expressed in (4.2).

$$THD = \frac{\sqrt{V_2^2+V_3^2+V_4^2+\cdots+V_n^2}}{V_1} \times 100\% \qquad (4.2)$$

Where:-

n is the harmonic order number.

(V_n) is the root-mean square (RMS) voltage of the nth order harmonic.

The necessity of using filters to reduce harmonics resulting from the increased use of power electronic interfaced technologies, such as battery chargers and photovoltaic systems in microgrids and distribution networks have been investigated by many researchers [200]. One of the ways to minimising harmonic distortion and eliminate undesirable frequency components brought into the grid is by the designing of an appropriate LC filter circuit (consisting of inductors and capacitors).

4.6.6.1 Design of LCL filters

The first 'L' in an LCL filter for a grid-connected rectifier (L_{rec}), is determined by using (4.3) [201-204]:

$$L_{rec} = \frac{V_{DC}}{8 \times f_{sw} \times I_{pp}} \tag{4.3}$$

Where:-

(V_{DC}) is the DC-link voltage (kV).

(f_{sw}) represents the rectifier's switching frequency (kHz).

(I_{pp}) is the peak-to-peak amplitude of the ripple current (kA).

The peak-to-peak amplitude of the ripple current may be calculated as follows [201]:

$$I_{pp} = \frac{S_{base}}{\sqrt{3} \times V_{L-L,rms}} \times \sqrt{2} \times 20\% \tag{4.4}$$

Where:-

(S_{base}) is the rectifier's base rating (kVA).

$(V_{L-L,rms})$ is the RMS line-to-line voltage at the point of charge and filter (i.e., between the grid and the rectifier terminal).

The multiplication of the peak-to-peak current with 20% is carried out, since the amplitude of the ripple current is assumed to be 20% of the nominal rated current as per design criteria [201-204]. Also, by multiplying the ripple current's amplitude by the square root of two, the peak maximum current is derived.

A cut-off frequency (f_{co}), may then be chosen to provide adequate filtering up to the nth order. Equation (4.5) shows the sizing of the filter capacitance (C_{filter}), required to achieve a desired cut-off frequency.

$$C_{filter} = \frac{1}{(2\times\pi\times f_{co})^2\times L_{rec}} \qquad (4.5)$$

200 Hz was chosen as the (f_{co}), which is a generic design requirement for grid applications with battery chargers [201].

As opined by [201, 204], to obtain a smoother voltage or current, additional design requirements, such as minimising oscillations in the output waveforms may be employed. This is achieved by the use of a damping circuit with damping capacitance, damping inductance, and damping resistance. Equations (4.6), (4.7), and (4,8) respectively show the calculation of each damping parameter.

$$C_{damp} = \frac{C_{filter}}{2} \qquad (4.6)$$

$$L_{damp} = L_{rec} \times 5 \quad (4.7)$$

$$R_{damp} = \sqrt{\frac{L_{damp}}{C_{damp}}} \quad (4.8)$$

In this research, the THD simulated measurements are made for phase current and voltage near the residential customers with a 3-kW AC charger, as well as for line current and voltage near the commercial customers with a 50-kW DC charger. Table 4.6 and Table 4.7 shows the harmonic content and THD measurements without and with chargers respectively. Harmonic distortion and the calculated THD for current and voltage are negligibly small without the battery chargers connected in the network. However, with battery chargers, the THD values for phase current and voltages are 5.6% and 39.5% respectively. The same measurements are repeated when a slow-speed charger is used to charge a 40-kWh Nissan Leaf SL at node N6. Simulation results indicating the harmonic distortion and transients resulting from the charging are shown in Fig. 4.19.

Table 4.6. THD simulated measurements without battery chargers.

Harmonic Order	**Phase Current (%)**	**Phase Voltage (%)**	**Line Current (%)**	**Line Voltage (%)**
1st	100	100	100	100
2nd	8e−8	0	7e−8	7e−8
3rd	6e−8	0	5e−8	5e−8
4th	5e−8	0	4e−8	4e−8
5th	4e−8	0	3e−8	3e−8
6th	4e−8	0	3e−8	3e−8
7th	0.0004	0	0.0004	0.0004
THD (%)	0.0004	0	0.0004	0.0004

Table 4.7. THD simulated measurements with battery chargers.

Harmonic Order	Phase Current (%)	Phase Voltage (%)	Line Current (%)	Line Voltage (%)
1st	100	100	100	100
2nd	5.5	37.2	0.001	10e−6
3rd	1.3	12.6	4.7	16.1
4th	0.3	3.5	0.0002	7.9e−6
5th	0.1	2.1	16.1	0.8
6th	0.05	1.3	0.0001	5.2e−6
7th	0.02	1.0	6.2	0.8
THD (%)	5.6	39.5	17.7	16.1

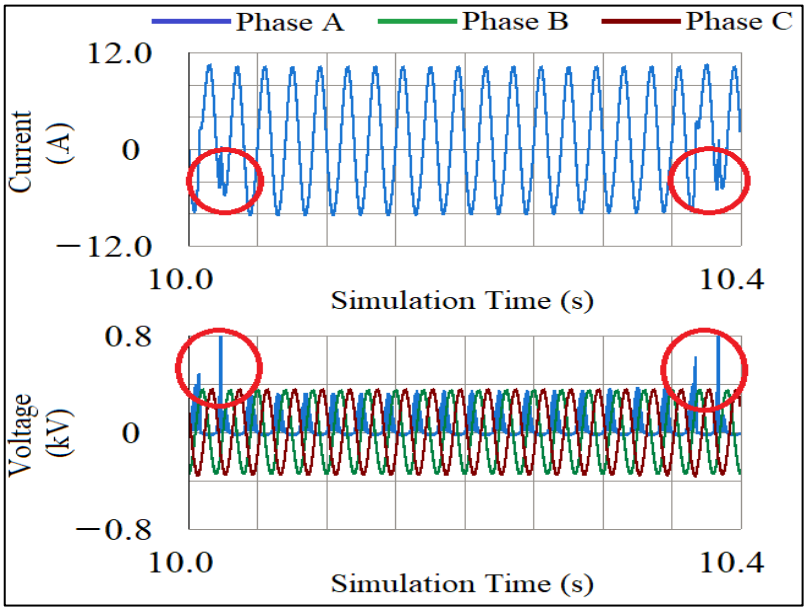

Fig. 4.19. Harmonic distortion in phase current (top) and voltage (down) at N6.

It can be observed that the peak-to-peak amplitude of the current waveform is not constant in Phase A as it shows transients at the red circled points. Since the charger only affects the phase where it is connected to, the current in other phases are excluded. Also, it is noticed that while the voltages on

Phase B and C stays constant, the voltage on Phase A is subjected to transients and increased harmonics throughout the simulation. Transients are randomly dispersed since the battery current fluctuates during the charging process.

Similar simulations are made when a fast-speed charger is connected at node point N14. In this case, the analysis only shows line current harmonics, since they are more severe because the battery charger withdraws current, creating distorted current waveforms that drive harmonic currents back into the network. Moreso, this situation causes an increase in the voltage drop across the system impedance, which results in voltage harmonics. Simulation results indicating current harmonic distortion due to charging are shown in Fig. 4.20.

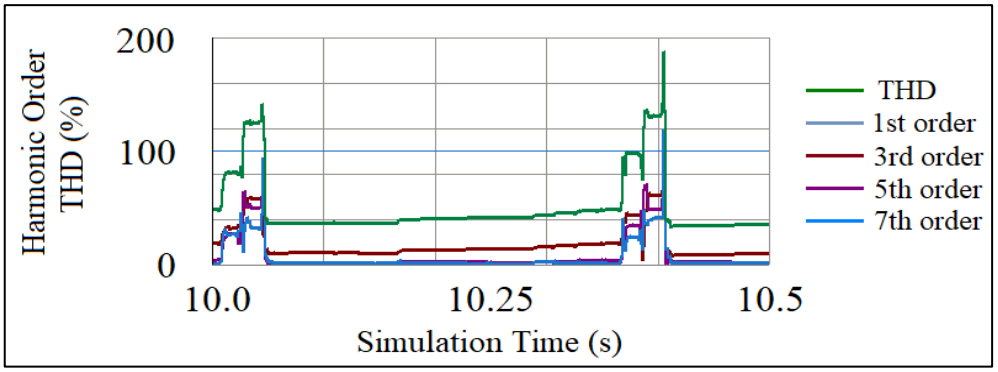

Fig. 4.20. Line current harmonic distortion due to commercial chargers at N14.

4.6.7 Effect of filters on current harmonics

Simulation results demonstrated that current harmonics increase significantly when the battery chargers are operational near the residential and commercial customers. THD measurements for all voltage and current waveforms surpass the IEEE harmonic threshold limit of 5% when the battery chargers are operational without the proposed filter deployment.

The effect of adapted filter design on the current harmonics observed along the line considering nodes N14–N16 with the operation of a 50-kW charger is compared and shown in Fig. 4.21.

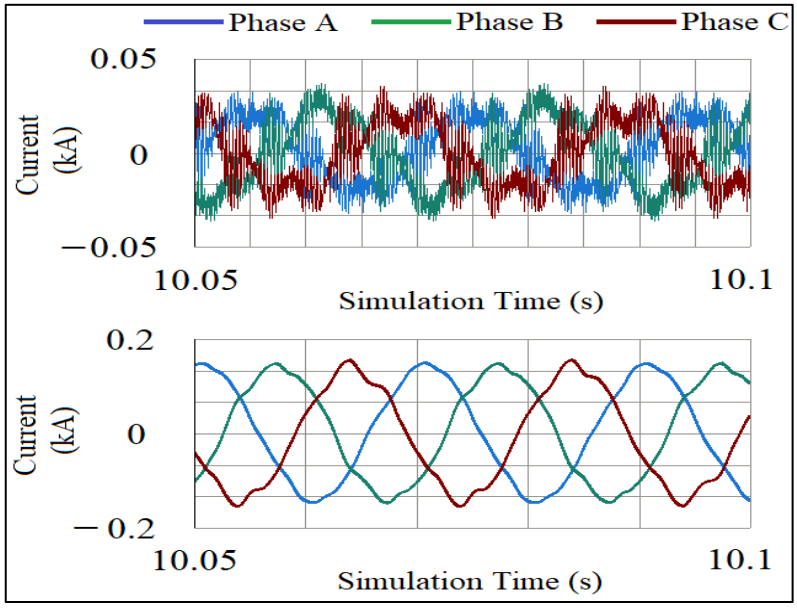

Fig. 4.21. Line current harmonics without (top) and with (below) LCL filters.

Current distortion is more noticeable than voltage distortion between three phases (as seen in Fig. 4.19 and Fig. 4.21), which is mostly caused by third and fifth order harmonics. The findings in Fig. 4.21 indicate that when a filter is utilised, harmonic distortion in line current is significantly reduced. Without an LCL filter located near the three-phase battery charger, THD value of 20% was measured for line current. As shown by the bottom graph in Fig. 4.21, although the current waveform is still not perfectly sinusoidal; however, an LCL filter reduces THD in the current to 4%.

4.7 Volt-VAr Optimization of the Distribution Network

In this section, a Volt-VAr Optimization of the DN is performed following the high penetration of PVs. Using the variable load profiles of different

consumers on all three feeders, the optimisation is carried out. The detailed nodal representation of each of the three feeder circuits is shown in Fig. 4.5, Fig. 4.13 and Fig. 4.22 for feeder circuits X, Z and Y respectively. The merged feeder representation incorporating 10 distributed PV inverters operating at maximum power point tracking (MPPT) is presented in Fig. 4.23. The connection nodes are still represented as 'N' with the various node branches serving different varied consumers.

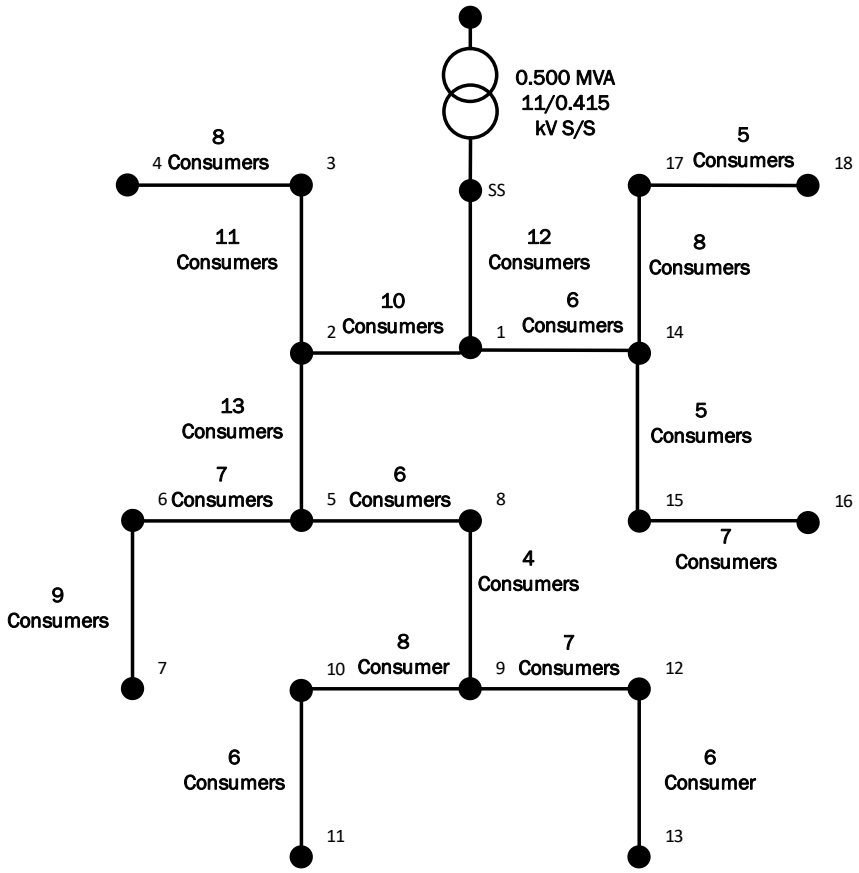

Fig. 4.22. Nodal representation of feeder circuit Y.

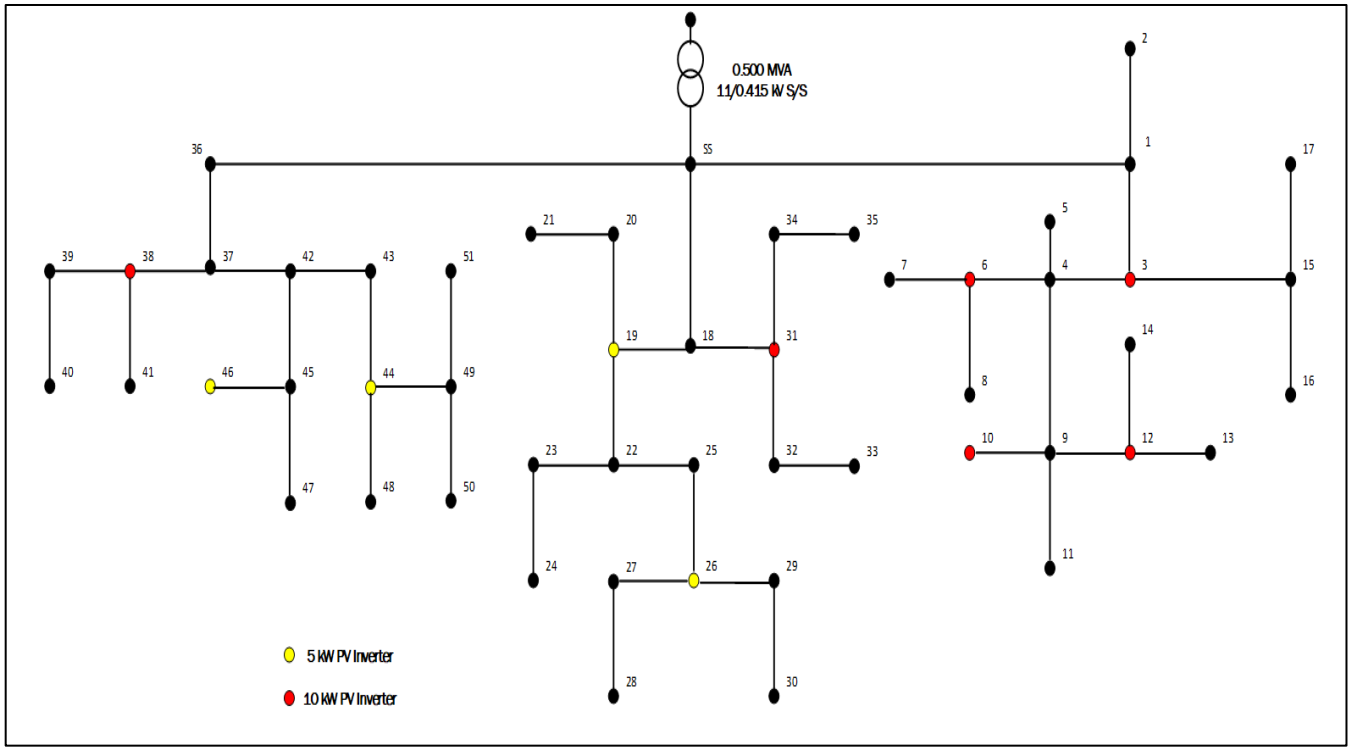

Fig. 4.23. Merged nodal representation of feeder circuits X, Y and Z.

4.7.1 Mathematical formulation of VVO

The graph theory model has been adopted in the representation of a DN. The indexing of the nodes is such that $\acute{\imath} \coloneqq \{0,1,2, \dots , \mathrm{n}\}$, where n is the total number of nodes in the network and $\grave{\mathrm{N}} = \mathrm{N}\backslash\{0\}.\mathrm{j}$ is defined as an alias of $\dot{\imath}$. The substation node with voltage fixed to the nominal value is represented as node 0 and known as the slack bus. The time index is captured as $t \in \mathrm{T}$, where t = $\{1,2, \dots , \mathrm{T}\}$ for T time intervals.

The complex voltage at node i is denoted by $V_{i,t} = V_{i,t}^{re} + jV_{i,t}^{im}$ at time t, hence $|V_{i,t}| = V_{i,t}$ and the net complex current at time t injected at node i is represented as $I_{i,t} = I_{i,t}^{re} + jI_{i,t}^{im}$. The net complex power injected at node i at time t, which is the sum of the consumers load demand subtracted from the

substation power generation and PV is expressed as $S_{i,t} = p_{i,t} + jq_{i,t}$. The (ij)th element of the bus admittance matrix is captured as $G_{ij} + jB_{ij}$.

The expression of the I-V distribution grid optimal power flow (DOPF) model in terms of the current-voltage relationship is presented in [205]. The underlining concept is the expression of network linearity such that the nonconvexities appear in the constraints relating bilinear terms in the load model [205]. Subject to some operating constraints, the model of the VVO for the DN is presented in equation (4.9) as a nonlinear programming problem (NLP).

$$OF_1 = min \sum_{i\in\mathcal{N}} \sum_{t\in\mathcal{T}} pi, t. \tag{4.9}$$

$$OF_2 = min \sum_{i\in\mathcal{N}}, \sum_{t\in\mathcal{T}} (|V_{i,t}| - |V_0|)^2. \tag{4.10}$$

The objective function OF_1 in equation (4.9) acts to minimise the total power loss in the DN and is equivalent to the sum of injections while the objective function OF_2 in equation (4.10) minimises the total voltage deviation in the DN.

The various constraints taken into account are as follows:

Current injection constraints

$$I_{i,t}^{re} = \sum_{j:(i,j)\in\varepsilon} V_{j,t}^{re} G_{ij} - V_{j,t}^{im} B_{ij,} \qquad \forall i \in \mathcal{N}, \forall t \in \mathcal{T} \tag{4.11}$$

$$I_{i,t}^{im} = \sum_{j:(i,j)\in\varepsilon} V_{j,t}^{re} B_{ij} + V_{j,t}^{im} G_{ij,} \qquad \forall i \in \mathcal{N}, \forall t \in \mathcal{T} \tag{4.12}$$

Power injection constraints

$$p_{i,t} = V_{i,t}^{re} I_{i,t}^{re} + V_{i,t}^{im} I_{i,t}^{im}, \quad \forall i \in \mathcal{N}, \forall t \in \mathcal{T} \tag{4.13}$$

$$q_{i,t} = V_{i,t}^{im} I_{i,t}^{re} - V_{i,t}^{re} I_{i,t}^{im}, \quad \forall i \in \mathcal{N}, \forall t \in \mathcal{T} \tag{4.14}$$

The underlying grid model is represented as the I-V DOPF function in equation (4.11) to (4.14). In equation (4.15), the reactive power of the inverter which is limited by its nameplate and active power rating has been expressed.

PV model

$$(q_{i,t}^{G})^2 \leq (s_i^{G})^2 - (p_{i,t}^{G})^2, \quad \forall i \in \mathcal{N}, \forall t \in \mathcal{T} \tag{4.15}$$

Where;

q_i^G is reactive power output of PV at node I at time t.

s_i^G is Capacity of PV inverter at node I at time t.

p_i^G is active power output of PV at node I at time t.

Voltage bounds

$$\underline{V_{i,t}}^2 \leq \left|V_{i,t}\right|^2 \leq \overline{V_{i,t}}^2, \quad \forall i \in \mathcal{N}, \forall t \in \mathcal{T} \tag{4.16}$$

The various consumer voltages constrained to operate within the pre-specified voltage boundaries is represented in equation (4.16).

4.7.2 Case studies analysis

The implementation of the VVO is carried out using the three distribution feeders of the LV-DN modelled in Fig. 4.3. The merged nodal representation

of feeders X, Y and Z is modelled in Fig. 4.23. Controlling the inverter reactive power and regulating the system voltage is being achieved by the VVO. In Fig. 4.24(a), an aggregated 1-hour resolution and time-series of the actual active and reactive power load demand for a day is presented. Furthermore, a 100% PV penetration operating at maximum power point tracking (MPPT) for a 4 kW system is assumed. The sizing of the PV system is such that the inverter's apparent power capacity is 10% above the PV active power rating. The normalised data of the PV generation is presented in Fig. 4.24(b).

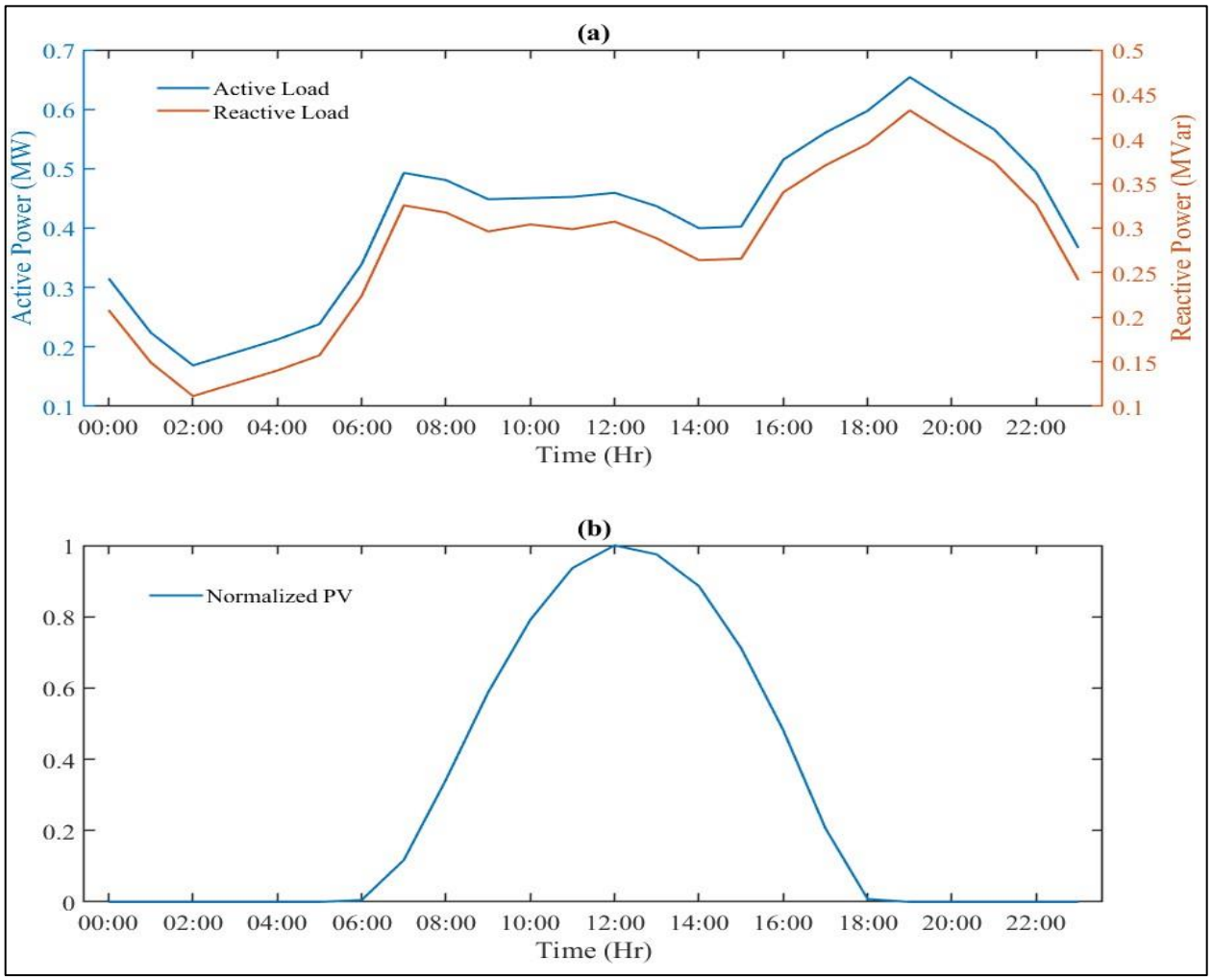

Fig. 4.24. Load and PV profiles: (a) aggregate active and reactive load; (b) normalised PV daily performance.

Another objective of the VVO is to control the reactive power of the PV systems connected to the DN so as to regulate the nodal voltages within the acceptable declared nominal limits of 225.6 V (0.94 p.u.) and 254.4 V (1.06 p.u.). The following case studies are considered in this research:

- Case study 1, no VVO is implemented, hence, the PV reactive power is not utilised.
- Case study 2, the VVO optimally dispatches the reactive power of the PV system by minimising the active power losses, i.e OF_1.
- Case study 3, the VVO optimally dispatches the reactive power of the PV system by minimising the voltage deviation of the consumer voltages from the nominal system voltage, i.e OF_2.

4.7.3 Case studies simulation results analysis

The minimum and maximum nodal voltages of the distribution feeder is analysed over a 24 hour duration in Fig. 4.25. At about 12 noon, a 0.12% violation of the upper voltage limit is observed due to the high penetration of PV in Case study 1 Fig. 4.25(a). Also, due to a peak in demand at about 19:00, the lower voltage limits of 0.23% is equally violated. The dotted lines in Fig. 4.25 indicates the upper and lower acceptable voltage limits respectively. During Case studies 2 and 3, the application of the VVO leads to a significant improvement in the voltage profiles as demonstrated in Fig. 4.25(b) and Fig. 4.25(c). The consumers voltages are all within the acceptable limits. Also, the operation of the PV system is at MPPT during the control case study considered and no curtailment of the PV active power is required. The participation of the inverter in the VVO helped to regulate the system voltages and mitigate voltage violations through injection and absorption of the reactive power of the inverter. However, for very high penetration of residential PV systems into the Nigerian grid, and to avoid

undervoltage resulting from critical load demands, the utilisation of the reactive power capability of the PV inverter would be essential.

In Table 4.8, the substation active and reactive power dispatch, the PV systems total reactive power dispatch, the total active power loss and the total voltage deviation over the days duration is presented. For Case study 1, the high penetration of PV system in the network results in a reverse active power flow (indicated by the negative sign) of 1.328 MW to the substation while there's an injection of 7.439 MVAr of reactive power from the substation. Such reverse power flow have significant impacts on the on load tap changer (OLTS) of the transformer.

For the controlled Case studies 2 and 3, the reactive power resources of the inverter helps eliminate the reverse power flow associated with the high PV penetration culminating to the injection of 7.281 MW from the substation. A net total of 1.359 MVAr and 1.301 MVAr respectively are utilized from the inverter to regulate voltage within the acceptable limits. With this, the substation reactive power is further reduced by 19.8% and 18.9% respectively during Case study 2 and 3. Also, with the application of VVO, during the controlled case, the total active power loss did reduce from 0.437 MW to 0.172 MW. Similarly, the deviation of consumer voltages from the nominal system voltage is reduced by 33.4% during these case studies.

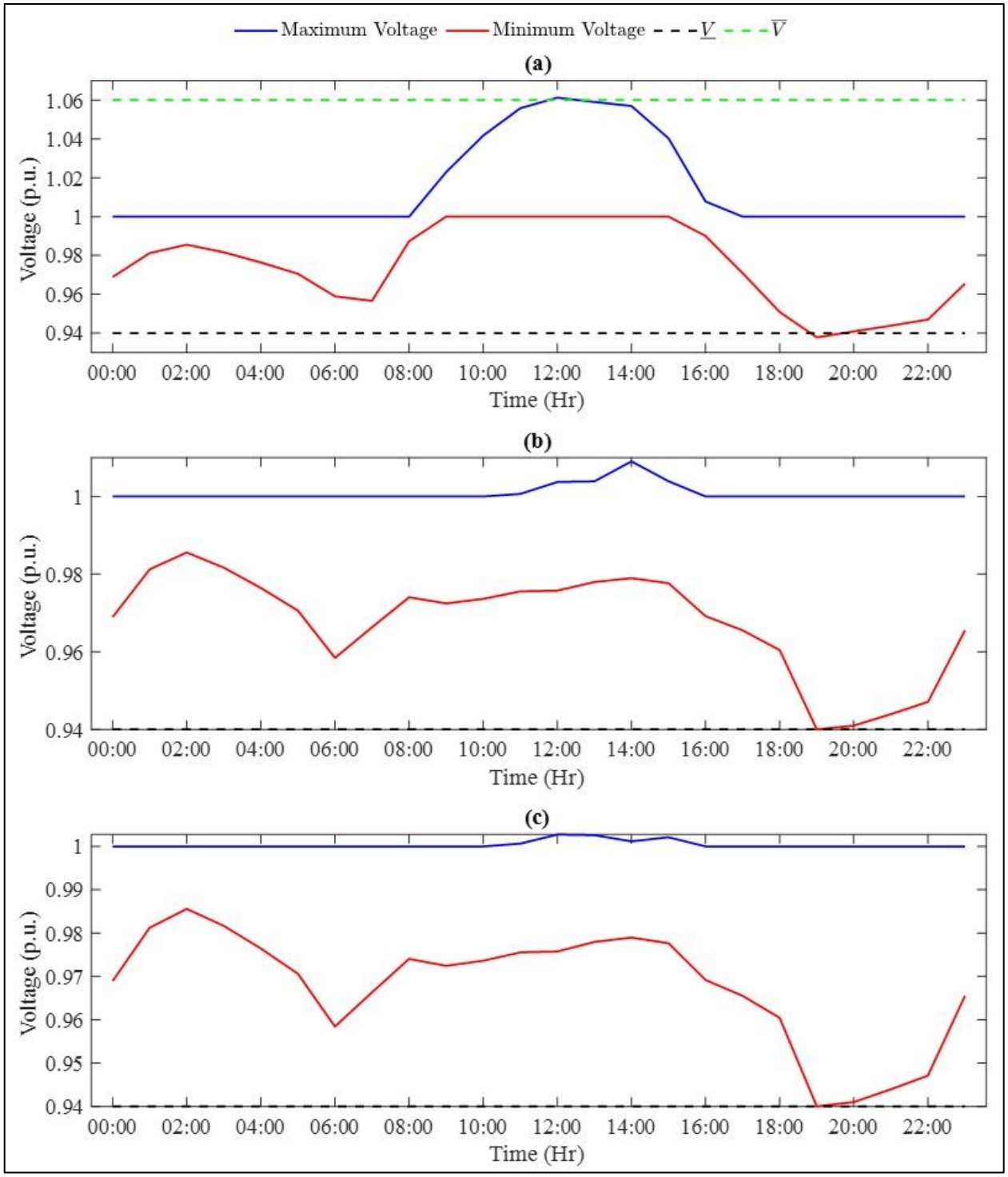

Fig. 4.25. Minimum and maximum voltage profiles for (a) Case study 1, (b) Case study 2; (c) Case study 3.

Table 4.8. Substation power, Total Reactive power dispatch, Total active power loss and Total voltage deviation.

	Case-1	**Case-2**	**Case-3**
Substation active power (MW)	-1.328	7.281	7.281
Substation reactive power (MVAr)	7.439	5.839	5.898
Total PV reactive power (MVAr)	-	1.359	1.301
Total active power loss (MW)	0.437	0.172	0.172
Total voltage deviation (p.u.)	0.772	0.514	0.514

4.8 Conclusion

This chapter uses the PSCAD/EMTDC dynamic software tool to investigate the various voltage and power quality issues that the potential introduction of EVs and DGs into the real Nigerian distribution network could cause. Also, a VVO was performed to enable the inverter-based PV systems participate actively in voltage regulation by the provision of flexible reactive power support.

A model of a real LV distribution system in Nigeria consisting of a 60 MVA 3-phase 33 kV ideal voltage source, connected to a 15 MVA, 33/11 kV YY0 transformers, and seven 11 kV outgoing feeder's substation was developed and analysed. Using both fixed and variable load profiles, the simulation was performed using the PSCAD/ EMTDC power system analysis software at various levels of EV and DG integration. Different case studies were considered. Voltage profile results using fixed load profile indicated voltage violations at some specified nodes resulting from excessive load connection at those node points. However, with the variable load profiles and application of VVO, the voltages operated within the acceptable limits.

Although the voltage violations were within the acceptable regulatory limits in the case of variable load profiles, the introduction of various battery chargers did increase the harmonics, especially the current, hence violating the IEEE permissible harmonic threshold limits. The installation of a LCL filter helped to mitigate harmonic distortion below 5% in the network.

Finally, to address the voltage concerns arising from high PV penetration, VVO was performed to enable the inverter-based PV systems participate actively in voltage regulation by the provision of flexible reactive power support. The VVO did improve the feeder voltage profile and reduced the active power losses in the network. With such improvements, the power system quality is enhanced, and the reliability of supply voltage guaranteed to the consumers.

The major contribution of this chapter is:

- A real Nigerian LV distribution network was modelled and simulated using PSCAD/EMTDC considering both fixed and variable load profiles.
- The modelled Nigerian LV network was used to perform dynamic analysis of the voltage and harmonic distortions with the introduction of DGs and EVs.
- The impacts of the introduction of various charger types into the network was investigated, recommending the installation of filters to mitigate the increase in the harmonic distortions.
- Recommendations were made for the distribution network operators to always maintain a secure and safe network operation with a significant increase in the load.
- VVO was implemented to allow inverter-based PV systems to participate actively in voltage regulation and optimisation by providing flexible reactive power support.

CHAPTER 5

5.0 BLACK START PROBLEM FORMULATION IN DISTRIBUTION NETWORK USING DERS

5.1 Introduction

A black start restoration (BSR) problem formulation method is presented in this chapter resulting from the frequent collapse of the Nigerian power grid discussed in previous chapters. This BSR method could be suitably applied in distribution management system (DMS) or microgrid control center (MGCC) to support in power system restoration operation. The formulated BSR problem was done as a dynamic optimisation problem to enable the effective coordination of the dispatching actions of the DERs along with the switching actions of RCSs over multiple decisions time steps. Having considered several linearisation techniques formulated by various researchers, the mixed-integer linear programming (MILP) technique was adopted and modelled to suit the nature of the BSR method developed. The simulation of the MILP model was achieved in MATLAB® using the IBM CPLEX™ solver. The results of this study have been peer reviewed and publish in [107, 206].

Power system restoration (PSR) using the bottom-up approach would usually involve using the power provided by the black start unit to power the generating stations and subsequently re-energising the various substations. The four categories of the black start units according to [126, 127] are: hydroelectric units, diesel generator sets, aero-derivative gas turbine generator sets and larger gas turbines.

As noted in [134, 135], latest technology has indicated that distributed energy resources and remote controllable switches can be utilized for black start restoration for distribution systems and microgrids. For some critical loads, photovoltaic battery backup systems and energy storage systems can be used to provide the power required while RCSs can be programmed to interconnect these power sources with the consumer loads by opening and closing thus temporarily operating as a dynamic microgrid [156].

Although there are ongoing research in the general area of black start, however, the use of DERs and plug-in electric vehicles in black start application is an emerging area. This chapter and the subsequent one therefore aims to assess the behaviour of the power system with a combination of renewable and non-renewable DERs as black start units, the system control during the power system restoration and the development of a viable restoration strategy that would permit a full-scale adoption of DERs without compromising the resilience of the power system.

As described in **Chapter 2**, during service restoration, the residual load tends to be higher than the normal or pre-outage demand level resulting from thermostatically controlled loads [128]. These unpredictable uncertainties resulting from the continuously changing load demand under CLPU conditions entails making available additional reserves when carrying on with load restoration. Studying the effects of the system restoration on cold load pickup with and without DGs and ESSs is also the focus of this research.

In the next section, the mathematical formulation of the BSR problem as a dynamic optimization problem is presented. This is followed by the introduction of the MILP model which is used to linearize the original

nonlinear dynamic optimization problem. Lastly, the solution methodology of the proposed modelled BSR method is presented.

5.2 BSR Mathematical Problem Formulation

According to [130, 207], the BSR problem can be formulated mathematically as a dynamic optimisation problem. [106] comprehensively documented the formulation principles which was adopted by [130] in the study. Using the same principles but with slight modifications, a similar BSR mathematical formulation has been adapted in this work. The dynamic optimization-based formulation addresses the issue of decision making over multiple time-step [207]. For example, the set points for controllable components such as; dispatchable DGs, controllable loads and controllable switches can be defined and optimised to meet various operational constraints for each time step. Also, the time horizon could be represented by a set of variables defined in discrete form; i.e., $zt \in \{z_0, z_1, z_2, \dots, z_N\}$. Assume N to be the total number of time steps, then $N = T/\Delta t$, where Δt is the length of each time step. Let $x(z_t)$ be defined as the state variable at time step z_t, and $u(z_t)$ as the control variable at time step z_t, $\tilde{f}[t, x(z_t), u(z_t)]$ as the transition equations determined by time step z_t, state variable $x(z_t)$ and control variable $u(z_t)$, and $\tilde{F}[z_t , x(z_t), u(z_t)]$ as the objective function. Then, according to [207], the discrete-time dynamic optimization problem can be described as captured in equation 5.1;

$$\mathrm{m}aximize\ or\ minimize \sum_{Z_0}^{Z_N=\frac{T}{\Delta t}} \tilde{\mathrm{F}}[Z_t, \mathrm{x}(Z_t), \mathrm{u}(Z_t)]\Delta \mathrm{t} \qquad (5.1)$$

$s.t.\ x(Z_{t+1}) - x(Z_t) = \tilde{f}[Z_t, x(Z_t), u(Z_t)] \rightarrow$ Equation of motion/transition equation.

$(Z_0) = A\ (A\ given), x(Z_N) = Z(T\ given, Z\ free) \rightarrow$ Transversality condition.

In the problem formulation, [207] asserted that the transition equation defines the inter-temporal (or inter-stage, inter-step) constraints among various variables, thereby relating the variables of different time steps. For instance, it would be expected that the difference of power output of DG between two consecutive steps should be smaller than a threshold (e.g., ramp rate constraint). Similarly, according to [207], transversality conditions defines the system operational conditions for each time step. For example, system model equations are typical transversality conditions. Furthermore, in order to facilitate the formulation of the BSR problem, [207] noted that three types of variables namely; time variables, state variables, and control variables are defined to formulate the dynamic optimization problems. A detailed illustrative example showing how the problem formulation based on dynamic optimization is achieved is presented in [130].

Mathematically, the BSR problem is formulated as:

$$\min F[\mathbf{x}(t), \mathbf{u}(t)] \tag{5.2}$$

$$\text{s. t. } G_i[\mathbf{x}(t), \mathbf{u}(t)] \leq 0, \; i = 1, \dots, m \tag{5.3}$$

$$H_j[\mathbf{x}(t), \mathbf{u}(t)] = 0, \; j = 1, \dots, n \tag{5.4}$$

$$t \in \{Z_0, Z_1, Z_2,, \dots, Z_N,\}, \tag{5.5}$$

Where:

$\boldsymbol{x}(t)$ represent the vector of state variables at each time instant.

$\boldsymbol{u}(t)$ represent the decision variables at each time instant.

$F[\boldsymbol{x}(t), \boldsymbol{u}(t)]$ represents the objective function of the BSR problem, as a function of $\boldsymbol{x}(t)$ and $\boldsymbol{u}(t)$.

Equation (5.3) represents m inequality constraints which can be magnitude limits for node voltage, capacity limits for DGs, etc.

Equation (5.4) represents n equality constraints such as power flow constraints.

The objective and constraints functions are introduced in the next section.

5.2.1 Objective function of the BSR problem

Power system restoration is pivotal to the unlocking of a power system blackout. As described in [124], it is a multi-objective, multi-stage, multi-variable and multi-constraint optimization issue which is full of non-linearity and uncertainty. Also, it is said to be a typical semi-structured decision-making but without complete solution process [124]. However, the primary objective of power system restoration as opined by [125] is to enable the immediate return of normalcy to the entire network with minimal loss and impacts to power consumers. In the light of the above, the cardinal objective as observed by [208, 209] is usually defined to maximise the total restored energy during the considered time-frame.

The objective function of the BSR problem can be formulated as:

$$\text{Max} \sum_{t\in\mathcal{T}} f\left(\boldsymbol{P}_{l,t}^{L}, \boldsymbol{P}_{g,t}^{\emptyset}, \boldsymbol{Q}_{g,t}^{\emptyset}, x_{ij,t}^{BR}, x_{l,t}^{L}\Delta\text{t}\right), \tag{5.6}$$

Where:

$t \in \mathcal{T} \coloneqq \{1,2, \dots, T\}$ represents the set of steps, and T is the length of the horizon.

$\boldsymbol{P}_{l,t}^{L}$ is a vector which represents the three-phase load demand on node l at step t.

$\boldsymbol{P}_{g,t}^{\emptyset}$ is a vectors representing the three-phase active power generated by a DG on node g at time step t.

$\boldsymbol{Q}_{g,t}^{\emptyset}$ is a vectors representing the three-phase reactive power generated by a DG on node g at time step t.

($x_{ij,t}^{BR}$) is the switching state of a switchable line between node i and j respectively, at time step t.

$x_{l,t}^{L}$ is the energization level of a load at node l at time step t.

Δt is the time span between two successive steps.

$f(\blacklozenge)$ is the function representing the restored load (e.g., in kW) as a result of the control variables.

Consequently, equation (5.6) represents the total amount of load restored at all the considered steps; i.e., the total restored energy (e.g., in kWh) over the considered time-frame or horizon.

5.2.2 BSR problem constraints

For a black start solution to be considered as viable, some operational constraints must be well defined for all the components involved in the black start process such as;- transformers, switches, lines and loads. Some of the models and constraints required for the implementation of functional black start problem are well documented in [130] and include but not limited to the ones presented in Table 5.1.

Table 5.1. Models and constraints of the BSR problem [130].

Category	**Models and Constraints**	**Description**
	Power Flow Model	Calculate voltage and line power, given an operating point
	Load Model: CLPU Load and ZIP Load	Calculate the load demand

System Model Constraints	Transformer/Voltage Regulator Mode Black Start DG Model Dispatchable DG Mode Renewable DG Model ESS Model Line Model Initial Condition	Model the behaviour of transformer and voltage regulators Ensure that each component is connected and operated properly Describe the initial state of the system
System Operational Constraints	Line kVA Capacity Constraints Voltage Limit Constraints Max Step Load Constraints	Ensure the apparent power going through each energised line is maintained below the thermal threshold Ensure the voltage magnitude of each energised bus is maintained within a permissible range Ensure the frequency stability
DG/ESS Operational Constraints	ESS Operation DG Current Unbalanced Operation DG Capacity Constraint DG Ramp Rate Constraint	Ensure each ESS is operated properly Protect each three-phase black start DG from being damaged by unbalanced conditions Prevent a DG from being overloaded and changing its output too fast
Topological Constraints	Connectivity Constraint Sequencing Constraint	Ensure the BSR sequence is feasible. Components are correctly connected Each isolated microgrid is in tree topology

5.3 Assumptions

The major phases of power system restoration following a blackout event namely; preparation, network restoration and load restoration has been described in details in [128], and during power restoration, the main consideration is usually to restore supply to the network and timely connect consumers to the grid in the best possible manner. However, in real life application, this process and its outcome can be quite complicated and unpredictable. Hence incorporating all possible concerns in the BSR problem formulation becomes unrealistic. [130], did however make several reasonable assumptions, some of which were adopted, modified and presented in this research.

- Between any two consecutive steps, the timeframe is assumed to be fixed.
- All the loads under CLPU conditions are modelled as constant PQ loads. However, loads can also be modelled as ZIP (constant impedance (Z), constant current (I), and constant power (P)) loads.
- For the control command to be timely performed for each time step, it is assumed that during the restoration process, a communication network is available and all the switches and DERs can be controlled remotely. Any component not controllable due to loss of communication is classified as a failed component.
- The predicted power output of renewable DGs and load profile are accurate.
- A restoration solutions that represent a series of operating points over multiple discrete time steps can be generated by the proposed method. In practice, the system operating conditions will continuously change from the operating point at one discrete step to the operating point at the next discrete step, due to continuously

changing variables such as energised loads under CLPU conditions. Therefore, it is necessary to assume that the intermediate system operating conditions always satisfy the constraints.

5.4 MILP Formulation

The MILP formulation for the modelled BSR problem is presented along with the nomenclature for various variables, parameters, and sets. Also presented is the objective function and various operational constraints.

5.4.1 Objective Function

The objective function is usually defined to maximise the total energy restored for each step considering the weight factor of each load l (denoted as β_l^L):

$$\text{Max} \sum_{l \epsilon \mathcal{L}} \sum_{t \epsilon J} \sum_{\phi \epsilon \{a,b,c\}} \beta_l^L . p_{l,t}^{\emptyset} \Delta \text{t} \qquad (5.7)$$

and subject to the following constraints:

- Linear three-phase power flow constraints.
- DG current unbalance constraints.
- Topological constraints.
- Initial condition constraints.
- Other constraints: line and transformer capacity constraint, DG output constraints, spinning reserve constraints, voltage limit constraints, ramp rate constraints, maximum load step constraints.

5.4.2 Optimisation function

The optimisation function expressed in equation 5.8 is used to capture all the variables used for the simulation and it is the same as equation 5.7.

$$\beta_l^L . p_{l,t}^{\emptyset} + 0p_{g,t}^{\emptyset} + 0Q_{g,t}^{\emptyset} + 0x_{ij,t}^{BR} + \ 0x_{l,t}^{L} \quad (5.8)$$

5.4.3 System model

The following system models were considered and used in the BSR analysis. Also, just like in most literatures, this study assumes a balanced three-phase distribution system.

5.4.3.1 Power flow model

The power flow model is required for the estimation of the node voltage magnitude and the line power which can be obtained by solving the nodal power balance equations. Using Kirchhoff's circuit law (KCL), the formulation of the general form of power flow model for distribution system is presented in [210].

The power flow model taking into consideration the energisation status of each line at each time step is formulated along with the power balance constraints for each bus at each step. Hence, we have:

$$0p_{l,t}^{L} + 0p_{g,t}^{\emptyset} + 0Q_{g,t}^{\emptyset} - Me_{ij}^{\emptyset} x_{ij,t}^{BR} + \ 0x_{l,t}^{L} \leq -\left\{\left(U_{i,t} - U_{j,t}\right) + Me_{ij}^{\emptyset} + \tilde{Z}_{ij} S_{ij}^{*} + \tilde{Z}_{ij}^{*} S_{ij}\right\} \quad (5.9)$$

$$\boldsymbol{U}_{i,t} - \boldsymbol{U}_{j,t} \ \leq \check{\mathrm{Z}}_{i,j} \boldsymbol{S}_{ij,t}^{*} + \ \check{\mathrm{Z}}_{ij}^{*} \boldsymbol{S}_{ij,t} + \mathrm{M}(1 - x_{ij,t}^{BR}) \boldsymbol{e}_{\boldsymbol{ij}}^{\emptyset}, \quad (5.10)$$

$$0p_{l,t}^{L} + 0p_{g,t}^{\emptyset} + 0Q_{g,t}^{\emptyset} + Me_{ij}^{\emptyset} x_{ij,t}^{BR} + \ 0x_{l,t}^{L} \leq \left(U_{i,t} - U_{j,t}\right) - \left(\tilde{Z}_{ij} S_{ij}^{*} + \tilde{Z}_{ij}^{*} S_{ij} - Me_{ij}^{\emptyset}\right) \quad (5.11)$$

$$\boldsymbol{U}_{i,t} - \boldsymbol{U}_{j,t} \ \geq \check{\mathrm{Z}}_{i,j} \boldsymbol{S}_{ij,t}^{*} + \ \check{\mathrm{Z}}_{ij}^{*} \boldsymbol{S}_{ij,t} + \mathrm{M}(1 - x_{ij,t}^{BR}) \boldsymbol{e}_{\boldsymbol{ij}}^{\emptyset}, \ (\mathrm{i}, \mathrm{j}) \in B/V, \mathrm{t} \in \mathcal{T}, \quad (5.12)$$

$$\sum_{l:l=i,l\in\mathcal{L}} p_{l,t}^{L} - \sum_{g:g=i,g\in\mathcal{G}} p_{g,t}^{\emptyset} + 0Q_{g,t}^{\emptyset} + 0x_{ij,t}^{BR} + 0\ x_{l,t}^{L} = \sum_{h:(h,i)\in B} p_{hi,t}^{BR} - \sum_{j:(i,j)\in B} p_{ij,t}^{BR} \tag{5.13}$$

$$\sum_{h:(h,i)\in B} \boldsymbol{P}_{hi,t}^{BR} + \sum_{g:g=i,g\in G} \boldsymbol{P}_{g,t}^{\emptyset} = \sum_{j:(i,j)\in B} \boldsymbol{P}_{ij,t}^{BR} + \sum_{l:l=i,l\in\mathcal{L}} \boldsymbol{P}_{l,t}^{L}, \tag{5.14}$$

$$0p_{l,t}^{L} + 0p_{g,t}^{\emptyset} - \sum_{g:g=i,g\in\mathcal{G}} Q_{g,t}^{\emptyset} + 0x_{ij,t}^{BR} + 0x_{l,t}^{L} = \sum_{l:l=i,l\in\mathcal{L}} Q_{l,t}^{L} - \sum_{h:(h,i)\in B} Q_{hi,t}^{BR} + \sum_{j:(i,j)\in B} Q_{ij,t}^{BR} \tag{5.15}$$

$$\sum_{h:(h,i)\in B} \boldsymbol{Q}_{hi,t}^{BR} + \sum_{g:g=i,g\in G} \boldsymbol{Q}_{g,t}^{\emptyset} = \sum_{j:(i,j)\in B} \boldsymbol{Q}_{ij,t}^{BR} + \sum_{l:l=i,l\in\mathcal{L}} \boldsymbol{Q}_{l,t}^{L}, \tag{5.16}$$

$$(i,j) \in B, \emptyset \in \emptyset_{i,j} t\ \in\ \mathcal{T} \tag{5.17}$$

Where:

$\boldsymbol{e}_{\boldsymbol{ij}}^{\emptyset} \in \mathbb{Z}_2^3$ is the vector with binary entries to represent the phases. Assuming a single-phase line for branch (i, j) (e.g., B-phase), then $\boldsymbol{e}_{\boldsymbol{ij}}^{\emptyset} = [0,1,0]^T$.

$\boldsymbol{S}_{ij,t} = \boldsymbol{P}_{ij,t}^{BR} + \boldsymbol{Q}_{ij,t}^{BR}$ is the vector of three-phase apparent power flowing from bus i to j through line (i, j) at step t.

$(\boldsymbol{P}_{l,t}^{L} + \boldsymbol{Q}_{l,t}^{L})$ is the three-phase load demand on node i at step t.

Except voltage regulators and transformers, equations (5.10) and (5.12) ensures that the constraints are applied only to energised lines. M, which is a big number, should be carefully selected to ensure that the constraints are only valid when the line is energised.

5.4.3.2 Load models

The loads in the distribution system are usually either wye-connected or delta-connected. In this research, only the load model under cold load pick-up condition was developed.

5.4.3.2.1 Load models under cold load pick-up condition

To model the behaviour of load demands at the various time steps, a linear CLPU model has been proposed. According to [130], the formulation of the three-phase CLPU which can be calculated in an accumulative manner is given as:

$$\boldsymbol{P}_{l,t}^{L} = \boldsymbol{P}_{l}^{L} \odot \left(\mathbf{S}^{\mathrm{u}} x_{l,t}^{L} - \Sigma_{k=1}^{t} \Delta \boldsymbol{P}_{l}(k) x_{l,t-k+1}^{L}\right), l \in \mathcal{L}, \mathrm{t} \in \mathcal{T}, \tag{5.18}$$

$$\boldsymbol{Q}_{l,t}^{L} = \boldsymbol{Q}_{l}^{L} \odot \left(\mathbf{S}^{\mathrm{u}} x_{l,t}^{L} - \Sigma_{k=1}^{t} \Delta \boldsymbol{Q}_{l}(k) x_{l,t-k+1}^{L}\right), l \in \mathcal{L}, \mathrm{t} \in \mathcal{T}, \tag{5.19}$$

Where:

$\boldsymbol{P}_{l}^{L}, \boldsymbol{Q}_{l}^{L}$ are pre-outage three-phase active and reactive power of load l.

$\mathbf{S}^{\mathrm{u}}$ is the vector representing undiversified loading factor for load l.

5.4.3.3 Voltage regulator and transformer model

Besides having a fixed ratio, the transformer and the voltage regulator have similar models. Hence, a single-phase voltage regulator is modelled as an ideal transformer connected with an equivalent line representing the leakage impedance, while a three-phase voltage regulator is modelled by connecting three single-phase voltage regulators.

5.4.3.4 Connectivity constraints for components

The physical connections of each component with the system is described by the connectivity constraints and is mathematically modelled as a set of equality and inequality constraints.

5.4.3.4.1 Connectivity constraints for DGs

Some of the rules governing the physical connections as it applies to different DGs types was elaborately enumerated in [130]. These according to [130] includes but not limited to:

- Black start DGs start at first time step.
- For a non-black start DG equipped with a switch, starting is enabled only if the terminal bus is energised.
- For a non-black start DG whose connection is directly tie to the terminal bus, starting is initiated once the terminal bus is energised.
- Non-participating DGs in the system restoration should not be energised.

The mathematical representation of these rules is formulated by the following constraints:

$$x_{g,t}^{G} \leq s_{g,t}^{N},\ \mathrm{g} \in \mathrm{G}/(\mathrm{G}^{\mathrm{S}} \cup \mathrm{G}^{\mathrm{F}}), \mathrm{t} \in \mathcal{T}, \tag{5.20}$$

$$x_{g,t}^{G} - x_{g,t-1}^{G} \geq 0, \mathrm{g} \in \mathrm{G}, \mathrm{t} \in \mathcal{T}, \mathrm{t} > 1 \tag{5.21}$$

$$x_{g,t}^{G} = 1, \mathrm{g} \in \mathrm{G}^{\mathrm{S}}/\mathrm{G}^{\mathrm{F}}, \mathrm{t} \in \mathcal{T} \tag{5.22}$$

Equations (5.20) and (5.21) respectively ensures that a dispatchable DG without black start capability should be able to start only when it's connected to an energised node and that once a DG is started, it cannot be tripped in the following steps. While equation (5.22) requires that the substation node and the black start DGs should be started at first step. The black start DGs capability to regulate voltage is formulated as:

$$U_{g,t} = 1.0, \mathrm{g} \in \mathrm{G}^{\mathrm{S}}/\mathrm{G}^{\mathrm{F}}, \mathrm{t} \in \mathcal{T} \quad (5.23)$$

5.4.3.4.2 Connectivity constraints for ESSs

The connectivity constraints for ESSs are defined to allow for ESS to charge and discharge power only when its terminal node is energised. These constraints are formulated as:

$$x_{e,t}^{ESS\_CH} + x_{e,t}^{ESS\_DISCH} \leq s_{e,t}^{N}, \ e \in E/\mathrm{E}^{\mathrm{F}}, t \in \mathcal{T}, \quad (5.24)$$

5.4.3.4.3 Connectivity constraints for loads

According to [130], the connectivity constraints for loads include the following:

- Loads can only be restored upon the energisation of the terminal buses.
- Restoration of switchable loads occurs immediately the terminal bus is energised.
- Once a load is restored, it shouldn't be shed.

The formulation of these constraints is as follows:

$$0p_{l,t}^{L} + 0p_{g,t}^{\emptyset} + 0Q_{g,t}^{\emptyset} + 0x_{ij,t}^{BR} + x_{l,t}^{L} \leq s_{l,t}^{N} \quad (5.25)$$

$$x_{l,t}^{L} \leq s_{l,t}^{N}, \ \mathrm{l} \in \mathcal{L}^{\mathrm{S}}/\mathcal{L}^{\mathrm{F}}, \mathrm{t} \in \mathcal{T}. \quad (5.26)$$

$$0p_{l,t}^{L} + 0p_{g,t}^{\emptyset} + 0Q_{g,t}^{\emptyset} + 0x_{ij,t}^{BR} + x_{l,t}^{L} = s_{l,t}^{N} \quad (5.27)$$

$$x_{l,t}^{L} = s_{l,t}^{N}, \ \mathrm{l} \in \mathcal{L}/, (\mathcal{L}^{\mathrm{S}} \cup \mathcal{L}^{\mathrm{F}}), \mathrm{t} \in \mathcal{T}. \quad (5.28)$$

$$x_{l,t}^{L} - x_{l,t-1}^{L} \geq 0,\ \mathrm{l} \in \mathcal{L}^{\mathrm{S}}, \mathrm{t}\ \in \mathcal{T}, \mathrm{t} > 1. \qquad (5.29)$$

Equation (5.26) requires that a switchable load should be energised only when it's connected to an energised node. For non-switchable load, equation (5.28) ensures that its gets energised immediately when it connects to an energised node. Equation (5.29) requires that once a load is restored, it cannot be tripped again.

$$x_{nl,t}^{L} \leq x_{cl,t}^{L},\ cl, nl \in\ \mathcal{L}/\mathcal{L}^{\mathrm{F}}, \mathrm{t}\ \in \mathcal{T}, \quad (5.30)$$

In addition, equation (5.30) provides that an optional constraint can be used to ensure that a set of loads (e.g., critical loads) can be restored prior to another set of loads. Hence, equation (5.30) ensures that once all critical loads are fully restored, non-critical loads can be restored. The subscripts $c\mathrm{l}$ in equation (5.30) represents a particular critical load, and $n\mathrm{l}$ represents a particular non-critical load.

5.4.3.4.4 Connectivity constraints for lines

The connectivity constraints for lines are summarily expressed as [130]:

- For a switchable line to be closed, one of the terminal buses needs to be energised.
- A terminal bus is energised immediately once a non-switchable line is closed.
- After being energised, a line cannot be tripped.

The mathematical formulation of the constraints is expressed as follows:

$$0p_{l,t}^{L} + 0p_{g,t}^{\emptyset} + 0Q_{g,t}^{\emptyset} + x_{ij,t}^{BR} + \ 0x_{l,t}^{L} \leq s_{i,t}^{N} \quad (5.31)$$

$$x_{ij,t}^{BR} \leq s_{i,t}^{N}, (i,j) \in \mathfrak{B}^{\mathrm{S}}/\mathfrak{B}^{\mathrm{F}}, \mathrm{t} \in \mathcal{T}, \quad (5.32)$$

$$0p_{l,t}^{L} + 0p_{g,t}^{\emptyset} + 0Q_{g,t}^{\emptyset} + x_{ij,t}^{BR} + 0x_{l,t}^{L} \leq s_{j,t}^{N} \quad (5.33)$$

$$x_{ij,t}^{BR} \leq s_{j,t}^{N}, (i,j) \in \mathfrak{B}^{\mathrm{S}}/\mathfrak{B}^{\mathrm{F}}, \mathrm{t} \in \mathcal{T}, \quad (5.34)$$

$$0p_{l,t}^{L} + 0p_{g,t}^{\emptyset} + 0Q_{g,t}^{\emptyset} + x_{ij,t}^{BR} + 0x_{l,t}^{L} = s_{i,t}^{N} \quad (5.35)$$

$$x_{ij,t}^{BR} = s_{i,t}^{N}, (i,j) \in \mathfrak{B}/(\mathfrak{B}^{\mathrm{S}} \cup \mathfrak{B}^{\mathrm{F}}), \mathrm{t} \in \mathcal{T}, \quad (5.36)$$

$$0p_{l,t}^{L} + 0p_{g,t}^{\emptyset} + 0Q_{g,t}^{\emptyset} + x_{ij,t}^{BR} + 0x_{l,t}^{L} = s_{j,t}^{N} \quad (5.37)$$

$$x_{ij,t}^{BR} = s_{j,t}^{N}, (i,j) \in \mathfrak{B}/(\mathfrak{B}^{\mathrm{S}} \cup \mathfrak{B}^{\mathrm{F}}), \mathrm{t} \in \mathcal{T}, \quad (5.38)$$

$$0p_{l,t}^{L} + 0p_{g,t}^{\emptyset} + 0Q_{g,t}^{\emptyset} - x_{ij,t}^{BR} + 0x_{l,t}^{L} \leq -x_{ij,t-1}^{BR} \quad (5.39)$$

$$x_{ij,t}^{BR} - x_{ij,t-1}^{BR} \geq 0, (i,j) \in \mathfrak{B}^{\mathrm{S}}/\mathfrak{B}^{\mathrm{F}}, \mathrm{t} \in \mathcal{T}, \mathrm{t} > 1. \quad (5.40)$$

Equations (5.32) and (5.34) ensures that both end nodes of a switchable line are energised if a switchable line is energised. Equations (5.36) and (5.38) makes provisions such that non-switchable lines are immediately energised once one of the end nodes is energised. Equation (5.40) guarantees that once a line is energised, it cannot be tripped.

5.4.3.5 Initial condition constraints

The energisation status of the damaged or non-damaged participating components is described by the initial condition constraints. The conditions describing the initial condition constraints is expressed as:

- At first time step, all lines are opened.

$$x_{ij,t}^{BR} = 0, (i,j) \in \mathfrak{B}^{\mathrm{S}}/\mathfrak{B}^{\mathrm{F}}, \mathrm{t} = 1. \quad (5.41)$$

- Non-participating DGs and ESS are kept de-energised.

$$x_{g,t}^{G} = 0, g \in \mathrm{G}^{\mathrm{F}}, \mathrm{t} \in \mathcal{T}. \quad (5.42)$$

$$x_{e,t}^{ESS\_CH} + x_{e,t}^{ESS\_DISCH} = 0, \ e \in \mathcal{E}^{\mathrm{F}}, t \in \mathcal{T}. \quad (5.43)$$

- A non-energised load should remain de-energised.

$$x_{l,t}^{L} = 0, l \in \mathcal{L}^{\mathrm{F}}, \mathrm{t} \in \mathcal{T} \quad (5.44)$$

- A line that is damaged or disconnected and hence cannot perform reclosing continues to be de-energised.

$$x_{ij,t}^{BR} = 0, (i,j) \in \mathfrak{B}^{\mathrm{F}}, \mathrm{t} \in \mathcal{T} \quad (5.45)$$

- Nodes that are damaged stays de-energised.

$$s_{i,t}^{N} = 0, i \in \mathbb{N}^{\mathrm{F}}, \mathrm{t} \in \mathcal{T} \quad (5.46)$$

5.4.4 System operational constraints

For the restoration process to be successfully implemented, various operational constraints must be satisfied. For instance, the voltage and the frequency of the energised system must be maintained at their acceptable nominal declared values. Hence in the following subsections, some of the models required to satisfy the various operational constraints are presented.

5.4.4.1 Transformer and line capacity constraints

The kVA rating of the transformer is used in determining its maximum permissible kVA capacity while the ampacity of the line at the rated voltage is used to determine the maximum permissive kVA of the line respectively. Hence it is assumed in this research that the loading of the line and

transformer does not exceed the maximum permissible capacity for each phase.

5.4.5 DG operational constraints

5.4.5.1 DG current unbalance constraints

To avoid overheating, the three-phase DGs operating under unbalanced conditions should satisfy the unbalance constraint [211].

5.4.5.2 DG ramp rate constraints

The DG ramp rate constraints usually requires two consecutive steps for each DG and is normally expected to be within the acceptable range. These constraints can be described as:

$$-x_{g,t}^{G} \cdot P_g^{RAMP} \cdot \Delta t \leq \sum_{\phi \in \{a,b,c\}} P_{g,t}^{\phi} - \sum_{\phi \in (a,b,c)} P_{g,t-1}^{\phi} \leq x_{g,t}^{G} \cdot P_g^{RAMP} \cdot \Delta t, g \in G, t \in \mathcal{T}, t > 1, \quad (5.47)$$

Where:

P_g^{RAMP} is the maximum ramp rate for DG g.

The output active and reactive power of the energised DG shall be maintained within the rated capacity.

$$x_{g,t}^{G} \cdot P_g^{min} \leq \sum_{\phi} P_{g,t}^{\phi} \leq x_{g,t}^{G} \cdot P_g^{max}, \quad (5.48)$$

$$x_{g,t}^{G} \cdot Q_g^{min} \leq \sum_{\phi} Q_{g,t}^{\phi} \leq x_{g,t}^{G} \cdot Q_g^{max}, g \in G, t \in \mathcal{T}, \quad (5.49)$$

Where:

P_g^{min} is minimum value of active output of DG g.

P_g^{max} is maximum value of active output of DG g.

Q_g^{min} is minimum value of reactive output of DG g.

Q_g^{max} is maximum value of reactive output of DG g.

These constraints also force the output of the de-energised DG to zero. Additionally, for dispatchable DG operating at fixed power factor, an optional constraints can be added thus;

$$\tan(\arccos\varphi_g) \cdot \sum_\phi P_{g,t}^\phi - \sum_\phi Q_{g,t}^\phi = 0, g \in \mathrm{G}/\mathrm{G}^{\mathrm{s}}, t \in, \mathcal{T} \quad (5.50)$$

Where:

φ_g is the fixed power factor for DG g. This constraint doesn't apply to the substation node or the black start DG.

5.4.6 ESS operational constraints

To adequately control an ESS, [212] proposed that a set of operational constraints should be adopted. These constraints can be described as given below for a single ESS:

$$P_e^{CH\_min} x_{e,t}^{ESS\_CH} \leq P_{e,t}^{ESS\_CH} \leq P_e^{CH\_max} x_{e,t}^{ESS\_CH}, \quad (5.51)$$

$$P_e^{DISCH\_min} x_{e,t}^{ESS\_DISCH} \leq P_{e,t}^{ESS\_DISCH} \leq P_e^{DISCH\_max} x_{e,t}^{ESS\_DISCH}, \quad (5.52)$$

$$Q_e^{CH\_min} x_{e,t}^{ESS\_CH} \leq Q_{e,t}^{ESS\_CH} \leq Q_e^{CH\_max} x_{e,t}^{ESS\_CH}, \quad (5.53)$$

$$Q_e^{DISCH\_min} x_{e,t}^{ESS\_DISCH} \leq Q_{e,t}^{ESS\_DISCH} \leq Q_e^{DISCH\_max} x_{e,t}^{ESS\_DISCH}, \quad (5.54)$$

$$x_{e,t}^{ESS\_CH} + x_{e,t}^{ESS\_DISCH} \leq s_{e,t}^N \quad (5.55)$$

$$SOC_{e,t}^{ESS} = SOC_{e,1}^{ESS} + \eta_e^{ESS\_CH} P_{e,t}^{ESS\_CH} \Delta t - \frac{1}{\eta_e^{ESS_{DISCH}}} P_{e,t}^{ESS_{DISCH}} \Delta t, t = 1, \quad (5.56)$$

$$SOC_{e,t}^{ESS} = SOC_{e,t-1}^{ESS} + \eta_e^{ESS\_CH} P_{e,t}^{ESS\_CH} \Delta t - \frac{1}{\eta_e^{ESS_{DISCH}}} P_{e,t}^{ESS_{DISCH}} \Delta t, t \geq 2, \quad (5.57)$$

$$SOC_e^{min} \leq SOC_{e,t}^{ESS} \leq SOC_e^{max}, e \in \mathcal{E}/\mathcal{E}^{F}, t \in \mathcal{T}, \quad (5.58)$$

Where:

$P_e^{CH\_min}$ and $P_e^{CH\_max}$ are minimum and maximum active charging power for ESS e.

$P_e^{DISCH\_min}$ and $P_e^{DISCH\_max}$ are minimum and maximum active discharging power for ESS e.

$Q_e^{CH\_min}$ and $Q_e^{CH\_max}$ are minimum and maximum absorbed reactive power for ESS e.

$Q_e^{DISCH\_min}$ and $Q_e^{DISCH\_max}$ are minimum and maximum generated reactive power for ESS e.

$\eta_e^{ESS\_CH}$ and $\eta_e^{ESS\_DISCH}$ are charging and discharging efficiency for ESS e.

SOC_e^{min} and SOC_e^{max} are minimum and maximum state of charge (SOC) for ESS e.

The energy stored in ESS is defined as the state of charge. The active and reactive power when charging and discharging is being limited by equations (5.51) to (5.54). The charging and discharging of an ESS can only be achieved when the connected node is energised. This process is made possible by equation (5.55). Also, the charging and discharging of an ESS cannot be carried out simultaneously.

5.4.7 Topological constraints

A series of rules which ensures the feasibility of a BSR sequence is described by the topological constraints. These rules which are based on the inter-temporal relationship among binary decision variables are defined for lines and nodes. Since most distribution system are operated using radial topology, this research adopts the tree topology which allows a bidirectional flow of power.

As noted in [130], the topological constraints can be expressed using the following rules:

- A bus block not connected to any black-start DG or substation can be energised by any lines connected to this bus.
- A bus block de-energised at step t – 1 and energised at step t, must be energised by at least one switchable line at step t.
- Each switchable line can only be energised if at least one of its end buses is energised at the previous interval.
- To avoid loop formation, if both end buses of a switchable line are energised, then the line cannot be closed.

The mathematically translation of these rules is represented by the following constraints:

$$0p_{l,t}^{L} + 0p_{g,t}^{\emptyset} + 0Q_{g,t}^{\emptyset} - \sum_{ij} x_{ij,t}^{BR} + 0x_{l,t}^{L} \leq \sum_{ki} x_{ki,t}^{BR} \qquad (5.59)$$

$$s_{i,t}^{N} \leq \sum_{i:\,(i,j)\in\mathcal{C}} x_{ij,t}^{BR} + \sum_{i:\,(k,i)\in\mathcal{C}} x_{ki,t}^{BR}, \mathrm{i} \in \mathcal{K}, \mathrm{t} \in \mathcal{T} \qquad (5.60)$$

$$0p_{l,t}^{L} + 0p_{g,t}^{\emptyset} + 0Q_{g,t}^{\emptyset} - \sum_{ij} x_{ij,t}^{BR} + 0x_{l,t}^{L} \leq -\sum_{ij} x_{ij,t-1}^{BR} - \sum_{ij}\left(x_{ki,t-1}^{BR} - x_{ki,t-1}^{BR}\right) + 1 + Ms_{i,t-1}^{N} \qquad (5.61)$$

$$\sum_{i:\,(i,j)\in\mathcal{C}}\left(x_{ij,t}^{BR}-\ x_{ij,t-1}^{BR}\right)+\sum_{i:\,(k,i)\in\mathcal{C}}\left(x_{ki,t}^{BR}-x_{ki,t-1}^{BR}\right)\leq 1+Ms_{i,t-1}^{N},\mathrm{i}\in\mathcal{K},\mathrm{t}\ \in\ \mathcal{T},\mathrm{t}>\ 1$$

(5.62)

$$0p_{l,t}^{L}+0p_{g,t}^{\emptyset}+0Q_{g,t}^{\emptyset}+x_{ij,t}^{BR}+\ 0x_{l,t}^{L}\leq s_{i,t-1}^{N}+s_{j,t-1}^{N} \quad (5.63)$$

$$x_{(i,j),t}^{BR}\leq s_{i,t-1}^{N}+s_{j,t-1,}^{N}(i,j)\in\mathcal{B}^{\mathrm{s}},\mathrm{t}\ \ \in\mathcal{T},\mathrm{t}>\ 1 \quad (5.64)$$

$$0p_{l,t}^{L}+0p_{g,t}^{\emptyset}+0Q_{g,t}^{\emptyset}+x_{ij,t}^{BR}+\ 0x_{l,t}^{L}\leq\left(s_{i,t}^{N}-s_{i,t-1}^{N}\right)+\left(s_{j,t}^{N}-s_{j,t-1}^{N}\right)-x_{ij,t-1}^{BR} \quad (5.65)$$

$$(s_{i,t}^{N}-s_{i,t-1,}^{N})+(s_{j,t}^{N}-s_{j,t-1,}^{N})\ \geq\ x_{(i,j),t}^{BR}-x_{(i,j),t-1}^{BR},(i,j)\in\mathcal{B}^{\mathrm{s}},\mathrm{t}\ \ \in\mathcal{T},\mathrm{t}>\ 1 \quad (5.66)$$

5.4.8 Formulation of matrix equation for CPLEX

To enhance the presentation in MATLAB environment and retain the CPLEX acceptable format, the power flow model incorporating both the inequality and equality constraints is created in a simple matrix form $Ax = B$, where *A* and *B* are the matrix and x is also a matrix containing variables of the objective function. The various limits for the variables have been expressed in the boundary conditions.

$$\begin{bmatrix} 0 & 0 & 0 & Me_{ij}^{\emptyset} & 0 \\ 0 & 0 & 0 & -Me_{ij}^{\emptyset} & 0 \\ 0 & 0 & 0 & 0 & 1 \\ 0 & 0 & 0 & 1 & 0 \\ 0 & 0 & 0 & 1 & 0 \\ 0 & 0 & 0 & -1 & 0 \\ 0 & 0 & 0 & -Sx_{ij,t}^{BR} & 0 \\ 0 & 0 & 0 & Sx_{ij,t}^{BR} & 0 \\ 0 & 0 & 0 & 1 & 0 \\ 0 & 0 & 0 & 1 & 0 \end{bmatrix} \begin{bmatrix} p_{l,t}^{L} \\ p_{g,t}^{\emptyset} \\ Q_{g,t}^{\emptyset} \\ x_{ij,t}^{BR} \\ x_{l,t}^{L} \end{bmatrix} = \begin{bmatrix} -\{(U_{i,t} - U_{j,t}) + Me_{ij}^{\emptyset} + \tilde{Z}_{ij}S_{ij}^{*} + \tilde{Z}_{ij}^{*}S_{ij}\} \\ (U_{i,t} - U_{j,t}) - (\tilde{Z}_{ij}S_{ij}^{*} + \tilde{Z}_{ij}^{*}S_{ij} - Me_{ij}^{\emptyset}) \\ s_{l,t}^{N} \\ s_{l,t}^{N} \\ s_{j,t}^{N} \\ -x_{ij,t-1}^{BR} \\ \sum_{ki} x_{ki,t}^{BR} \\ -\sum_{ij} x_{ij,t-1}^{BR} - \sum_{ij} (x_{ki,t-1}^{BR} - x_{ki,t-1}^{BR}) + 1 + Ms_{i,t-1}^{N} \\ s_{i,t-1}^{N} + s_{j,t-1}^{N} \\ (s_{i,t}^{N} - s_{i,t-1}^{N}) + (s_{j,t}^{N} - s_{j,t-1}^{N}) - x_{ij,t-1}^{BR} \end{bmatrix}$$

$$\begin{bmatrix} \sum_{l:l=i,l\in\mathcal{L}} p_{l,t}^{L} & -\sum_{g:g=i,g\in\mathcal{G}} p_{g,t}^{\emptyset} & 0 & 0 & 0 \\ 0 & 0 & \sum_{g:g=i,g\in\mathcal{G}} Q_{g,t}^{\emptyset} & 0 & 0 \\ 0 & 0 & 0 & 0 & 1 \\ 0 & 0 & 0 & 1 & 0 \\ 0 & 0 & 0 & 1 & 0 \end{bmatrix} \begin{bmatrix} p_{l,t}^{L} \\ p_{g,t}^{\emptyset} \\ Q_{g,t}^{\emptyset} \\ x_{ij,t}^{BR} \\ x_{l,t}^{L} \end{bmatrix}$$

$$= \begin{bmatrix} \sum_{h:(h,i)\in B} p_{hi,t}^{BR} - \sum_{j:(i,j)\in B} p_{ij,t}^{BR} \\ \sum_{l:l=i,l\in\mathcal{L}} Q_{l,t}^{L} - \sum_{h:(h,i)\in B} Q_{hi,t}^{BR} + \sum_{j:(i,j)\in B} Q_{ij,t}^{BR} \\ s_{l,t}^{N} \\ s_{i,t}^{N} \\ s_{j,t}^{N} \end{bmatrix}$$

Bounds:

$0 \le p_{l,t}^{L} \ge P_{load\_max}$

$x_{g,t}^{G}.P_{gen\_min} \le p_{g,t}^{\emptyset} \ge P_{gen\_max}$

$x_{g,t}^{G}.Q_{gen\_min} \le Q_{g,t}^{\emptyset} \ge Q_{gen\_max}$

$0 \le x_{ij,t}^{BR} \ge 1$

$0 \le x_{l,t}^{L} \ge 1$

5.5 Methodological Solution of the BSR

The hub of the BSR solution method is the mixed-integer linear programming technique which has been adopted and modelled in this study. As a dynamic optimisation problem, the determination of the state and decision variables must be at each time step to facilitate the coordination of the dispatching actions of the DERs along with the switching actions of RCSs. The simulation of the MILP model was implemented in MATLAB using the IBM CPLEX solver.

The flow chart of the black start power restoration sequence following a blackout event is presented in Fig. 5.1.

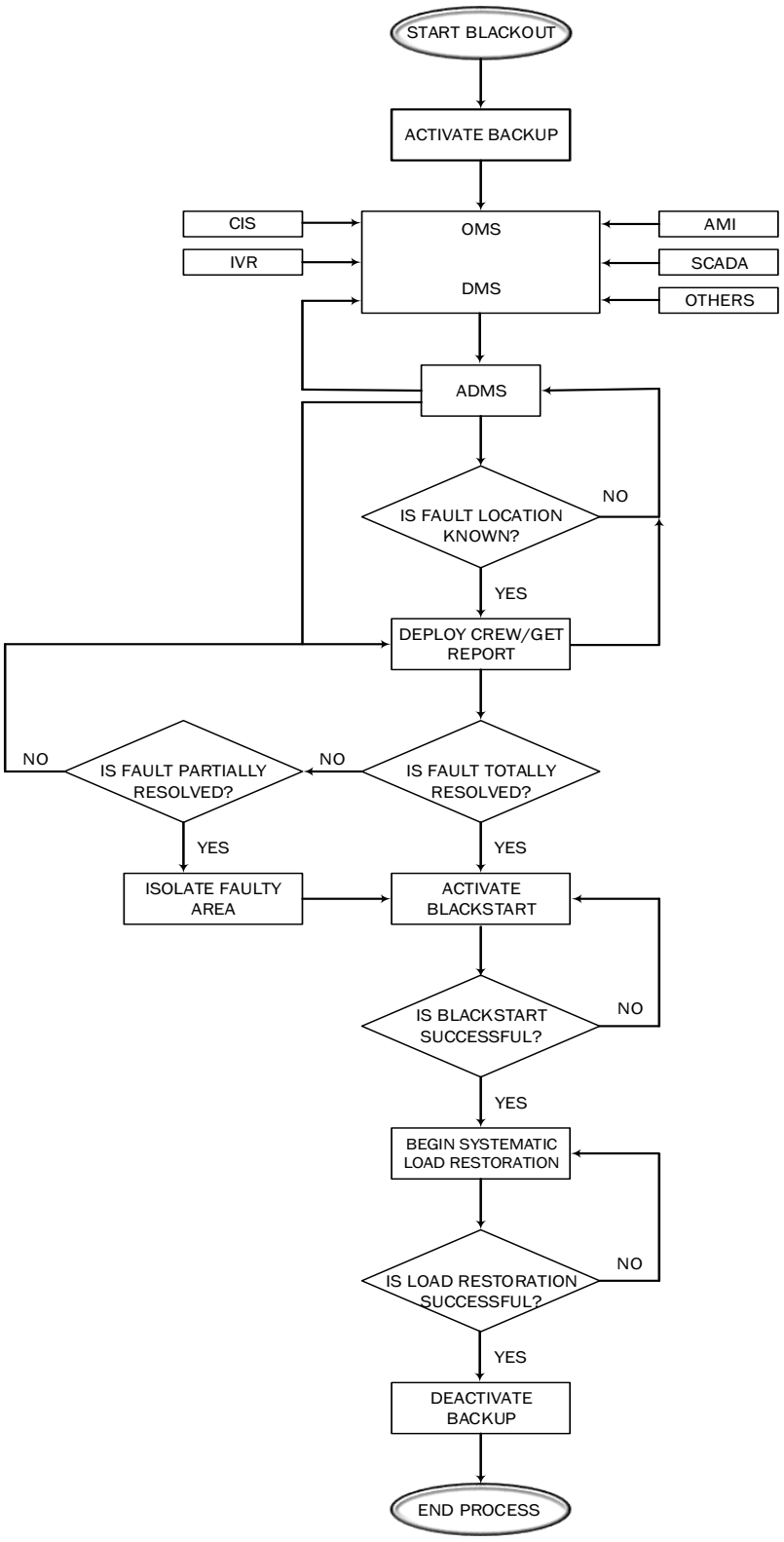

Fig. 5.1. Black start power restoration sequence following a blackout event.

When a blackout event occurs, the backup supply is immediately triggered so that critical facilities can still operate with minimum disruption. The ADMS coordinates the inputs from the various real time tools and sends signals regarding fault type and location. The magnitude of the outage is identified during this analysis phase and all parties updated on the blackout status. The ground maintenance crew deployed to fault locations provides regular updates as repairs progresses. Resulting from the successful repairs, the black start procedure is initiated. A systematic load restoration is carried out with attention paid to CLPU. The entire process is structured to follow a series of *if-else* conditions. The process is ended if all *yes* conditions are successful *else* the loop continues until the *yes* condition is satisfied. The detailed BSR implementation framework as well as the structured flowchart of its implementation is presented in Fig. 5.2.

The architectural framework adopted for the sequential execution of the modelled BSR solution is succinctly described as captured in the flowchart. Using MATLAB, the MILP model was implemented and solved using the IBM CPLEX solver. The procedural steps that were deployed are discussed in detail.

The distribution system load model data such as load demand $P_{l,t0}^{\emptyset} + jQ_{l,t0}^{\emptyset}$, load type, load status, type of load connection, load location, weight coefficients β_l^L, and CLPU parameters S_l^U, S_l^D, αl , Dl were obtained and inputted in MATLAB. Also inputted are the system model parameters for the bus, node, line, transformer, and generator data respectively. The parameters for the DGs as well as that of the ESS are also obtained and inputted.

The formulation of the objective function using the load weight coefficients β_l^L is implemented followed by the system model as well as the system operational constraints. The DGs and the ESS operational constraints along with the topological constraints' formulation are introduced. With the complete formulation of the MILP model, the IBM CPLEX solver is activated in MATLAB and called to run the simulation. The generated solution by the CPLEX solver is further sent to MATLAB for processing. In MATLAB, the various variables (power flow results, objective values, control sequence, etc.,) obtained in the solution are collected and assembled together.

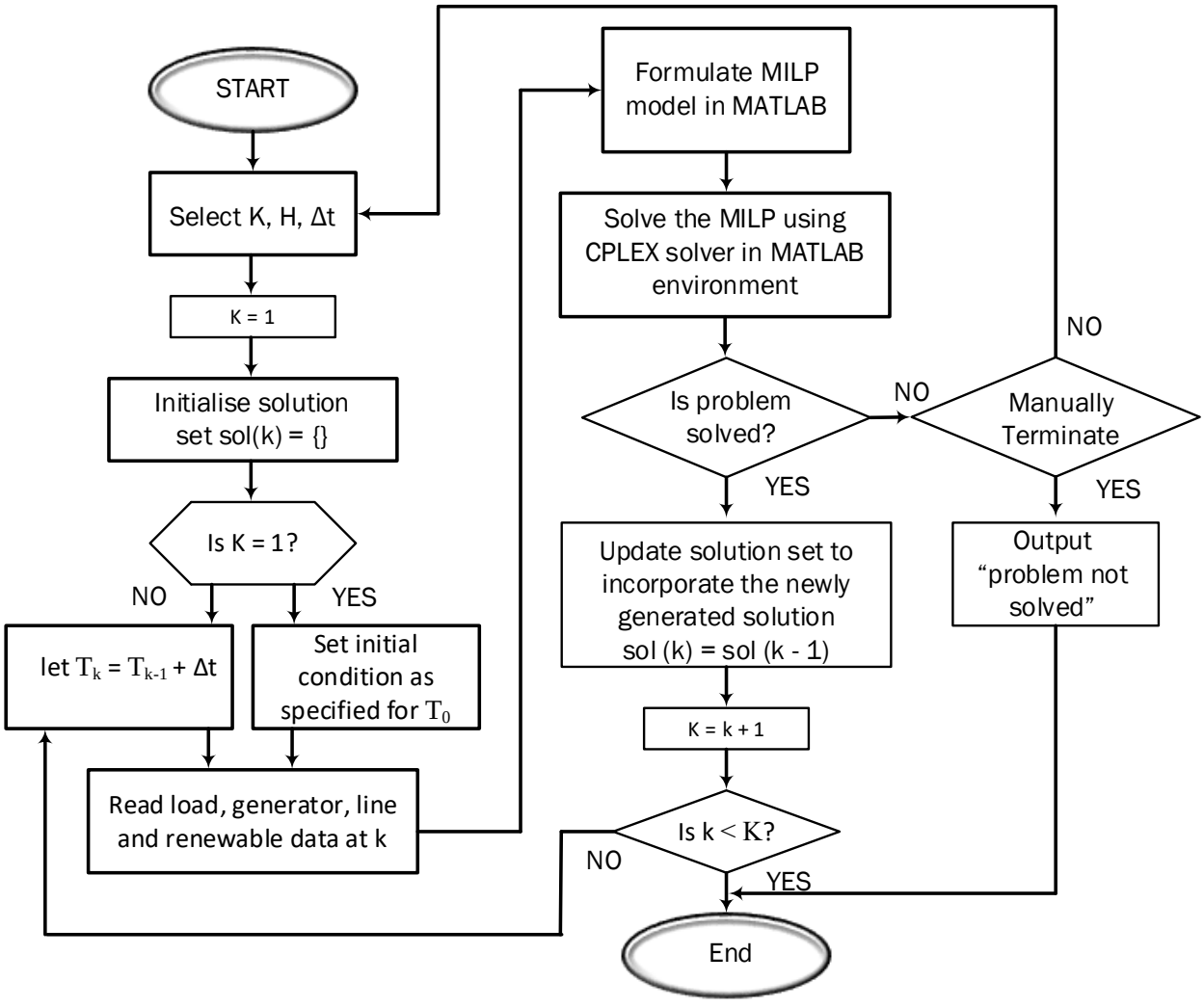

Fig. 5.2. Black start restoration implementation methodology flowchart.

At time T_0, the BSR method is assumed to be initialised, with a fixed horizontal length *H*, having a maximum iteration number *K*. Next, a structured object *sol {}* which stores all control action is created in MATLAB. This is in the form of dummy cells for example *xbr = zeros (48, k).* MATLAB interprets these instructions to mean that the values will be in *48* by *k* matrix and replaces the dummy values with the real values as the simulation progresses. At time *T*, which is T_0 for the initial condition constraints, the first iteration begins. It is important for the initial condition constraints to be identical with the decision variables determined in the previous iteration. The next procedure requires reading of the load, generator, line and renewable energy data into the BSR model. It is expected that at the end of each iteration, assuming a valid solution outcome, *sol {}* should be updated to include the solution obtained from the current horizon. A solution is reached when there is no further change in the optimised value. This value can be reached before the end of the horizon. The horizon is designed to accommodate each step of restoration of actual constructive actions, thus it can be adjusted depending on the result. The adjustment can be manually or reprogrammed as the case may be otherwise, the problem cannot be solved by the MILP solver.

5.6 BSR Implementation Coding in MATLAB

The coding of the Power flow model of the matrix equation for CPLEX incorporating both the inequality and equality constraints was formulated in MATLAB and used for the BSR simulation in Chapter 6.

5.7 Conclusion

The BSR problem was mathematically formulated as a dynamic optimisation problem using the formulation principles established by [207] and adopted by [130]. The dynamic optimisation-based formulation addresses the issue of decision making over multiple time-step. Also, a restoration strategy capable of improving the resilience of the power grid in the unlikely events of a blackout was developed. The uniqueness of the developed black start restoration sequence is the real time coordination of the restoration process by employing the advanced distribution management system. Lastly, the detailed BSR implementation framework as well as the structured flowchart of its implementation was presented.

The major contribution of this chapter is as follows:

- The BSR problem was formulated as a dynamic optimisation problem capable of determining the dispatching actions of DERs and the switching actions of RCSs over several time steps.
- The mixed-integer linear programming technique was adopted and modelled to linearised the nonlinear dynamic optimisation problem which was capable of being solved by commercial software such as IBM CPLEX [213] and GUROBI [214] as noted by [130].
- A power flow model of the matrix equation for CPLEX incorporating both the inequality and equality constraints was formulated in MATLAB and used for the BSR simulation in Chapter 6.
- A unique restoration sequence capable of improving the resilience of the power grid in the unlikely events of a blackout was developed along with the structured flowchart used in implementing the BSR solution framework.

CHAPTER 6

6.0 BLACK START PERFORMANCE ANALYSIS ON NIGERIAN POWER NETWORK

6.1 Introduction

To validate the proposed black start restoration method developed in **Chapter 5**, the Nigerian 48-bus system was used in a case study to assess its performance. The choice of the Nigerian 48-bus system for this research was intentional because of the frequent blackout events and load shedding the country has continued to experience. The results of this research addresses an important gap in the state of the art especially in the part of the world where blackouts are a reoccurring concern. The test system model and the various simulation results of the load restoration performance analysis are presented in this chapter. The results of this study have been peer reviewed and published in [215].

6.2 Modelled Test System

The Nigerian 48-bus system which was modelled in NEPLAN is used as the simulated test system to assess the performance of the proposed BSR method. NEPLAN Electricity is a software tool which is used to plan, analyse, optimise and simulate electrical network. The friendly graphical user interface makes it easier for users to model and simulate their case studies efficiently. The line diagrams and respective data were obtained from the Transmission Company of Nigeria (TCN). The model of the Nigerian 48-bus system modelled in NEPLAN is presented in Fig. 6.1.

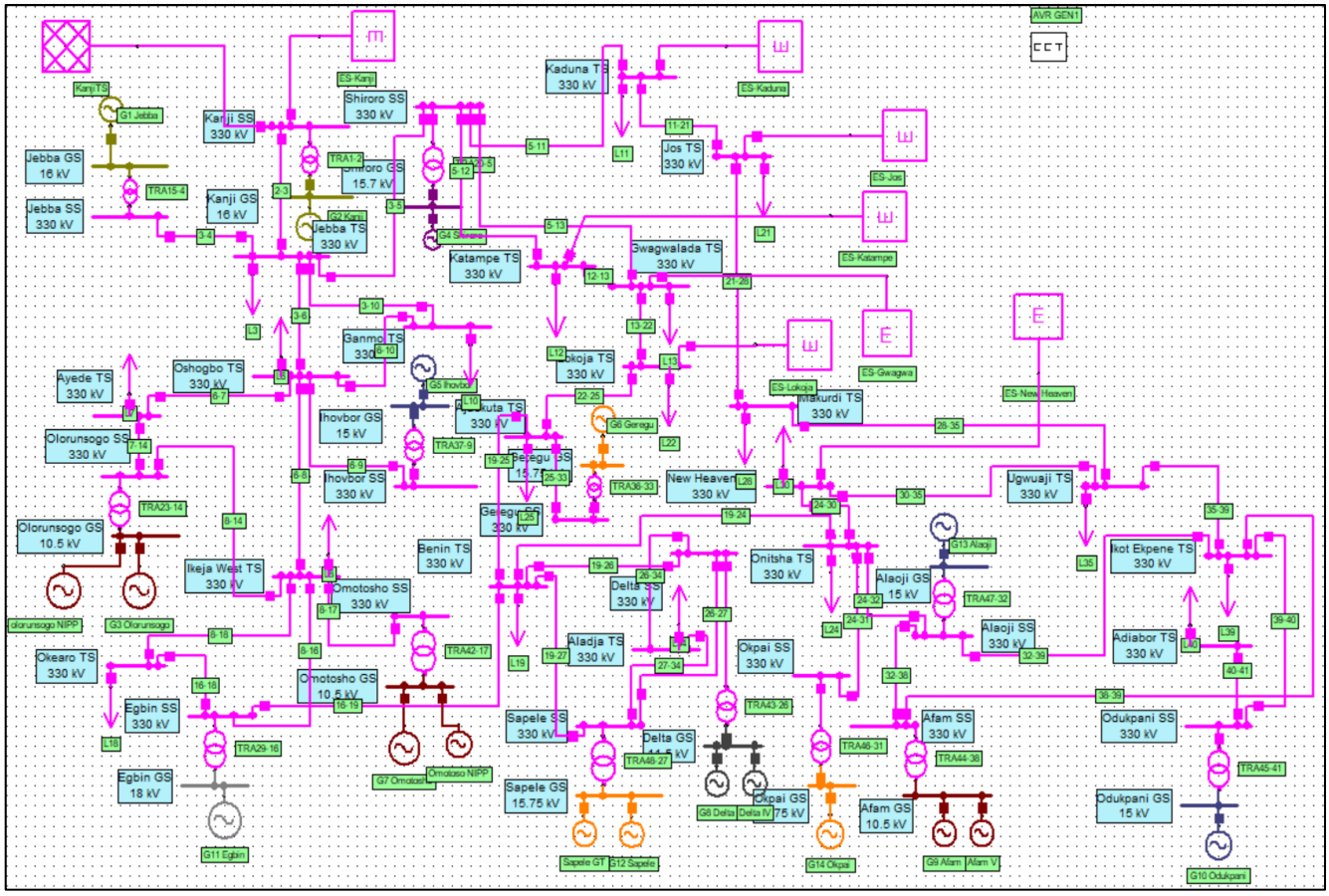

Fig. 6.1. Model of Nigerian 48-bus system modelled in NEPLAN.

6.2.1 Test system description

The Nigerian 48-bus system consists of the various generating stations and transmission system interconnectivity. As reported in [216], the transmission system currently comprises of 5523.8 km of 330 kV, 6801.49 km of 132 kV, 32 substations of 330/132 kV with total installed transformer capacity of 7688 MVA. The average available capacity on the 330/132 kV is 7364 MVA. The geographical structure of TCN as well as the various data set used in the system modelling of the Nigerian 48-bus system are provided in **Appendix F**. Using the available information, and by making necessary inference, the model of the 48-bus system was developed and built in NEPLAN and used to implement the black start analysis.

The projected load switching possibility of the participating generators in the network are tabulated in terms of switching time in Table 6.1. Participating transmission lines routes taken to switch the various desired loads are included in Tables G.1 to G.20 (**in Appendix G**). These Tables show the possible switching routes of the various loads on the different transmission substation (TS) buses by participating generators in the network. The switching sequence of the various loads during restoration takes into consideration the anticipated drop for all the restoration route and choses the route with least voltage and frequency drop. Also taken into consideration is the optimal restoration time for the load which is important as well as the quality of the power supply during restoration.

Table 6.1. Possible switching time of load by generators.

S/N	**Bus**	**Name**	**Time step from generator to load considering the entire network (min)**													
			G 1	**G 2**	**G3**	**G4**	**G5**	**G6**	**G7**	**G8**	**G9**	**G10**	**G11**	**G12**	**G13**	**G14**
1	3	Jebba TS	2	2	4	2	3	6	4	6	8	8	4	6	7	7
2	6	Oshogbo TS	3	3	3	3	2	5	3	5	7	8	3	5	6	6
3	7	Ayede TS	4	4	2	4	3	7	4	6	8	9	4	6	7	7
4	8	Ikeja West TS	4	4	2	4	3	5	2	4	6	7	2	4	5	5
5	10	Ganmo TS	3	3	4	3	3	7	4	6	8	9	4	6	7	8
6	11	Kaduna TS	4	4	6	2	4	5	6	6	8	8	6	6	7	7
7	12	Katampe TS	4	4	6	2	4	5	6	6	8	8	6	8	7	7
8	13	Gwagwalada TS	4	4	6	2	5	4	6	5	6	8	6	5	6	6
9	18	Okearo TS	5	5	5	3	5	4	5	3	4	5	7	2	5	5
10	19	Benin TS	6	6	4	6	5	3	4	2	4	6	2	2	3	3
11	21	Jos TS	5	5	7	3	6	7	7	7	5	6	7	7	5	6
12	22	Lokoja TS	5	5	7	2	6	3	6	4	6	8	4	4	5	5
13	24	Onitsha TS	7	7	5	7	6	4	5	3	3	5	3	3	2	2
14	25	Ajaokuta TS	6	6	5	4	6	2	5	3	5	7	3	3	4	4
15	28	Makurdi TS	6	6	8	4	7	7	8	6	4	5	6	6	4	5
16	30	New Heaven TS	8	8	6	6	7	5	6	4	4	5	4	4	3	3
17	34	Aladja TS	8	8	6	8	7	5	6	2	6	8	4	2	5	8

18	35	Ugwuaji TS	7	7	7	5	8	6	6	5	3	4	5	5	3	4
19	39	Ikot Ekpene TS	8	8	6	5	8	6	7	5	2	3	5	5	2	4
20	40	Adiabor TS	9	9	9	9	10	8	9	7	3	2	7	6	3	5

6.2.2 Modelled system sectioning

For analytical expediency, the 48-bus system is sectioned into five regions namely: Shiroro, Oshogbo, Benin, Enugu and Port Harcourt (see Fig. F1 in **Appendix F**). These regions are intentionally sectioned to accommodate the operating sectors of the distribution companies since the sectioning of the distribution sector are for convenience and ease of loads controllability. The modelling of these various regions in NEPLAN is presented in Fig. 6.2 to Fig. 6.6.

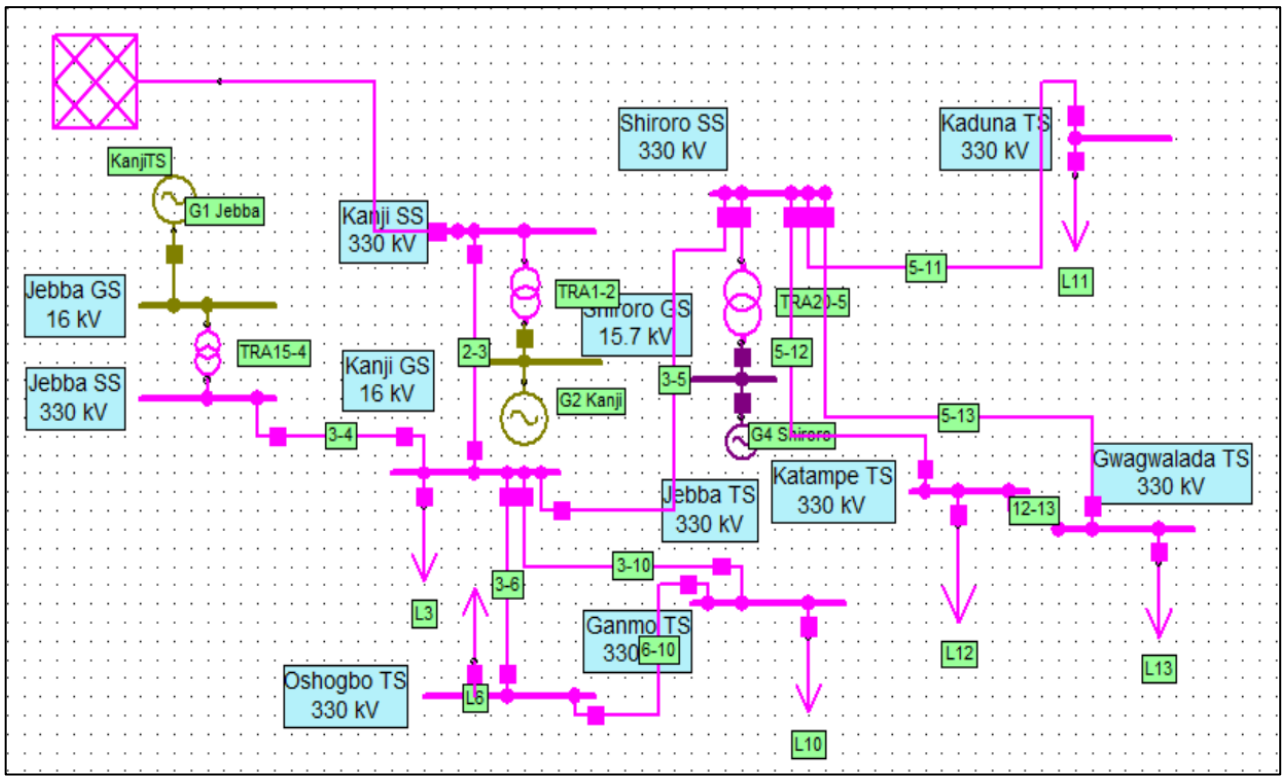

Fig. 6.2. Sectional model of Nigerian 48-bus system showing Shiroro region.

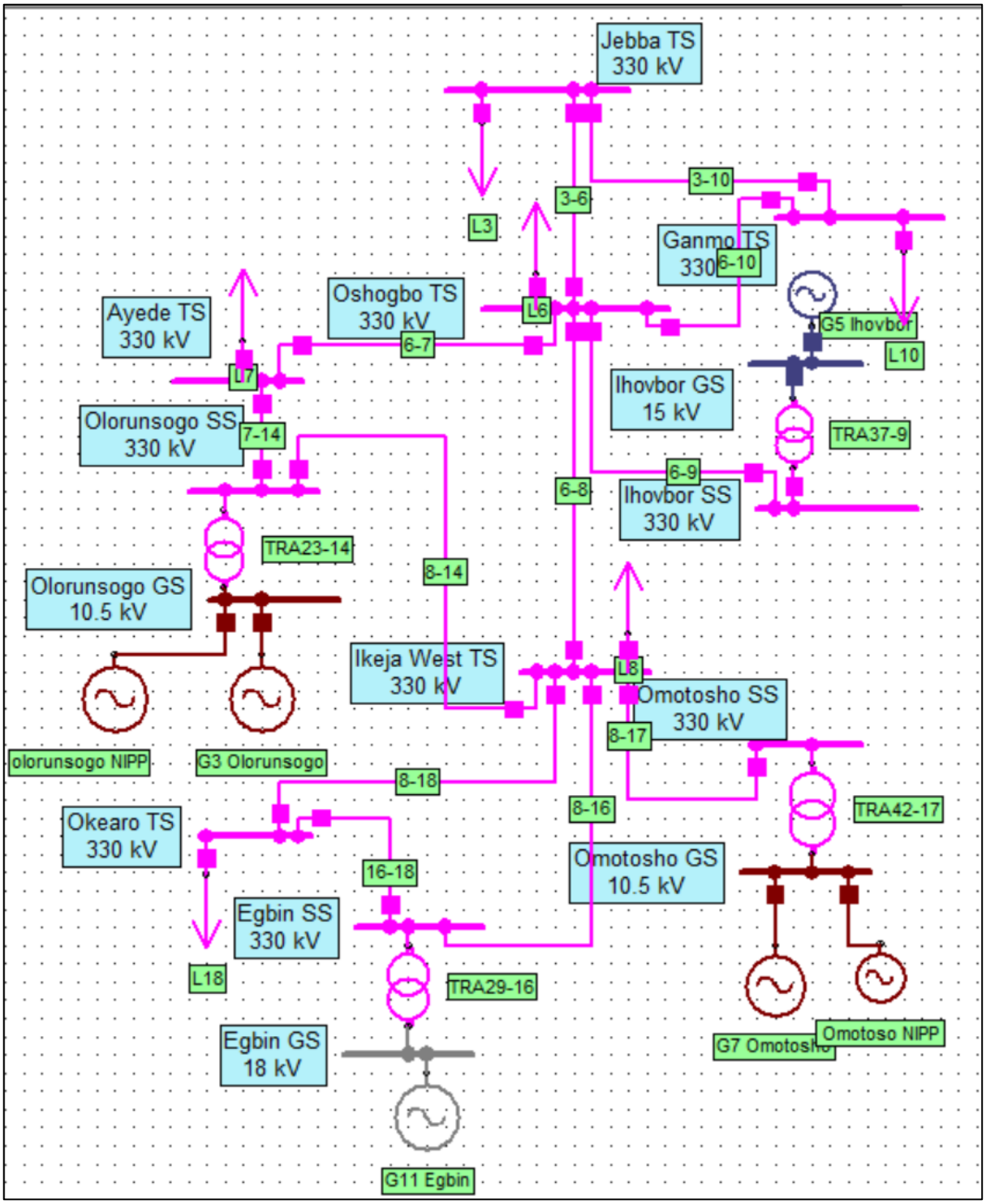

Fig. 6.3. Sectional model of Nigerian 48-bus system showing Oshogbo region.

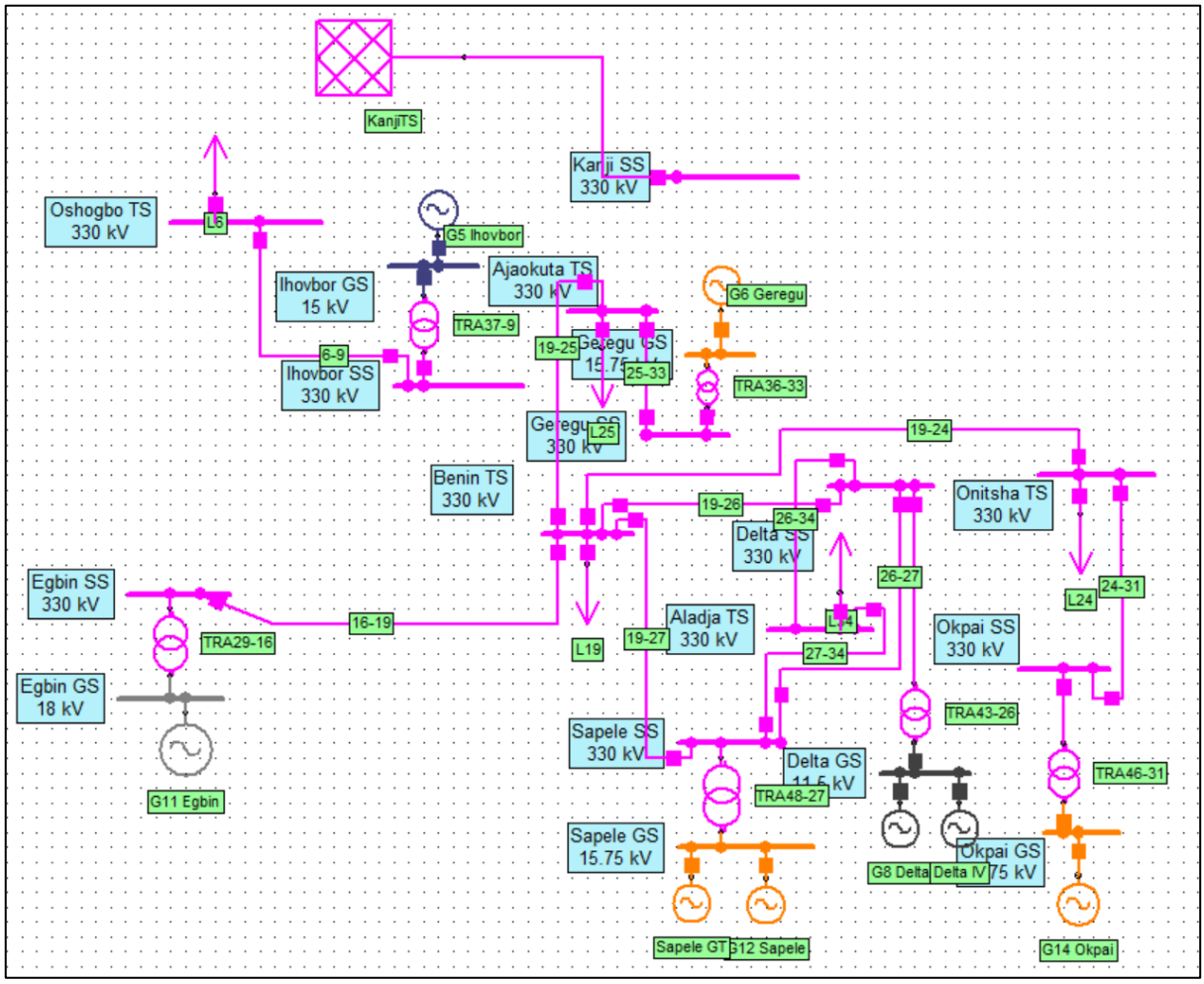

Fig. 6.4. Sectional model of Nigerian 48-bus system showing Benin region.

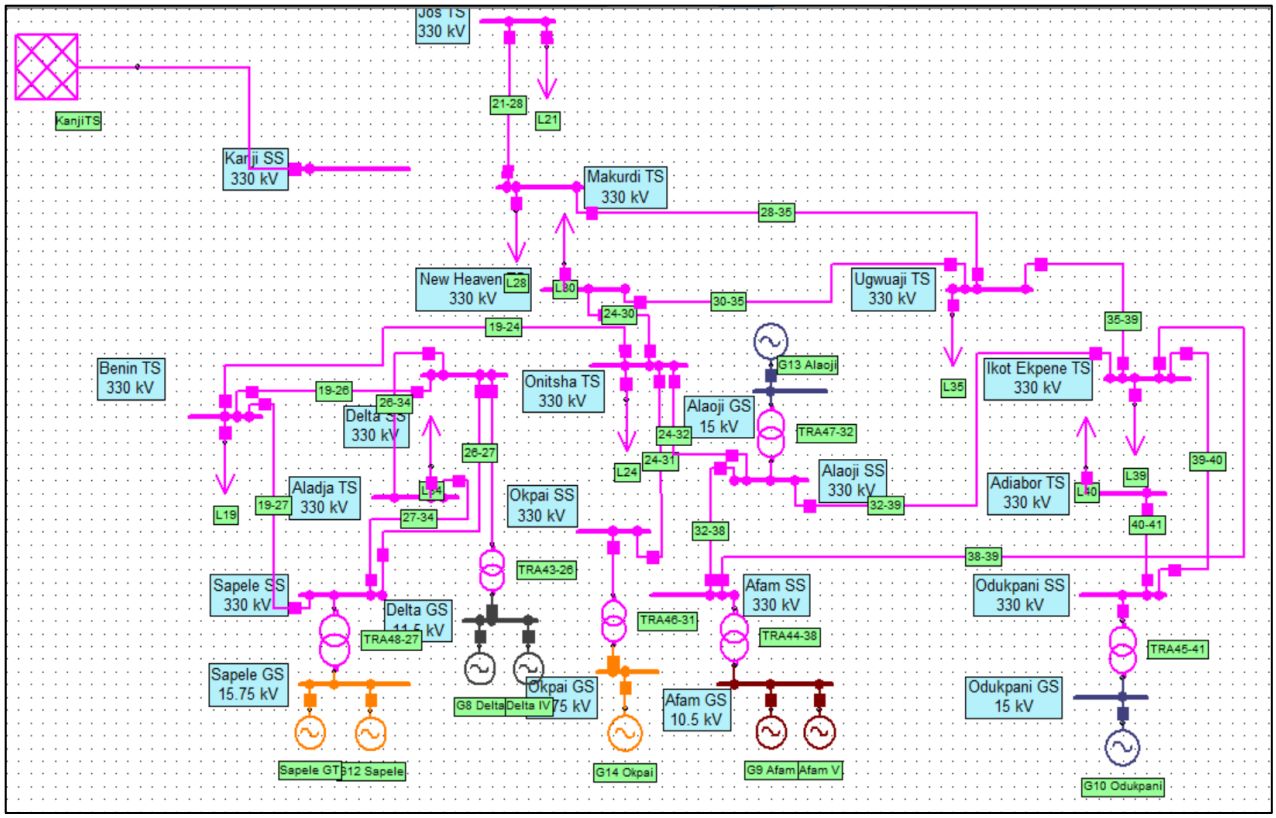

Fig. 6.5. Sectional model of Nigerian 48-bus system showing Enugu region.

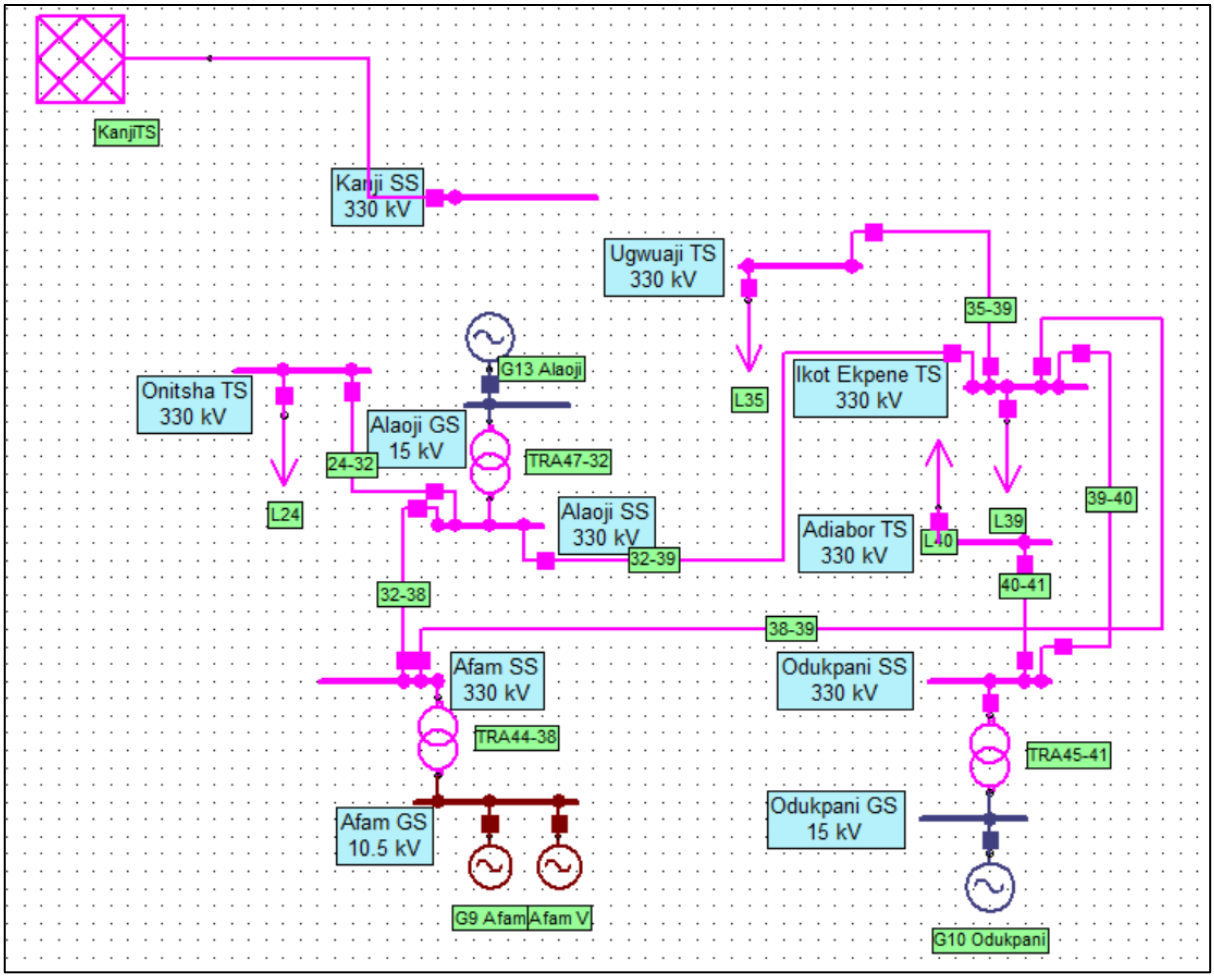

Fig. 6.6. Sectional model of Nigerian 48-bus system showing Port Harcourt region.

Table 6.2 shows the energy generation, energy transfer and the load availability in the different regions. In this study, (see Table 6.3), Abuja, Kaduna and Jos are added to the Shiroro region, while Ibadan, Ikeja and Eko are considered as Oshogbo region.

Table 6.2. Power generation and transfer [217].

	Generation (MW)		**Load (MW)**	**Power Transfer**		
			MW	From	To	MW
1	Ikeja	1349	1250	4	1	965
2	Ibadan	590	1225	4	2	462
3	Abuja	1950	745	4	3	0
4	Benin	2280	1273	4	9	636
5	Kaduna	200	590	8	4	491
6	Jos	100	442	7	4	766
7	Enugu	840	1090	2	1	1286
8	PH	3443	946	3	2	171
9	Eko	0	1320	3	5	1217
10	Kano	9	705	5	10	0
11	Yola	0	309	10	6	0
	Nigeria	10761	9896	5	6	46
	Export	387		6	3	1068
	PV	0		8	7	1296
	Total load	10283		7	6	844
	NIPP	1340		6	11	269
				1	9	258

The 48-bus system comprising of generation, transmission and load buses are sectioned into the various regions as captured in Table 6.3. Also included in Table 6.3 is the potential future PV installation in the different regions. The PV installations closest to the buses are considered to participate directly in the BSR, while the PV installations that are farther from the buses are considered as energy reserves, and by extension deployed as an additional generating capacity of the region. The optimal PV rating is 209 MW, and from Table 6.2, Jos also receives 442 MW from the grid.

Table 6.3. Power generation and consumption regions [217].

S/N	TCN regions and sectors		Bus	Load		Generator
				P (MW)	Q (MVAr)	(MW)
1	Shiroro	Kainji GS G2	1			600
		Kainji SS	2			55
		Jebba TS	3	260	119	
		Jebba SS	4			
		Shiroro SS	5			
		Katampe TS	12	201	107	50
		Shiroro GS G4	20			600
		Jebba GS G1	15			607
		KVK (sokoto)				55
		Gurara (Niger)				30
	Abuja	Ajaokuta TS	25	120	70	
		Lokoja TS	22	100	60	80
		Gwagwalada TS	13	120	65	100
		Geregu SS	33			
		Geregu GS G6	36			634
		Afrinergia Solar				50
		LR Aaron (Abuja) PV				100
		Middle Band Solar (kogi)				100
	Kaduna	Kaduna TS	11	102	51	605
		Anjeed Kafachan Solar (Nassarawa)				100
		EN Consult (Kaduna) PV				100
		Kaduna GS				215
		Kashimbilla (katsina)				40
		Nova Scotia (Jigawa)				80
		NOVA Solar (katsina)				100
		Pan-African (katsina)				75
		Oriental (Jigawa)				50
		Quaint Energy (kaduna)				50
		Zungeru				700

	Bauchi	Jos TS	21	232	110	
		CT cosmos (plateau)				70
		Dadin Kowa (gombe)				39
		Hydro				
		Nigeria Solar Capital				100
		Patners (bauchi)				
2	Osogbo	Oshogbo TS	6	107	56	
		Ayede TS	7	114	68	
		Omotosho SS	17			
		Ganmo TS	10	100	57	
		Omotosho GS G7	42			544
		Olorunsogo SS	14			
		Olorunsogo GS G3	23			695
	Lagos	Ikeja West TS	8	447	195	
		Egbin GS G11	29			1320
		Egbin SS	16			
		Okearo TS	18	220	100	
		PARAS (Ogun)				170
3	Benin	Benin TS	19	257	108	
		Delta SS	26			
		Sapele SS	27			
		Sapele GS G12	48			854
		Delta GS G8	43			881
		Ihovbor SS	9			
		Okpai SS	31			
		Aladja TS	34	182	77	
		Ihovbor GS G5	37			339
		Okpai GS G14	46			440
		AZURA (Edo)				450
4	Enugu	New Heaven TS	30	136	77	
		Makurdi TS	28	160	72	
		Onitsha TS	24	180	85	
		Ugwuaji TS	35	125	69	
		Motir Dusable				100
5	Port	Afam GS G9	44			1316
	Harcourt	Ikot Ekpene TS	39	165	74	
		Afam SS	38			
		Odukpani SS	41			

Odukpani GSG 10	45			338
Alaoji SS	32			
Adiabor TS	40	90	48	
Alaoji GS G13	47			480
Omoku				150
Gbarain (bayelsa)				226
Ibom				390
Rivers				191
Trans-Amadi				100
Egbema (owerri)				339

The spot load parameters of the participating loads is presented in Table 6.4. A three-phase balanced load is assumed, and the load demand is determined as the average value of the total demand of presenting phase(s). $S_l^U, S_l^D, D_l and\ a_l$ are cold load pick-up (CLPU) coefficients used in cold load modelling. Their values of [1.8, 3.0], [1.0, 1.3], [1, 4] and [0.5, 1.5] respectively were generated using the uniform distribution [130]. For the analysis of the network, a weight coefficient of 1.0 for all loads was assumed.

To ensure a systematic load energisation, some of the alternative load switching routes (alternate routes) have the same switching step, hence, utilising the same number of lines to the load. The alternate route to a load for restoration is presented as '**alternate**' route in Table 6.4. During the network model sectioning process, for lines that have multiple loading, delay in switching of the load was incorporated and termed as "**horizon**" as reflected on Table 6.4. This was done to ensure that the effect of CLPU along the various routes has subsided before energising the desired loads.

Table 6.4. Spot load parameter.

S/N	Load bus no		Weight	S_l^y/S_l^p	$D_l(\min)$			a_l
					Main	Alternate	Horizon	
1	3	Jebba TS	1	2.0/1.2	2.0			0.7
2	6	Oshogbo TS	1	1.8/1.1	2.0	3.0		0.8
3	7	Ayede TS	1	2.4/1.1	2.0			1.0
4	8	Ikeja West TS	1	2.5/1.1	2.0			0.7
5	10	Ganmo TS	1	2.3/1.0	3.0		7.0	1.3
6	11	Kaduna TS	1	2.7/1.0	2.0			0.6
7	12	Katampe TS	1	1.8/1.3	2.0		21.0	0.7
8	13	Gwagwalada TS	1	2.1/1.3	3.0		9.0	0.6
9	18	Okearo TS	1	3.0/1.1	2.0		5.0	0.9
10	19	Benin TS	1	2.0/1.2	2.0			0.7
11	21	Jos TS	1	2.0/1.2	3.0			0.7
12	22	Lokoja TS	1	1.8/1.1	3.0	3.0	12.0	0.8
13	24	Onitsha TS	1	2.4/1.1	2.0		7.0	1.0
14	25	Ajaokuta TS	1	2.5/1.1	2.0		6.0	0.7
15	28	Makurdi TS	1	2.3/1.0	4.0			1.3
16	30	New Heaven TS	1	2.7/1.0	3.0			0.6
17	34	Aladja TS	1	3.4/1.3	2.0			0.7
18	35	Ugwuaji TS	1	2.1/1.3	3.0			0.6
19	39	Ikot Ekpene TS	1	3.0/1.1	2.0			0.9
20	40	Adiabor TS	1	2.0/1.2	2.0			0.7

The spot active and reactive loads for the different regions namely: Shiroro, Oshogbo, Enugu, Benin and Port Harcourt with CLPU condition are presented in Fig. 6.7 to Fig. 6.16. The Load plots are based on switching status of Table 6.4, where D_l(min) has a main status and takes into consideration the nearest route to restoration.

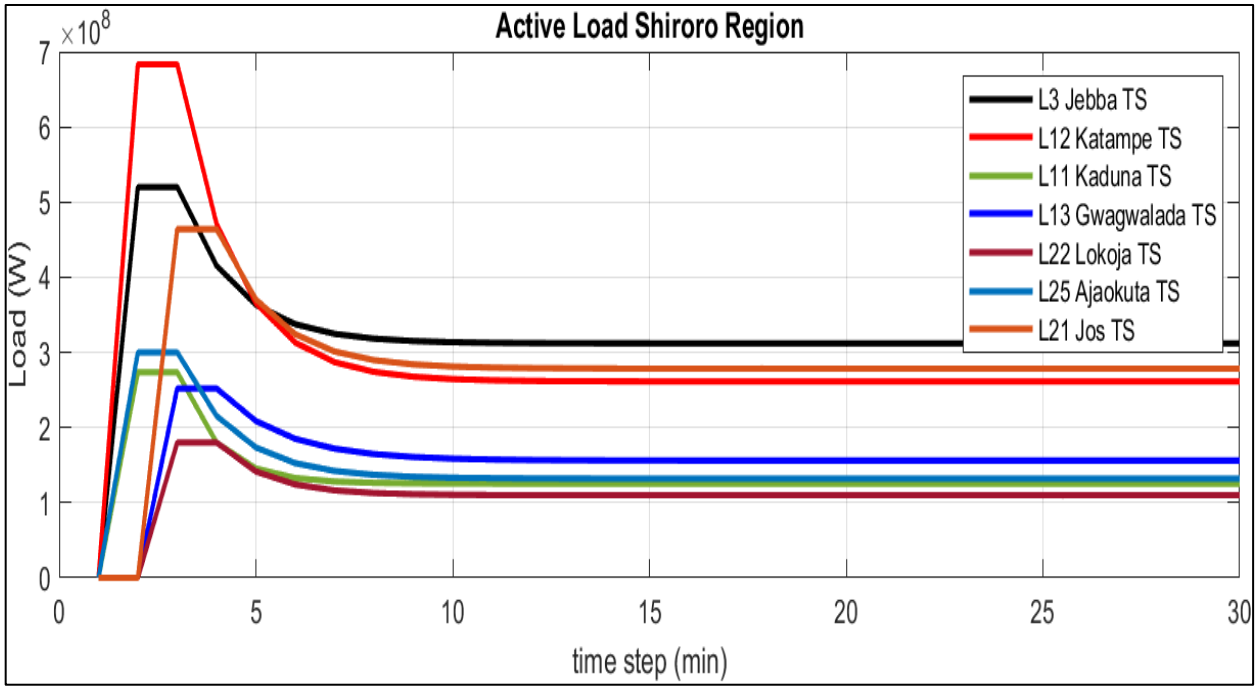

Fig. 6.7. Active loads in Shiroro region.

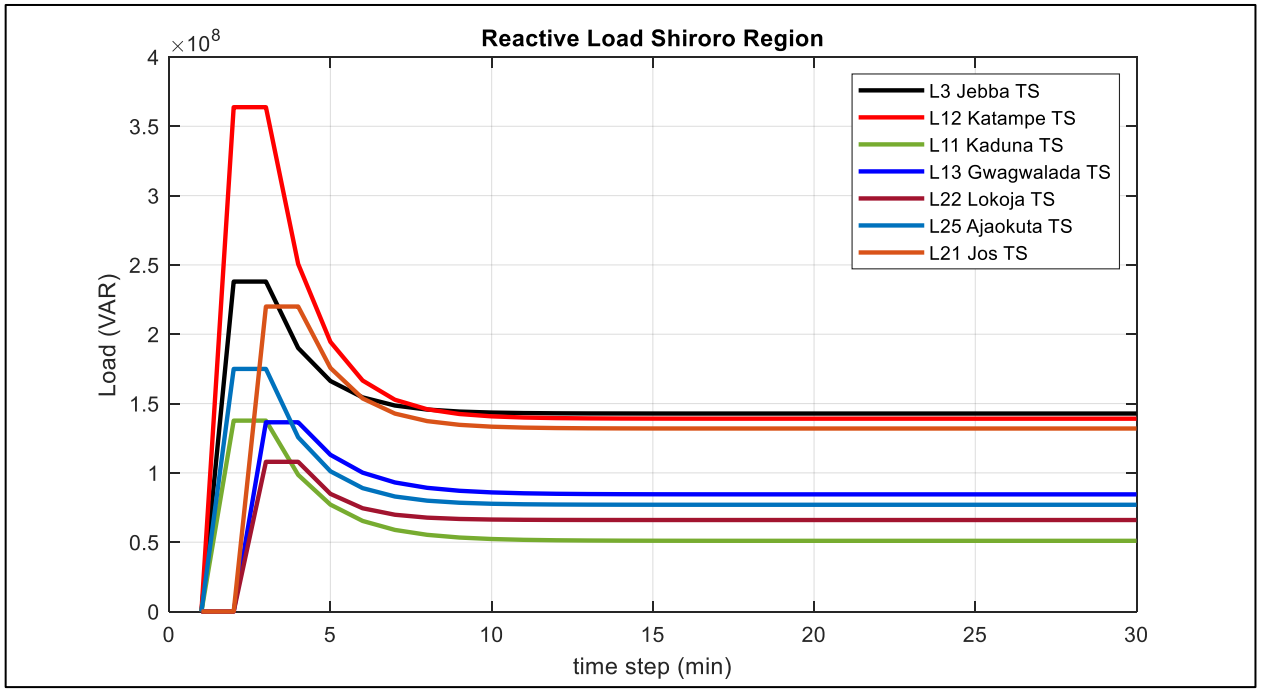

Fig. 6.8. Reactive loads in Shiroro region.

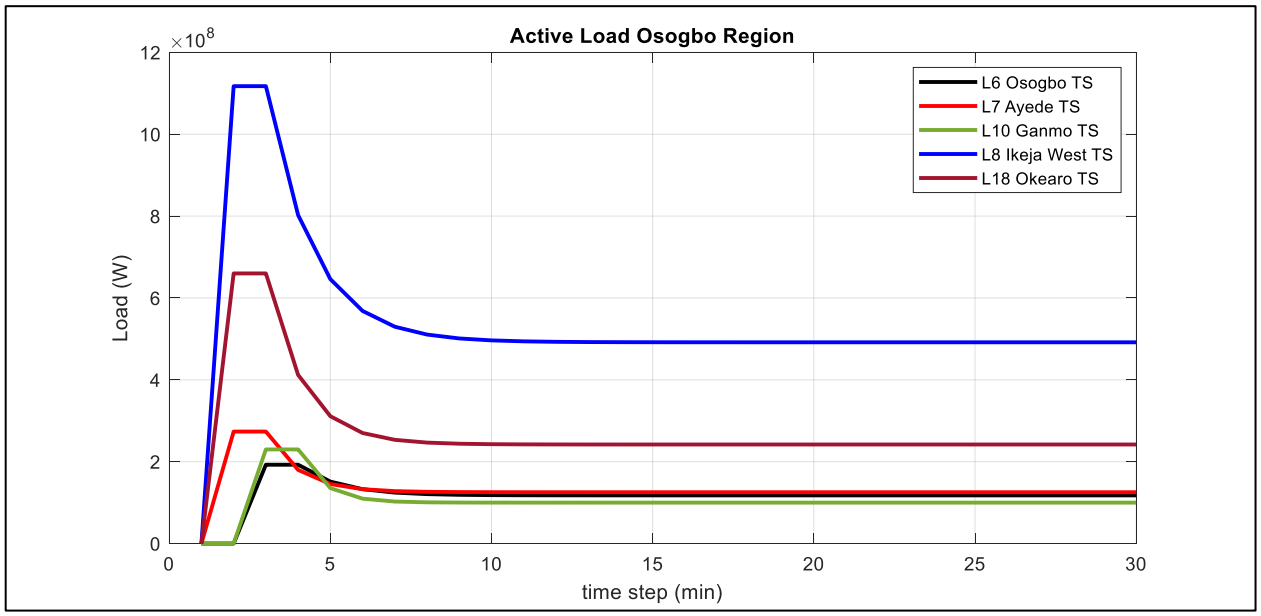

Fig. 6.9. Active loads in Oshogbo region.

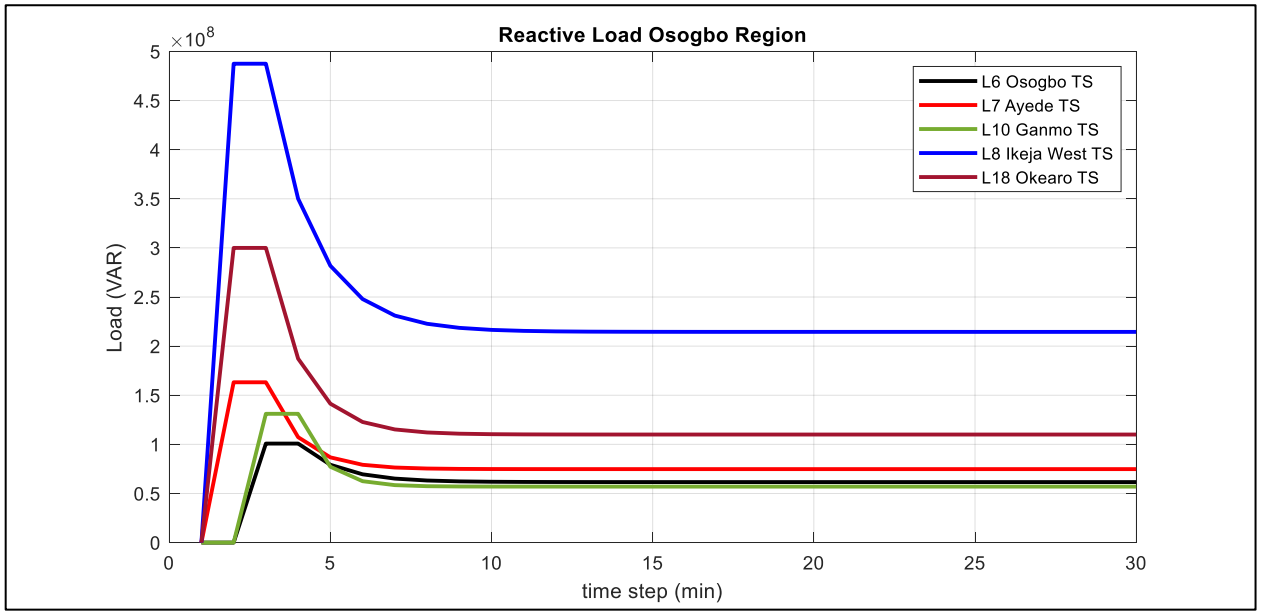

Fig. 6.10. Reactive loads in Oshogbo region.

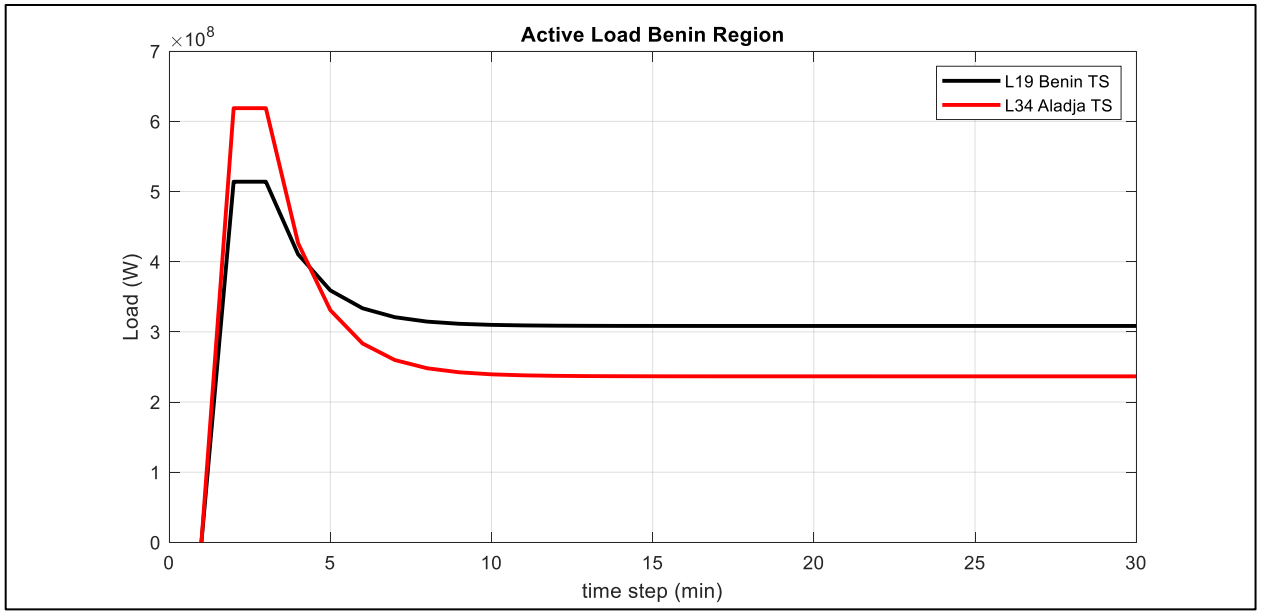

Fig. 6.11. Active loads in Benin region.

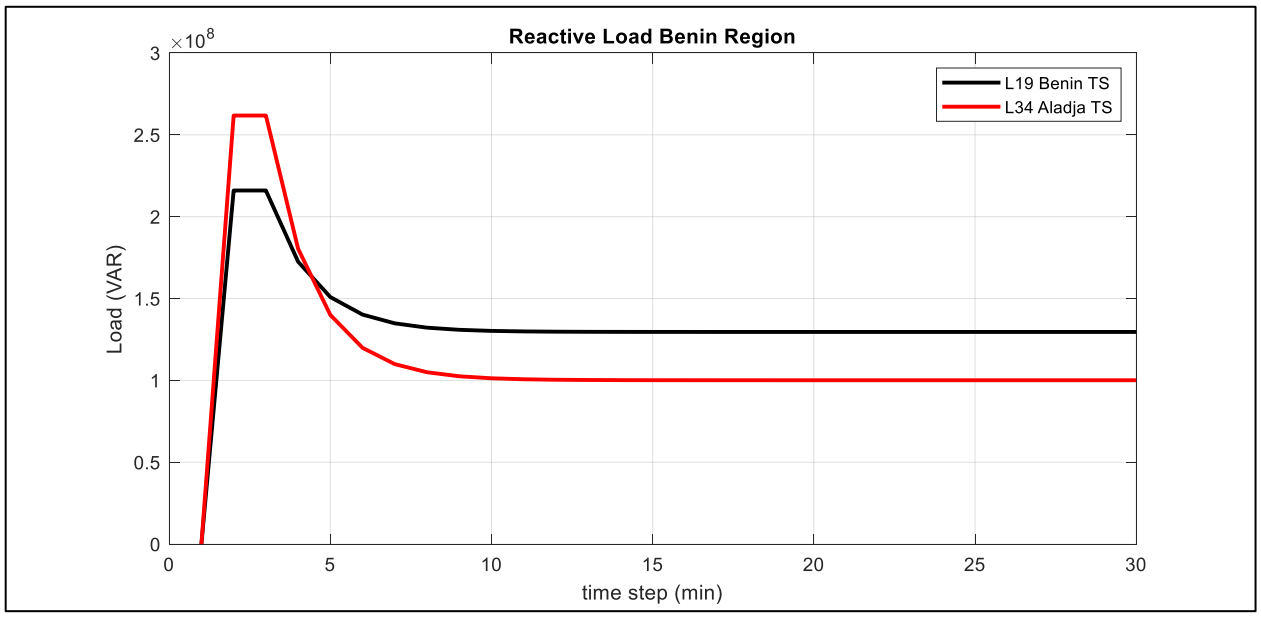

Fig. 6.12. Reactive loads in Benin region.

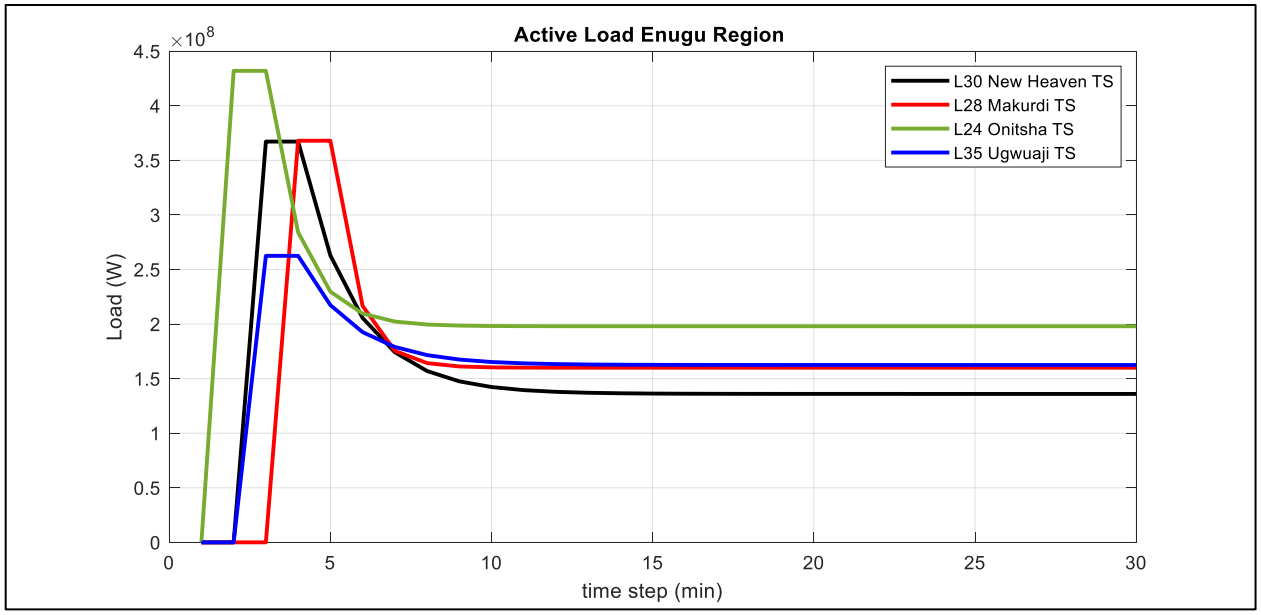

Fig. 6.13. Active loads in Enugu region.

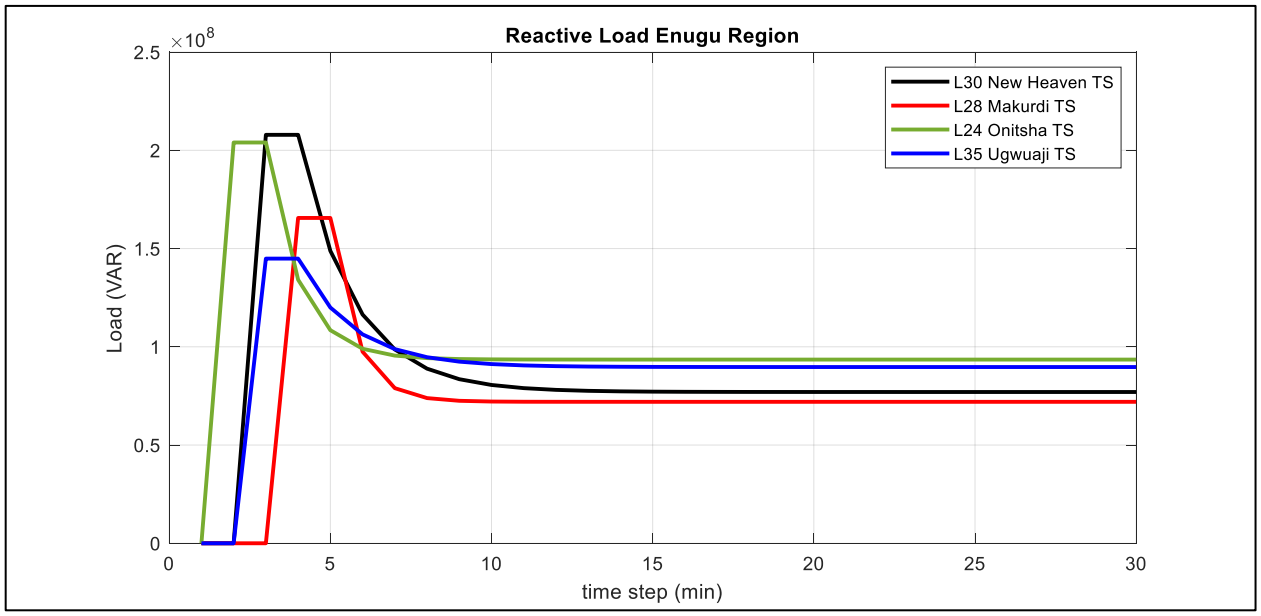

Fig. 6.14. Reactive loads in Enugu region.

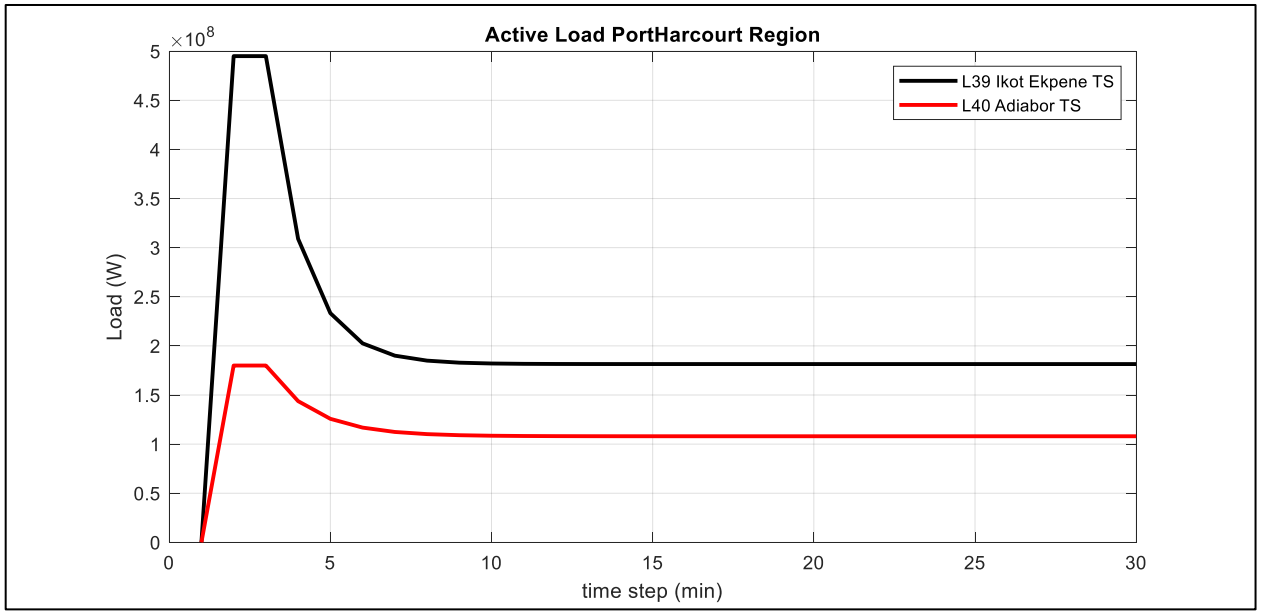

Fig. 6.15. Active loads in Port Harcourt region.

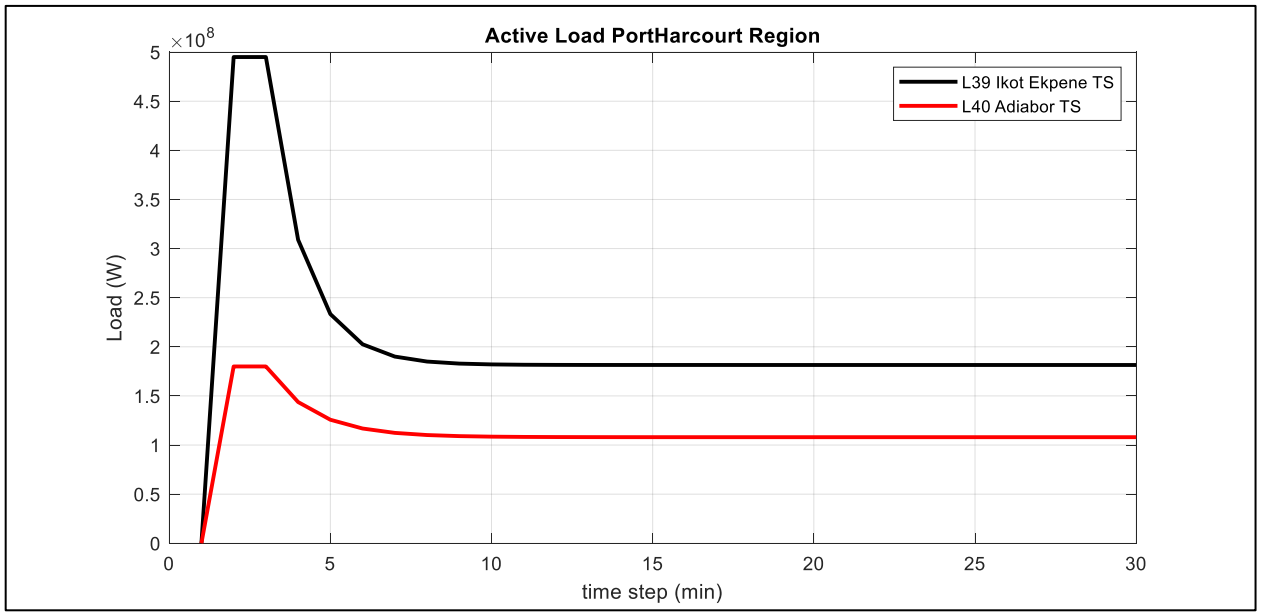

Fig. 6.16. Reactive loads in Port Harcourt region.

The shape of the active and reactive power plot in Fig. 6.7 to Fig. 6.16 can be seen to mimic that of the load restoration plots in section 6.3.1. Since

the objective of the BSR is to ensure the immediate return of normalcy and stability to the system, the power system must meet its demand for reactive power. As the restored load begins to normalise, the active and reactive power is seen to also normalise as it approaches the 15^{th} time step.

6.3 Results Analysis and Discussion

To evaluate the performance of the modelled BSR method, the developed model of the MILP was used to simulate the Nigerian 330 kV 48-bus system. In order to further demonstrate its workability, in the simulated network, dispatchable distributed generations, (renewable DGs - hydro, ESSs, and RCSs) were connected. The simulated results shows that the developed BSR method is capable of generating black start restoration sequences in response to varying operating conditions such as CLPU conditions, and the assistance of PV on the BSR time was assessed. The effect of CLPU on the system restoration while considering a time horizon corresponding to a subsided effect of the CLPU and subsequent PV contributions to the restoration process was also assessed.

The performance characteristics of voltage and frequency in response to the loading during restoration was monitored in the different regions noting that energy transfer exist between the regions. As highlighted in **Chapter 2**, the transmission region is different from the distribution regions in terms of overlapping boundaries, as can be seen in the case of Shiroro and Kaduna existing in the transmission region (see **Appendix F**), while it's being sectioned into Kaduna and Abuja in the distribution region. The same is applicable for Oshogbo and Lagos transmission regions which is being sectioned to Lagos, Ibadan and Ikeja for the distribution regions. Irrespective of the sectioning, the grid is designed to ensure that all

generated power including those of the independent power plant (IPP) are fed to the grid for subsequent distribution by the distribution companies.

The operation and dispatch of power in the transmission system is aligned with the Grid Code. In Nigeria, the nominal system frequency is 50 Hz, however, a narrow operating band of +/- 0.5% (49.75 – 50.25 Hz) and +/- 2.5% (48.75 – 51.25 Hz) is permissible during normal and under system stress conditions respectively. Under normal operating conditions, the voltage limits of the 330 kV network are 0.8 p.u. lower limit and 1.1 p.u. upper limit and for 132 kV network are 0.8 p.u. and 1.15 p.u. [217]. For most regions, the various simulation results obtained in subsequent sections are within these stipulated frequencies and voltages limits, hence maintaining the security and integrity of the transmission system.

6.3.1 Load restoration in Shiroro region

The Shiroro region partial network model is shown in Fig. 6.2 with additional information given in Table 6.3. The voltage and frequency characteristics of the buses are shown in Fig. 6.17 and Fig. 6.18 respectively. In Fig. 6.17, Katampe TS has the highest voltage drop with a value of 0.3897 p.u. and settling at a value of 0.6449 p.u., while Ajaokuta TS has the lowest drop with a value of 1.0450 p.u. on loading and settling at a value of 1.0478 p.u.

The highest frequency dip is recorded at Katampe TS with a dip value of -2.7700 Hz on loading and settling at a value of -2.7652 Hz, while the lowest value is recorded at Ajaokuta TS with a value of -0.0292 Hz on loading and settling at a value of -0.0194 from the system frequency of 50 Hz (Fig. 6.18). For the restoration of load L22 at Lokoja TS, the main route of 22a (supplied from bus 25) gives better characteristics on loading and settling

value than the alternate route of 22b (supplied from bus 13). The region's performance characteristics upon loading is presented in Table 6.5.

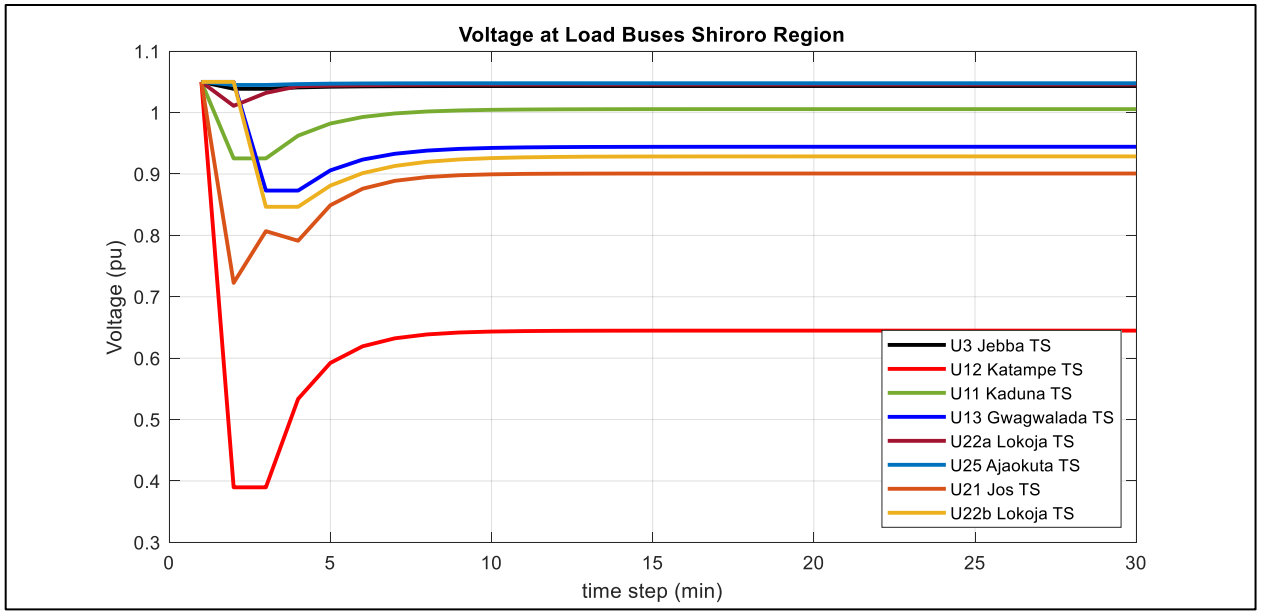

Fig. 6.17. Voltage at load buses for Shiroro region.

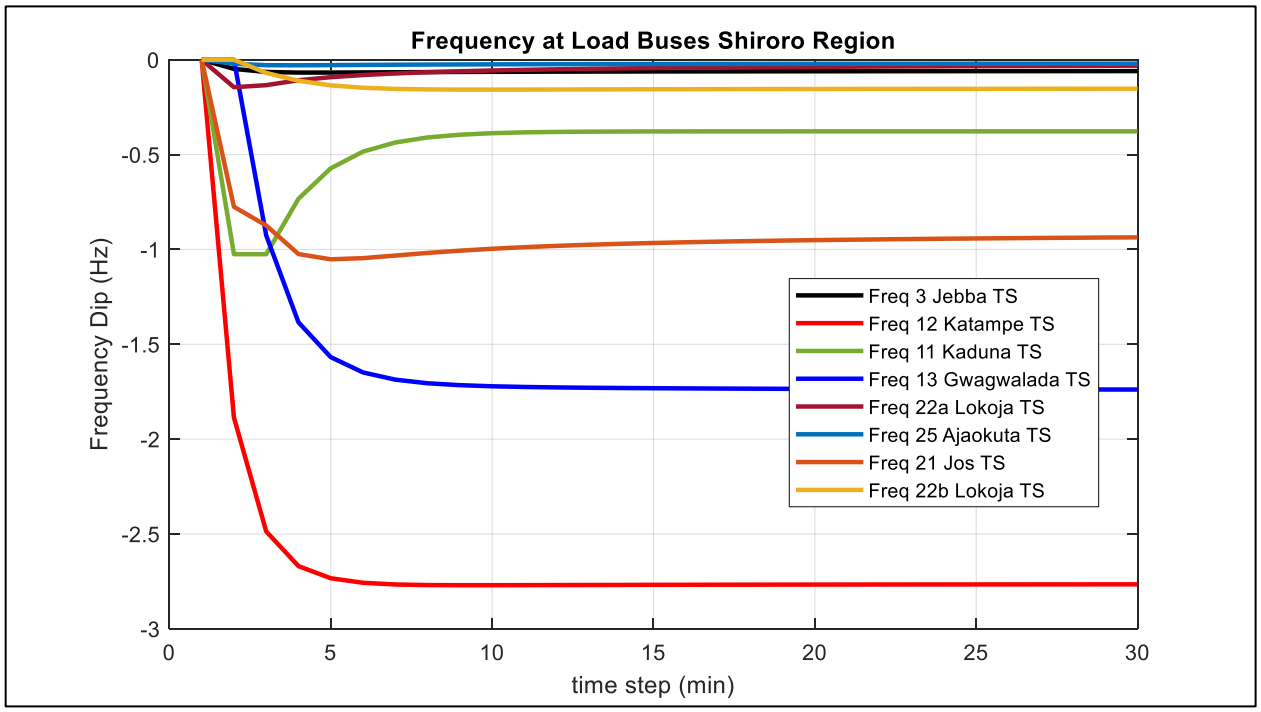

Fig. 6.18. Frequency dip at load buses for Shiroro region.

Table 6.5. Shiroro region performance characteristics on loading.

S/N	Bus no.	Load bus	Voltage (p.u.)		Frequency (dip from 50 Hz)	
			Maximum drop	Settling value	Maximum dip	Settling value
1	3	Jebba TS	1.0388	1.0433	-0.0676	-0.0599
2	12	Katampe TS	0.3897	0.6449	-2.7700	-2.7652
3	11	Kaduna TS	0.9254	1.0057	-1.0249	-0.3774
4	13	Gwagwalada TS	0.8730	0.9443	-1.7434	-1.7434
5	22a	Lokoja TS	1.0110	1.0456	-0.1448	-0.0225
6	22b	Lokoja (alternate)	0.8466	0.9287	-0.1574	-0.1506
7	25	Ajaokuta TS	1.0450	1.0478	-0.0292	-0.0194
8	21	Jos TS	0.7226	0.9008	-1.0519	-0.9158

6.3.2 Load restoration in Oshogbo region

In Fig. 6.3, the partial network model of the Oshogbo region is presented along with additional information provided in Table 6.3. The voltage and frequency characteristics of the buses are shown in Fig. 6.19 and Fig. 6.20 respectively, while the performance characteristics of the region upon loading is presented in Table 6.6. Oshogbo TS has the highest voltage drop, with a value of 0.3844 p.u. and settling at a value of 0.8545 p.u., while Okearo TS has the lowest voltage drop with a value of 0.9475 p.u. on loading and settling at a value of 1.0136 p.u..

Ayede TS with a dip value of -1.6969 Hz on loading, records the highest frequency dip which eventually settles to a value of -1.5208 Hz from the system frequency of 50 Hz. The lowest frequency value is recorded at Ganmo TS with a value of -0.5134 Hz on loading and settles at a value of -0.0750 Hz as depicted in the frequency dip at load buses for Oshogbo region in Fig. 6.20. For the restoration of load L6 at Oshogbo TS, the alternate route of 6d (supplied from bus 9) presents better characteristics on loading and settling value than the main route of 6a (supplied from bus 7).

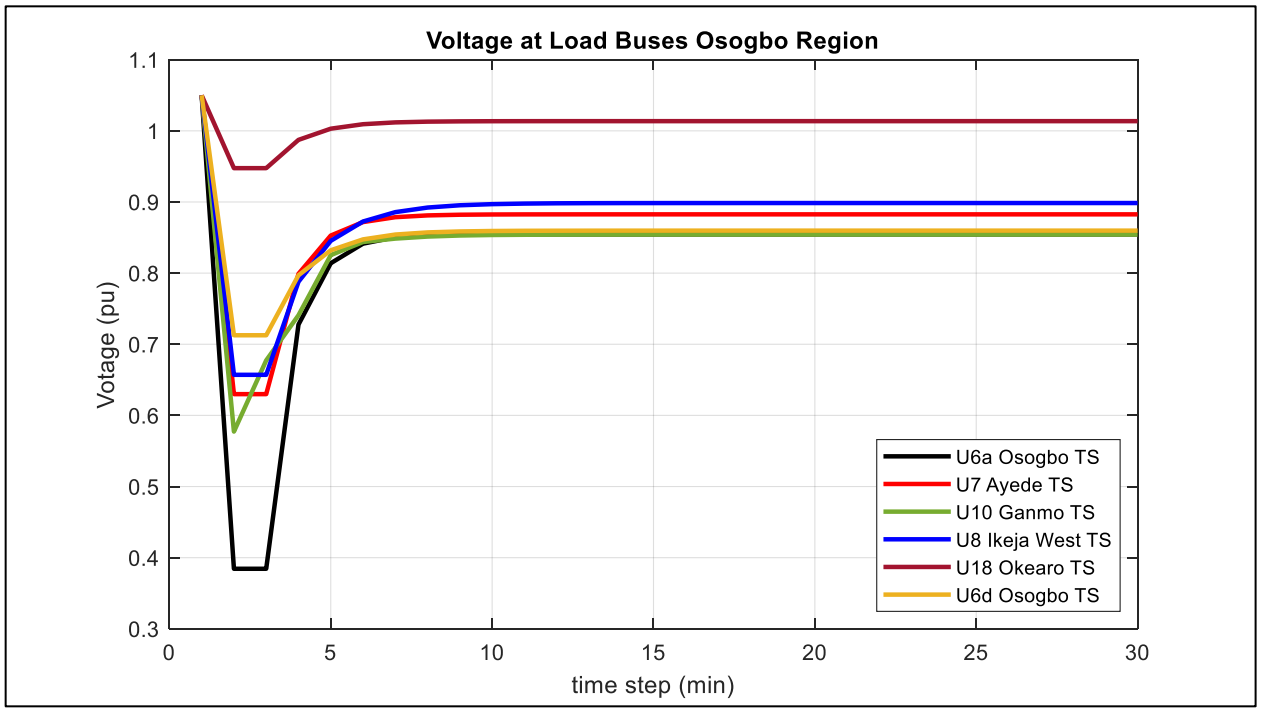

Fig. 6.19. Voltage at load buses for Oshogbo region.

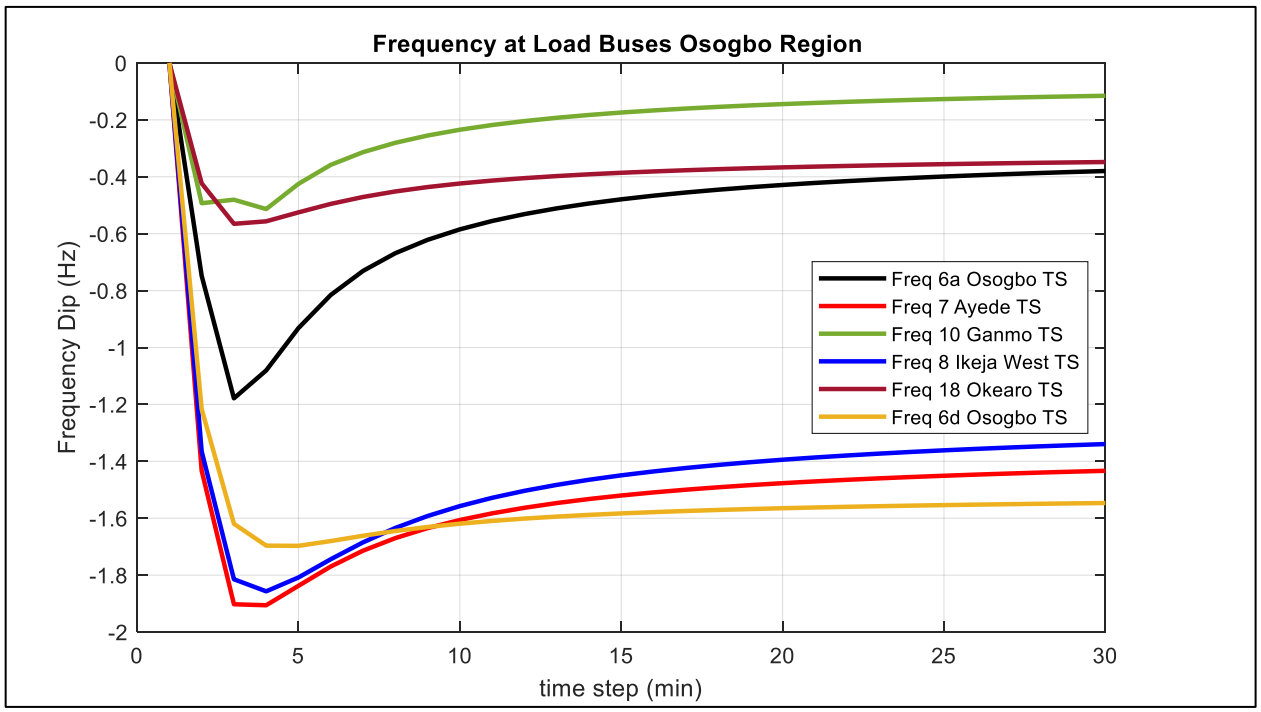

Fig. 6.20. Frequency dip at load buses for Oshogbo region.

Table 6.6. Oshogbo region performance characteristics on loading.

S/N	Bus no.	Load bus	Voltage (p.u.)		Frequency (dip from 50 Hz)	
			Maximum drop	Settling value	Maximum dip	Settling value
1	6a	Oshogbo TS	0.3844	0.8545	-1.1785	-0.3133
2	6d	Oshogbo (alternate)	0.7127	0.8597	-1.6969	-1.5208
3	7	Ayede TS	0.6299	0.8836	-1.9058	-1.3722
4	10	Ganmo TS	0.5772	0.8542	-0.5134	-0.0750
5	8	Ikeja West TS	0.6570	0.8985	-1.8568	-1.2620
6	18	Okearo TS	0.9475	1.0136	-0.5653	-0.3217

6.3.3 Load restoration in Benin region

The model of the Benin region partial network is captured in Fig. 6.4 with the corresponding additional information tabulated in Table 6.3. The respective voltage and frequency characteristics of the buses are shown in Fig. 6.21 and Fig. 6.22. As illustrated in Fig. 6.21, Benin TS experiences the highest voltage drop, with a value of 0.6481 p.u. and settling at a value of 0.8325 p.u., while Aladja TS has the lowest voltage drop with a value of 0.6766 p.u. on loading and settling at a value of 0.9252 p.u. Also, as seen in the frequency dip at load buses for Benin region Fig. 6.22., the highest frequency dip is recorded at Benin TS with a dip value of -1.9457 Hz on loading and settling at a value of -1.7127 Hz, while the lowest value is recorded at Aladja TS with a value of -1.7700 Hz on loading and settles at a value of -1.0648 Hz from the system frequency of 50Hz. The performance characteristics of Benin region upon loading is captured in Table 6.7.

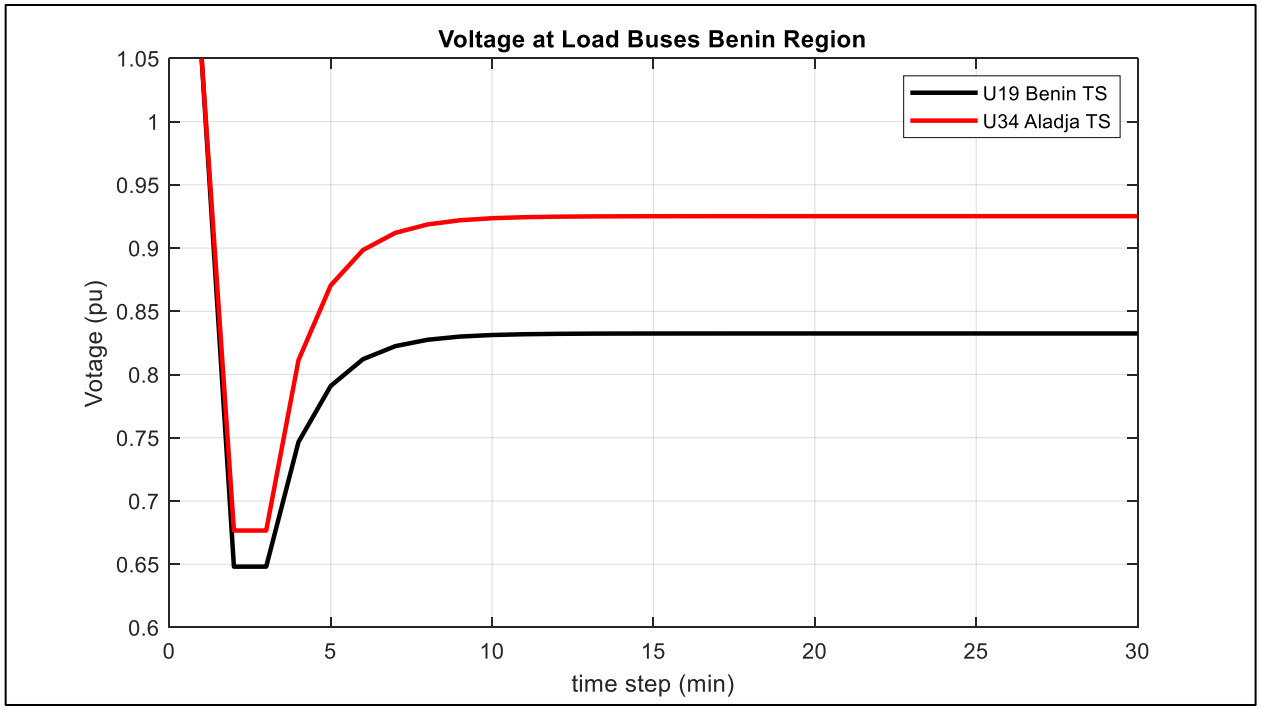

Fig. 6.21. Voltage at load buses for Benin region.

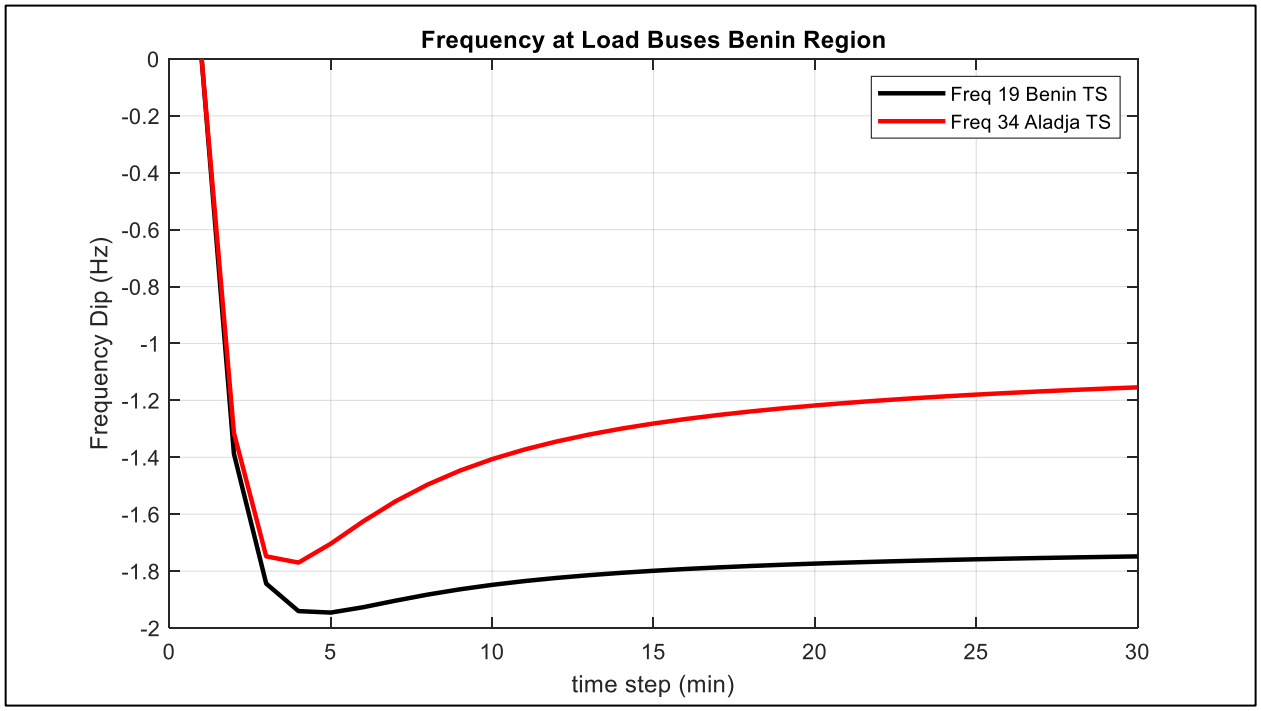

Fig. 6.22. Frequency dip at load buses for Benin region.

Table 6.7. Benin region performance characteristics on loading.

S/N	Bus no.	Load bus	Voltage (p.u.)		Frequency (dip from 50 Hz)	
			Maximum drop	Settling value	Maximum dip	Settling value
1	19	Benin TS	0.6481	0.8325	-1.9457	-1.7127
2	34	Aladja TS	0.6766	0.9252	-1.7700	-1.0648

6.3.4 Load restoration in Enugu region

The partial network model of Enugu region as well as the required additional information is presented in Fig. 6.5 and Table 6.3 respectively. In Fig. 6.23 and Fig. 6.23 respectively, the voltage and frequency characteristics of the buses are plotted. As can be seen in Fig. 6.23, Onitsha TS main route has the highest voltage drop, with a value of 0.2096 p.u. and settling at a value of 0.7857 p.u., while Onitsha alternate route 2 TS has the lowest voltage drop with a value of 0.9382 p.u. on loading and settling at a value of 1.003 p.u.

The highest frequency dip is recorded at Onitsha TS main route with a dip value of -2.7428 Hz on loading and settling at a value of -2.0361 Hz, while the lowest value is recorded at Onitsha TS alternate route 2 with a value of -0.5134 Hz on loading and settles at a value of -0.0750 Hz from the system frequency of 50 Hz, as captured in frequency dip at load buses for Enugu region Fig. 6.24. For the restoration of load L24 at Onitsha TS, the alternate route of 24c (supplied from bus 31) gives better characteristics on loading and settling value than the main route of 22a (supplied from bus 32). In restoring the load at Makurdi TS, the main route of 28a (supplied from bus 21) presents better characteristics on loading and settling value than the main route of 28b (supplied from bus 35). The performance characteristics of the region upon loading and settling is presented in Table 6.8.

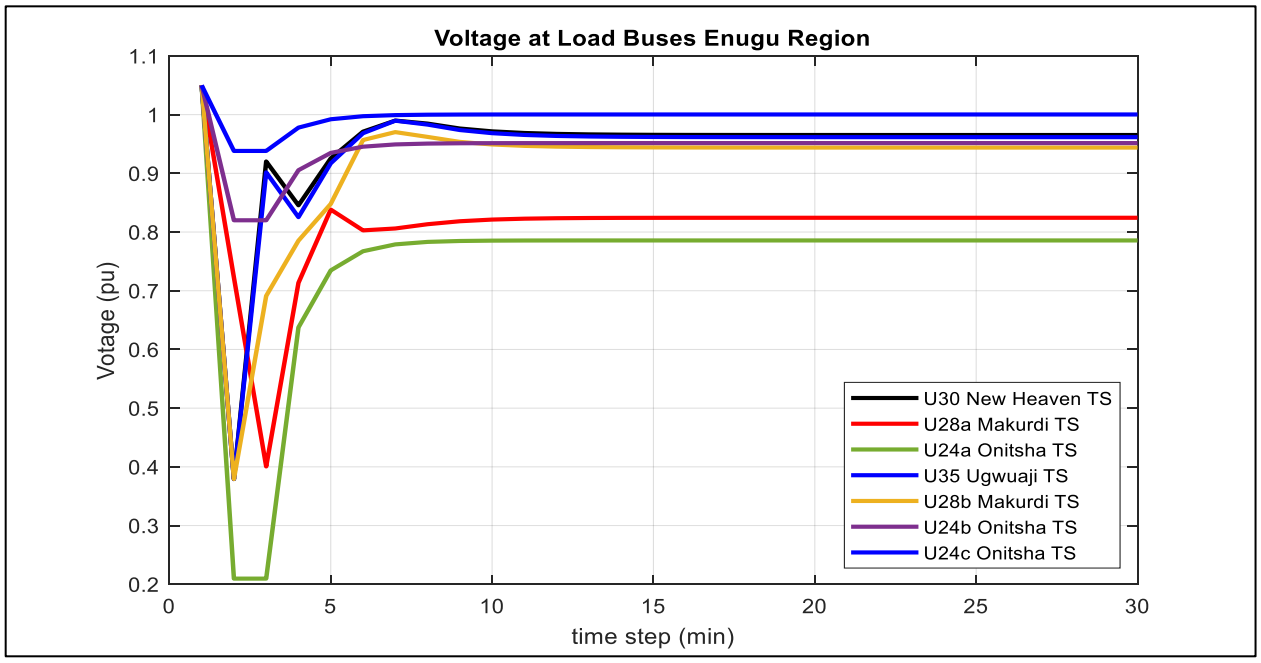

Fig. 6.23. Voltage at load buses for Enugu region.

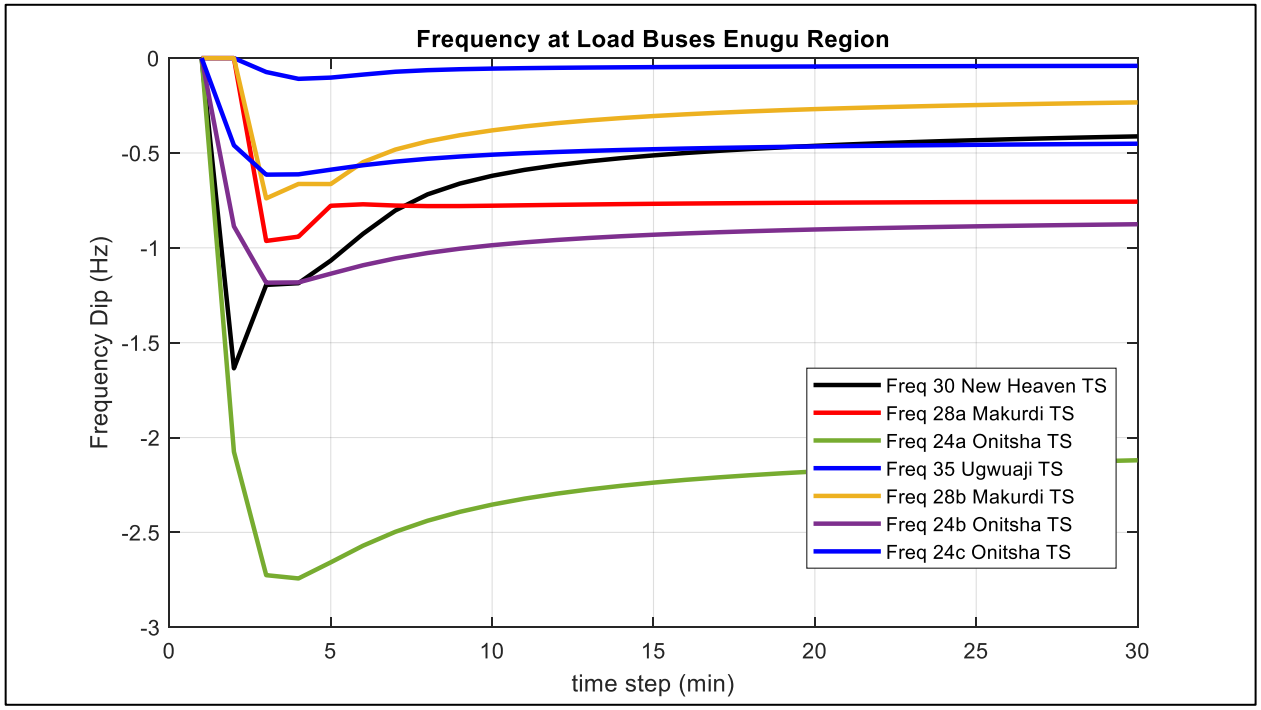

Fig. 6.24. Frequency dip at load buses for Enugu region.

Table 6.8. Enugu region performance characteristics on loading.

S/N	Bus no.	Load bus	Voltage (p.u.)		Frequency (dip from 50 Hz)	
			Maximum drop	Settling value	Maximum dip	Settling value
1	24a	Onitsha TS	0.2096	0.7857	-2.7428	-2.0361
2	24b	Onitsha (alternate1)	0.8200	0.9515	-1.1836	-0.8386
3	24c	Onitsha (alternate2)	0.9382	1.003	-0.6143	-0.4309
4	28a	Markurdi TS	0.4007	0.8243	-0.9635	-0.7488
5	28b	Markurdi (alternate)	0.3792	0.9439	-0.7392	-0.1858
6	30	New Heaven TS	0.3792	0.9653	-1.6352	-0.3430
7	35	Ugwuaji TS	0.3792	0.9616	-0.1092	-0.0364

6.3.5 Load restoration in Port Harcourt region

Model of the Port Harcourt region partial network is shown in Fig. 6.6 with additional information provided in Table 6.3. Fig. 6.25 and Fig. 6.26 show the voltage and frequency characteristics of the buses respectively while the region's performance characteristics upon loading is captured in Table 6.9. In Fig. 6.25, Ikot Ekpene TS main route has the highest voltage drop with a value of 0.6466 p.u. and settling at a value of 0.9228 p.u., while Ikot Ekpene alternate route 2 TS has the lowest drop with a value of 0.9515 p.u. on loading and settling at a value of 1.0150 p.u.

From Fig. 6.26, the highest frequency dip is recorded at Ikot Ekpene TS main route with a dip value of -1.8486 Hz on loading and settling at a value of -1.0820 Hz, while the lowest value is recorded at Ikot Ekpene TS alternate route 2 with a value of -0.5447 Hz on loading and settles at a value of -0.3354 Hz from the system frequency of 50Hz. When considering the restoration of load L39 at Ikot Ekpene TS, the alternate route 2 of 39c (supplied from bus 32) shows a better characteristics on loading and settling

value than the main route of 39a (supplied from bus 38) and alternate route 1 of 39b (supplied from bus 40).

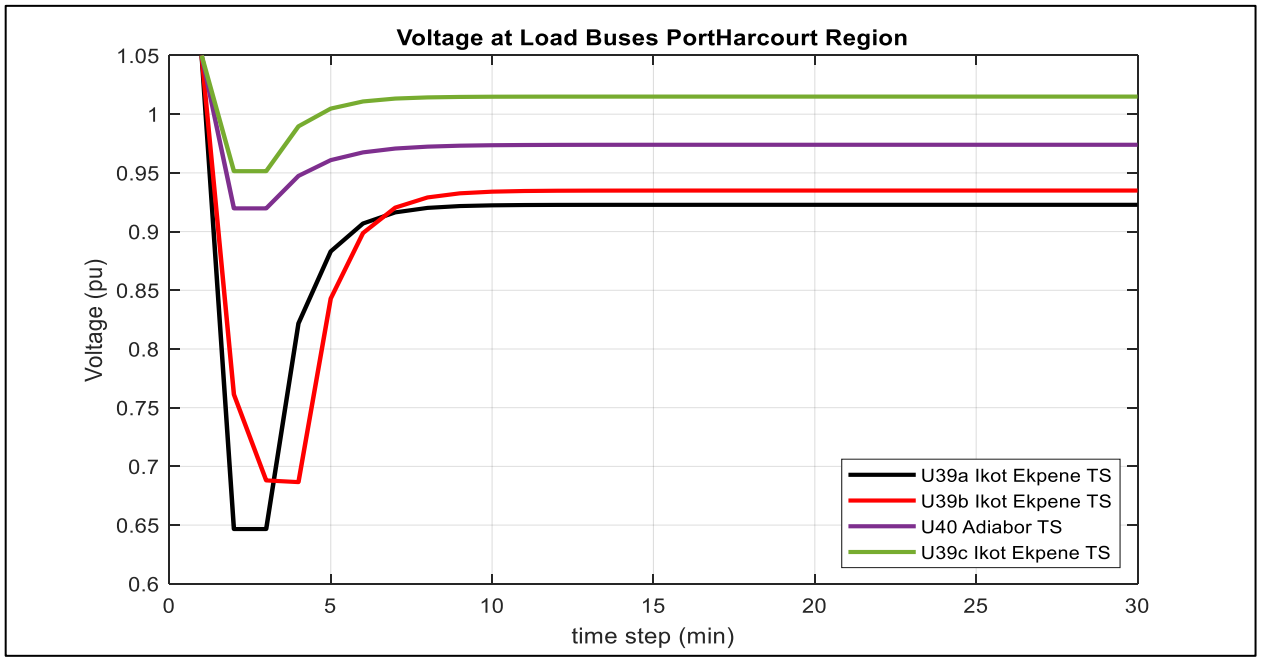

Fig. 6.25. Voltage at load buses for Port Harcourt region.

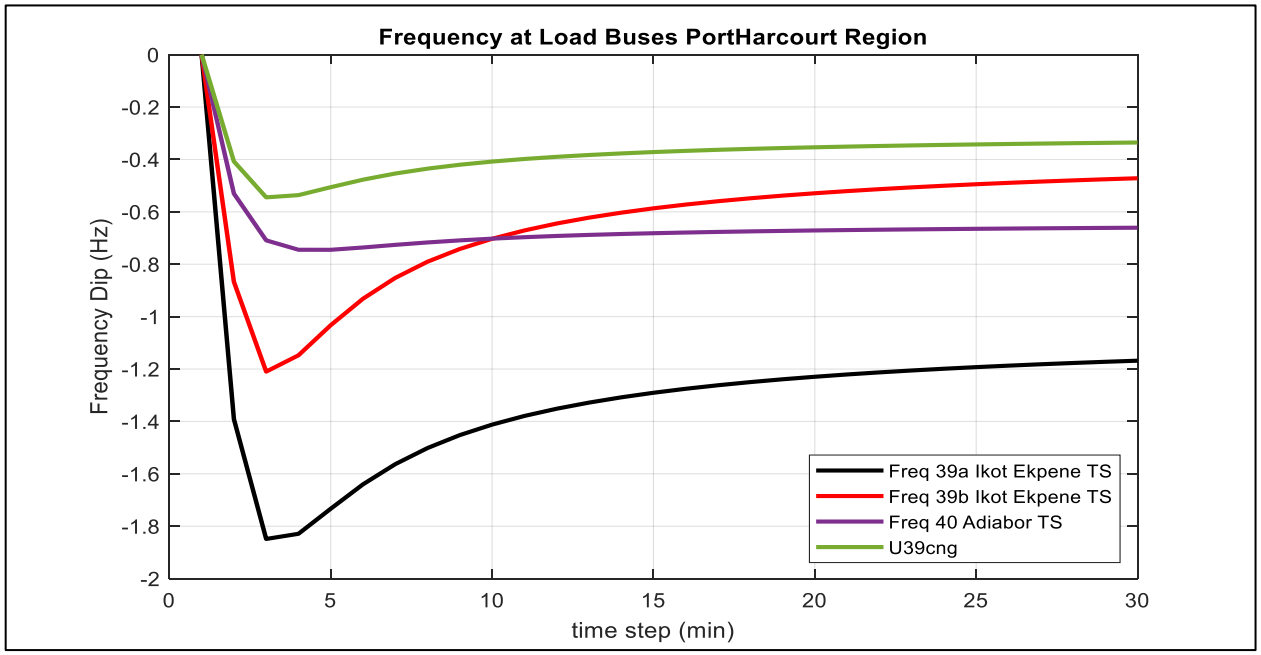

Fig. 6.26. Frequency dip at load buses for Port Harcourt region.

Table 6.9. Port Harcourt region performance characteristics on loading.

S/N	Bus no.	Load bus	Voltage (p.u.)		Frequency (dip from 50 Hz)	
			Maximum drop	Settling value	Maximum dip	Settling value
1	39a	Ikot Ekpene TS	0.6466	0.9228	-1.8486	-1.0820
2	39b	Ikot Ekpene (alternate1)	0.6881	0.9350	-1.2099	-0.3921
3	39c	Ikot Ekpene (alternate2)	0.9515	1.0150	-0.5447	-0.3354
4	40	Adiabor TS	0.9198	0.9739	-0.7448	-0.6458

6.4 Restoration Considering the Horizon

Due to the nature of CLPU characteristics settling at a load value at a particular time step, the sequence of the restoration can be adjusted to ensure that energy availability for restoration is maximised. With this consideration, there is a tradeoff on time before restoration since loads can be restored successively depending on energy consumption of the previous restored load at the anticipated time of restoration.

6.4.1 Restoration in Shiroro region considering the horizon

The voltage and frequency characteristics of the Shiroro region buses are shown in Fig. 6.27 and Fig. 6.28 respectively. In Fig. 6.27, Katampe TS has the highest voltage drop, with a value of 0.3897 p.u. and settling at a value of 0.6449 p.u., while Ajaokuta TS has the lowest drop with a value of 1.0450 p.u. on loading and settling at a value of 1.0478 p.u. These values are the same as those without the horizon. For the frequency characteristics, the highest dip value is recorded at Katampe TS with a dip value of -2.2478 Hz

on loading and settling at a value of -2.2478 Hz from the system frequency of 50Hz. The lower frequency dip value is as a result of a longer time step needed for steady state value to be recorded.

In the restoration process of the load L13 at Gwagwalada TS, the model with horizon shows a greater voltage drop from a value of 0.8253 p.u. to 0.6494 p.u. Nonetheless, in the restoration of load Lokoja TS, a better voltage performance is recorded with a value of 1.0472 p.u., when compared to the previous value of 1.0110 p.u. without the horizon. However, when considering the alternate restoration route, the performance is contrary as the voltage drop value reduces to a value of 0.4674 p.u. as opposed to a value of 0.8466 p.u. without the horizon. Shiroro's region performance characteristics on loading considering the horizon is presented in Table 6.10.

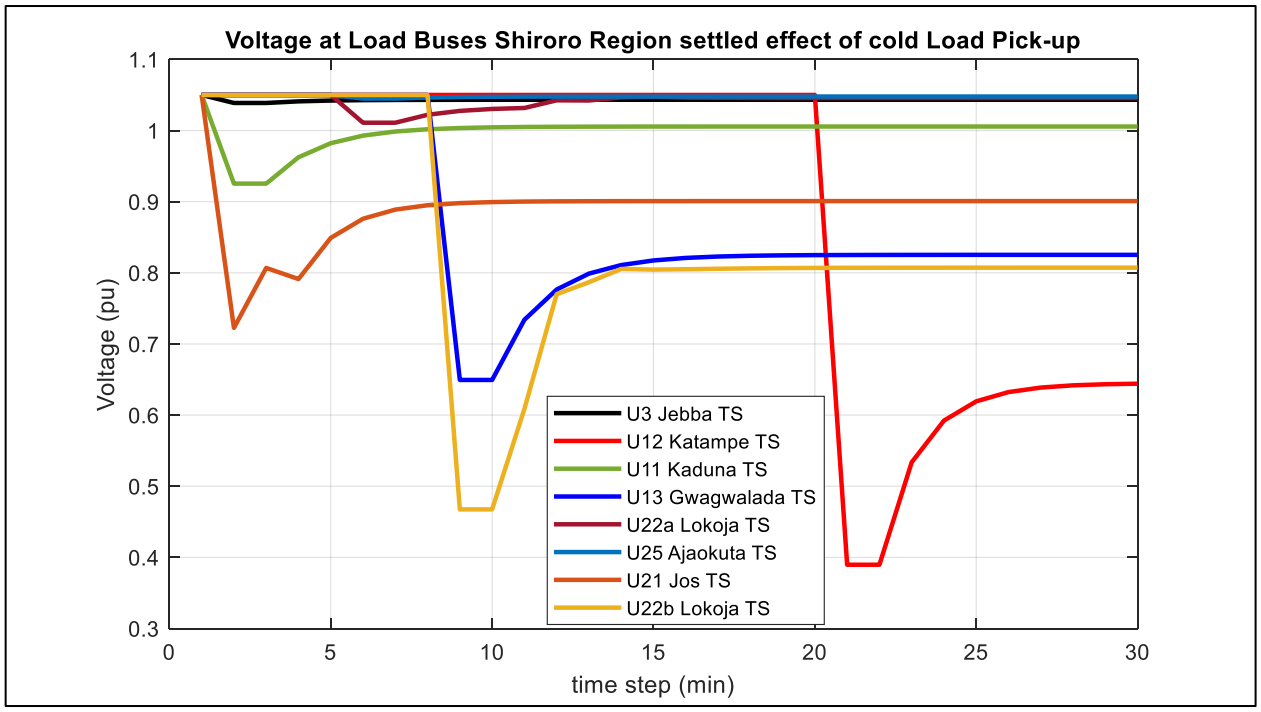

Fig. 6.27. Voltage at load buses for Shiroro region with horizon.

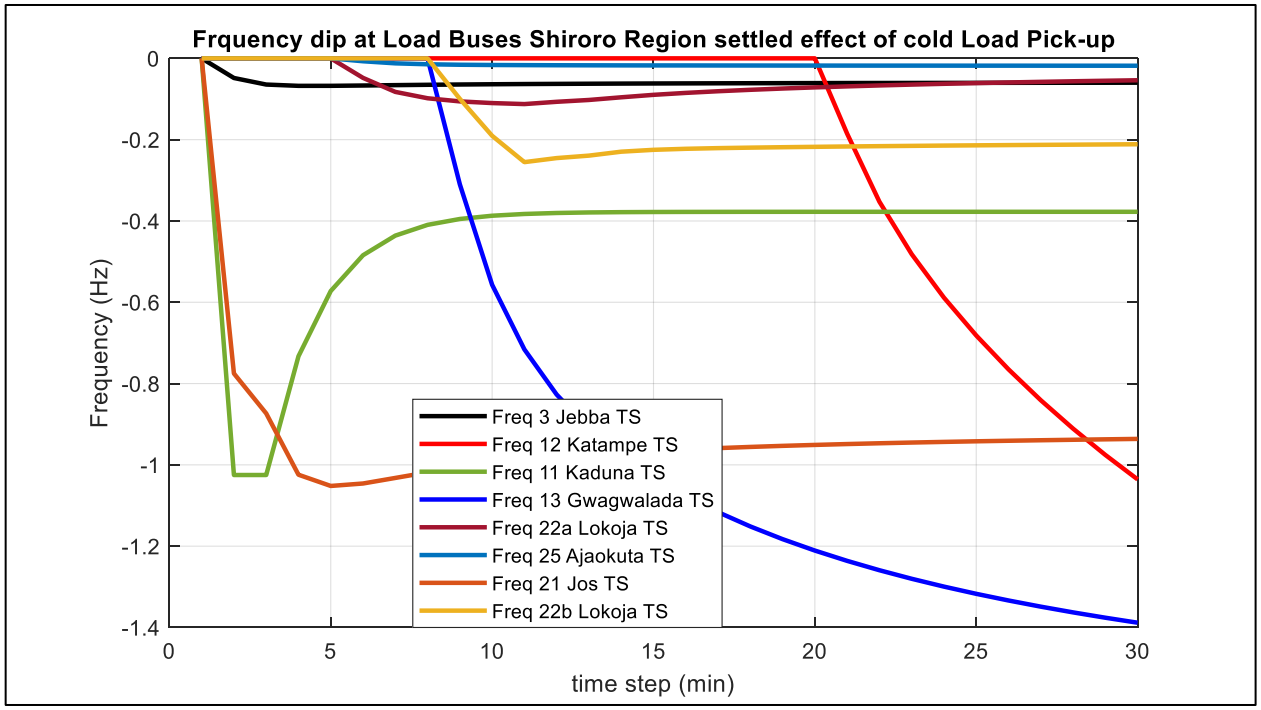

Fig. 6.28. Frequency dip at load buses for Shiroro region with horizon.

Table 6.10. Shiroro region performance characteristics on loading considering the horizon.

S/N	Bus no.	Load bus	Voltage (p.u.)		Frequency (dip from 50 Hz)	
			Maximum drop	Settling value	Maximum dip	Settling value
1	3	Jebba TS	1.0388	1.0433	-0.0676	-0.0599
2	12	Katampe TS	0.3897	0.6449	-2.2478	-2.2478
3	11	Kaduna TS	0.9254	1.0057	-1.0249	-0.3774
4	13	Gwagwalada TS	0.6494	0.8253	-1.6380	-1.6380
5	22a	Lokoja TS	1.0472	1.0456	-0.1125	-0.0292
6	22b	Lokoja (alternate)	0.4674	0.8073	-0.2553	-0.2012
7	25	Ajaokuta TS	1.0450	1.0478	-0.0292	-0.0194
8	21	Jos TS	0.7226	0.9008	-1.0519	-0.9158

6.4.2 Load restoration in Oshogbo region considering the horizon

The voltage and frequency characteristics of the buses are shown in Fig. 6.29 and Fig. 6.30 respectively. In Fig. 6.29, the restoration of load L10, at Ganmo TS show a voltage drop with a value of 0.0577 p.u. and settling at a value of 0.8542 p.u. Both values of voltage drop, and frequency dip are the same as the ones previously obtained when not considering horizon. In the restoration of load L18 at Okearo TS, the voltage value is the same as that without horizon. However, an improvement is recorded in the frequency dip value which is -0.3292 Hz at loading and -0.3123 Hz upon settling as against the values of -0.5653 Hz and -0.3217 Hz upon loading and settling respectively recorded in Oshogbo region performance characteristics Table 6.6 and Oshogbo region performance characteristics on loading considering horizon Table 6.11.

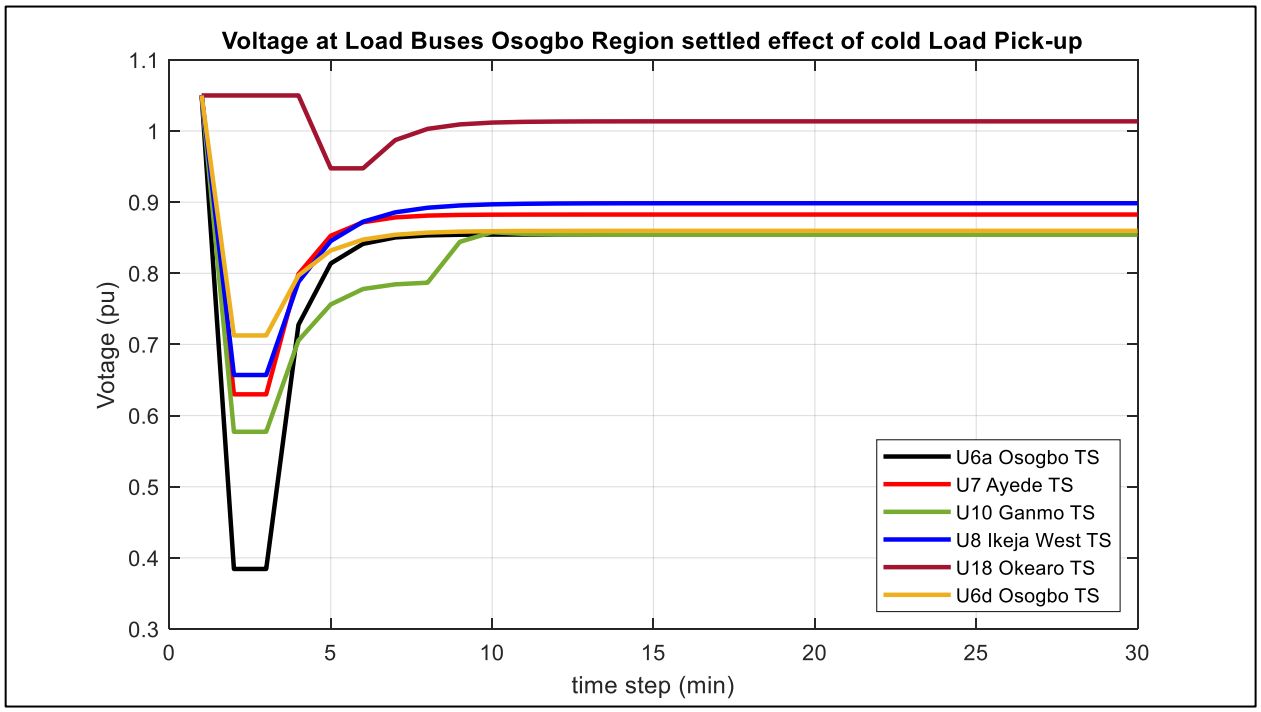

Fig. 6.29. Voltage at load buses for Oshogbo region with horizon.

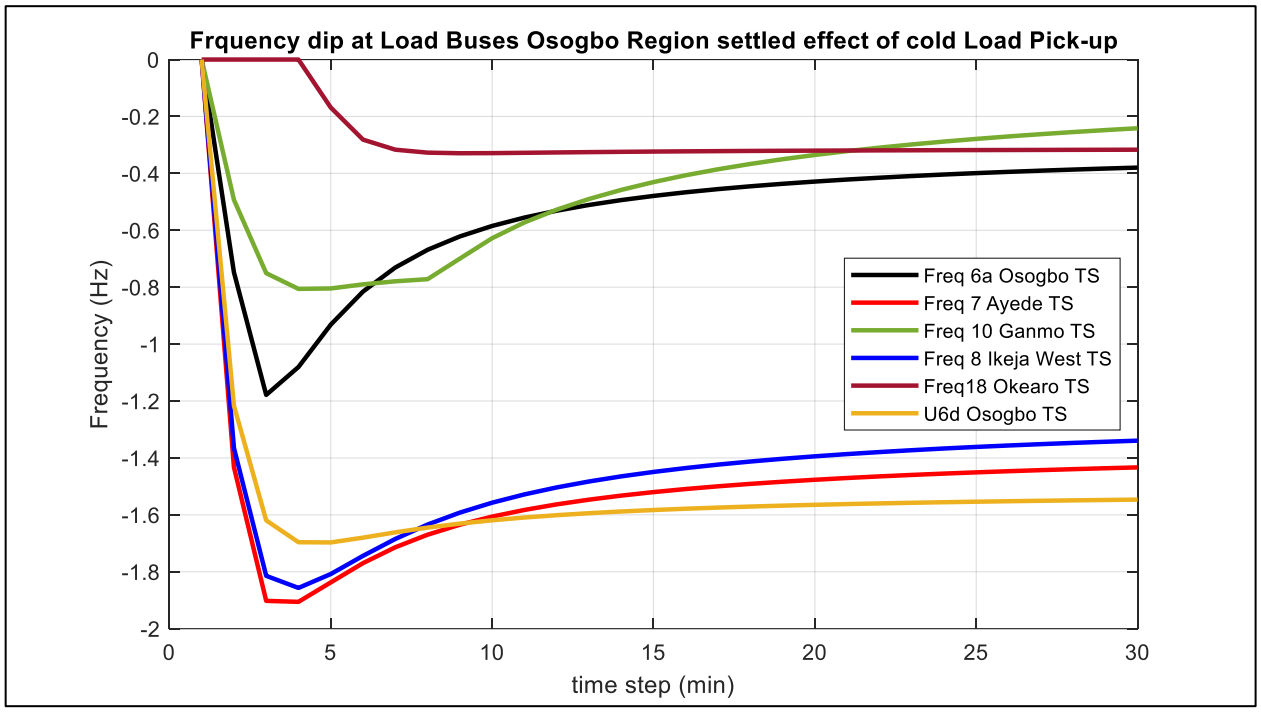

Fig. 6.30. Frequency dip at load buses for Oshogbo region with horizon.

Table 6.11. Oshogbo region performance characteristics on loading considering the horizon.

S/N	Bus no.	Load bus	Voltage (p.u.)		Frequency (dip from 50 Hz)	
			Maximum drop	Settling value	Maximum dip	Settling value
1	6a	Oshogbo TS	0.3844	0.8545	-1.1785	-0.3133
2	6d	Oshogbo (alternate)	0.7127	0.8597	-1.6969	-1.5208
3	7	Ayede TS	0.6299	0.8836	-1.9058	-1.3722
4	10	Ganmo TS	0.5772	0.8542	-0.5134	-0.0750
5	8	Ikeja West TS	0.6570	0.8985	-1.8568	-1.2620
6	18	Okearo TS	0.9475	1.0136	-0.3292	-0.3123

6.4.3 Restoration in Enugu region considering the horizon

Fig. 6.31 and Fig. 6.32 shows the respective voltage and frequency characteristics of the various buses considered within the region. The restoration of load L24 at Onitsha TS in Fig. 6.31 show the same value of voltage drop for all the considered routes similar to the results obtained without horizon both in drop at loading and the settling value. For the frequency dip, a better dip value is obtained from all the routes at a considered time step of 30 minutes, when compared to the values obtained without considering horizon. These performance characteristics is detailed in Table 6.12.

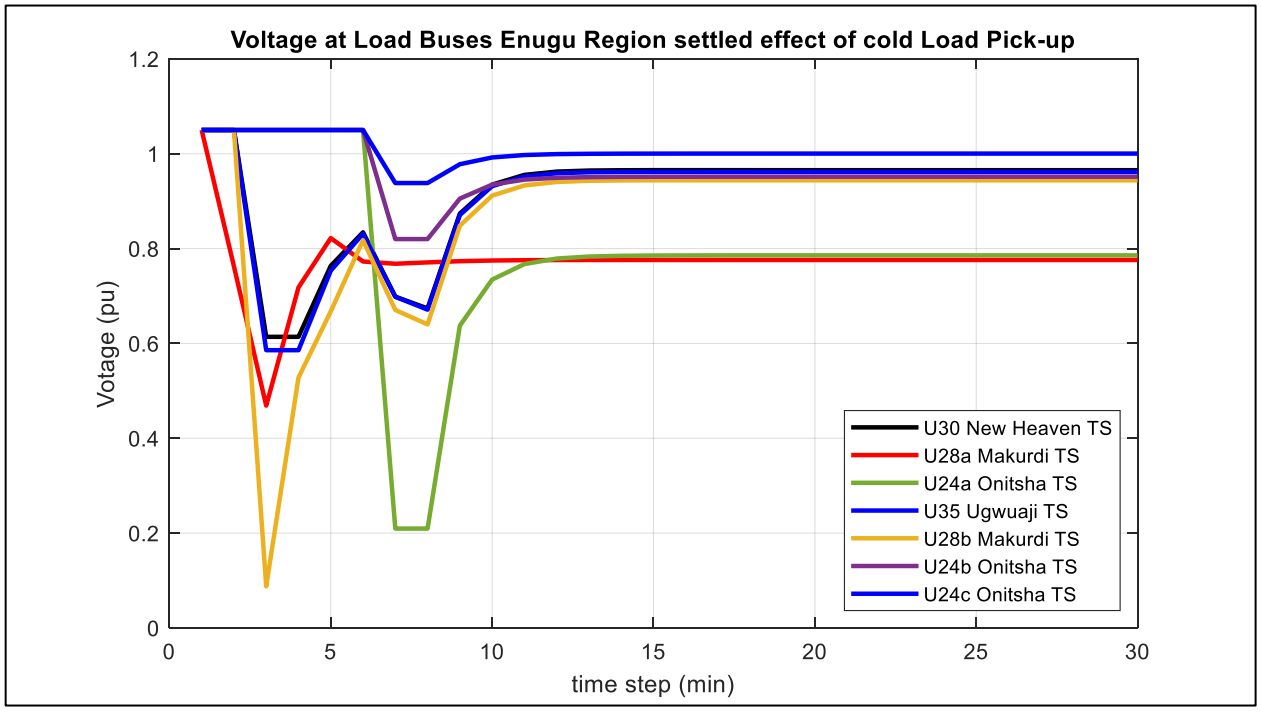

Fig. 6.31. Voltage at load buses for Enugu region with horizon.

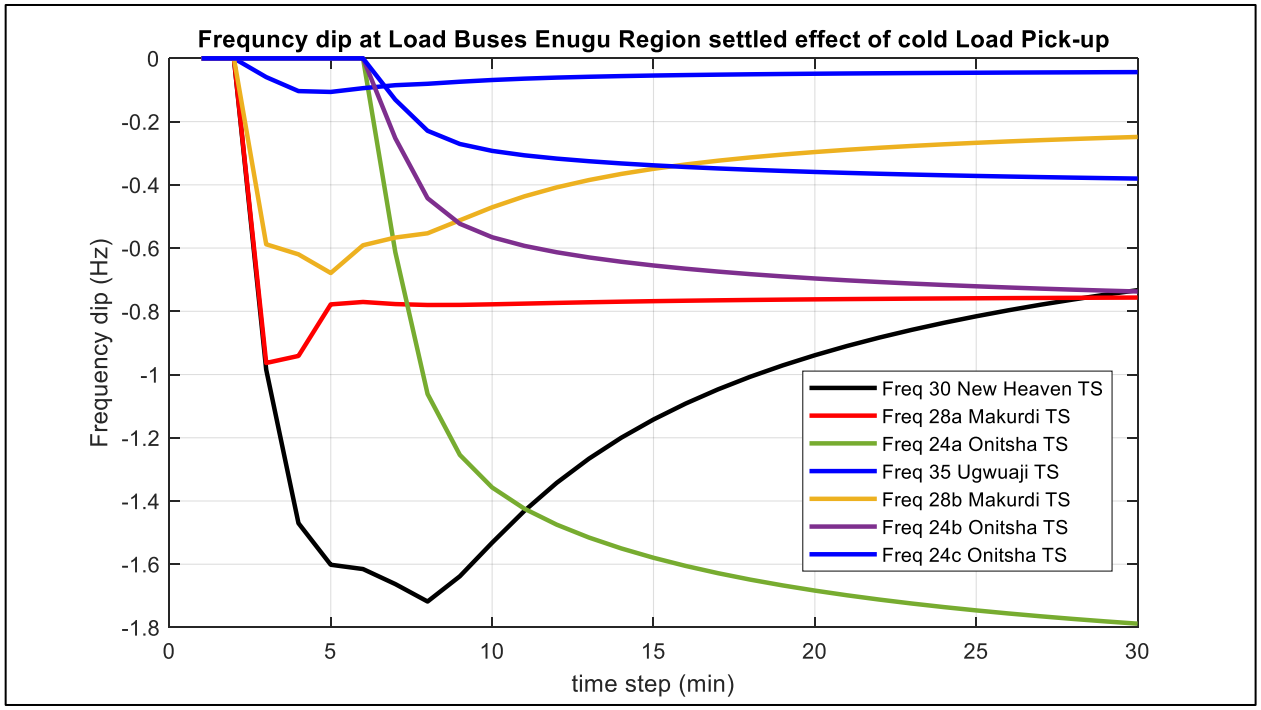

Fig. 6.32. Frequency dip at load buses for Enugu region with horizon.

Table 6.12. Enugu region performance characteristics on loading considering the horizon.

S/N	Bus no.	Load bus	Voltage (p.u.)		Frequency (dip from 50 Hz)	
			Maximum drop	Settling value	Maximum dip	Settling value
1	24a	Onitsha TS	0.2096	0.7857	-1.9360	-1.9360
2	24b	Onitsha (alternate1)	0.8200	0.9515	-0.7953	-0.7953
3	24c	Onitsha (alternate2)	0.9382	1.003	-0.4096	-0.4096
4	28a	Markurdi TS	0.4007	0.8243	-0.9635	-0.7488
5	28b	Markurdi (alternate)	0.3792	0.9439	-0.7392	-0.1858
6	30	New Heaven TS	0.3792	0.9653	-1.6352	-0.3430
7	35	Ugwuaji TS	0.3792	0.9616	-0.1092	-0.0364

6.5 Energy Storage System and PV Assistance in Restoration

Due to the power generation and transmission challenges experience within the network, various regions and states are resorting to PV installations and energy storage systems to meet their varied energy needs. These installations are mostly situated around the northern part of the country. To assess the contribution of potential PV generated energy to load restoration, seven PV installations close to some selected load buses were incorporated into the model. The various PV locations and capacity are presented in Table 6.2. The PVs were modelled to participate in the BSR, while monitoring their assistance to voltage and frequency. The contribution of the PV was considered for Shiroro and Enugu regions.

6.5.1 Restoration in Gwagwalada with PV assistance

The voltage drop and the frequency dip at Gwagwalada bus is measured considering loading L13 (i) with and without PV, (ii) with horizon and (iii) with a combination of PV and horizon. The corresponding characteristics are presented in Fig. 6.33 for voltage drop, Fig. 6.34 and Fig. 6.35 for frequency dip at 30- and 240-minutes time step respectively. The detailed performance characteristics are presented in Table 6.13. An improved performance is recorded with the use of PV without the horizon for both the voltage drop and the frequency dip. In Fig. 6.35, the time step of 240 minutes help to present a better settling time for the frequency.

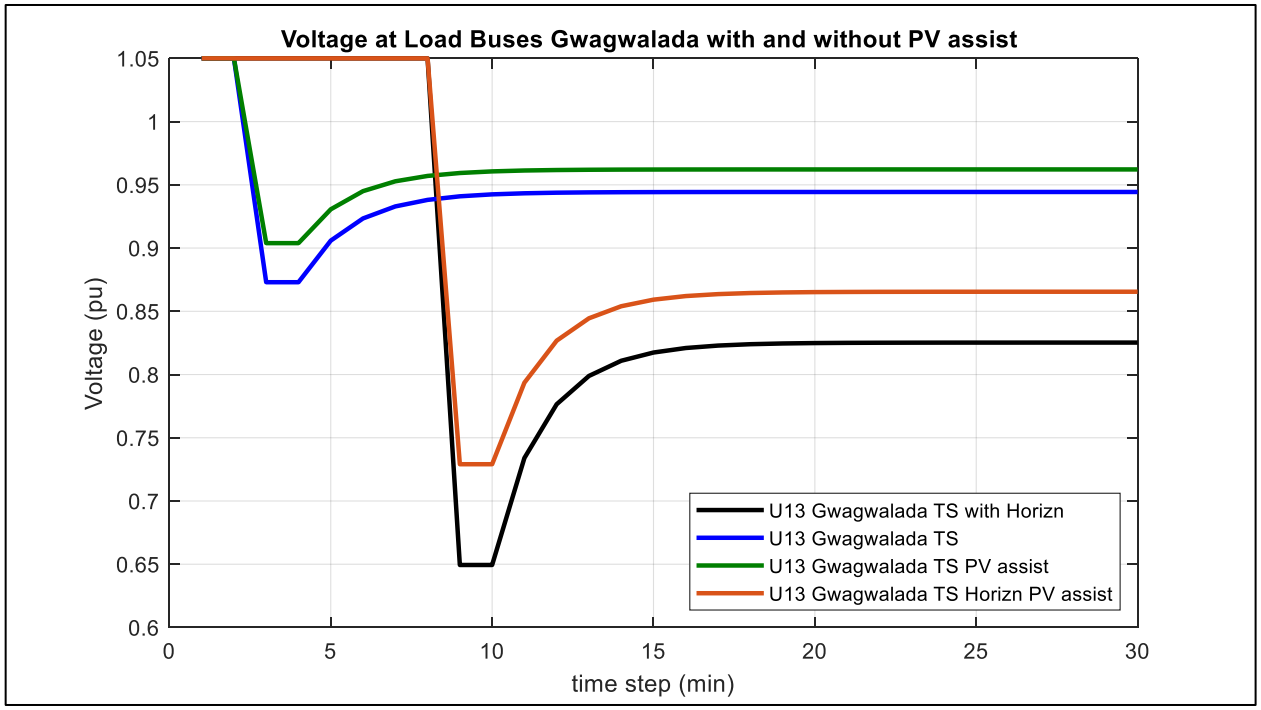

Fig. 6.33. Voltage at load buses for Gwagwalada with and without PV assist.

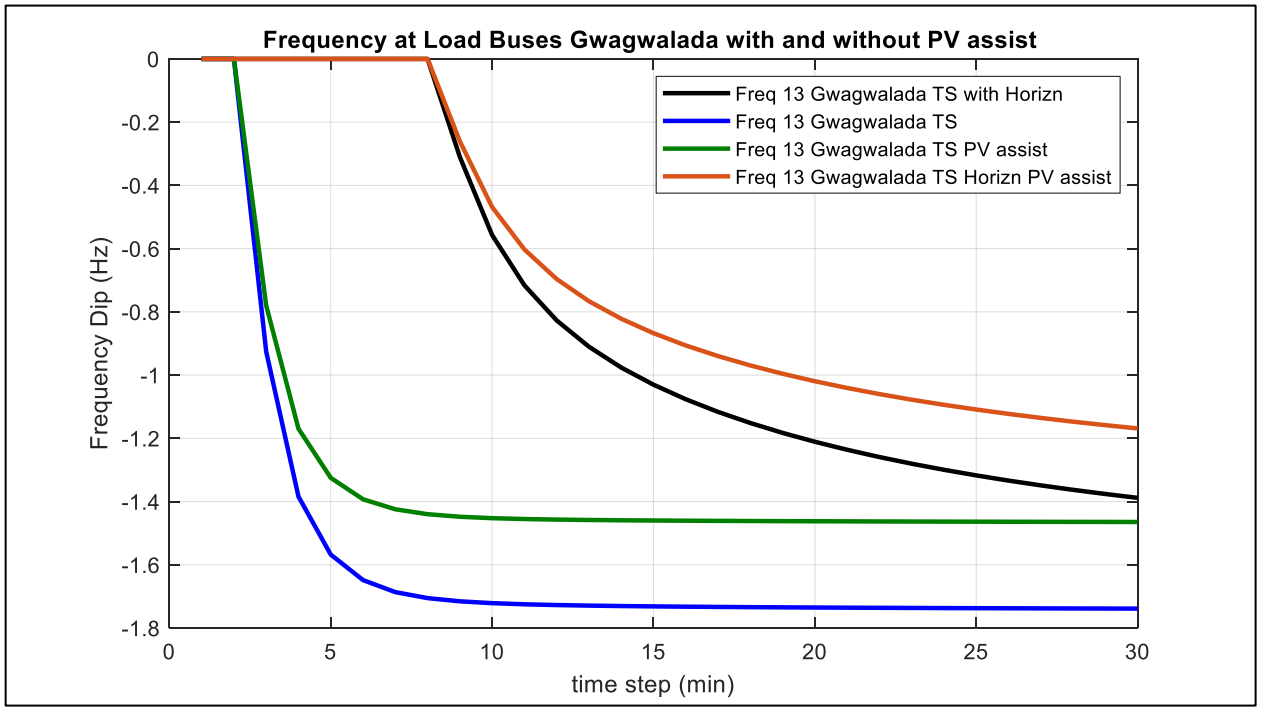

Fig. 6.34. Frequency dip at load buses for Gwagwalada with and without PV assist.

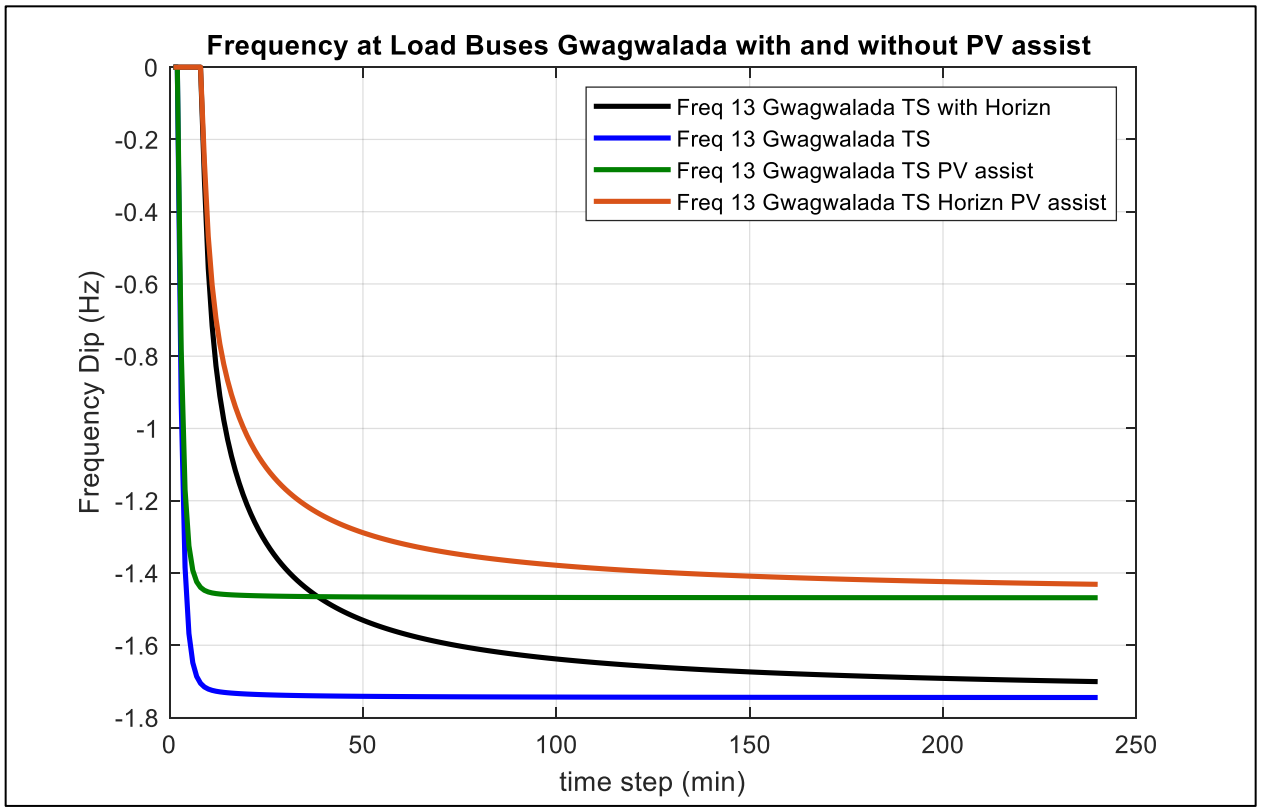

Fig. 6.35. Frequency dip at load buses for Gwagwalada with and without PV assist (240 minutes).

Table 6.13. Gwagwalada performance characteristics on loading.

S/N	Gwagwalada TS Bus 13	Voltage (p.u.)		Frequency (dip from 50 Hz)	
		Maximum drop	Settling value	Maximum dip	Settling value
1	Without PV	0.8730	0.9443	-1.7447	-1.7447
2	With PV	0.9039	0.9622	-1.4685	-1.4685
3	With Horizon	0.6494	0.8253	-1.7007	-1.7007
4	With Horizon & PV	0.7291	0.8665	-1.4314	-1.4314

6.5.2 Restoration in Lokoja with PV assistance

The performance characteristics upon loading of the Lokoja bus with PV assistance is presented in Table 6.14. The voltage drop and the frequency dip at Lokoja bus on loading L22, is considered with and without PV, with horizon and with the combination of PV and horizon. These characteristics are presented in Fig. 6.36 for voltage drop, Fig. 6.37 and Fig. 6.38 for frequency dip at 30- and 240-minutes time step respectively. Route 1 with PV assistance offers a better voltage settling value while for the alternate route, the use of PV without the horizon gives an improved voltage drop and frequency dip values. The 240 minutes time step in Fig. 6.38 help to present a better settling time for the frequency.

For the main route, the voltage drop upon loading are the same, while improvement is recorded in the settling time with PV assistance recording a value of 1.0459 p.u. when compared to 1.0456 p.u. without PV assistance. Also, an improvement in the frequency dip settling value was achieved having attained a dip value of -0.0181 Hz. For the alternate route with PV assistance, an improvement is recorded in both with and without horizon, having recorded a voltage value of 0.8630 p.u. and 0.6008 p.u. respectively when compared to the values without PV assistance of 0.8466 p.u. and 0.4674 p.u. respectively. These are well tabulated in Table 6.14.

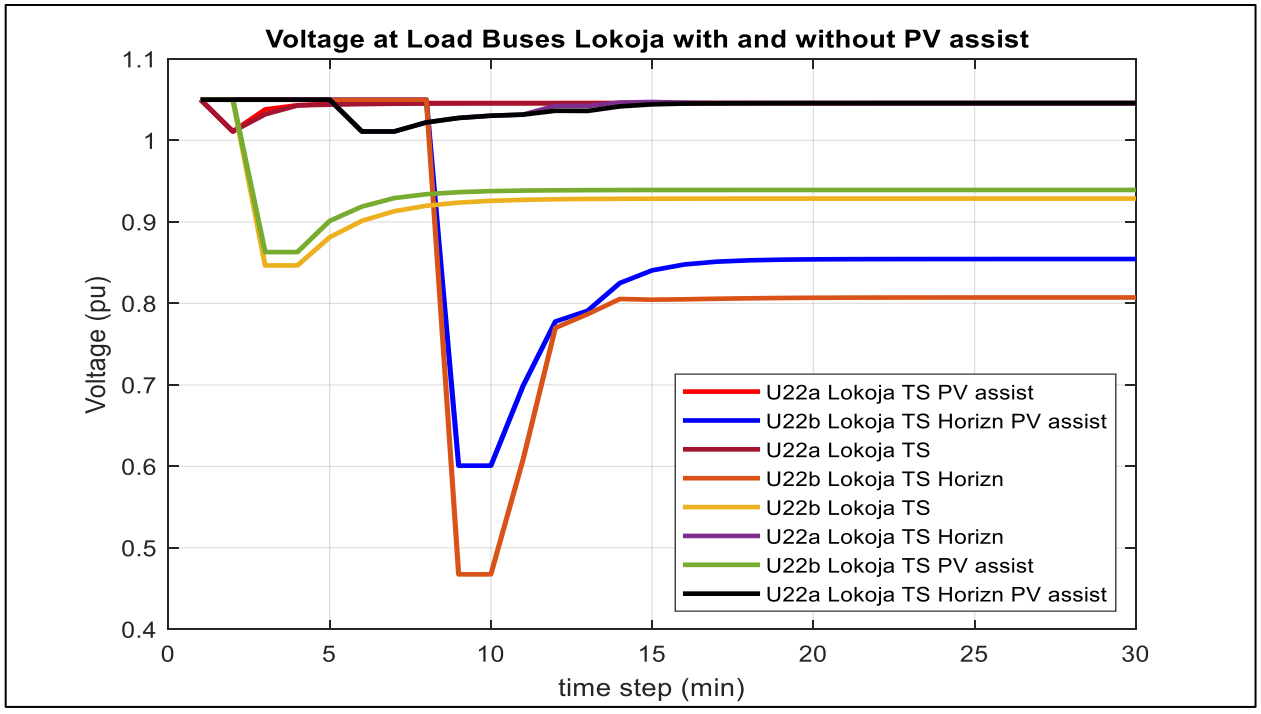

Fig. 6.36. Voltage at load buses for Lokoja with and without PV assist.

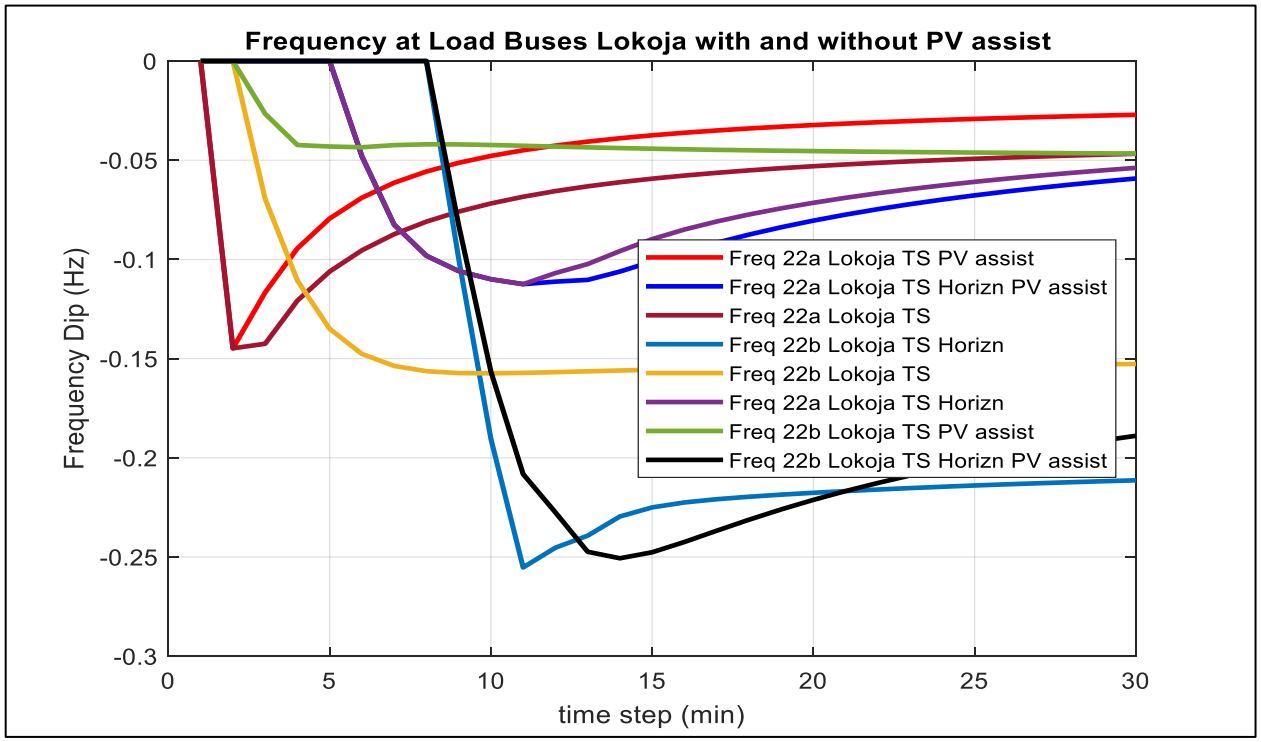

Fig. 6.37. Frequency dip at load buses for Lokoja with and without PV assist.

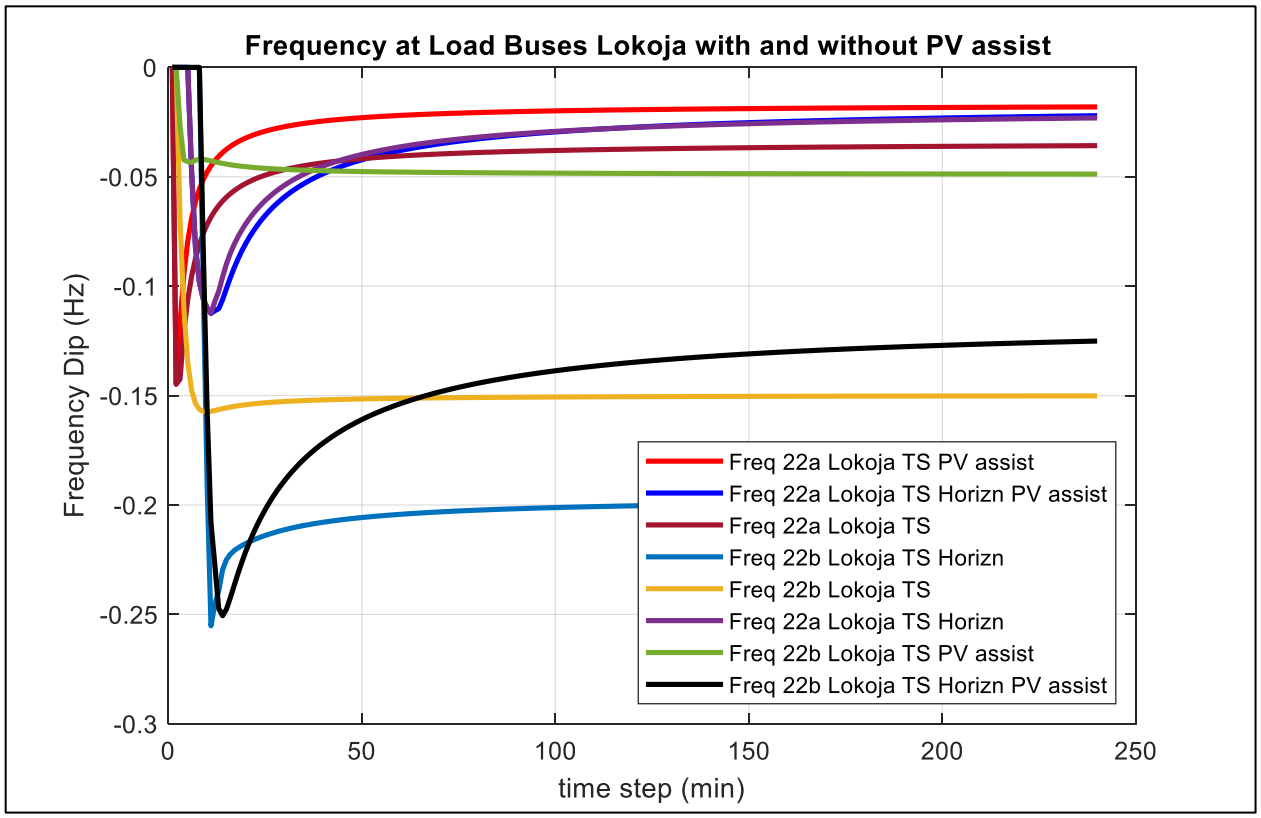

Fig. 6.38. Frequency dip at load buses for Lokoja with and without PV assist (240 minutes).

Table 6.14. Lokoja performance characteristics on loading.

S/N	Bus no.	Lokoja Load bus 22	Voltage (p.u.)		Frequency (dip from 50 Hz)	
			Maximum drop	Settling value	Maximum dip	Settling value
1	22a	Without PV	1.0110	1.0456	-0.1448	-0.0203
2		With PV	1.0110	1.0459	-0.1448	-0.0181
3		With Horizon	1.0110	1.0456	-0.1125	-0.0231
4		With Horizon & PV	1.0110	1.0459	-0.1125	-0.0221
5	22b	Without PV	0.8466	0.9287	-0.1574	-0.1501
6		With PV	0.8630	0.9392	-0.1448	-0.0488
7		With Horizon	0.4674	0.8073	-0.2553	-0.1984
8		With Horizon & PV	0.6008	0.8544	-0.2506	-0.1251

6.5.3 Restoration in Katampe with PV assistance

The voltage drop and the frequency dip at Katampe bus upon loading L12 with and without PV, with horizon and with a combination of PV and horizon is presented. The corresponding characteristics plots are presented in Fig. 6.39 for voltage drop, Fig. 6.40 and Fig. 6.41 for frequency dip at 30- and 240-minutes time step respectively. Table 6.15 captures the various performance characteristics. With PV assistance, a better settling value is observed with the voltage drop, while for the alternate route, restoration with PV without the horizon presents better results for both the voltage drop and the frequency dip values. Also, the time step of 240 minutes in Fig. 6.41 help to present a better settling time for the frequency.

With PV assistance, the voltage drop value noticeably improves to 0.4453 p.u., when compared to the voltage drop value of 0.3897 p.u. without PV assistance. Also, a voltage drop value of 0.4453 p.u. is recorded for PV assistance with horizon, compared to a voltage drop value of 0.3897 p.u. without PV assistance with horizon. The same improvement is recorded in the frequency dip values both for with and without horizon with PV assistance as seen in Table 6.15.

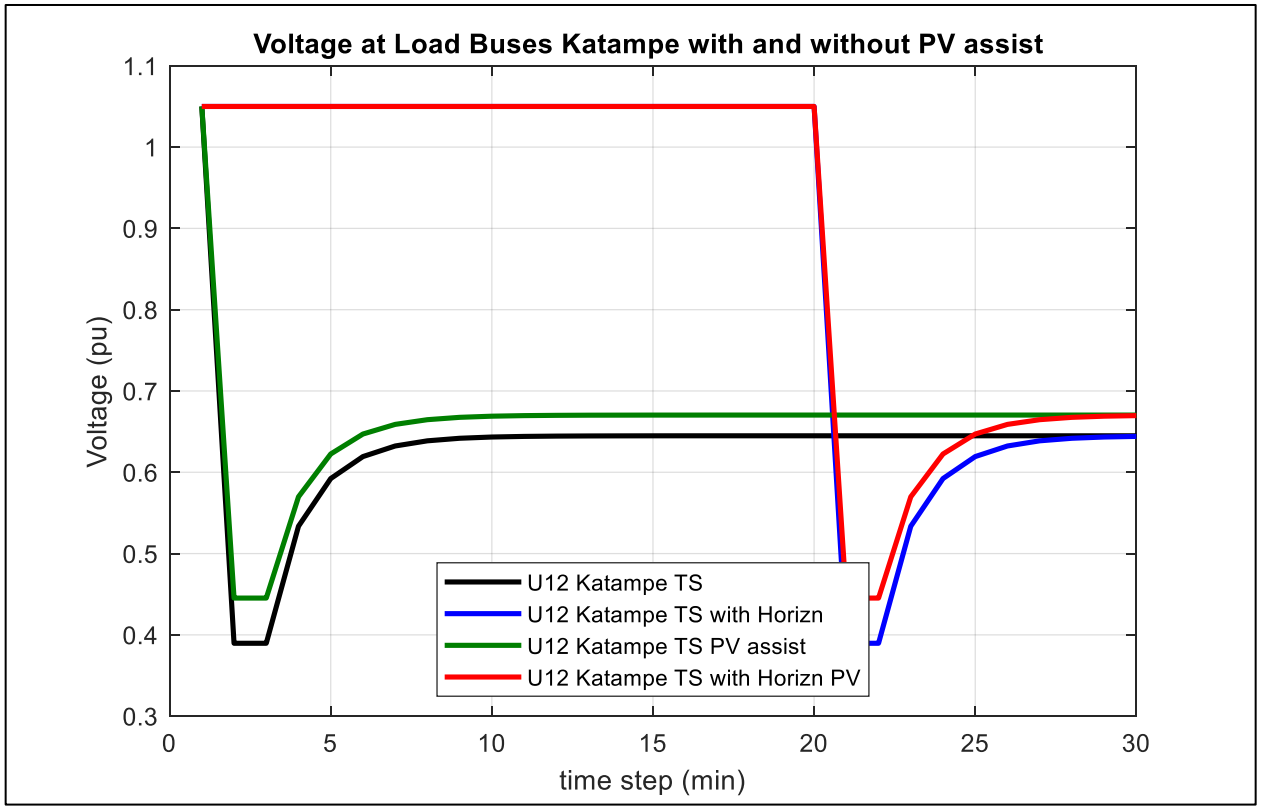

Fig. 6.39. Voltage at load buses for Katampe with and without PV assist.

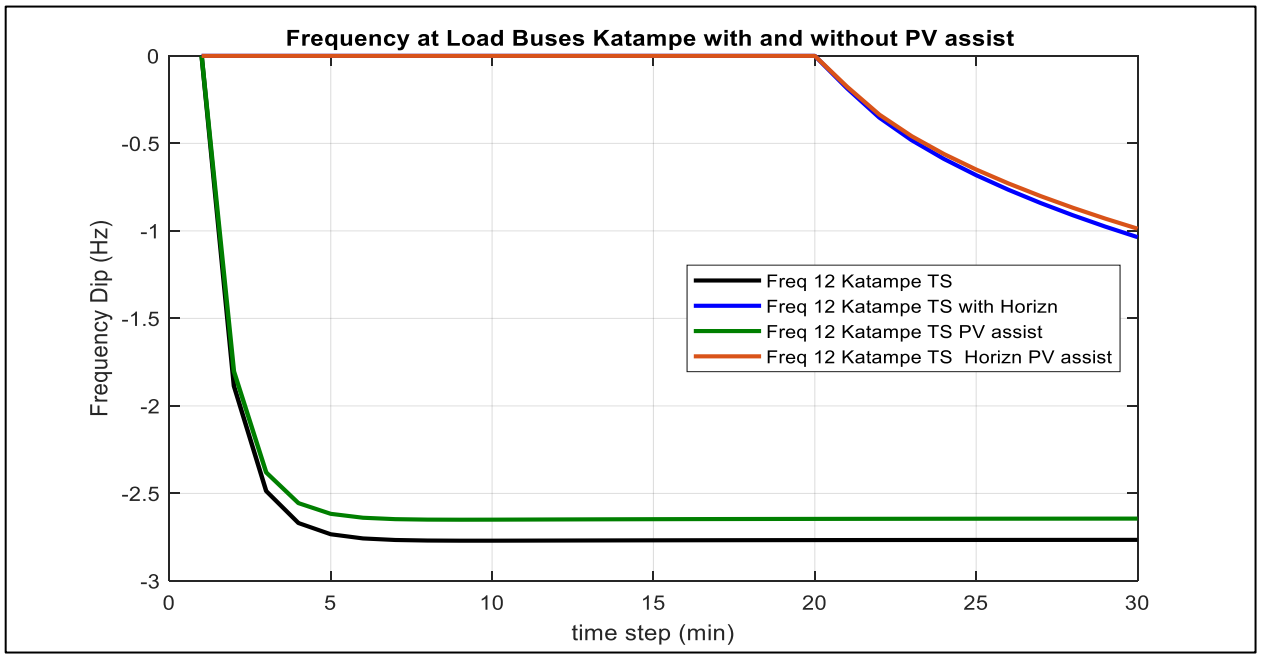

Fig. 6.40. Frequency dip at load buses for Katampe with and without PV assist.

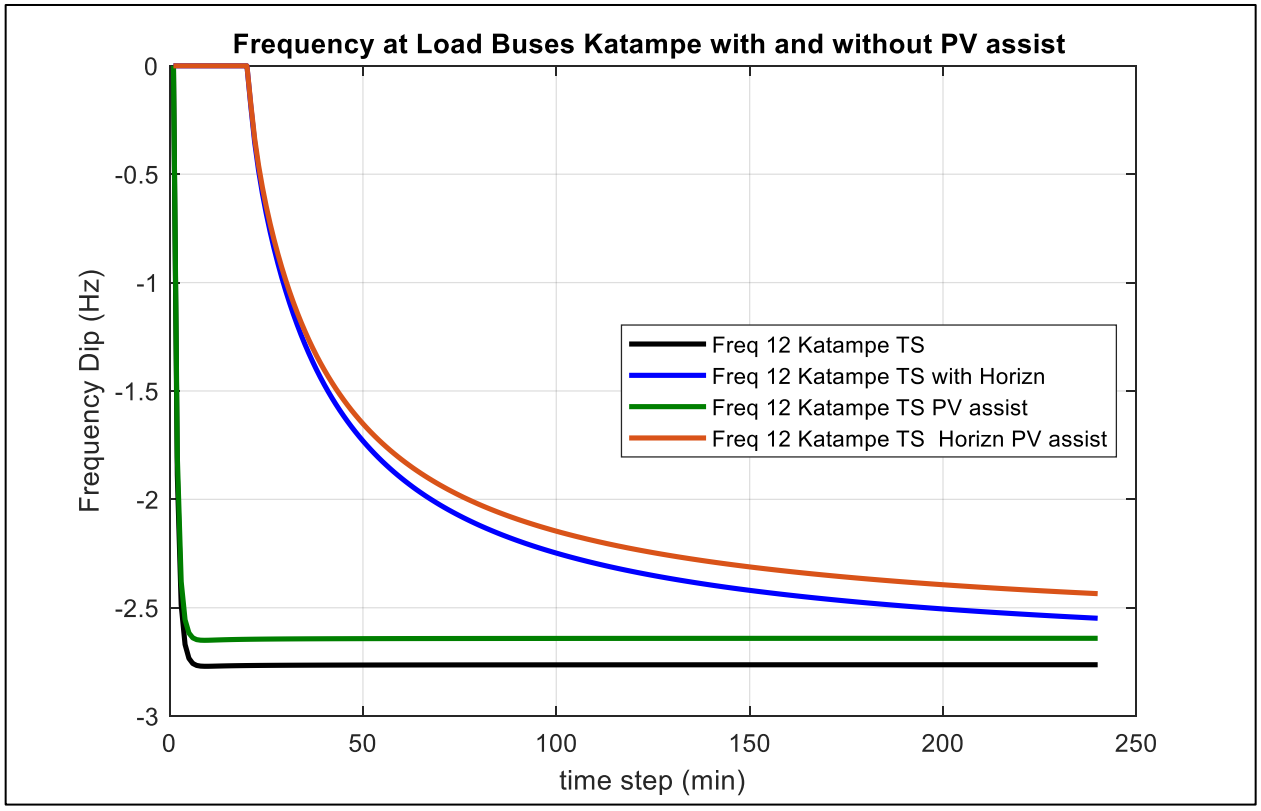

Fig. 6.41. Frequency dip at load buses for Katampe with and without PV assist (240 minutes).

Table 6.15. Katampe performance characteristics on loading.

S/N	Katampe Load bus 12	Voltage (p.u.)		Frequency (dip from 50 Hz)	
		Maximum drop	Settling value	Maximum dip	Settling value
1	Without PV	0.3897	0.6449	-2.7700	-2.7629
2	With PV	0.4453	0.6704	-2.605	-2.6409
3	With Horizon	0.3897	0.6449	-2.5484	-2.5484
4	With Horizon & PV	0.4453	0.6704	-2.4349	-2.4349

6.5.4 Restoration in Jos with PV assistance

The voltage drop and the frequency dip at Jos bus upon loading L21 with and without PV is explored. The various bus loading characteristics are presented in Fig. 6.42 for voltage drop, Fig. 6.43 and Fig. 6.44 for frequency

dip at 30- and 240-minutes time steps. The summarised results of the performance loading characteristics are reflected in Table 6.16. A better settling value is observed with the voltage when PV assistance is considered. In Fig. 6.44, the time step of 240-minutes help to present a better settling time for the frequency.

With PV assistance, the voltage value is improved. A settling voltage value of 0.9196 p.u. is recorded compared to a value 0.9008 p.u. without PV assistance. The frequency dips to a lower value of -0.9647 Hz when compared to a value of -1.0519 Hz without PV assistance. Generally, this is a significant improvement in the frequency value with PV assistance as depicted in Table 6.16.

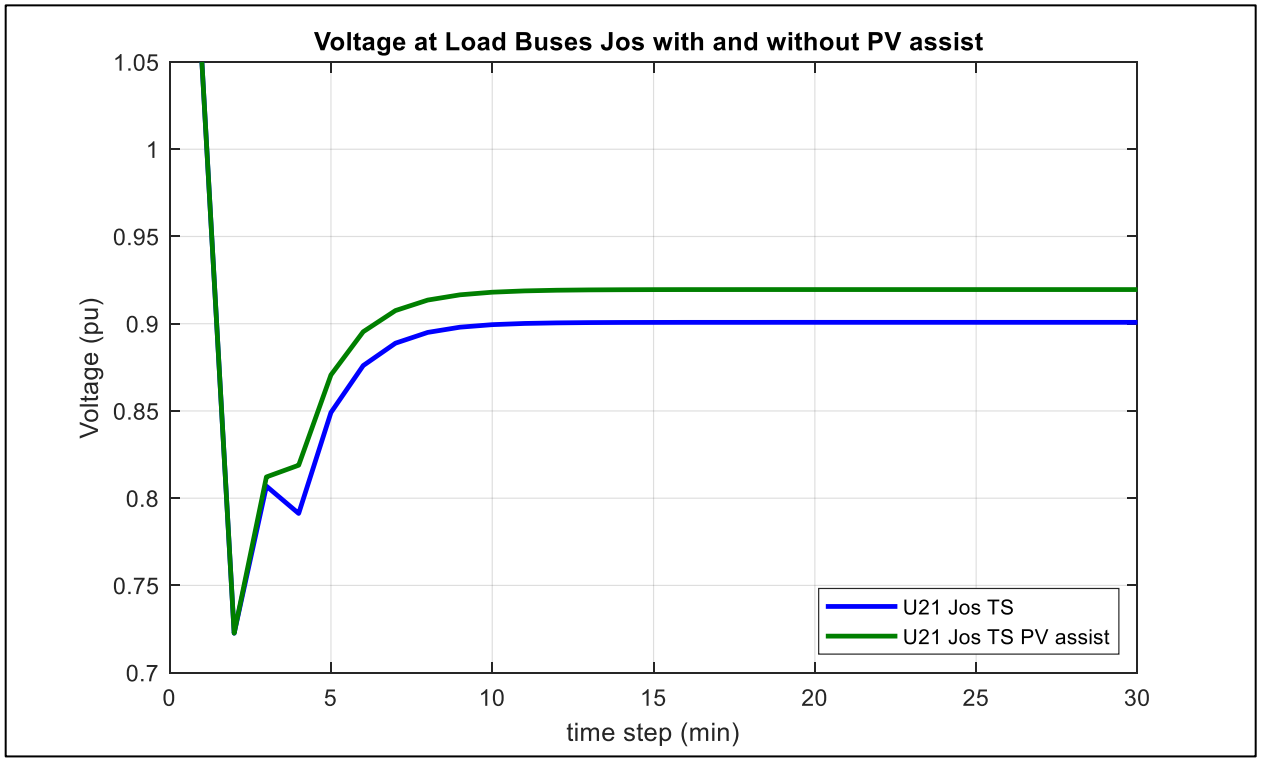

Fig. 6.42. Voltage at load buses for Jos with and without PV assist.

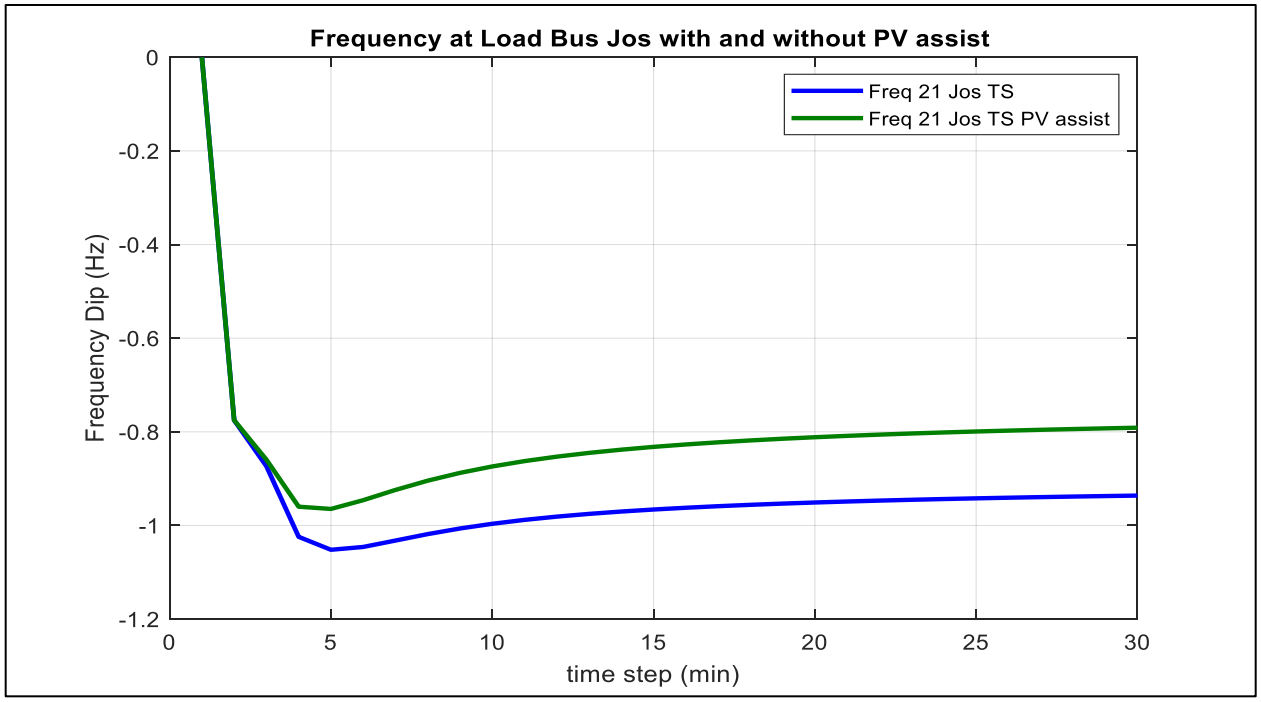

Fig. 6.43. Frequency dip at load buses for Jos with and without PV assist.

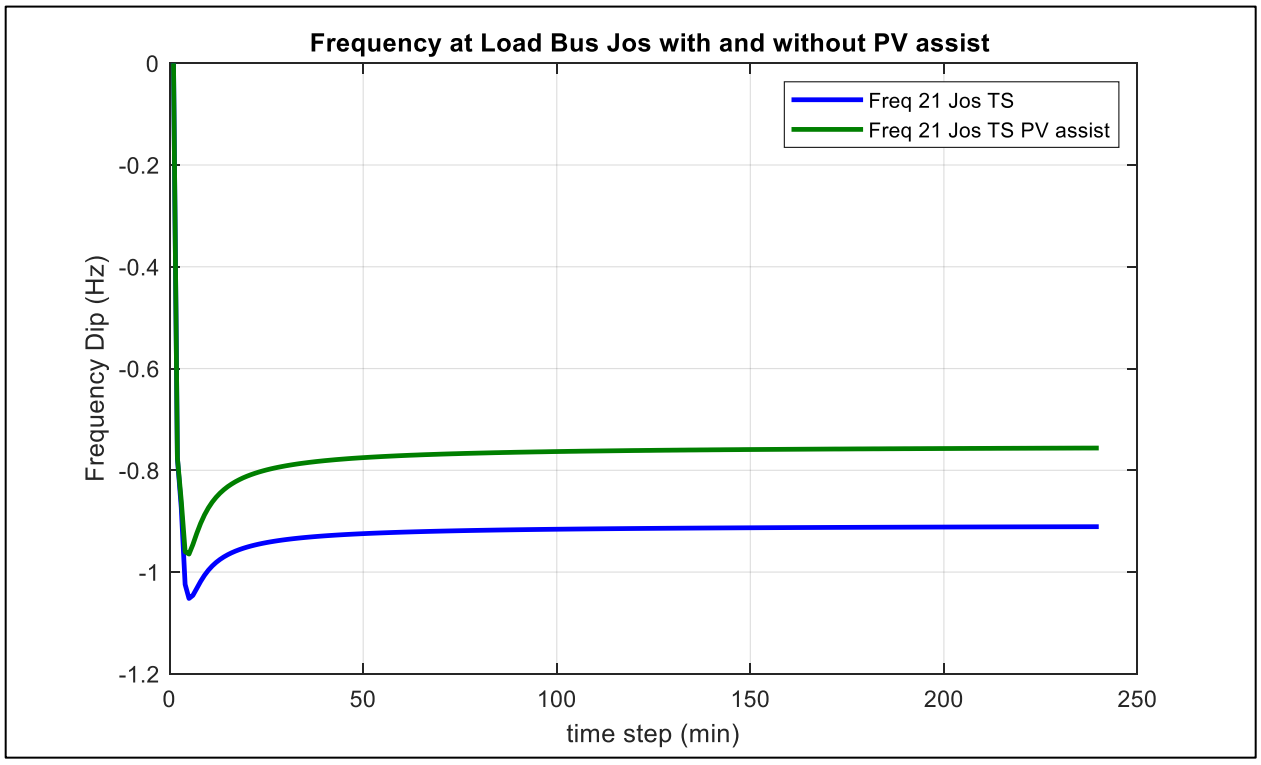

Fig. 6.44. Frequency dip at load buses for Jos with and without PV assist (240 minutes).

Table 6.16. Jos performance characteristics on loading.

S/N	Jos Load bus 21	Voltage (p.u.)		Frequency (dip from 50 Hz)	
		Maximum drop	Settling value	Maximum dip	Settling value
1	Without PV	0.7226	0.9008	-1.0519	-0.9108
2	With PV	0.7226	0.9196	-0.9647	-0.7562

6.6 Conclusion

The Nigerian 48-bus system was modelled in NEPLAN and used as the simulated test system to assess the performance of the BSR method proposed. To be able to provide an enhanced and detailed analysis of the network, a sectional model of the 330 kV 48-bus system indicative of the various regions was further created and used to perform various simulated load restoration analysis. Various possible switching logic sequence was generated and used to determine the viability of different transmission routes. Based on the switching status of Table 6.4, the active and reactive loads for the different regions namely: Shiroro, Oshogbo, Enugu, Benin and Port Harcourt with CLPU condition were plotted. The shape of the active and reactive power plot can be seen to mimic that of the load restoration plots. As the restored load begins to normalise, the active and reactive power also normalise as it approaches the 15^{th} time step.

The effect of cold load pickup on the system restoration was equally assessed while considering a time horizon corresponding to a subsided effect of the CLPU and subsequent PV contributions to the restoration process. The performance characteristics of voltage and frequency in response to the loading during restoration was monitored in the different regions. Voltage and frequency profile results indicated various levels of voltage and frequency dips at some specified nodes resulting from excessive inrush

currents experience during the load restoration events. However, with the PV assistance, the voltage and frequency values recorded a significant level of improvement as tabulated on the various loading performance Tables. Also, in most locations, improved performance is recorded with the use of PV without the horizon for both the voltage drop and the frequency dip.

The general response of the load, is typically because of the cold-Load pick-up consideration. Without the applied method, the switching can just be done considering only optimisation of switching time, but with the applied method, the path with the least anticipated voltage and frequency drop is taken into consideration in the choice of the restoration route. This is applicable when alternative route for restoration is considered.

Summarily, the performance analysis of the modelled BSR method on the Nigerian 330 kV 48 bus system indicated that, when considering the whole system, BSR is effective since restoration can be initiated at the same time in different sections of the network. It was also possible to energise the system by implementing the restoration sequence step by step, while satisfying various operational constraints during the restoration process. However, some operating conditions resulted in infeasible solutions, such as heavy loading conditions, load demands and limited DG ramp rate and capacity.

The major contributions of this chapter are:-

- The Nigerian 330 kV 48-bus system was modelled in NEPLAN and used to examine the workability of the modelled black start restoration (BSR) method. The network was integrated with dispatchable distributed generations (DGs), renewable DGs, and Remote controllable switches (RCSs).
- A sectional model of the 330 kV 48-bus system indicative of the various regions was developed and used to perform various load restoration analysis.

- A switching logic sequence of the various loads on the different transmission substation buses by participating generators was developed and used to achieve effective restoration.
- The modelled BSR method was able to generate restoration sequences in response to varying operating conditions.
- The modelled BSR method could generate multiple step solutions accommodating up to 240-time steps. However, for the Nigerian 330 kV 48 bus system analysed, it was observed that most loads were restored optimally before the 30^{th} time step for a black start operation.
- The network sectioning enhanced systematic load restoration along with contribution from PV.

CHAPTER 7

7.0 EXPERIMENTAL VALIDATION OF BLACK START BATTERY STORAGE OPERATIONS WITH PV SYSTEMS ANALYSIS

7.1 Introduction

To experimentally validate the characteristics of the ESS adopted for the BSR simulated study carried out in the previous chapter, this chapter describes the experimental method used in conducting the battery state of charge (SOC) analysis. The description of both the experimental and numerical methodology is presented alongside a detailed analysis of the various scenarios created.

7.2 Overview of Energy Storage Systems

To successfully manage the various grid integrated RE sources, storage forms a critical component which would enable the coordinated release of energy to and from the grid during peak and off-peak hours. According to [218], the major asset possessed by these ESS are their energy density (up to 150 Wh/kg and 2000 Wh/kg for lithium) alongside the technological maturity as indicated in Fig. 7.1. The discussions and analysis in this chapter will only be limited to the practical applications of the basic category of ESS.

As noted by [219], the ESS are maintaining a stable voltage as a function of charge level. Also, the minimum discharge period of the electrochemical accumulators is reached below 15 mins. Despite having a notable drawback of low durability for large-amplitude cycling, [219] maintains that they are mostly used for renewable storage which is the focus of this research. A

detailed description of the main characteristics of storage systems have been succinctly captured by [219] and was referenced in Chapter 2 of this thesis.

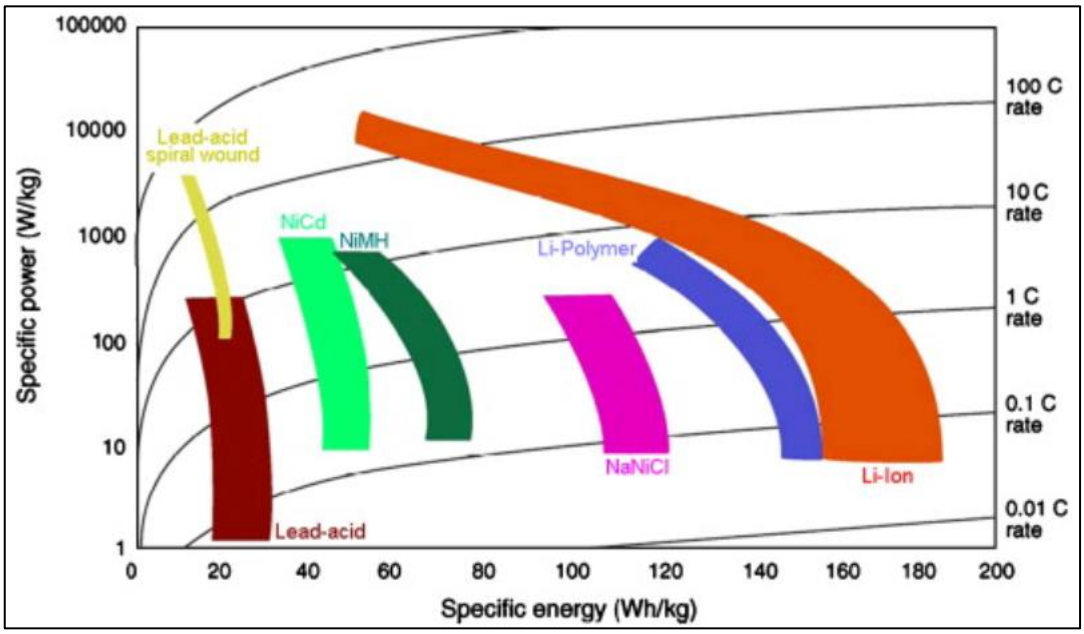

Fig. 7.1. Distribution of the different electrochemical accumulators according to their energy densities and power [218].

7.3 Energy Storage Systems in Power Restoration

The application of RE as well as ESS in power system restoration is an emerging area of research because of its variable nature and users' lack of in-depth knowledge of managing the associated complexities thereof. Acting as emergency backup source for critical infrastructures during power system blackout, [134, 135] highlighted the successes of PV battery backup systems and ESS. To consolidate on and improve upon the current level of achievements recorded in this area, research on efficient ways of integrating and implementing ESS into the power system restoration plans is discussed in this chapter.

The significant improvements in battery technology as well as the important advances in the EV technologies have propelled a major shift in vehicle to grid (V2G) applications. As opined in [156], Photovoltaic battery backup systems (PVBBSs) and ESSs are increasingly being deployed to provide backup power for critical loads due to its fast response and capability of being used to maintain transient stability if chosen to regulate voltage and frequency. Besides this, during periods of high demand, the battery packs of idle or stationary EVs can be leveraged to send power back to the grid while also recharging during periods of low demand. [157], reported of such contributions in the use of electric buses as a means of proving resilience in the distribution system.

7.4 ESS Operational Constraints

To systematically control the operation of an ESS, a set of operational constraints were proposed by [212]. These constraints was formulated and presented in section 5.4.6. Inferring from the description of these constraints for a single ESS and the basic characteristics of energy storage devices, the experimental ideas for this chapter was developed and implemented.

7.5 ESS Experimental Materials

The experiments which aims to simulate the behaviour of the ESS integrated into the BSR study in this thesis were conducted in the Electronics & Battery Laboratory of Cardiff University School of Engineering. The description of the universal battery charger & analyzer equipment as well as the data acquisition tool is presented below.

7.5.1 Universal battery charger & analyser

The SKYRC MC3000 battery charger is designed to have four independent charging bays and suitable for charging round cylindrical single cell batteries. The 11~18V (60W) DC power adaptor plug is first connected to the device before the 110/220V AC power cable plug is connected to the mains supply socket. The MC3000 has a maximum charge rate of 3A constant current for charging and 2A for discharging. The user-friendly interface of this device allows for the data acquisition system to be easily interfaced. The pictorial representation of this device is shown in Fig. 7.2 while the complete setup with the device plugged and interfaced to a computer for data acquisition is shown in Fig. 7.3.

7.5.2 Universal battery charger setup & interfacing

The SKYRC MC3000 battery charger is interfaced to a windows personal computer (PC) using the PC link universal serial bus (USB) cable terminated on one end with A-plug and the opposite end with micro-B plug which connects to the charger directly Fig. 7.3. The synchronisation of the two devices is achieved by downloading and installing the free PC link software which is then launched to enable data visualization. The synchronisation of the two devices is achieved by downloading and installing the free PC link software which is then launched to enable data visualisation. With the setup successfully implemented, the details of the charging algorithms as well as the battery performance analysis was observed in real-time.

Fig. 7.2. Pictorial representation of the SKYRC MC3000 battery charger.

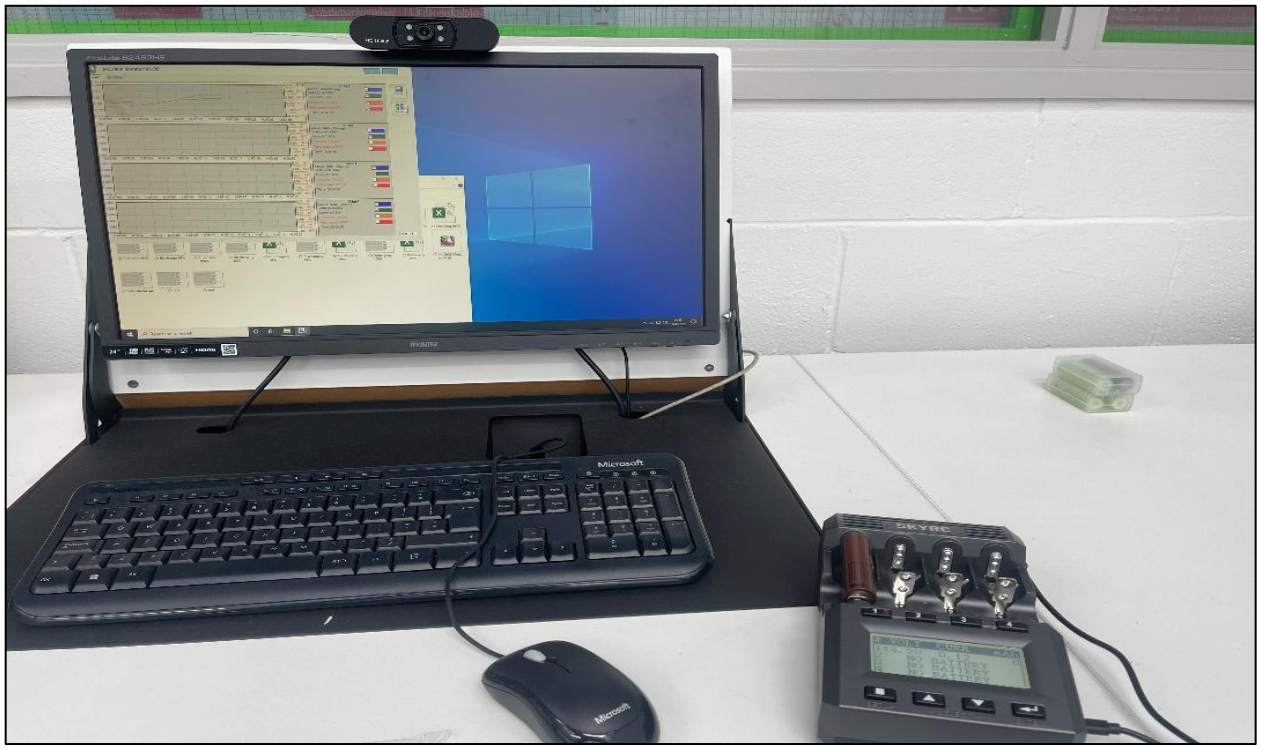

Fig. 7.3. The complete setup with the device plugged and interfaced to a computer for data acquisition.

When the batteries are inserted into the various charger slots as shown in Fig. 7.2, and PC link software launched, the software automatically retrieves the program settings of each respective slot and displays it graphically. This enables the user to adjust the various settings as desired and then monitor the displayed important battery qualities as well as track their respective charge and discharge capacities. The data of the various charge and discharge cycles obtained in this experiment were exported to the .csv-spreadsheet format. These were subsequently imported to MS Excel and MATLAB for post-processing and analysis. The resulting plots of the various charging and discharging analysis are presented in Fig. 7.5 to Fig. 7.8 respectively.

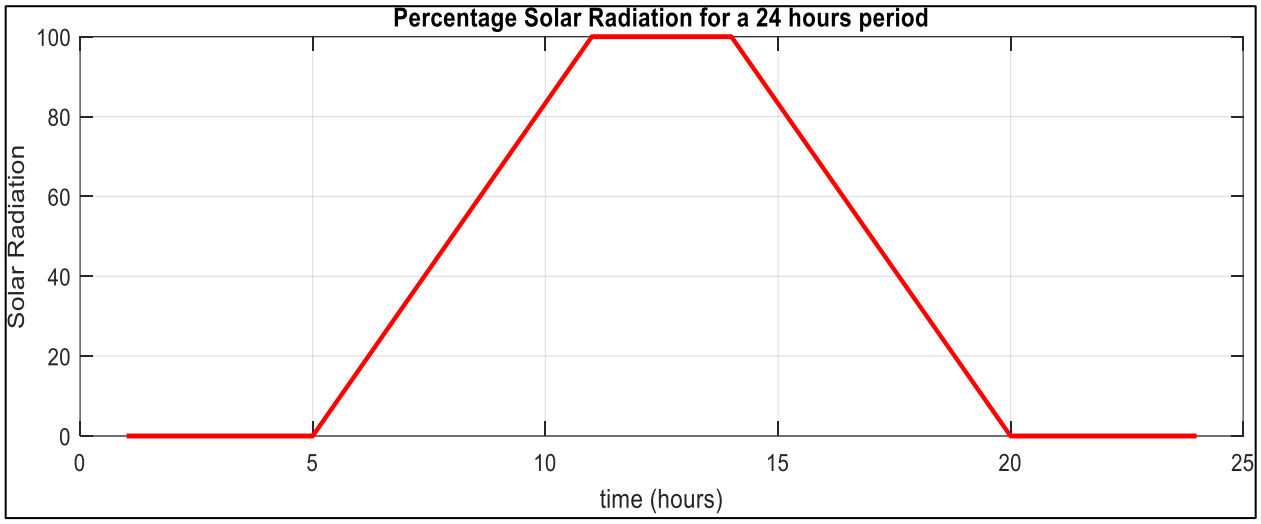

Fig. 7.4. Estimated percentage hourly solar radiation availability in Nigeria [215].

In Fig. 7.4, the percentage of solar radiation availability for a 24 hour period in Nigeria estimated by [215] is presented. By inspection, it can be observed that it is only between 11:00 to 14:00 that 100% PV solar availability is guaranteed, while 50% PV availability is guaranteed between 08:00 and 17:00. At least between 08:00 to 11:00, and 14:00 to 17:00, other

percentage levels (60%, 70%, 80% and 90%) of solar availability is attainable. 20% PV solar availability is achieved by 06:00 and 17:00 respectively. Inferring from the solar availability data in [215], the charging current in this experiment was set to vary from 20% to 100% representing the intensity of solar radiation, with a 20% intensity expected at 08:00 and 100% intensity expected between 11:00 to 14:00 respectively.

A plot of current against time is shown in Fig. 7.5. From the plot, it takes 6 seconds to reach a steady state charging current for 1 A, but takes 8700 seconds for the ESS unit to be completely charged when compared to a charging current of 3 A which reaches steady state at 22 seconds and completely charges the ESS unit at 2500 seconds as shown in charging plots at various percentage of charging current (indicating drop in current at full charge) Fig. 7.6.

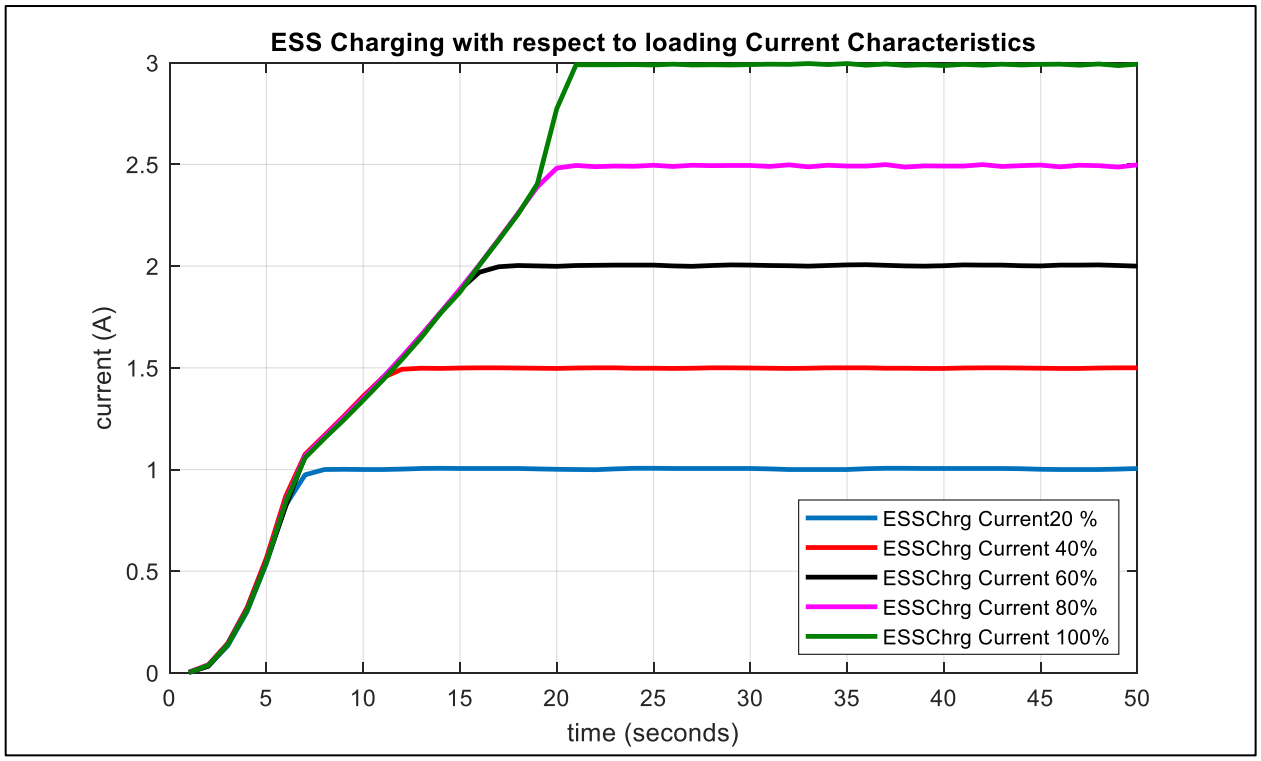

Fig. 7.5. Charging plots at various percentage of charging current.

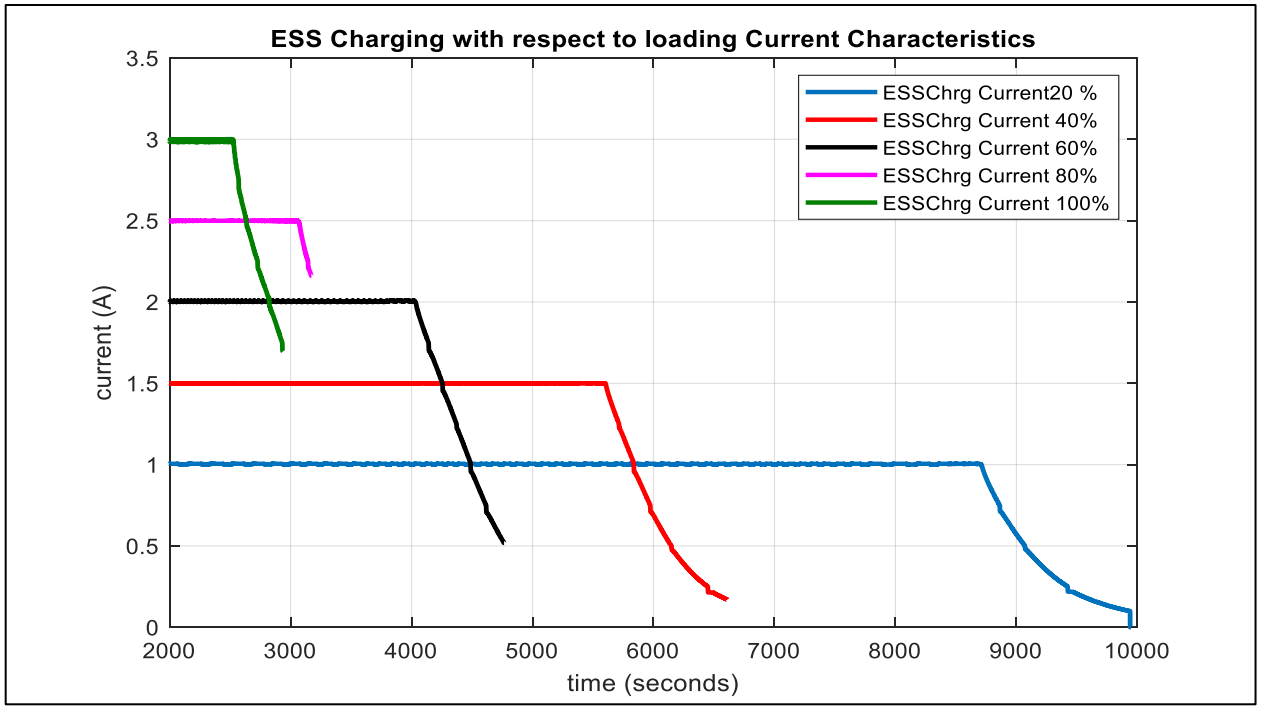

Fig. 7.6. Charging plots at various percentage of charging current (indicating drop in current at full charge).

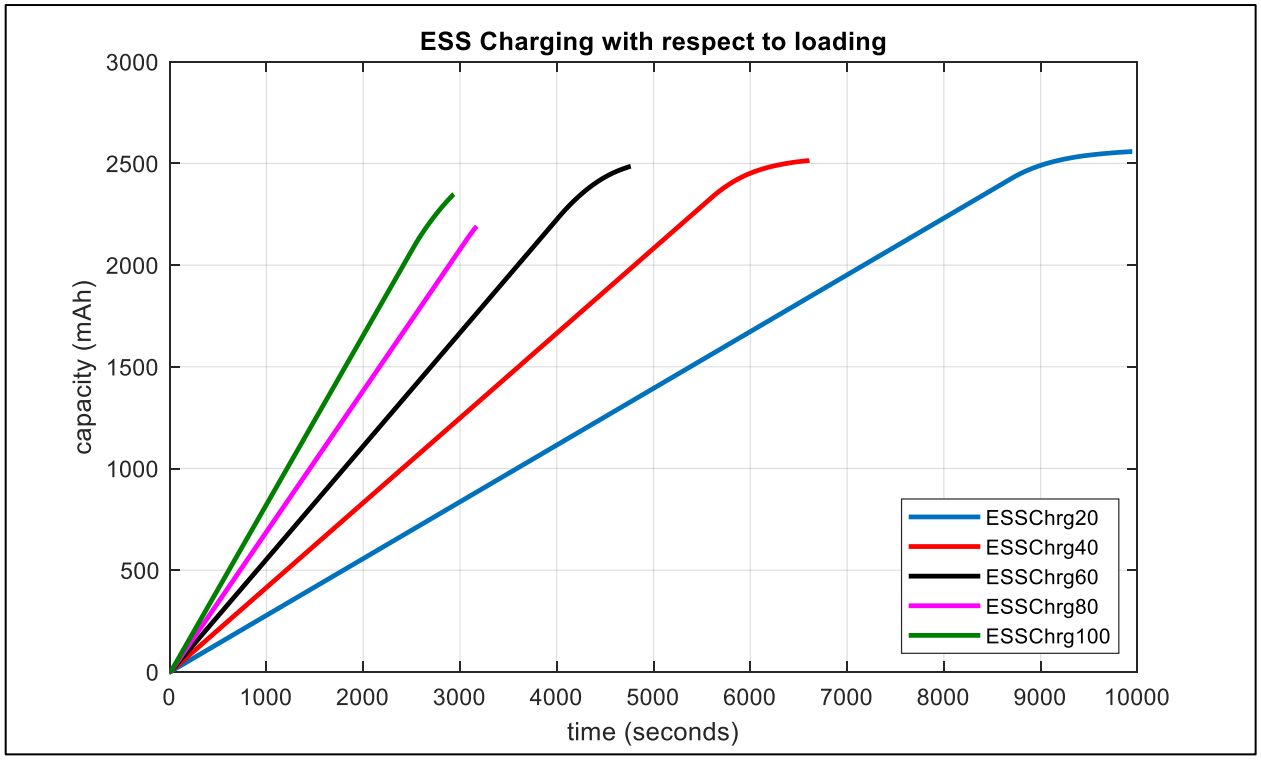

Fig. 7.7. Charging plots at various percentage of charging current (time to reach full capacity).

In Fig. 7.7, the charging time to reach full capacity is plotted. At 20% charging capacity, it takes a longer time to reach the ESS full capacity of 2500 mAh. However, as the charging percentage increases, the charging time to full capacity also decreases. For instance, at 100% charging capacity, the ESS full capacity is reached in less than 3000 seconds when compared to the charging time of 9000 seconds at a 20% charging capacity. The same characteristics are observed for the voltage against time plot Fig. 7.8. The maximum value of 4.2 V is recorded in less than 3000 seconds for a 100% charging capacity. The corresponding charging plots at various percentage charging capacities is highlighted Fig. 7.8.

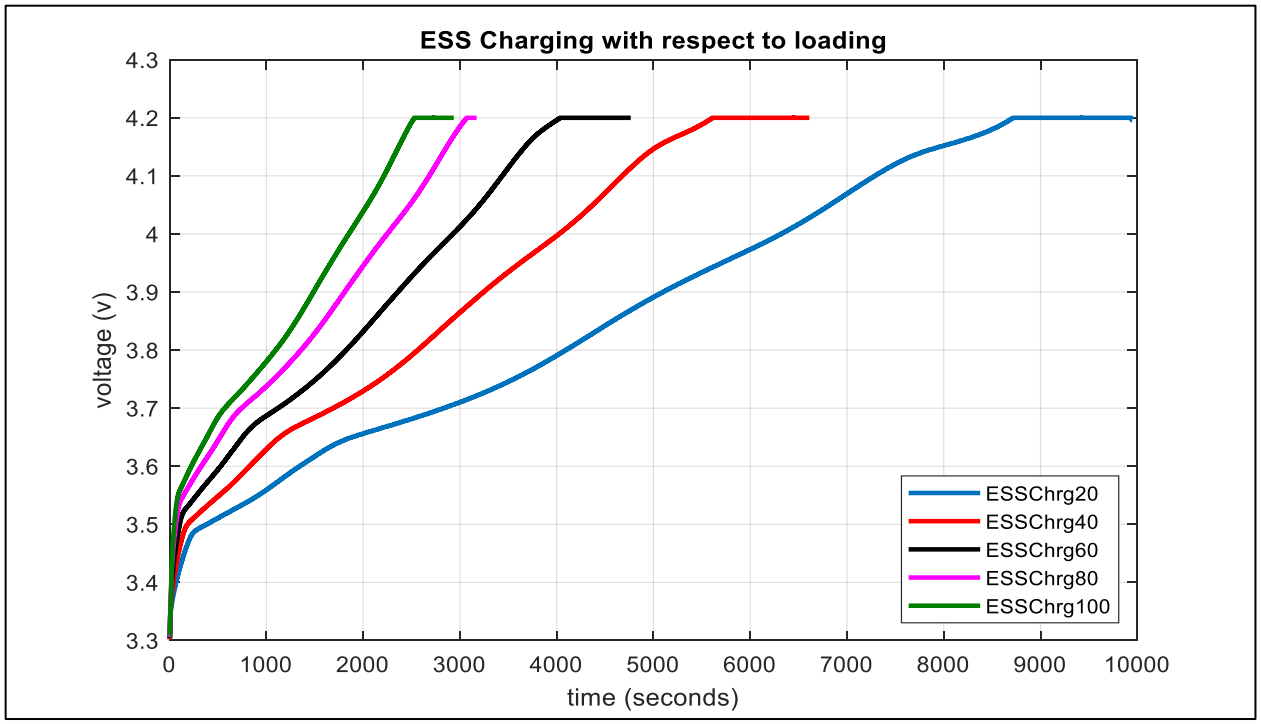

Fig. 7.8. Charging plots at various percentage charging capacities.

The discharging of the ESS unit was also initiated with varying steps of 20% to 100% representing the loading capacity assigned to the ESS unit. This is significant when part of the load of a particular bus is sectioned to be

powered by an ESS unit during a BSR. The plot of discharging of the ESS unit for varying percentage of 20% is shown in Fig. 7.9.

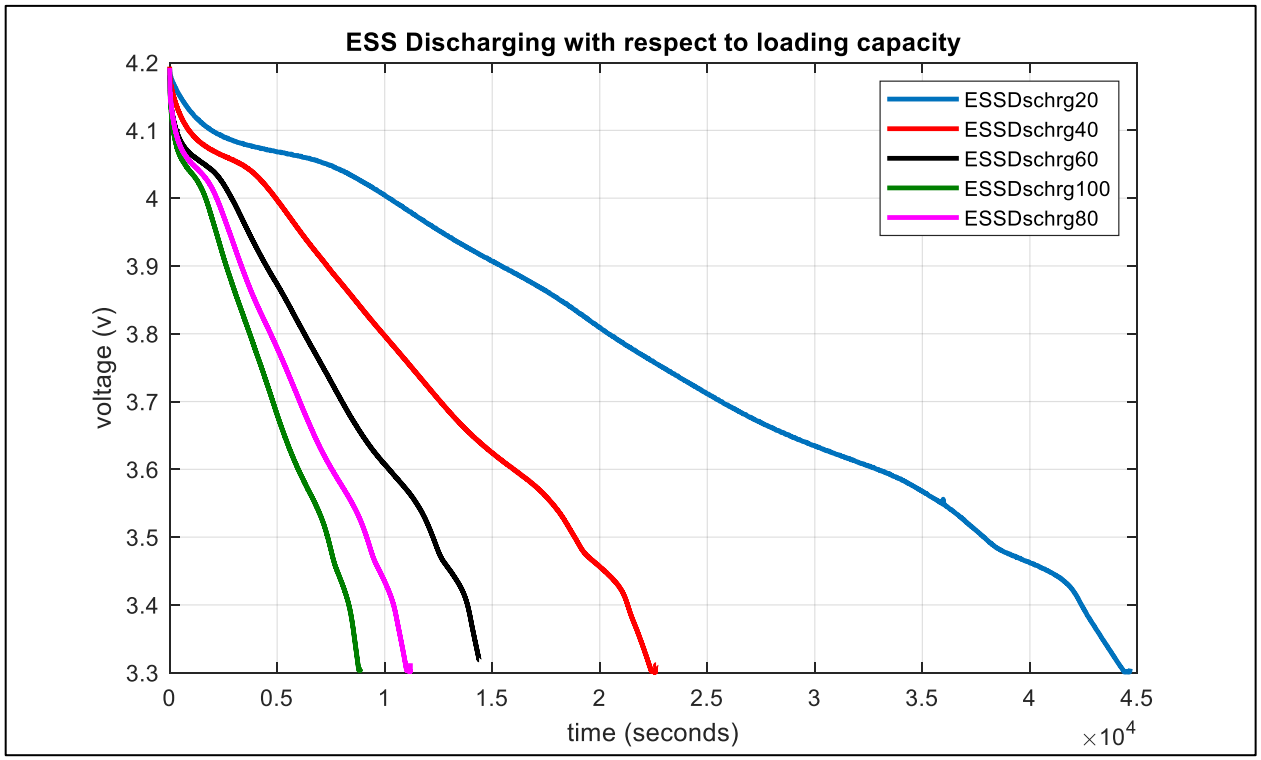

Fig. 7.9. The plot of discharging of the ESS unit for varying percentage (%) of 20.

For the 100 % charging of the ESS, the PV supplies at rated capacity, anticipating maximum sunshine for both Kaduna and Jos, thus a total ESS capacity is available to contribute for restoration. The ESS rate of charge and discharge is tabulated in Table 7.1.

Table 7.1. ESS rate of charging and discharging.

Rate (VA/min)	**20%**	**40%**	**60%**	**80%**	**100%**
Charging	6.279e-3	9.8182e-3	1.3500e-2	1.7419e-2	2.1600e-2
Discharging	1.2135e-3	2.4000e-3	3.7241e-3	4.9091e-3	0.6e-2

7.6 Deduction from Experimental Data and Incorporation into the BSR Model

The charging of the ESS unit was modelled and integrated into the restoration strategy implemented for the 48-bus system. With reference to the energy generation and consumption regions (Table 6.3), Kanji, Kaduna, Gwagwalada and Jos with a corresponding ESS capacity labelled as ESS 1, ESS 2, ESS 4 and ESS 5 respectively participated in the BSR. Katampe, Lokoja and New Heaven were omitted because their ESS capacities are the same as that of Jos and the resultant plots would be superimposed on each other. Also, ESS is assumed to be a non-black start unit, thus can only assist in restoration except the ones that the Load can be accommodated by the ESS unit. In Table 7.2, the ESS parameters is captured. The plots of ESS capacity during a 20% charging cycle are projected to represent an anticipated solar radiation between 07:00 – 08:00 and 17:00 – 18:00 respectively as shown in Fig. 7.10.

Table 7.2. ESS Parameters.

Parameters	**Kanji**	**Kaduna**	**Katampe**	**Gwagwalada**	**Jos**	**Lokoja**	**New Heaven**
$E_e^{ESS\_R}$ (MWh)	2.2	24.2	4	2	6.8	4	4
p_e^{min} (%)	10	10	10	10	10	10	10
p_e^{max} (%)	100	100	100	100	100	100	100
η_e^C	0.90	0.90	0.90	0.90	0.90	0.90	0.90
η_e^D	0.90	0.90	0.90	0.90	0.90	0.90	0.90
$p_e^{C\_min}/p_e^{C\_max}$ (MW)	10/55	121/605	10/50	20/100	34/170	20/100	20/100
$Q_e^{C\_min}/Q_e^{C\_max}$ (MVar)	0/20	0/200	0/20	0/20	0/20	0/20	0/20

$p_e^{D\_min}/p_e^{D\_max}$ (MW)	20/55	242/605	20/50	40/100	68/170	40/100	40/100
$Q_e^{D\_min}/Q_e^{D\_max}$ (MVar)	0/20	0/200	0/20	0/20	0/20	0/20	0/20

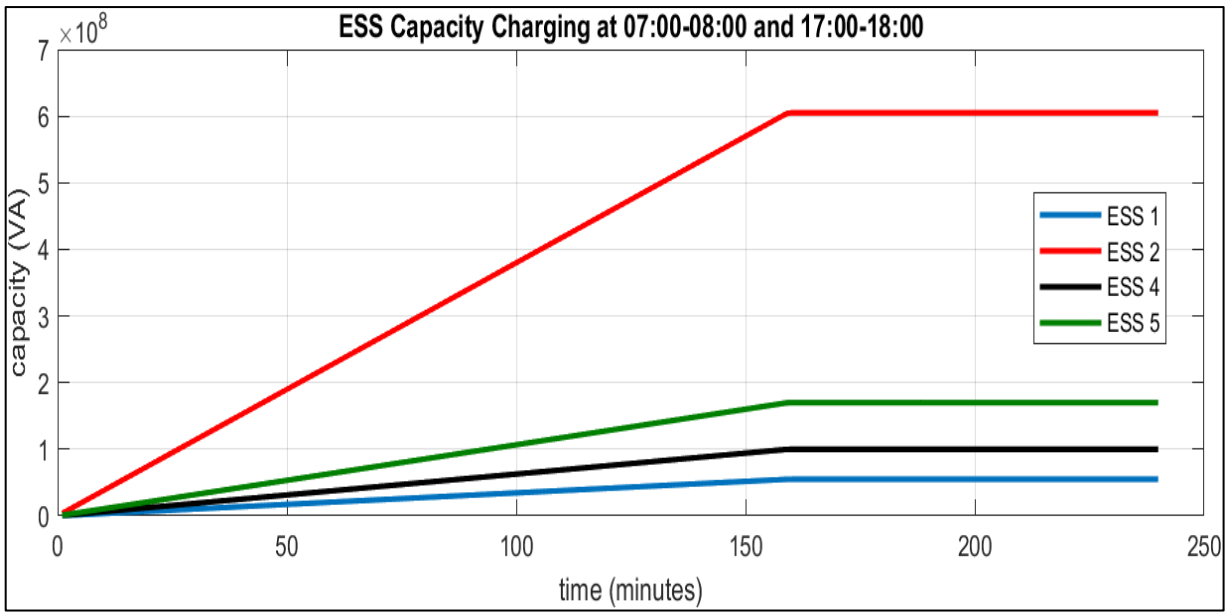

Fig. 7.10. Plots showing ESS charging capacity between 07:00 – 08:00 and 17:00 – 18:00.

It can be observed that for a 20% charging capacity, it takes 160 minutes to reach a steady state value. In Fig. 7.11 to Fig. 7.14, the plots for 40%, 60%, 80% and 100% charging capacities, reaching steady state values of 102 minutes, 75 minutes, 58 minutes and 47 minutes respectively are shown.

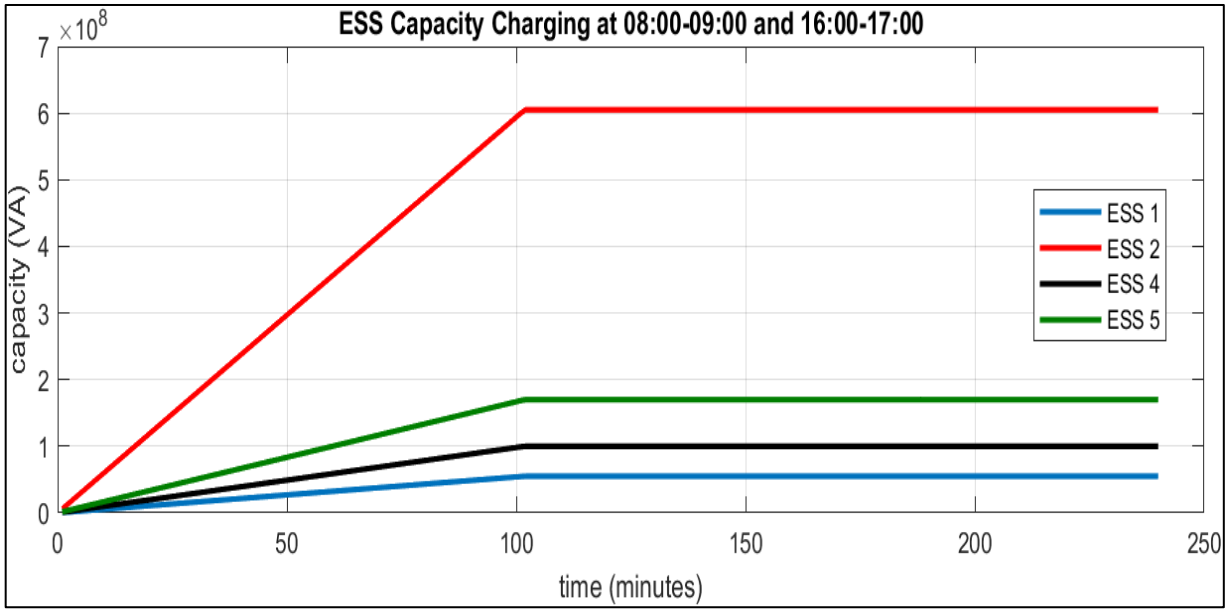

Fig. 7.11. Plots showing ESS charging capacity between 08:00 – 09:00 and 16:00 – 17:00.

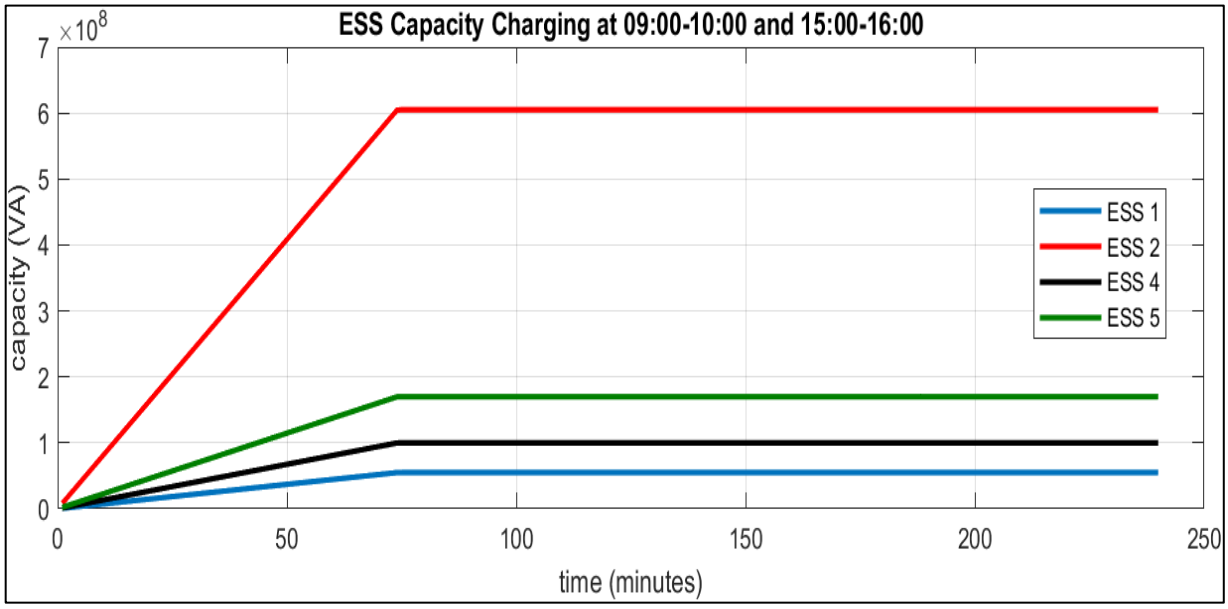

Fig. 7.12. Plots showing ESS charging capacity between 09:00 – 10:00 and 15:00 – 16:00.

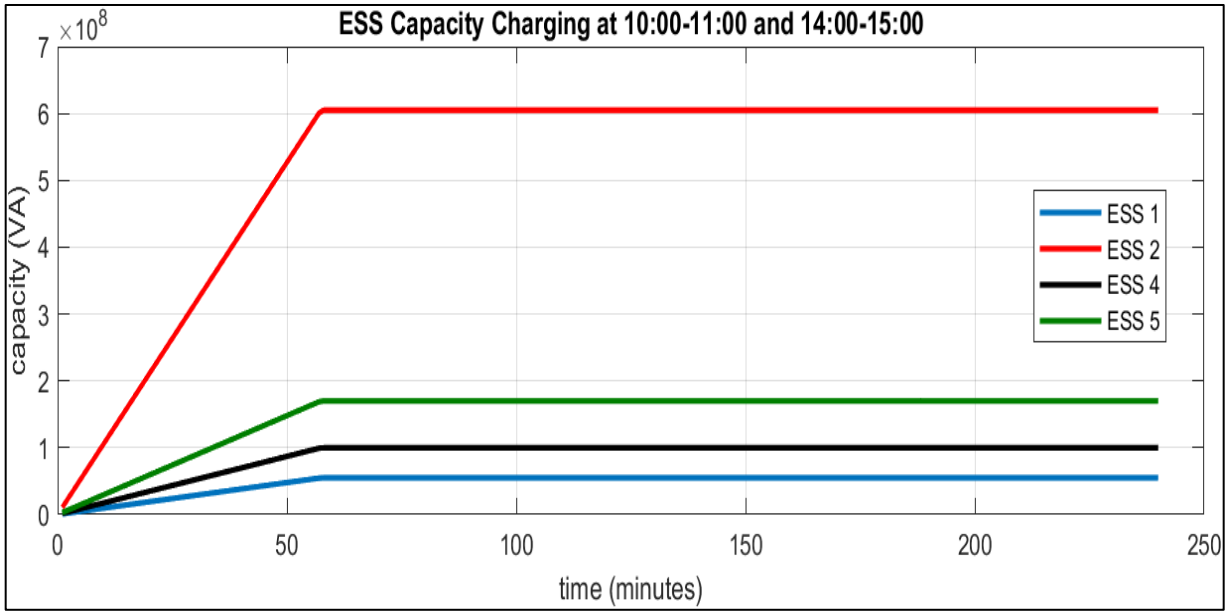

Fig. 7.13. Plots showing ESS charging capacity between10:00 -11:00 and 14:00 – 15:00.

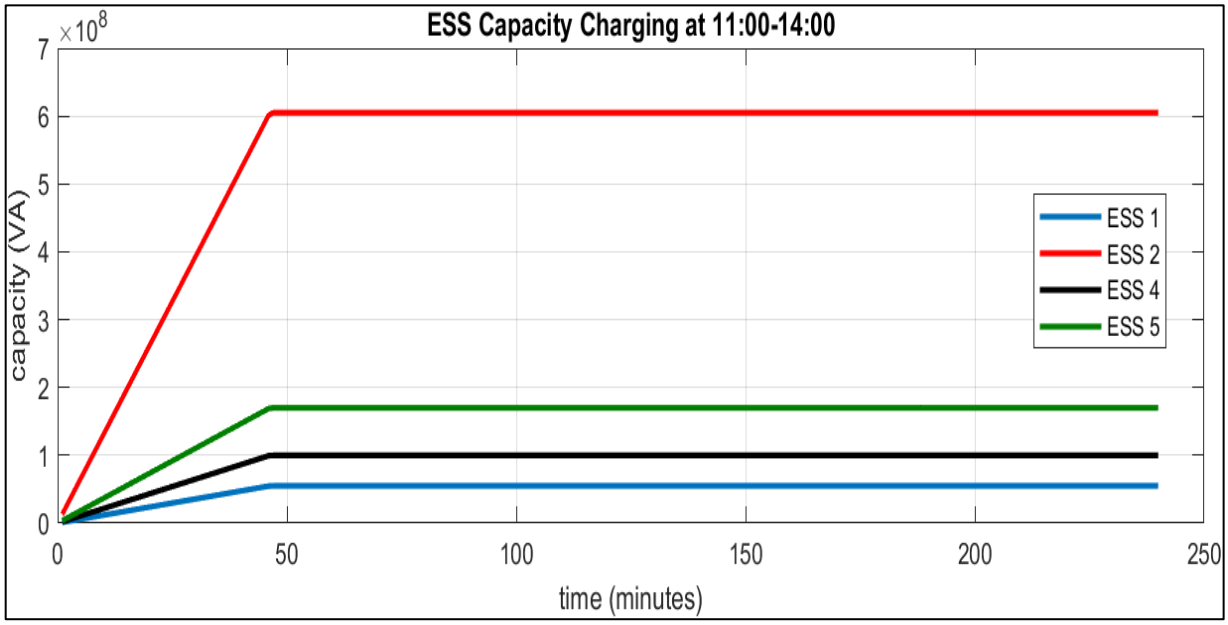

Fig. 7.14. Plots showing ESS charging capacity between 11:00 -12:00 and 13:00 – 14:00.

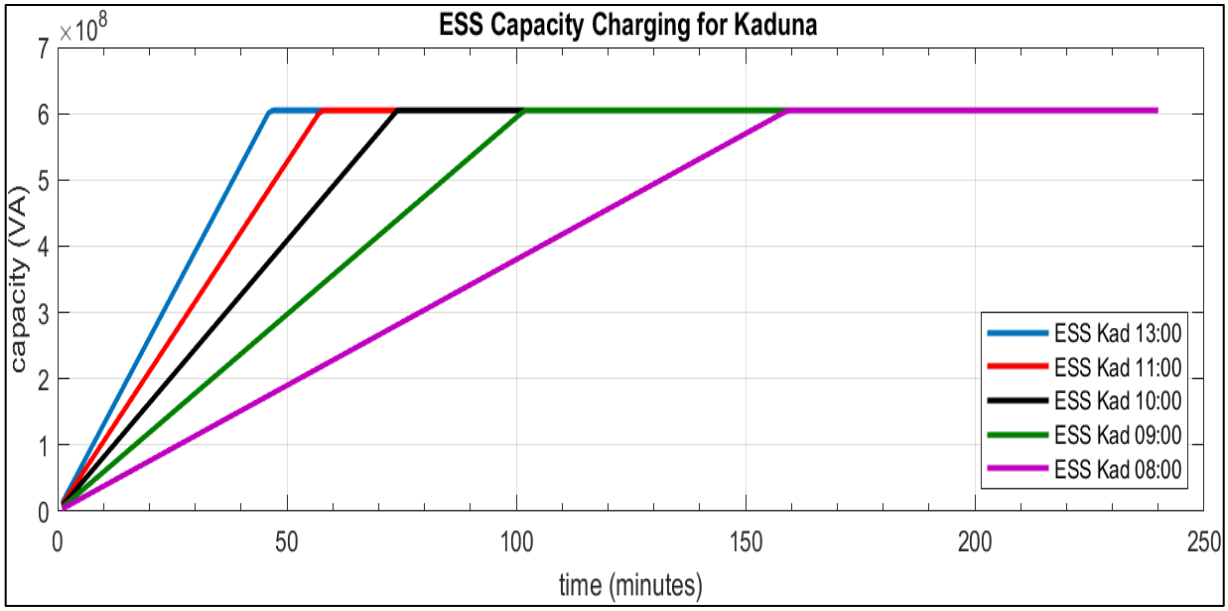

Fig. 7.15. Plots showing capacity of ESS during charging at Kaduna.

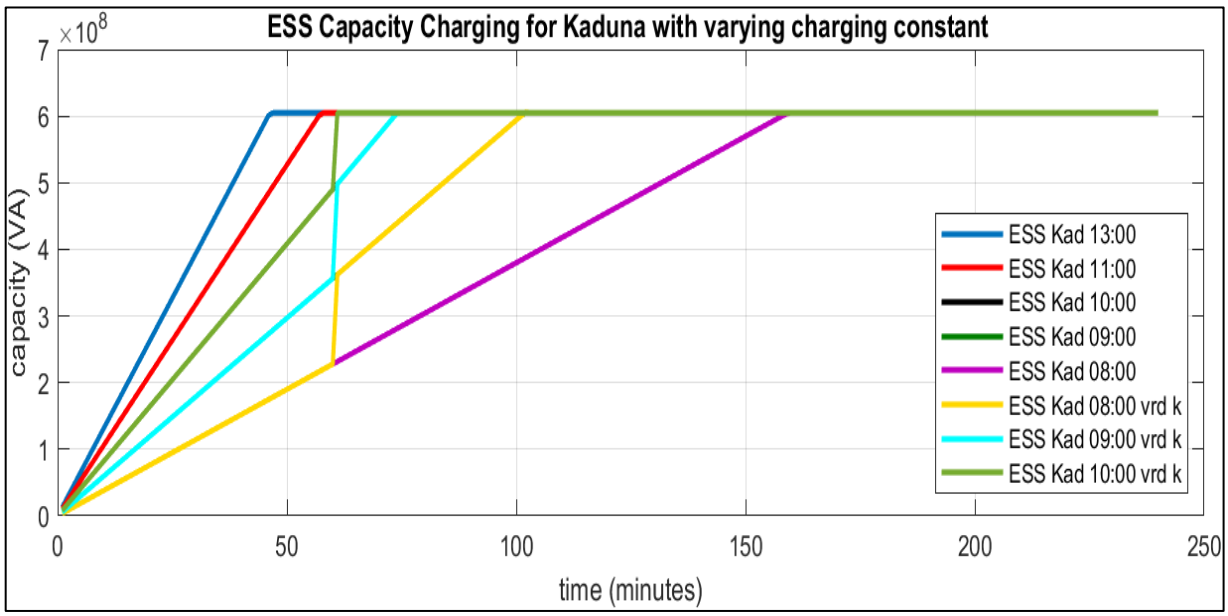

Fig. 7.16. Plots showing capacity of ESS during charging at Kaduna with varied k.

The various PV charging capacity of 20% to 100% illustrated (charging at 08:00, 09:00, 10:00, 11:00 and 13:00) for Kaduna TS are co-plotted for

the various times of the day and presented in Fig. 7.15. Considering the charging rates of 20%, 40% and 60% respectively, it can be observed that it takes more than an hour (60 minutes) to fully charge the ESS unit (Fig. 7.16). The adjusted plots for a charging time overlap of more than 60 minutes indicating the subsequent charging cycle is illustrated in Fig. 7.17. The resultant angular shift of the rate of charging coefficient for the time axis is tabulated in Table 7.3. With the full energisation of the load at Kaduna, assuming 20% to 100% loading capacity, the discharge of the ESS is triggered and shown in Fig. 7.18. The different energy availability scenarios are further analysed with varied assumptions made.

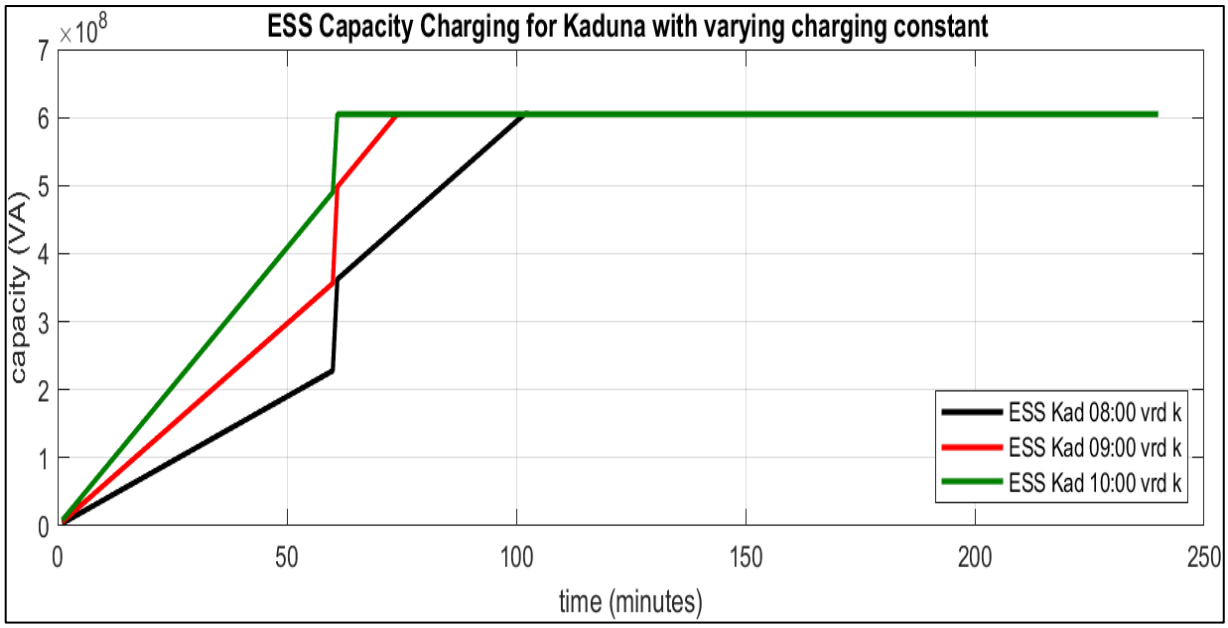

Fig. 7.17. Plots showing capacity of ESS during charging at Kaduna varying charging constant.

Table 7.3. Table showing angular value of the charging constant at different percentage.

Rate of charging showing charging constant angles (Degree)					
PV Buses	20%	40%	60%	80%	100%
Kanji	89.9906	89.9937	89.9953	89.9958	89.9968
Kaduna	89.9991	89.9994	89.9995	89.9996	89.9997
Katampe	89.9896	89.9931	89.9948	89.9954	89.9965
Gwagwalada	89.9948	89.9965	89.9974	89.9977	89.9982
Jos	89.9969	89.9979	89.9984	89.9986	89.9989
Lokoja	89.9948	89.9965	89.9974	89.9977	89.9982
New Heaven	89.9948	89.9965	89.9974	89.9977	89.9982

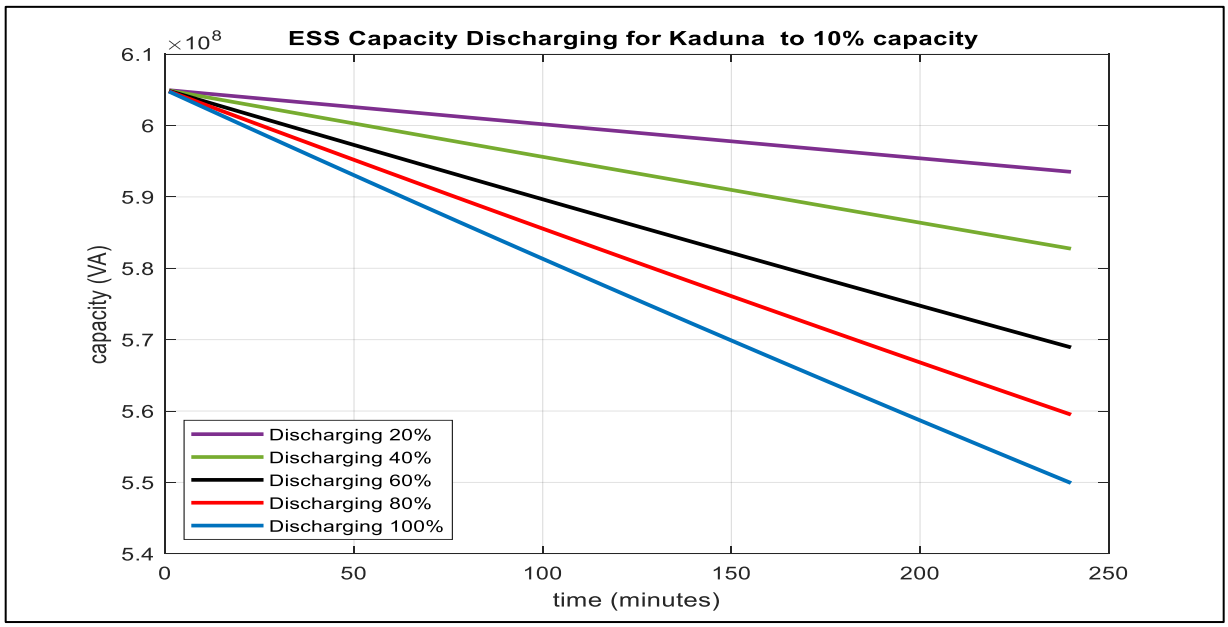

Fig. 7.18. Plots showing capacity of ESS during discharging at Kaduna bus.

7.6.1 Scenario 1

Energy availability for restoration at Jos bus 04:00.

- No sunshine available hence 0% charging.

- ESS previously charged to 100% capacity.
- Load energised at time step 3.
- 20% to 100% level of discharge of ESS implemented.

For all scenarios, before the initiation of BSR, the available energy sources includes: (i) generator at Shiroro, (ii) PV and ESS at Kaduna TS, and (iii) subsequently PV at Jos TS. A maximum power availability of 1,310.9 MVA for Kaduna TS is recorded, but a minimum drop to 1,003 MVA is recorded on loading, which decreased to a value of 1,002.4 MVA at a 100% discharge capacity. Conversely, at Jos TS, a maximum power availability of 1,480.9 MVA is recorded, but a minimum drop to 920.4 MVA is recorded on loading, which decreased to a value of 919.6 MVA at a 100% discharge capacity.

A decrease in the settling value is observed as the discharging is increased. A settling value of 1,185.5 MVA is recorded for 20% discharge capacity, decreasing to a value of 1,141.9 MVA for 100% discharge capacity for Kaduna, while at Jos TS, a settling value of 1,200.7 MVA is recorded for 20% discharge capacity, decreasing to a value of 1,144.8MVA for 100% discharge capacity as can be seen in Fig. 7.19 and Fig. 7.20 for Kaduna TS and Jos TS respectively, and tabulated in Table 7.4.

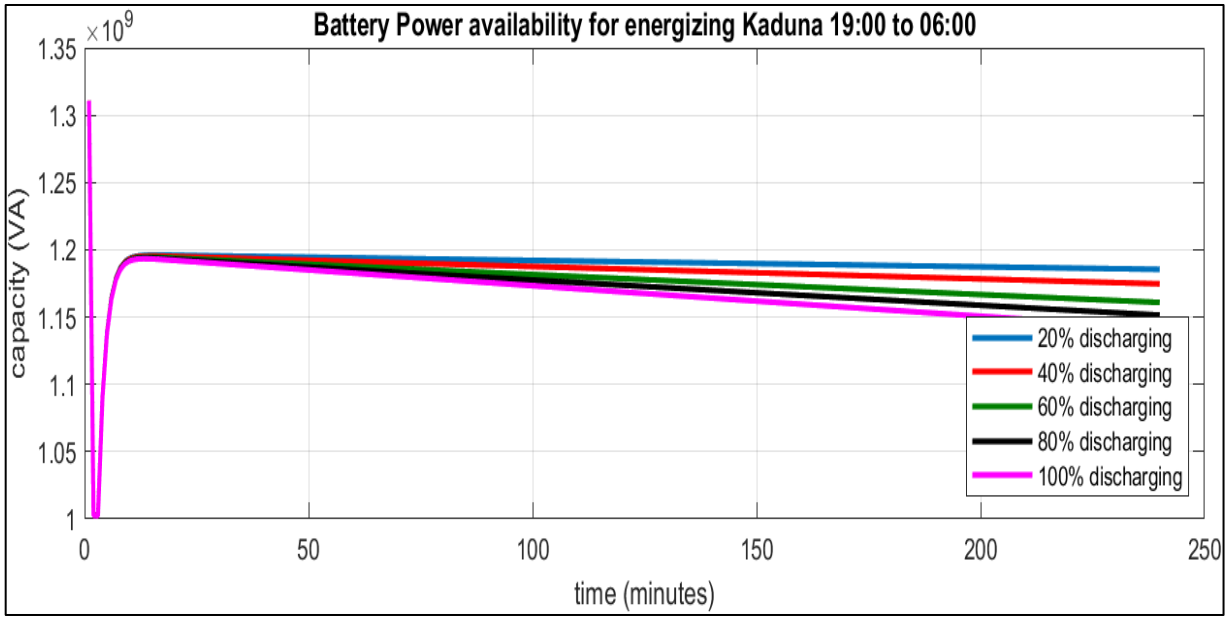

Fig. 7.19. Plots showing capacity of ESS during discharging at Kaduna bus (0% charging).

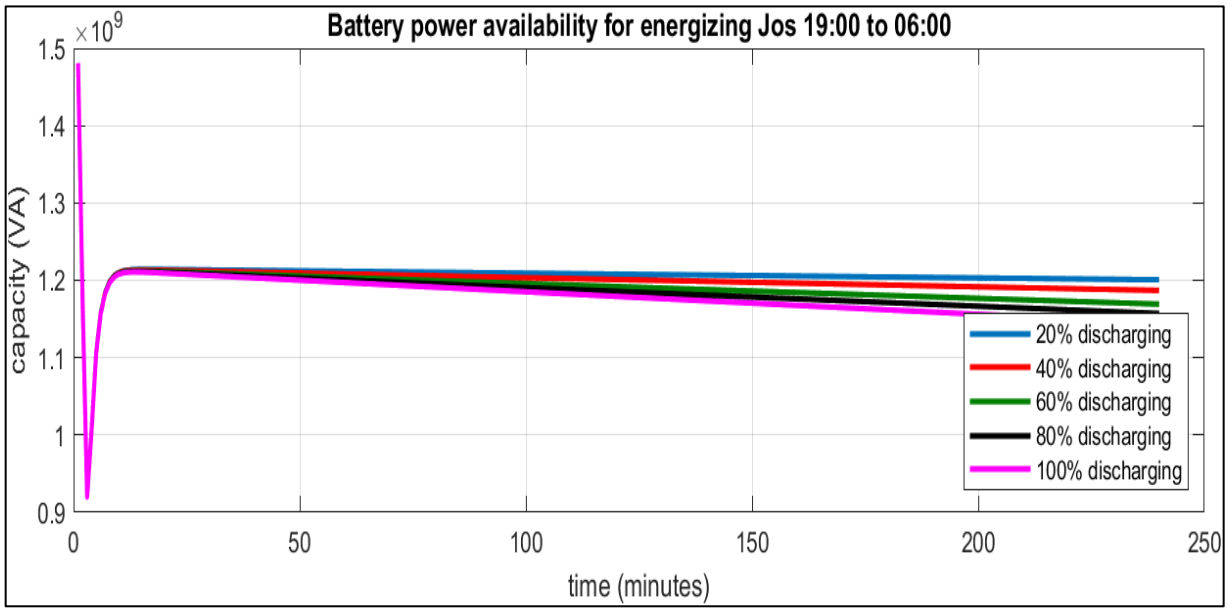

Fig. 7.20. Plots showing capacity of ESS during discharging at Jos bus (0% charging).

Table 7.4. Restoration at Kaduna TS and Jos TS 0% charging (20% - 100%) discharging.

Energy availability for restoration at 04:00 at Kaduna TS and Jos TS (0% charging)						
Discharging (20% to 100%)						
Bus	Value (MVA× 10^3)	20%	40%	60%	80%	100%
Kaduna	Max	1.3109	1.3109	1.3108	1.3108	1.3108
	Min	1.0030	1.0028	1.0026	1.0025	1.0024
	Settling value	1.1855	1.1747	1.1609	1.1515	1.1419
Jos	Max	1.4809	1.4809	1.4808	1.4807	1.4807
	Min	0.9204	0.9202	0.9200	0.9198	0.9196
	Settling value	1.2007	1.1869	1.1692	1.1571	1.1448

7.6.2 Scenarios 2

Energy availability for restoration at Jos bus 07:00 to 18:00.

- Sunshine available and charging done at 20% to 100%.
- ESS previously charged to 100% capacity.
- Load energised at time step 3.
- 20% level of discharge of ESS implemented.

A maximum power availability of 1,208.9 MVA for Kaduna TS is recorded. Upon loading, a minimum drop of 405.8 MVA is noted, with a resultant increase to a value of 424.3 MVA at a 100% discharge capacity. At Jos TS, a maximum power availability of 1,230.2 MVA is recorded, with a minimum drop to a value of 160.4 MVA experienced on loading. At a 100% discharge capacity, the value increases to 196.0 MVA.

A settling value of 1,208.4 MVA is recorded for 20% charge capacity, maintaining a steady state value for 100% charge capacity for Kaduna, while

at Jos TS, a settling value of 1,230.2 MVA is recorded for 20% charge capacity and also maintaining a steady state value for 100% charge capacity as can be seen in Fig. 7.21 and Fig. 7.25 for Kaduna TS and Jos TS respectively, and tabulated in Table 7.5.

Table 7.5. Restoration at Kaduna TS and Jos TS 20% discharging (20% - 100%) charging.

Energy availability for restoration at Kaduna TS and Jos TS (20% discharging)						
		Charging (20% to 100%)				
Bus	Value (MVA$\times 10^3$)	20%	40%	60%	80%	100%
Kaduna	Max	1.2084	1.2084	1.0284	1.2084	1.2084
	Min	0.4058	0.4101	0.4145	0.4193	0.4243
	Settling value	1.2084	1.2084	1.0284	1.2084	1.2084
Jos	Max	1.2302	1.2302	1.2302	1.2302	1.2302
	Min	0.1604	0.1686	0.1771	0.1863	0.1960
	Settling value	1.2302	1.2302	1.2302	1.2302	1.2302

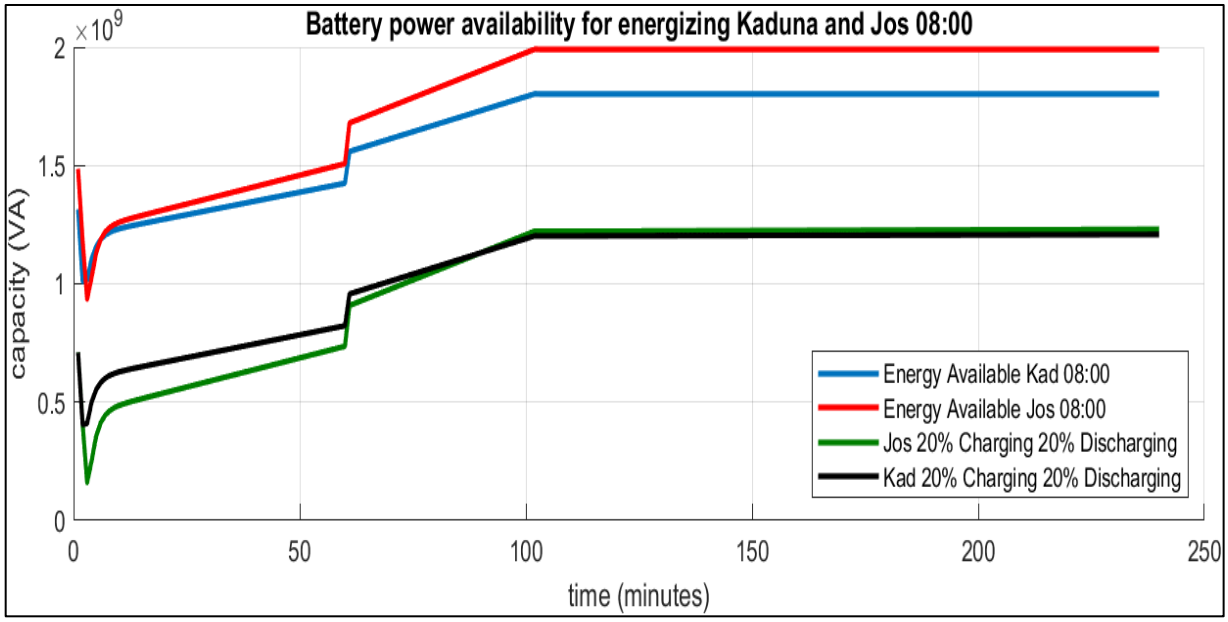

Fig. 7.21. Plots showing energy capacity at 20% with 20% discharging at Kaduna and Jos.

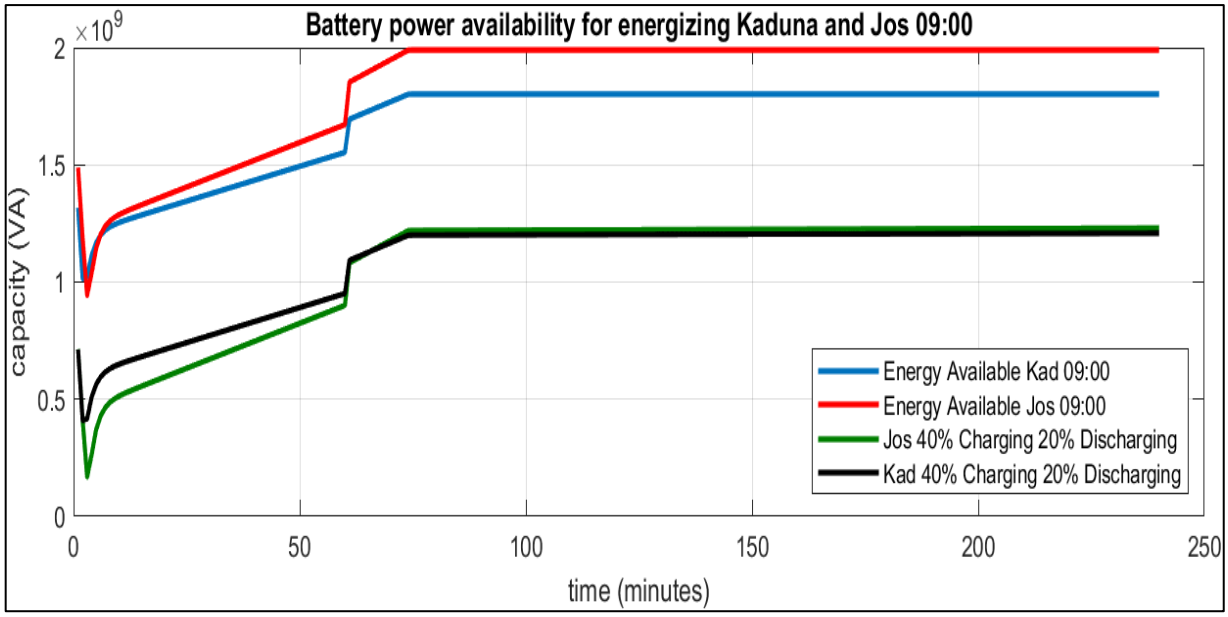

Fig. 7.22. Plots showing energy capacity at 40% with 20% discharging at Kaduna and Jos.

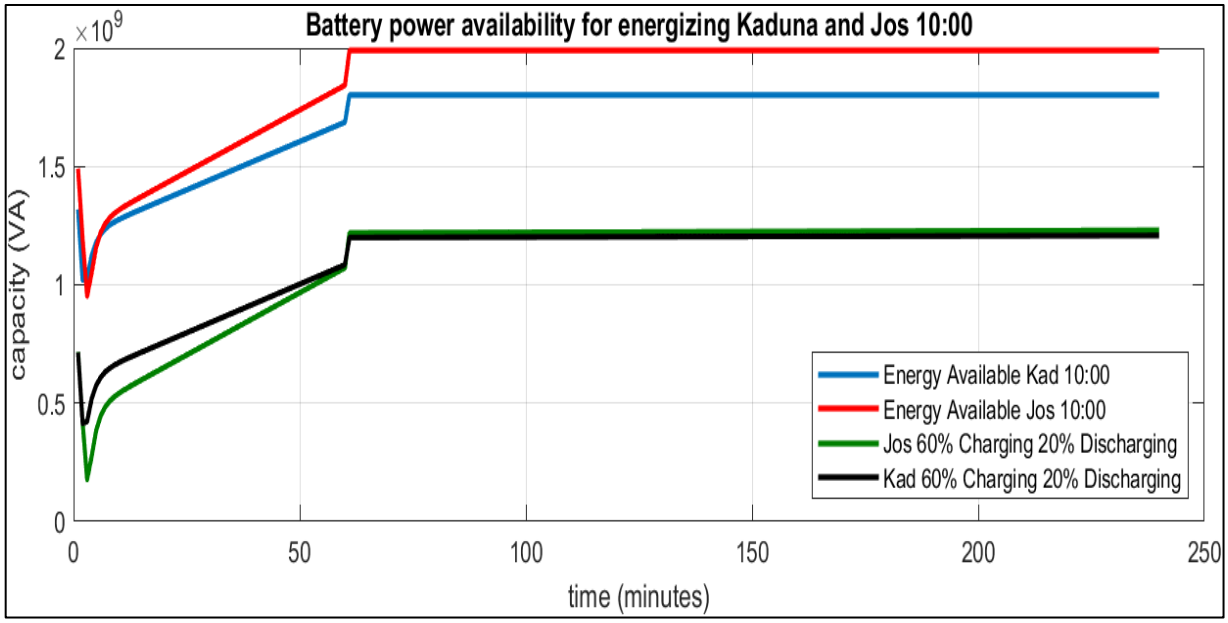

Fig. 7.23. Plots showing energy capacity at 60% with 20% discharging at Kaduna and Jos.

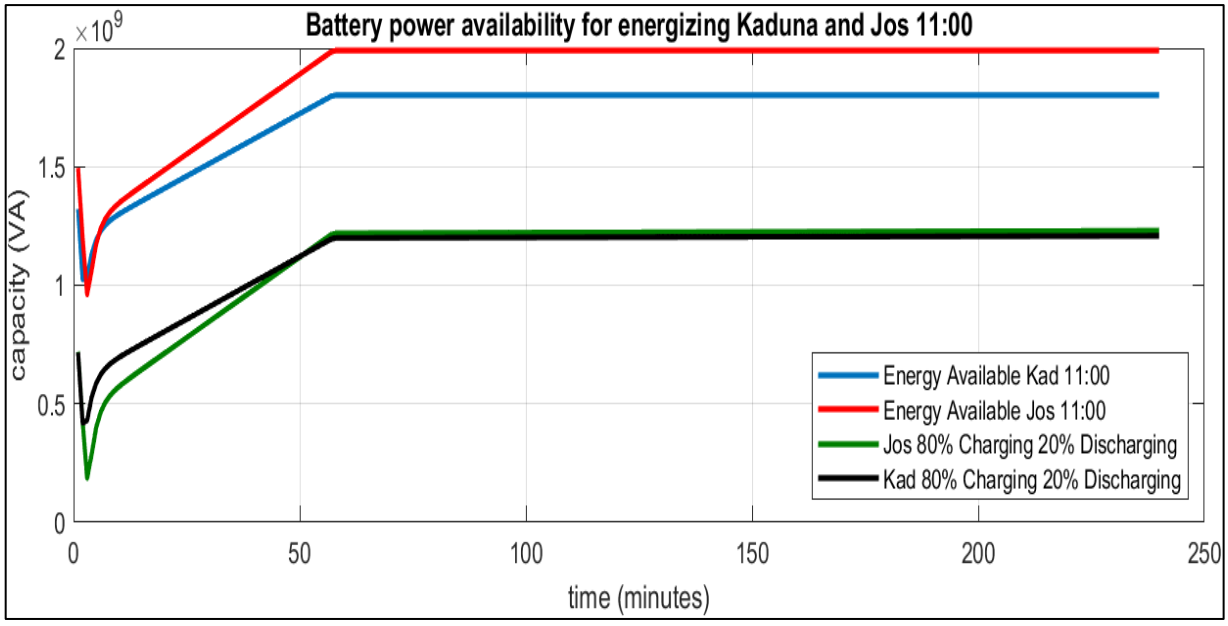

Fig. 7.24. Plots showing energy capacity at 80% with 20% discharging at Kaduna and Jos.

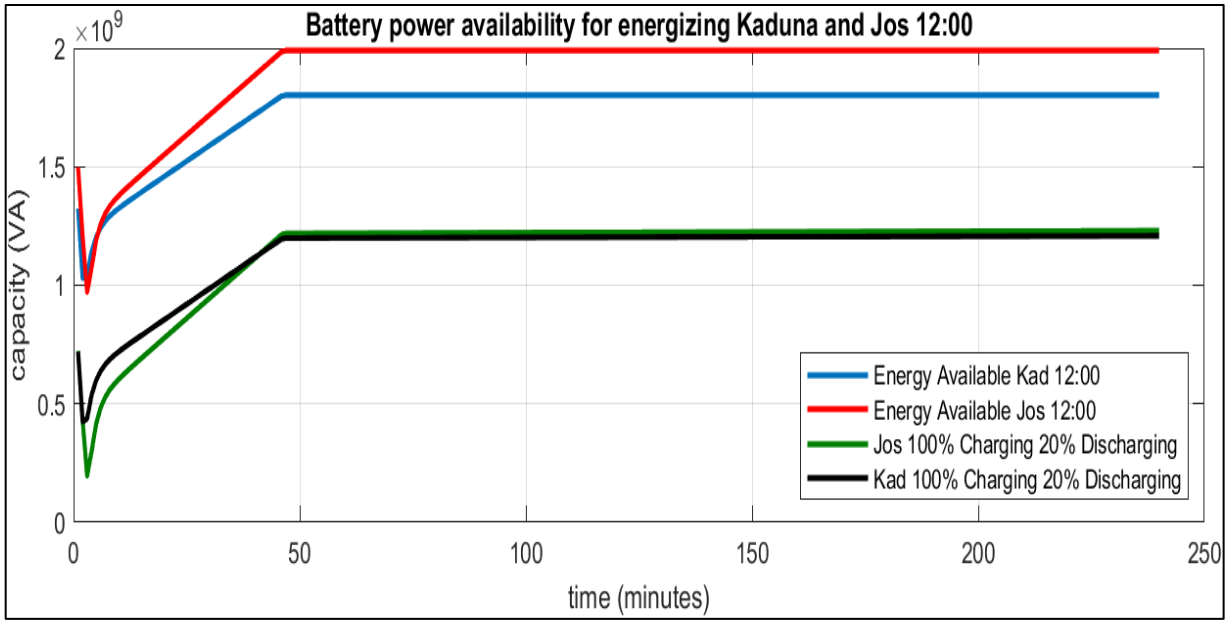

Fig. 7.25. Plots showing energy capacity at 100% with 20% discharging at Kaduna and Jos.

7.6.3 Scenarios 3

Energy availability for restoration at Jos bus 07:00 to 18:00.

- Sunshine available and charging done at 20% to 100%.
- ESS previously charged to 100% capacity.
- Load energised at time step 3.
- 40% level of discharge of ESS implemented.

The maximum power availability for Kaduna TS is 1,219.2 MVA. When loaded, a minimum drop to a value of 405.9 MVA is recorded, which increased to a value of 424.4 MVA at a 100% discharge capacity. Similarly, at Jos TS, a maximum power availability of 1,243.9 MVA is recorded, but upon loading, a minimum drop to 160.5 MVA is observed. This value is noted to have increased to 196.2 MVA at a 100% discharge capacity.

For Kaduna and Jos, a settling value of 1,219.2 MVA and 1,243.9 MVA respectively is recorded for 20% charge capacity, hence maintaining a steady state value for 100% charge capacity as shown in Fig. 7.26 and Fig. 7.30 for Kaduna TS and Jos TS respectively, and tabulated in Table 7.6.

Table 7.6. Restoration at Kaduna TS and Jos TS 40% discharging (20% - 100%) charging.

Energy availability for restoration at Kaduna TS and Jos TS (40% discharging)						
Charging (20% to 100%)						
Bus	Value (MVA$\times 10^3$)	20%	40%	60%	80%	100%
Kaduna	Max	1.2192	1.2192	1.2192	1.2192	1.2192
	Min	0.4059	0.4102	0.4146	0.4194	0.4244
	Settling value	1.2192	1.2192	1.2192	1.2192	1.2192
Jos	Max	1.2439	1.2439	1.2439	1.2439	1.2439
	Min	0.1605	0.1688	0.1773	0.1864	0.1962
	Settling value	1.2439	1.2439	1.2439	1.2439	1.2439

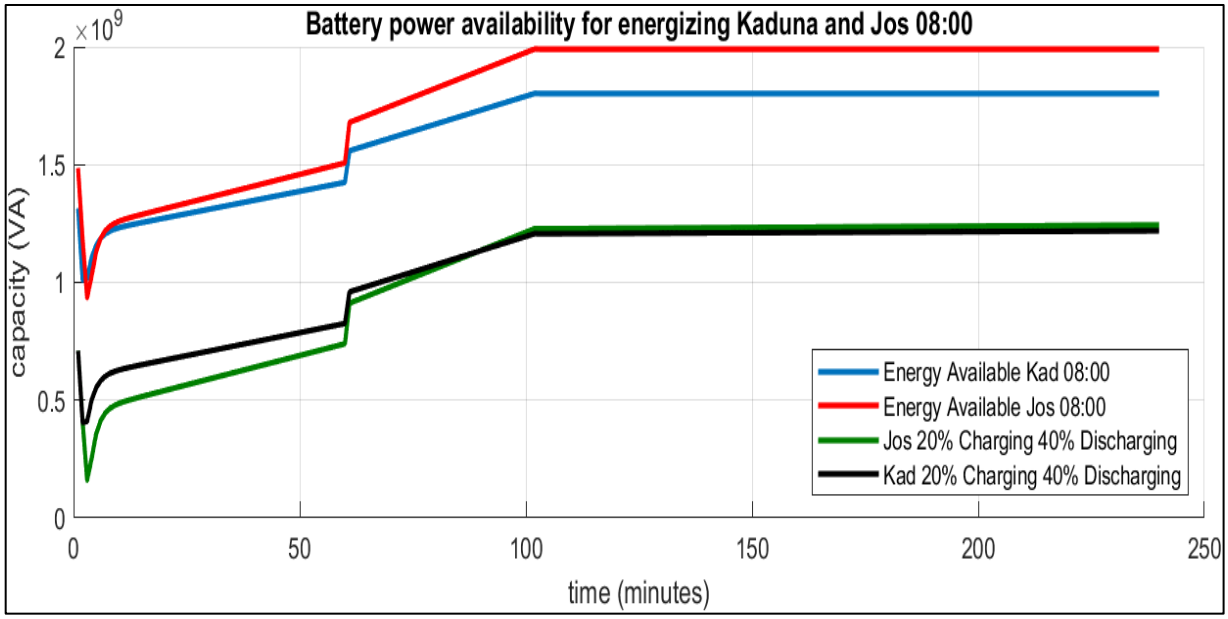

Fig. 7.26. Plots showing energy capacity at 20% with 40% discharging at Kaduna and Jos.

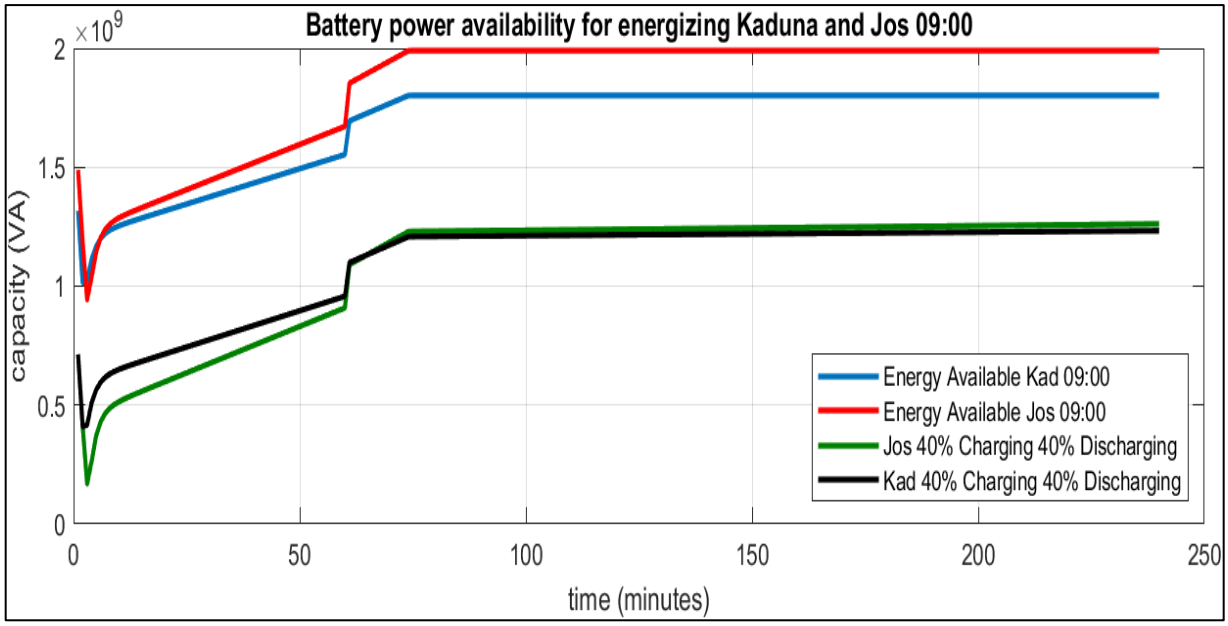

Fig. 7.27. Plots showing energy capacity at 40% with 40% discharging at Kaduna and Jos.

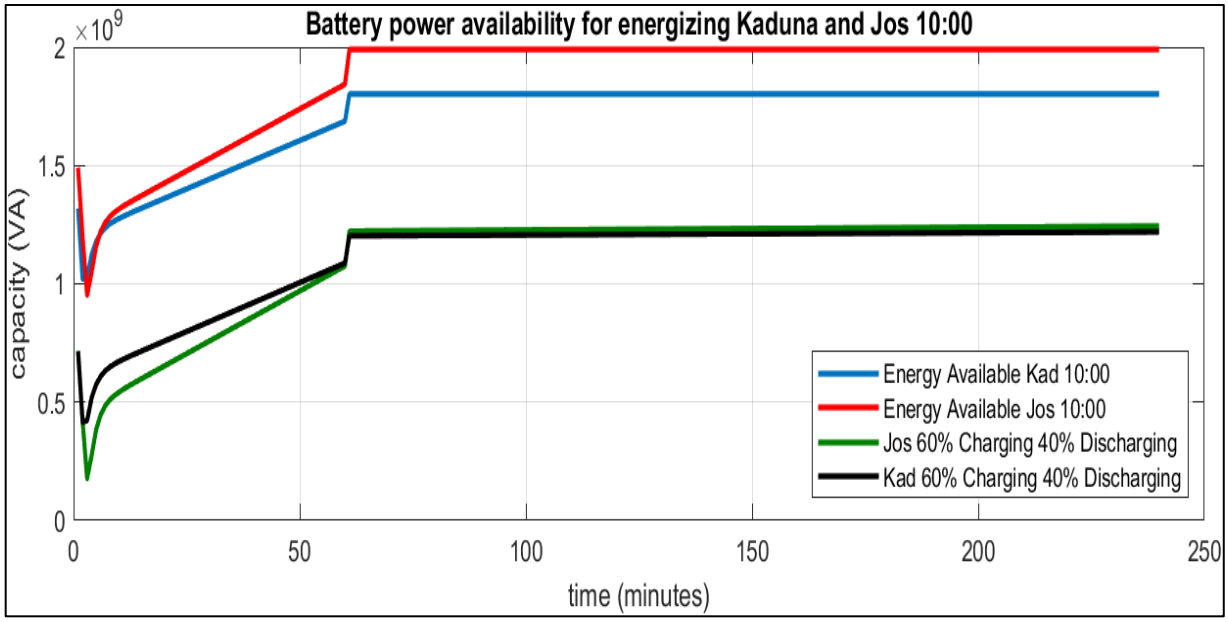

Fig. 7.28. Plots showing energy capacity at 60% with 40% discharging at Kaduna and Jos.

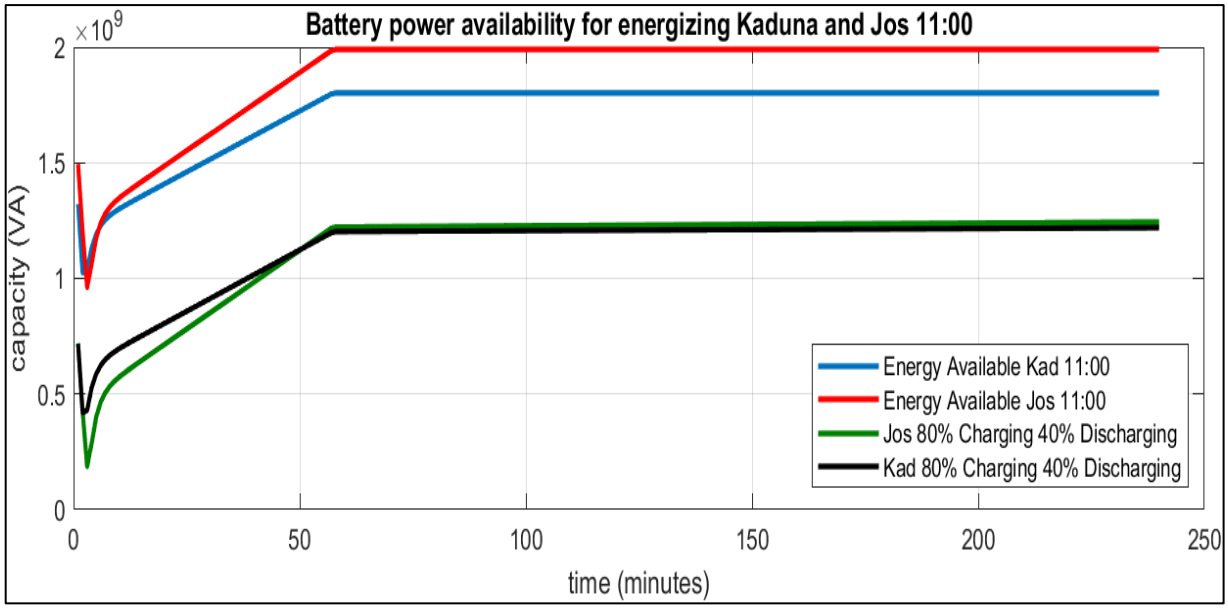

Fig. 7.29. Plots showing energy capacity at 80% with 40% discharging at Kaduna and Jos.

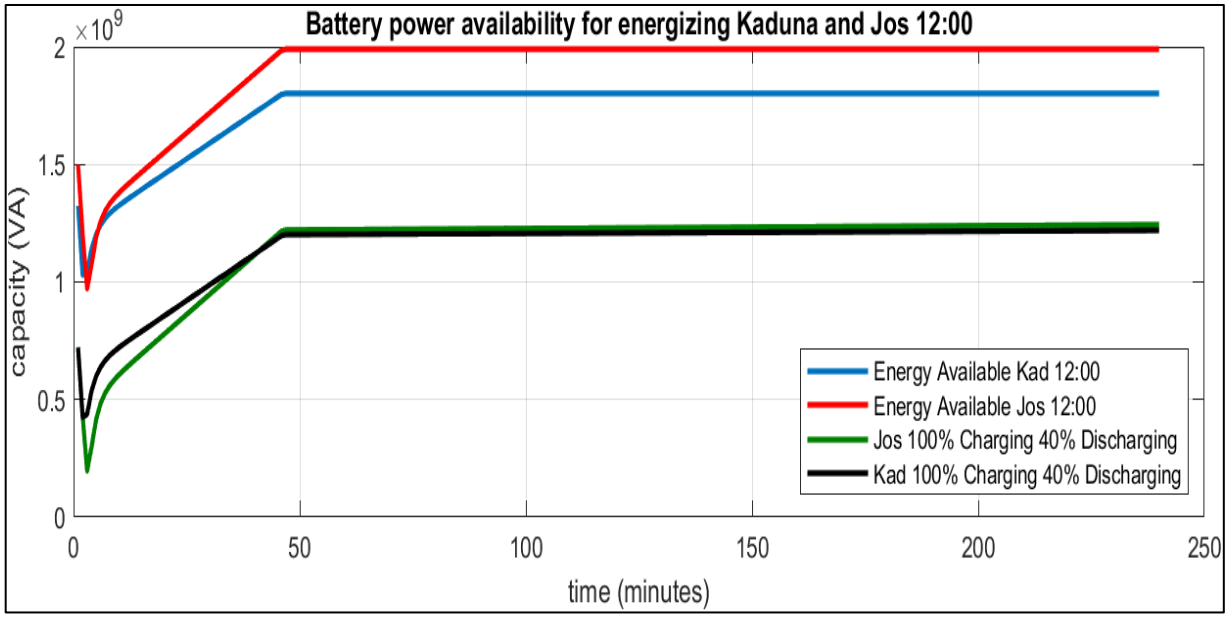

Fig. 7.30. Plots showing energy capacity at 100% with 40% discharging at Kaduna and Jos.

7.6.4 Scenarios 4

Energy availability for restoration at Jos bus 07:00 to 18:00.

- Sunshine available and charging done at 20% to 100%.
- ESS previously charged to 100% capacity.
- Load energised at time step 3.
- 60% level of discharge of ESS implemented.

Kaduna TS maximum power availability is 1,233.0 MVA. When loaded, a minimum of 406.0 MVA is recorded, which subsequently increased to a value of 424.5 MVA at a 100% discharge capacity. Likewise at Jos TS, a maximum power availability of 1,261.7 MVA is recorded. However, upon loading a minimum drop of 160.8 MVA is noted, which increased to a value of 196.4 MVA at a 100% discharge capacity.

A settling value of 1,233.0 MVA and 1,261.7 MVA respectively is recorded at 20% charge capacity for Kaduna and Jos, maintaining a steady state value even for 100% charge capacity. This is captured in Fig. 7.31 and Fig. 7.35 for Kaduna TS and Jos TS respectively and tabulated in Table 7.7.

Table 7.7. Restoration at Kaduna TS and Jos TS 60% discharging (20% - 100%) charging.

Energy availability for restoration at Kaduna TS and Jos TS (60% discharging)						
Charging (20% to 100%)						
Bus	Value (MVA$\times 10^3$)	20%	40%	60%	80%	100%
Kaduna	Max	1.2330	1.2330	1.2330	1.2330	1.2330
	Min	0.4060	0.4103	0.4147	0.4195	0.4245
	Settling value	1.2330	1.2330	1.2330	1.2330	1.2330
Jos	Max	1.2617	1.2617	1.2617	1.2617	1.2617
	Min	0.1608	0.1690	0.1776	0.1867	0.1964
	Settling value	1.2617	1.2617	1.2617	1.2617	1.2617

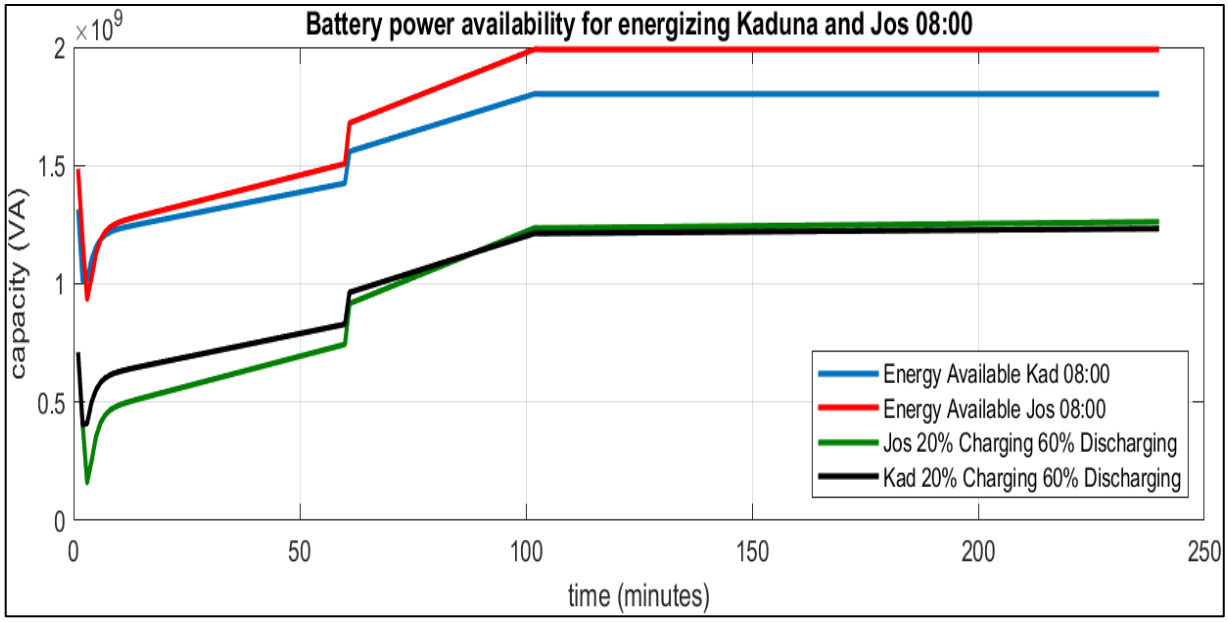

Fig. 7.31. Plots showing energy capacity at 20% with 60% discharging at Kaduna and Jos.

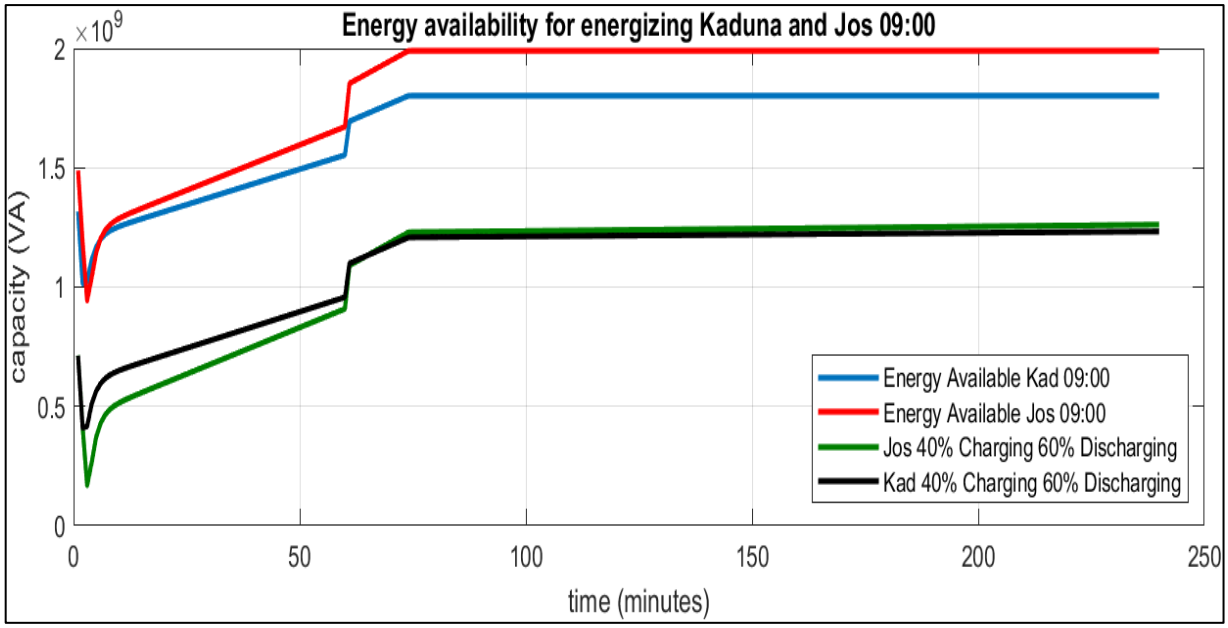

Fig. 7.32. Plots showing energy capacity at 40% with 60% discharging at Kaduna and Jos.

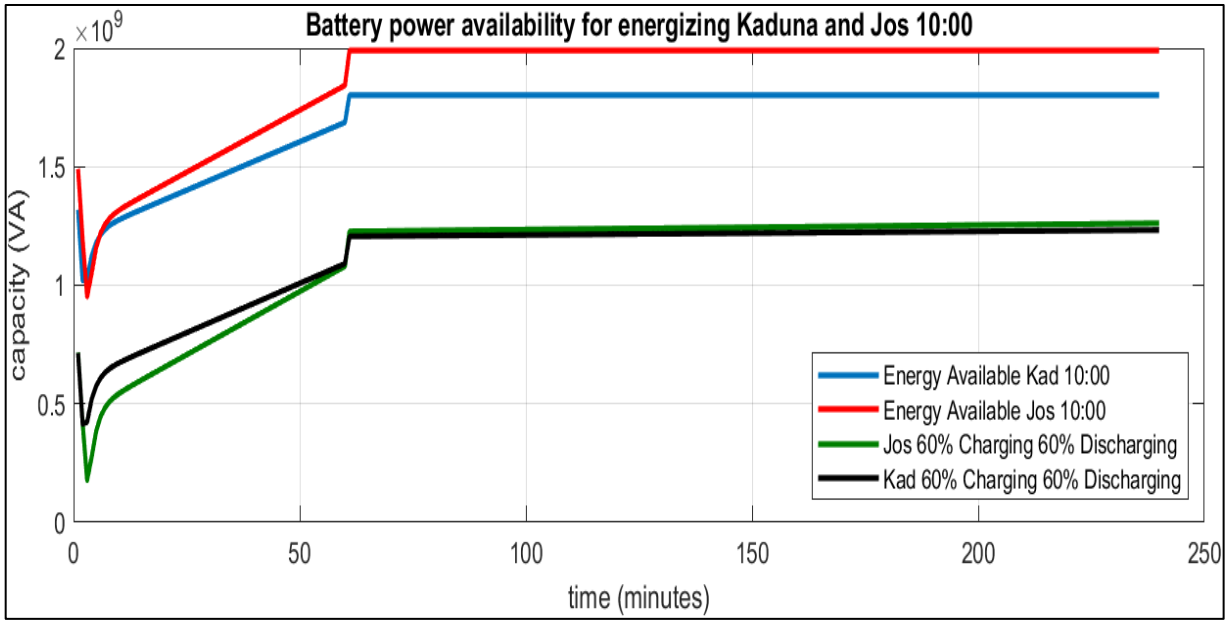

Fig. 7.33. Plots showing energy capacity at 60% with 60% discharging at Kaduna and Jos.

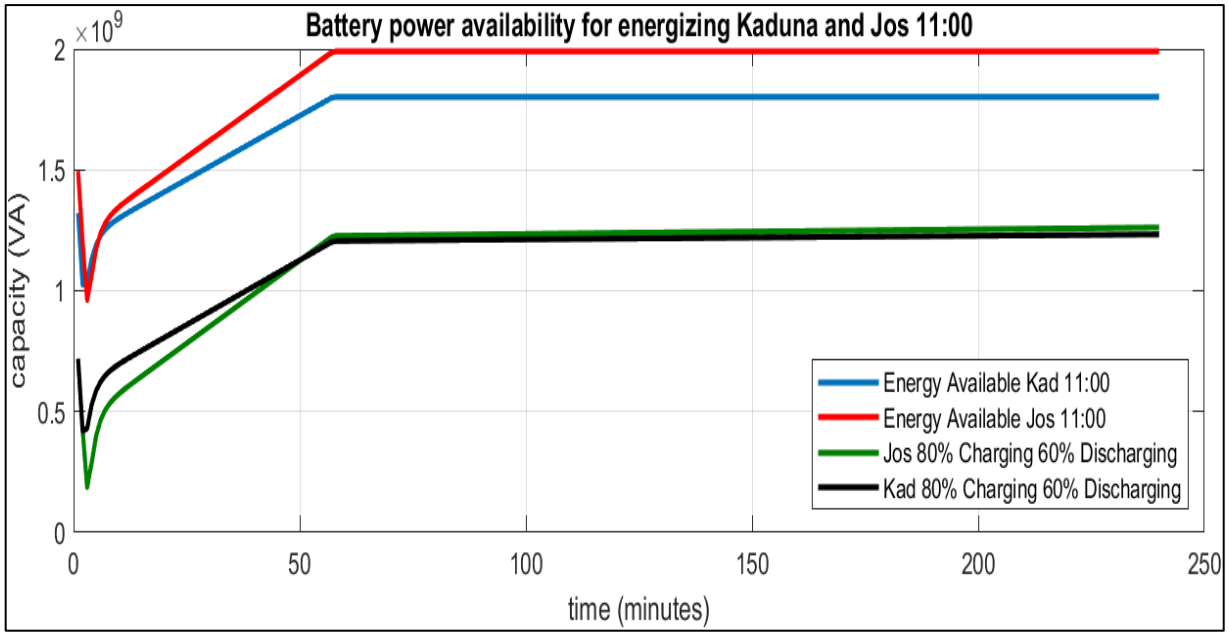

Fig. 7.34. Plots showing energy capacity at 80% with 60% discharging at Kaduna and Jos.

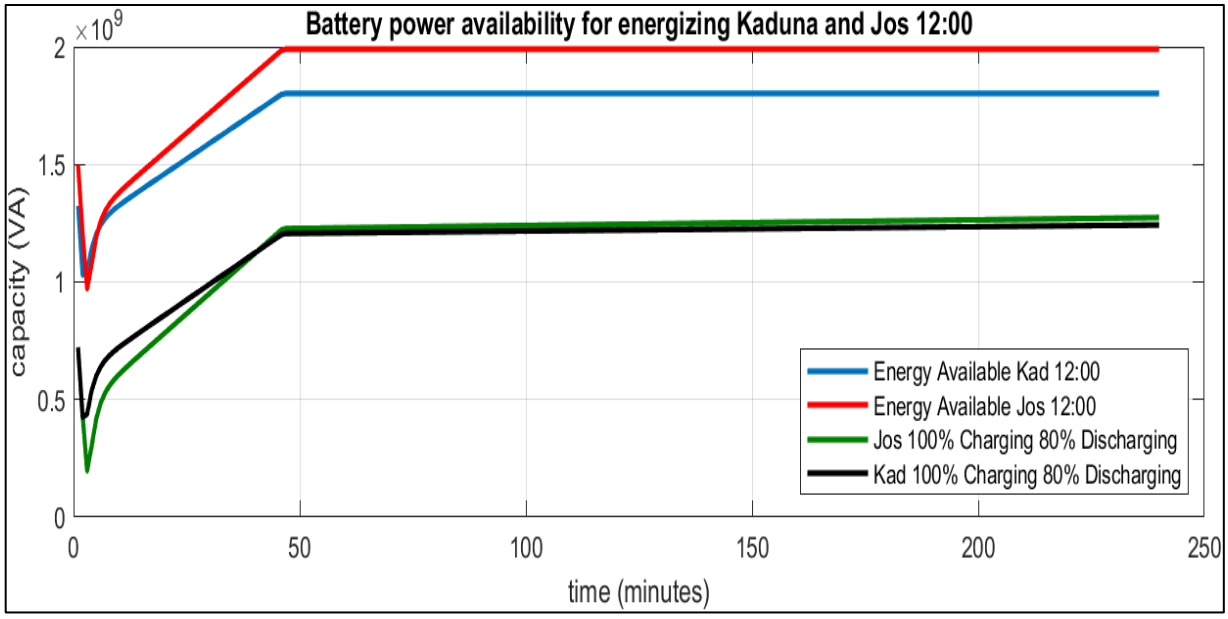

Fig. 7.35. Plots showing energy capacity at 100% with 60% discharging at Kaduna and Jos.

7.6.5 Scenarios 5

Energy availability for restoration at Jos bus 07:00 to 18:00.

- Sunshine available and charging done at 20% to 100%.
- ESS previously charged to 100% capacity.
- Load energised at time step 3.
- 80% level of discharge of ESS implemented.

A maximum power availability of 1,242.4 MVA for Kaduna TS is recorded at no load. When loaded, a minimum drop to a value 406.9 MVA is observed, with a subsequent increase to a value of 424.6 MVA at a 100% discharge capacity. Comparatively, at Jos TS, a maximum power availability of 1,273.7 MVA is recorded, but with a subsequent minimum drop to a value of 160.9 MVA upon loading. At a 100% discharge capacity, an increase to a value of 196.5 MVA is noted.

The respective settling values for Kaduna and Jos recorded for a 20% charge capacity is 1,242.4 MVA and 1,273.7 MVA. As can be seen in Fig. 7.36 and Fig. 7.40 for Kaduna TS and Jos TS respectively and tabulated in Table 7.8, both locations maintained a steady state value even for a 100% charge capacity.

Table 7.8. Restoration at Kaduna TS and Jos TS 80% discharging (20 - 100%) charging.

Energy availability for restoration at Kaduna TS and Jos TS (80% discharging)						
Charging (20% to 100%)						
Bus	Value (MVA$\times 10^3$)	20%	40%	60%	80%	100%
Kaduna	Max	1.2424	1.2425	1.2425	1.2424	1.2424
	Min	0.4609	0.4104	0.4148	0.4195	0.4246
	Settling value	1.2424	1.2425	1.2425	1.2424	1.2424
Jos	Max	1.2737	1.2737	1.2737	1.2737	1.2737
	Min	0.1609	1.6716	0.1777	0.1868	0.1965
	Settling value	1.2737	1.2737	1.2737	1.2737	1.2737

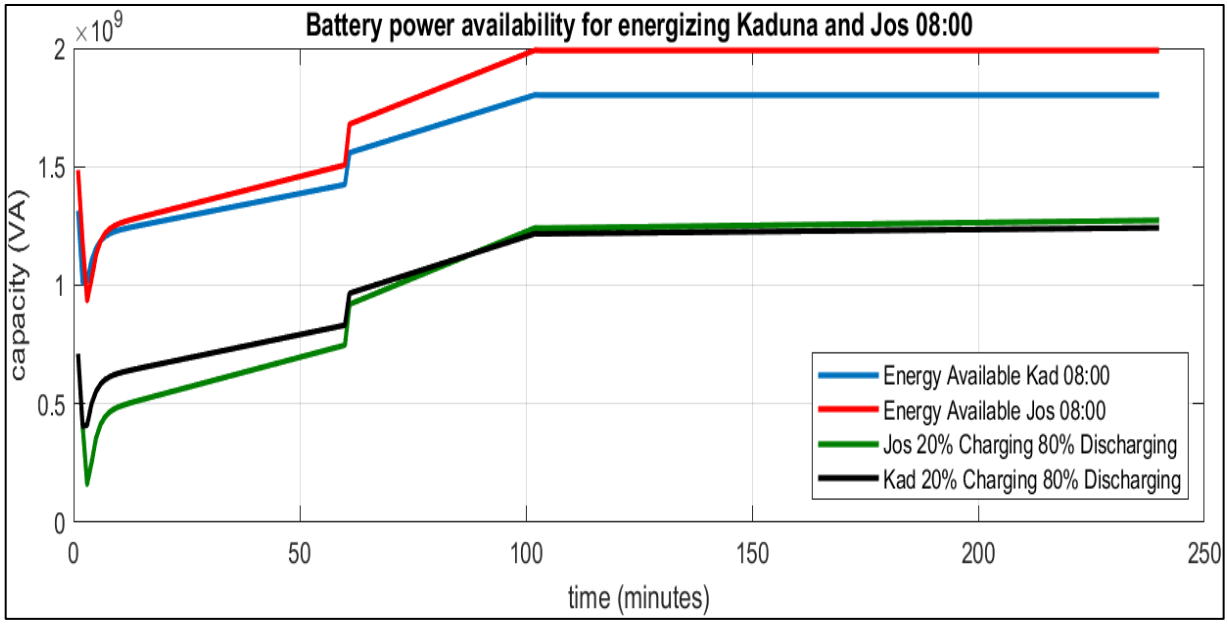

Fig. 7.36. Plots showing energy capacity at 20% with 80% discharging at Kaduna and Jos.

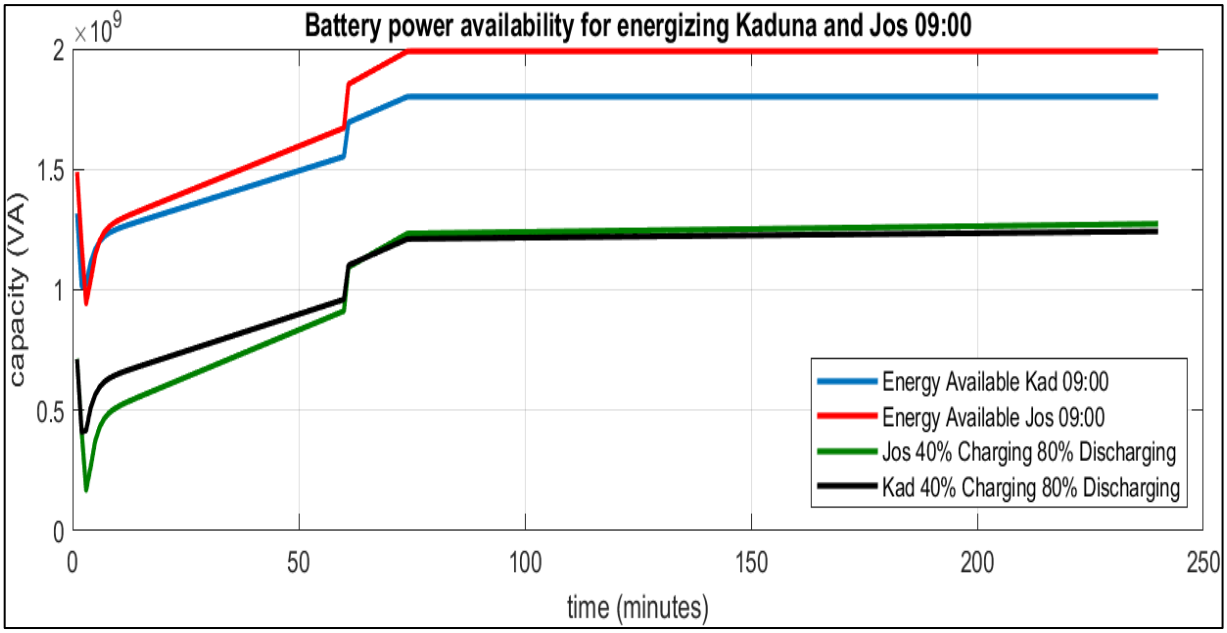

Fig. 7.37. Plots showing energy capacity at 40% with 80% discharging at Kaduna and Jos.

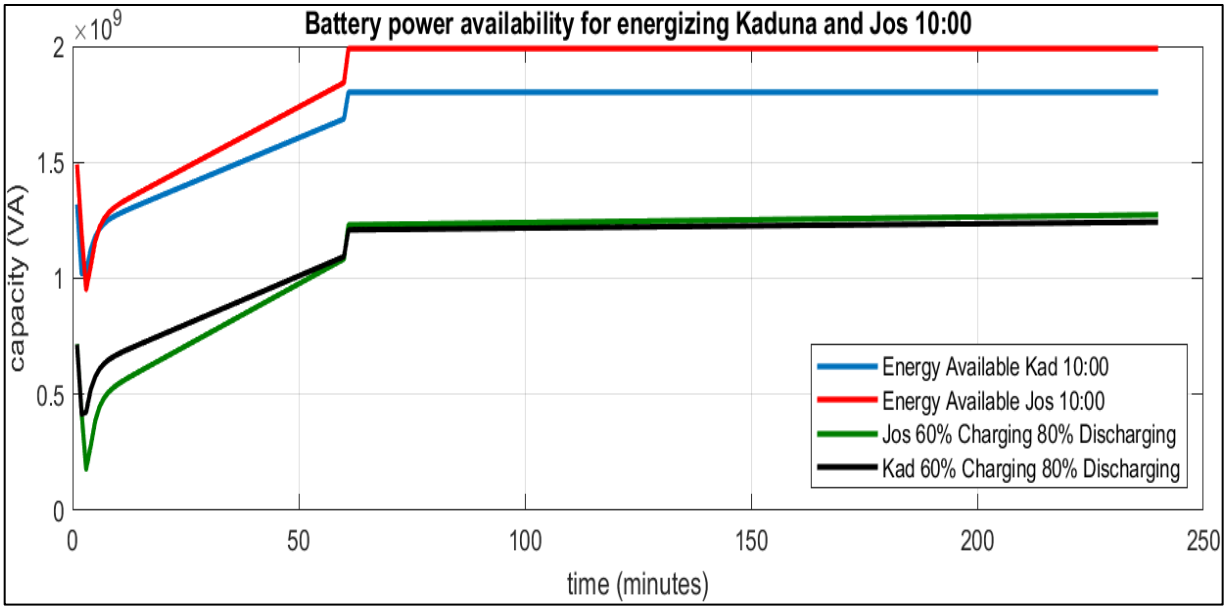

Fig. 7.38. Plots showing energy capacity at 60% with 80% discharging at Kaduna and Jos.

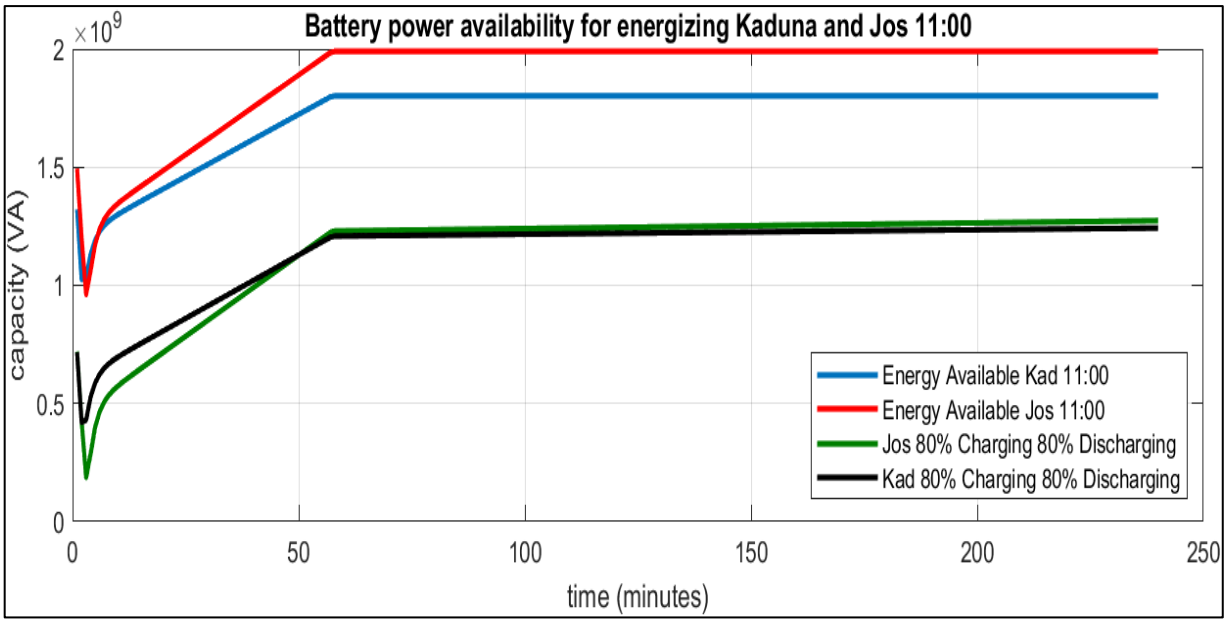

Fig. 7.39. Plots showing energy capacity at 80% with 80% discharging at Kaduna and Jos.

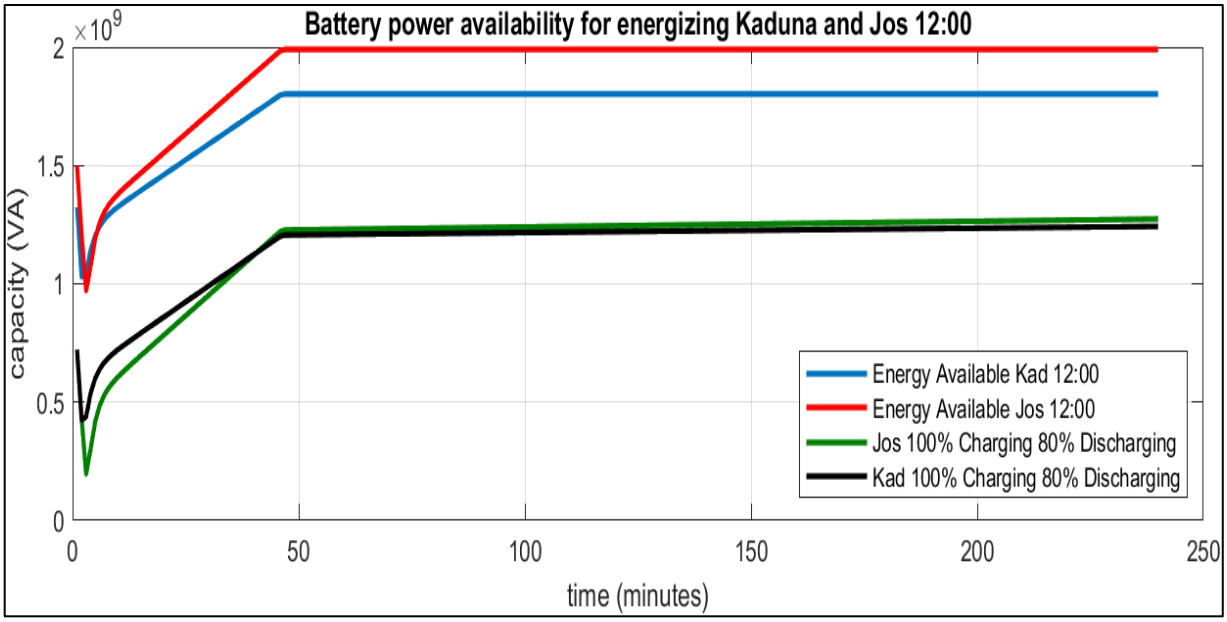

Fig. 7.40. Plots showing energy capacity at 100% with 80% discharging at Kaduna and Jos.

7.6.6 Scenarios 6

Energy availability for restoration at Jos bus 07:00 to 18:00.

- Sunshine available and charging done at 20% to 100%.
- ESS previously charged to 100% capacity.
- Load energised at time step 3.
- 100% level of discharge of ESS implemented.

At no load condition, the maximum power availability for Kaduna TS is 1,252.0 MVA. Upon loading, a minimum drop to a value of 406.2 MVA is noted. An increase to a value of 424.7 MVA at a 100% discharge capacity is recorded. Furthermore, at Jos TS, a maximum power availability of 1286.0 MVA is recorded at no load, but with a minimum drop to a value of 161.1 MVA upon loading. Moreso, an increase to a value of 196.7 MVA is observed at a 100% discharge capacity.

A settling value of 1,232.0 MVA and 1,286.0 MVA is recorded at 20% charge capacity for Kaduna and Jos respectively. As illustrated in Fig. 7.41 and Fig. 7.45 for Kaduna TS and Jos TS respectively, and tabulated in Table 7.9, a steady state value for 100% charge capacity was maintained by both locations.

Table 7.9. Restoration at Kaduna TS and Jos TS 100% discharging (20% - 100%) charging.

Energy availability for restoration at Kaduna TS and Jos TS (100% discharging)						
Charging (20% to 100%)						
Bus	Value (MVA$\times 10^3$)	20%	40%	60%	80%	100%
Kaduna	Max	1.2520	1.2520	1.2520	1.2520	1.2520
	Min	0.4062	0.4105	0.4149	0.4197	0.4247
	Settling value	1.2520	1.2520	1.2520	1.2520	1.2520
Jos	Max	1.2860	1.2860	1.2860	1.2860	1.2860
	Min	0.1611	0.1693	0.1779	0.1870	0.1967
	Settling value	1.2860	1.2860	1.2860	1.2860	1.2860

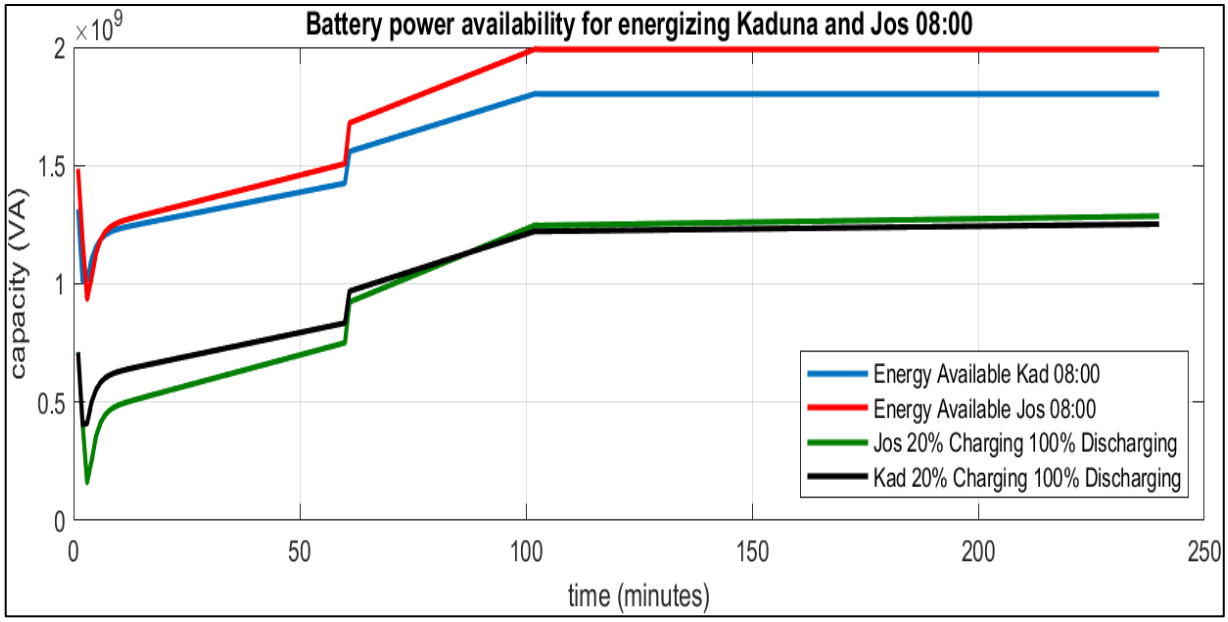

Fig. 7.41. Plots showing energy capacity at 20% with 100% discharging at Kaduna and Jos.

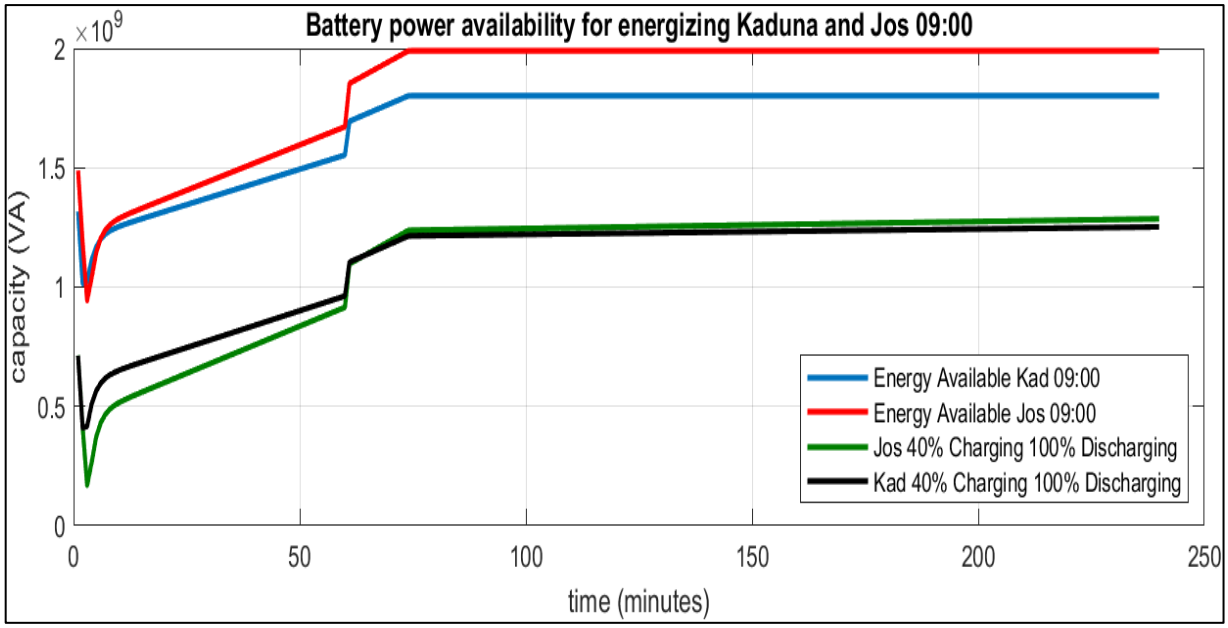

Fig. 7.42. Plots showing energy capacity at 40% with 100% discharging at Kaduna and Jos.

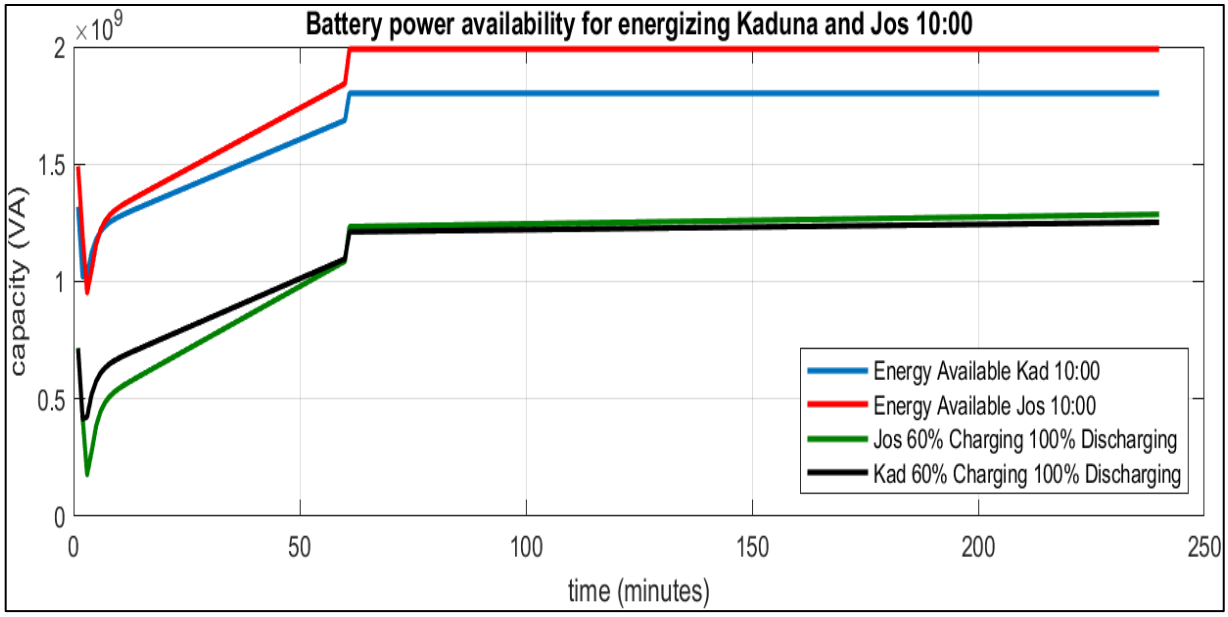

Fig. 7.43. Plots showing energy capacity at 60% with 100% discharging at Kaduna and Jos.

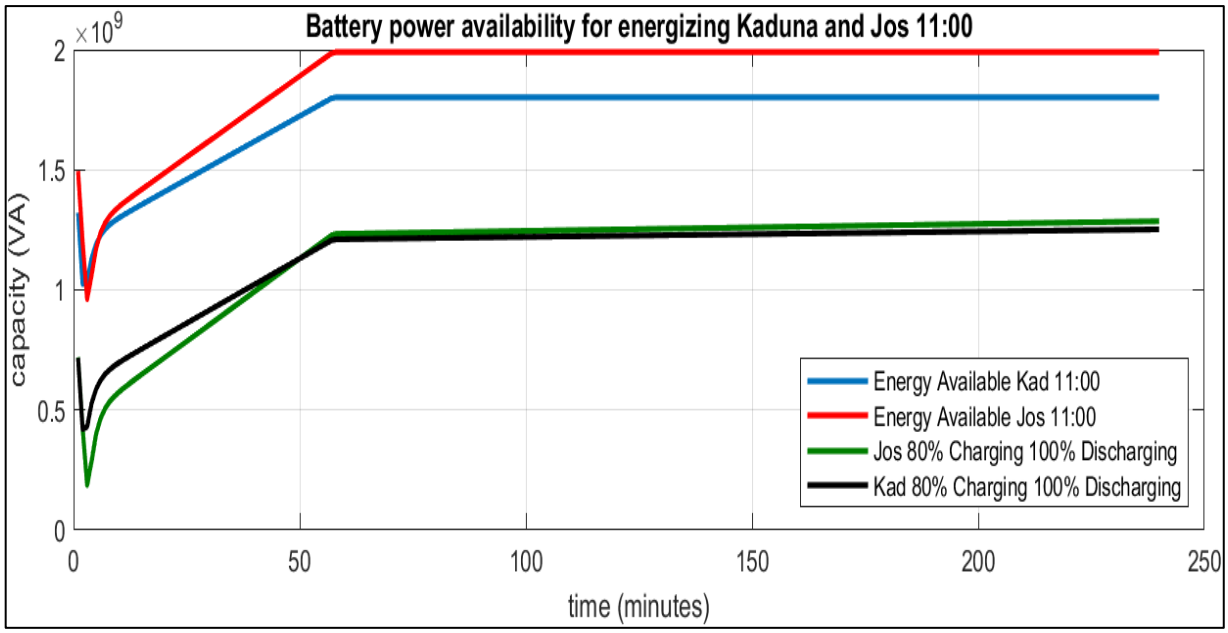

Fig. 7.44. Plots showing energy capacity at 80% with 100% discharging at Kaduna and Jos.

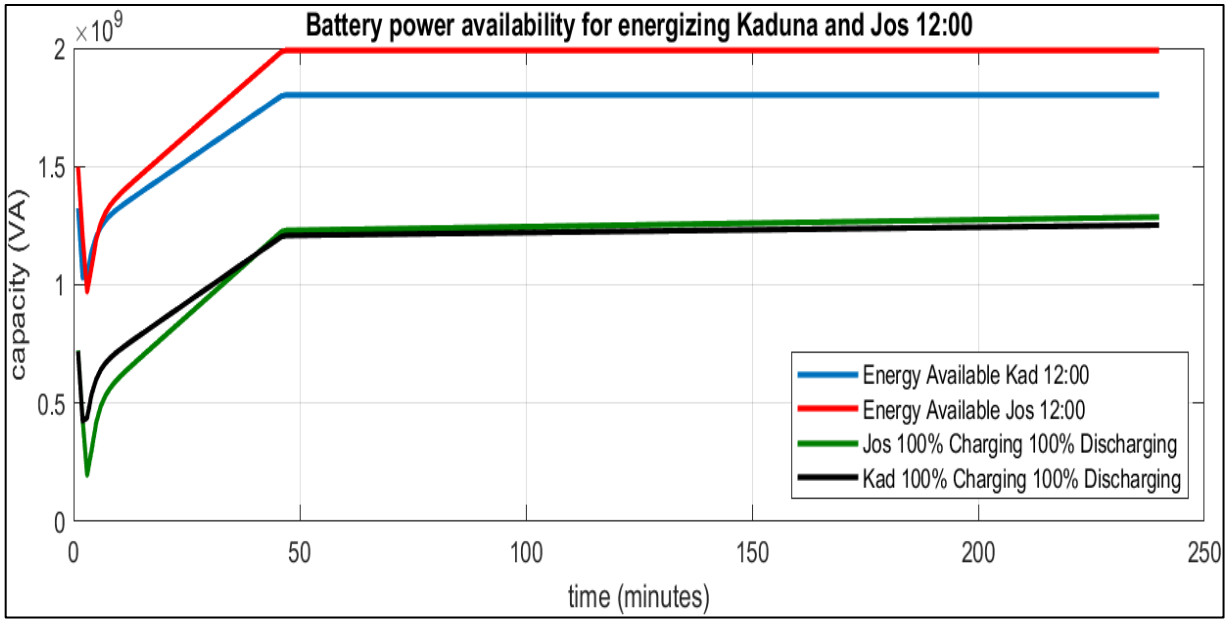

Fig. 7.45. Plots showing energy capacity at 100% with 100% discharging at Kaduna and Jos.

For all scenarios except the first, it is seen that despite the varying percentages of discharge, the optimal battery power availability for participating in restoration is reached in less than 50 minutes. Hence, Fig. 7.25, Fig. 7.30, Fig. 7.35, Fig. 7.40, and Fig. 7.45 is the optimal for each scenario respectively. However, since for black start, short transient power capability might be more important than long term energy capability, further analysis of the contribution of ESS to power restoration at a 100% discharge rate considering all the scenarios is carried out and presented in Table 7.10.

For scenario 1, with no sunshine available and hence 0% charging, upon loading, the minimum drop decreased further from 1,003 MVA to 1,002.4 MVA at Kaduna and from to 920.4 MVA to 919.6 MVA at Jos respectively at 100% ESS discharge capacity. However, for all other scenarios, where there was availability of sunshine and hence charging implemented at varying levels, the contribution of ESS to the power restoration was quite significant in both locations as can be seen in Table 7.10.

Table 7.10. ESS % contribution for restoration at Kaduna TS and Jos TS for all scenarios.

ESS % contribution for restoration at Kaduna TS and Jos TS for all scenarios (100% initial charging and 100% discharging)							
Value		Scenarios					
Bus	(MVA)	1	2	3	4	5	6
Kad	Max	1310.9	1208.9	1219.2	1233.0	1242.4	1252.0
	Drop	1003	405.8	405.9	406.0	406.9	406.2
	Min	1002.4	424.3	424.4	424.5	424.6	424.7
	ESS cont. (%)	-	4.3	4.4	4.4	4.2	4.3
Jos	Max	1480.9	1230.2	1243.9	1261.7	1273.7	1286.0
	Drop	920.4	160.4	160.5	160.8	160.9	161.1
	Min	919.6	196.0	196.2	196.4	196.5	196.7
	ESS cont. (%)	-	18.0	18.2	18.1	18.0	18.1

7.7 Conclusion

The experimental validation of the characteristics of the ESS adopted for the proposed BSR simulated study carried out as well as the evaluation of the PV contributions to system restoration were performed. The contribution of both PV and ESS to system restoration are quite significant and optimally contribute to improving the settling values of the restoration zones. The various percentages of ESS contribution to power restoration in the two locations is well represented in Table 7.10. The various PV and ESS energy availability plots during the peak period of solar irradiation also demonstrates that it is possible to quickly energise a section of the network by the combination of PV and ESS systems.

The major contributions of this chapter are:

- The experimental charging and discharging of the ESS system was conceptualised and integrated into the BSR methodology implemented using the 48-bus system.
- The experimental validation of the ESS system implemented using the 48-bus system showed that the charging and discharging at various percentages during system restoration was possible.
- Different scenarios were created and used to validate the contribution of ESS to load restoration.
- The percentage contributions of ESS and PV to system restoration was demonstrated.
- The battery ESS contributed optimally to the system restoration by reducing the restoration time step as illustrated in Chapter 6.

CHAPTER 8

8.0 CONCLUSIONS AND RECOMMENDATIONS FOR FUTURE RESEARCH

8.1 Conclusions

The major focus of this research was to model and analysis a smart localised energy system for a sustainable future power network. Achieving a sustainable future power system requires an application of a whole system approach to energy generation, distribution and utilisation. Starting from power utilisation, the study investigated the dynamics of residential power demand and modelled the residential energy consumption profile.

Moreover, to enhance the estimation of the urban residential energy use of different residential types in the absence of smart meters or historical data, an excel-based algorithm was developed and applied to the developed model. The results, which was based on the appliance energy end use methodology, was used to develop a load profile indicative of a typical urban residential energy demand and employed to predict the effects of residential loads on the power system. Several case studies demonstrating how to optimise energy consumption and improve energy efficiency were also carried out.

In addition, a techno-economic analysis of the energy cost of public lighting was carried out using metrics such as Life Cycle Cost (LCC), Annualized Life Cycle Cost (ALCC), Net Present Cost (NPC), Cost of Energy (COE), and Return on Investment (ROI). The LCC of the SPV system which is the main index adopted in the economic assessment of a project's viability was the lowest. On the contrary, the grid-connected system had both the highest

LCC and ALCC. To further simulate the performance of the generator and solar PV connected street lighting systems, HOMER Pro 3.13.1 software was used. For both the generator and SPV systems, the simulated NPC cost was determined along with the LCOE. Lastly, the emissions resulting from the generator powered lighting system was also estimated.

Furthermore, an assessment of the response of the power system to the integration of DERs and EVs was performed. Data from a real low voltage (LV) distribution network in Nigeria was obtained and used in modelling the network using PSCAD/EMTDC software package. Using the network, different impact studies considering an increase in the load and addition of distributed generation sources were performed. The introduction of an LCL filter did reduce the THD in the line current from 20% to 4%. Resulting from PV systems integration into the network, Volt-VAr optimisation (VVO) was performed to enable the inverter-based PV systems participate actively in voltage regulation by the provision of flexible reactive power support. For the controlled Case studies 2 and 3, a net total of 1.359 MVAr and 1.301 MVAr respectively are utilised from the inverter to regulate the voltage within the acceptable limits, hence reducing the substation reactive power by 19.8% and 18.9% respectively. The application of VVO reduced the deviation of consumer voltages from the nominal system voltage by 33.4% thereby enhancing power quality and reliability by improving the feeder volage profile and further reducing the active power losses in the network from 0.437 MW to 0.172 MW.

Besides the aforementioned, since the resilience of the power system is constantly been threatened as a consequence of the devastating effects of climate change impact, oftentimes culminating to blackout, a DER integrated black start restoration strategy was implemented. The formulated BSR

problem was implemented as a dynamic optimisation problem to enable the effective coordination of the dispatching actions of the DERs along with the switching actions of RCSs over multiple decisions time steps. The mixed-integer linear programming (MILP) technique was adopted and modelled to suit the nature of the BSR method developed. The black start power restoration sequence and the development of a viable restoration strategy were actualised. The simulation of the MILP model was achieved in MATLAB® using the IBM CPLEX™ solver.

Consequently, to validate the proposed BSR method developed, the Nigerian 330 kV 48-bus system was modelled in NEPLAN and used as a case study to assess its performance. The performance analysis indicated that BSR was effectively executed since restoration could be sequentially initiated at various times in different sections of the network. Most loads were optimally restored before the 30th time step for a black start operation. The switching sequence of the various loads on the different transmission substation buses by participating generators was developed and used to achieve effective restoration. The performance characteristics of voltage and frequency in response to the loading during restoration monitored in the different regions witnessed appreciable level of improvement especially with PV assistance. Also, it was possible to energise the system by implementing the restoration sequence step by step, while satisfying various operational constraints during the restoration process.

Equally important is the experimental and numerical methodology adopted in the validation of energy storage system (ESS) adopted for the proposed BSR simulated study. The optimal battery power availability for participating in restoration was reached in less than 50 minutes. The contribution of both PV and ESS to system restoration were quite significant, with ESS optimally

contributing to power restoration achieving 4.3% & 18.1% for Kaduna and Jos respectively culminating to a reduce restoration time. During the peak period of solar irradiation, it was also possible to energise a section of the network by the combination of PV and ESS systems.

Finally, the novelty of this work lies in the development of a unique restoration sequence capable of improving the resilience of the power grid in the unlikely events of a blackout. The developed structured flowchart incorporates DERs in implementing the BSR solution framework. Without the applied method, the switching can only be done considering optimisation of switching time, but with the applied method, the path with the least anticipated voltage and frequency drop is taken into consideration in the choice of the restoration route. This is applicable when alternative route for restoration is considered. Besides this, the implementation of different impact studies considering an increase in the load and addition of distributed generation sources using data from a real low voltage distribution network in Nigeria also makes this work unique. Prior to this study, to the best of the reseacher's knowledge, there seems to be no existing detailed technical work assessing the Nigerian power network for BSR, LV urban distribution network for DG, EV and slow and fast charging infrastructures. This is the first of such comprehensive study in these areas. Although, the Nigerian 48-bus system was used as a case study to assess the performance of the black start restoration method developed, however, its application is relevant for some other countries facing similar challenging issues.

In summary, the main contributions of this thesis are:

- The modelling the Nigerian 330 kV 48-bus system and its use in the validation of the BSR methodology.
- The development of an optimal retoration strategy, which takes into consideration the path with the least anticipated voltage and frequency drop in the choice of its restoration routes.

- Demonstrating the significant contributions of ESS and PV to system restoration.
- The development of a unique BSR restoration sequence incorporating DERs and capable of improving the resilience of the power grid in the unlikely events of a blackout.
- The formulation and implementation of the BSR problem as a dynamic optimisation problem to enable the effective coordination of the dispatching actions of the DERs along with the switching actions of RCSs over multiple decisions time steps.
- The modelling of a real low voltage (LV) distribution network in Nigeria and the implementation of different impact studies.
- The adoption of appliance energy end use methodology in the estimation of consumer energy use and development of load profiles.

8.2 Recommendations for Future Research

This research was carried out using information and tools that were readily available as at the time of a global pandemic which culminated in new working conditions. Constrained by some of these conditions, reasonable adjustments were made which no doubts placed a limit to the extent in which some aspects of this research would have been stretched. For instance, it would be interesting to use long range energy alternatives planning (LEAP), to predict the long term residential load demands. While the focus of the early part of this study was on residential loads, further insights into the nature of commercial and industrial loads could be explored as well. Also, municipal street lighting is only a study case considered in this research, other sectors could be investigated as well. This research did focus on urban networks, extending similar analysis to rural networks and performing a comparative analysis between both networks would be exciting to see.

Furthermore, the application of DERs in distribution networks is a fast moving field and it would be interesting to further investigate how both the

urban and rural networks in Nigeria would be impacted by a full scale introduction of DERs into the network. Moreso, with the proposed EVs integration into the Nigerian market, carrying out further detailed studies and analysing the various connections and charging scenarios would be expedient.

Another very exciting area of this study that could be expanded upon is the black start applications. It would be great to see a restoration strategy developed for applications in urban, rural, residential, commercial, airports settings, etc. Although this study had comprehensively modelled and simulated the Nigerian 330 kV 48-bus system, getting a chance to implement the simulated model in real time on the Nigerian power network and examining its performance with assumed blackout events would be worth investigating. Lastly, the comprehensive updated network parameters with newly added generation and transmission capacities can be obtained and used in performing a similar study and comparison done.

Appendices

Appendix A Various buildings layout schematics

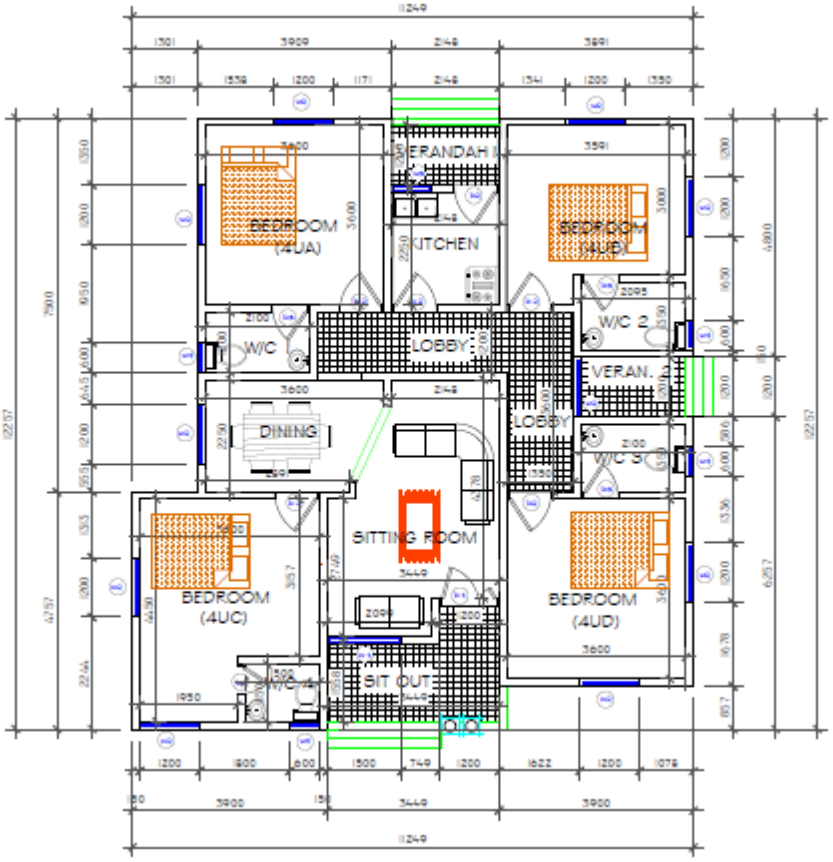

Fig. A1. 4 bedroom apartment floor plan.

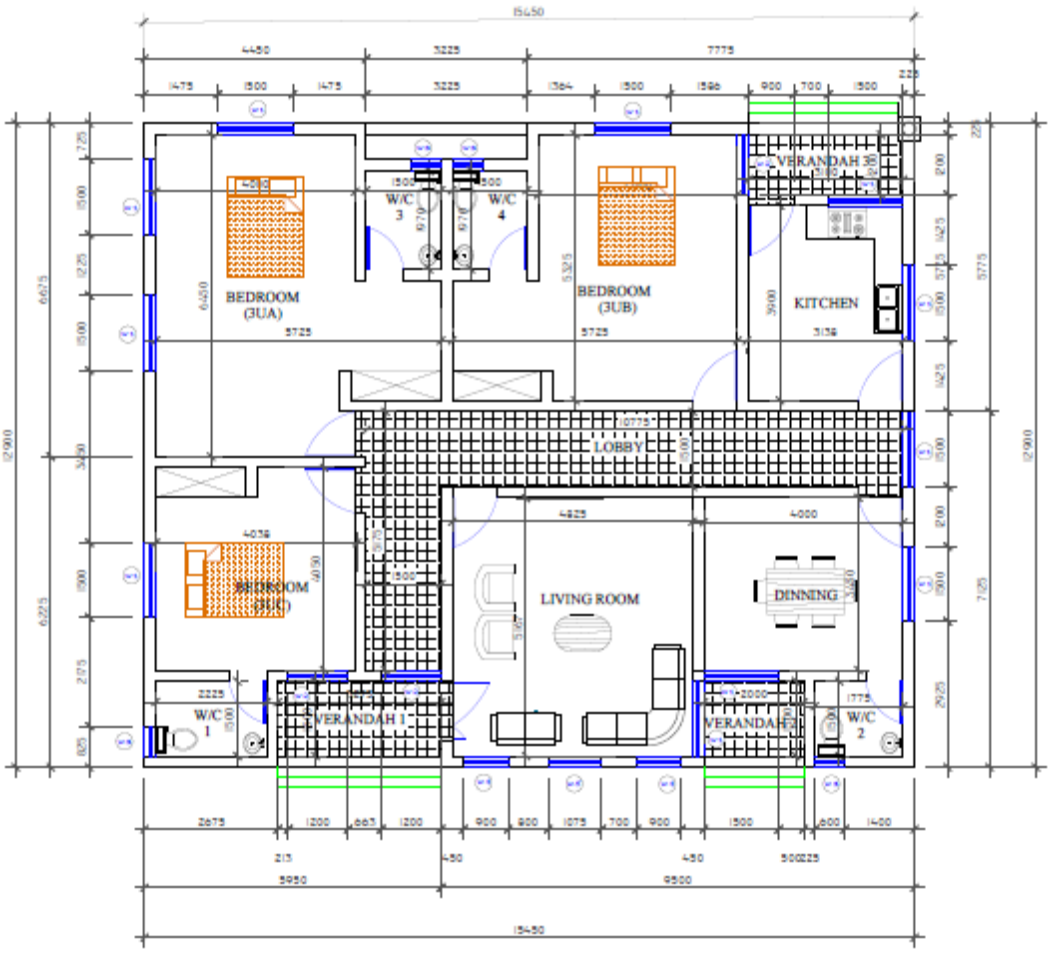

Fig. A2. 3 bedroom apartment floor plan.

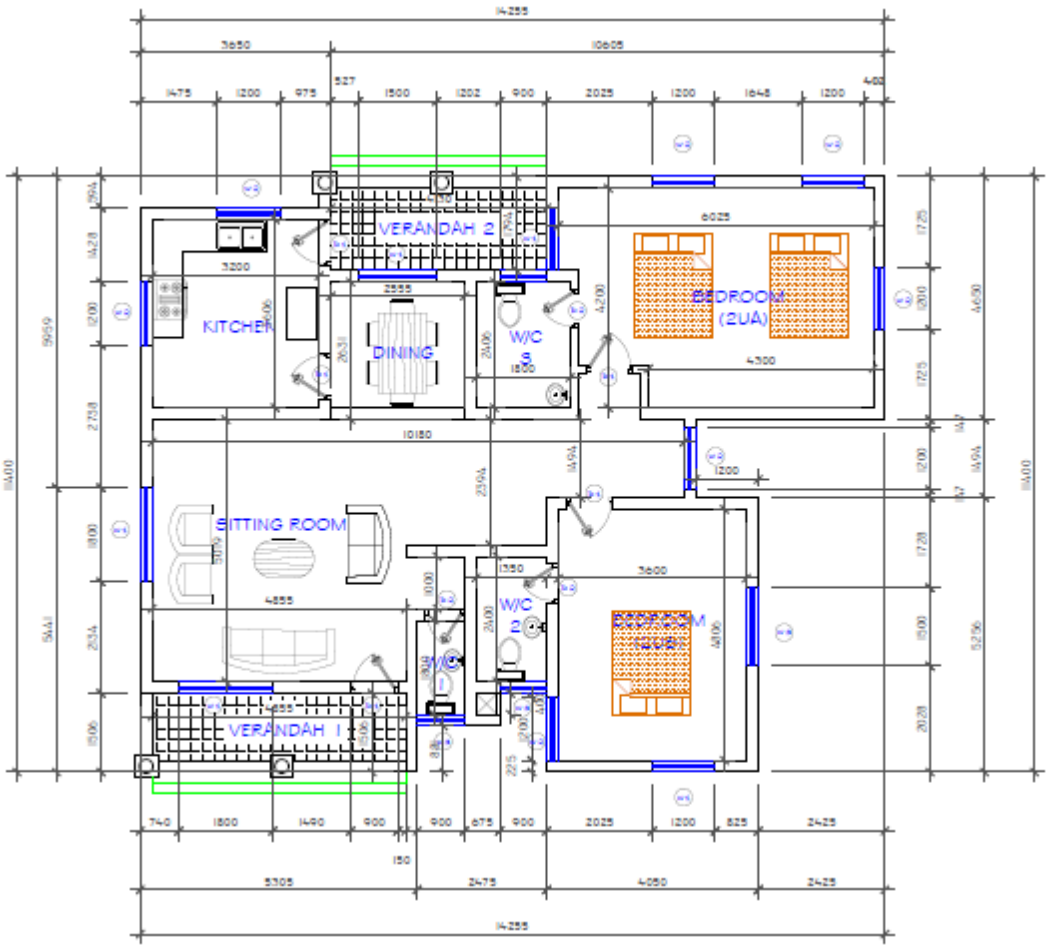

Fig. A3. 2 bedroom apartment floor plan.

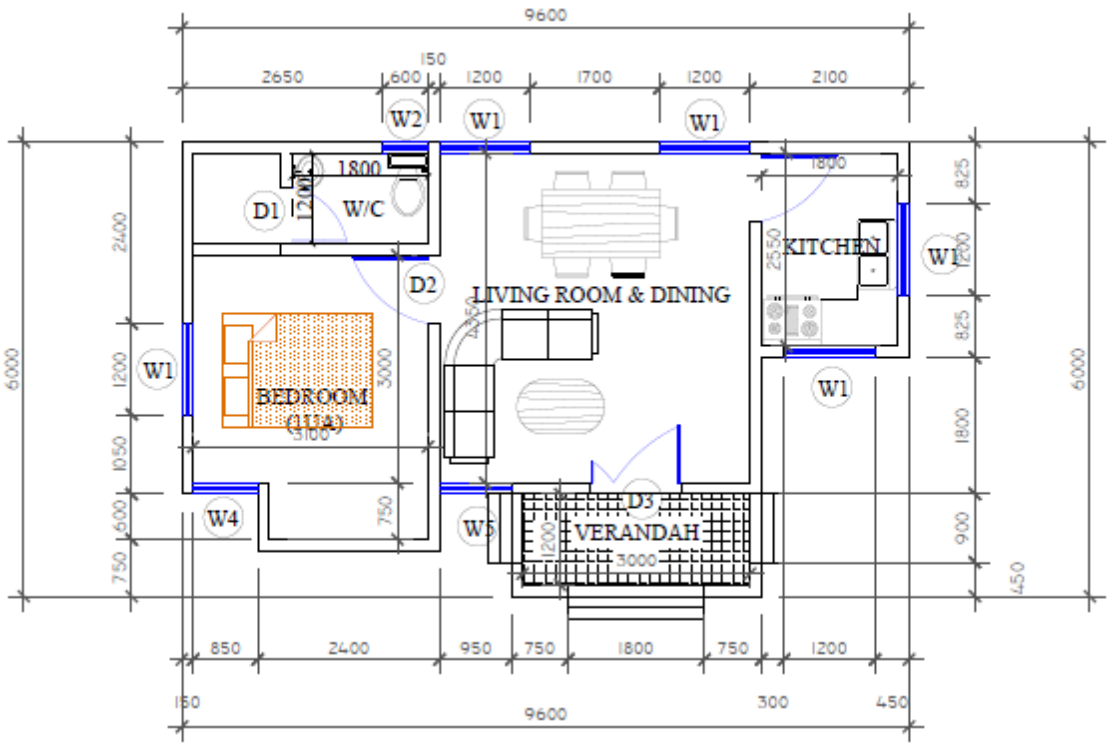

Fig. A4. 1 bedroom apartment floor plan.

Appendix B Seasonal daily load profile of various residential consumer types

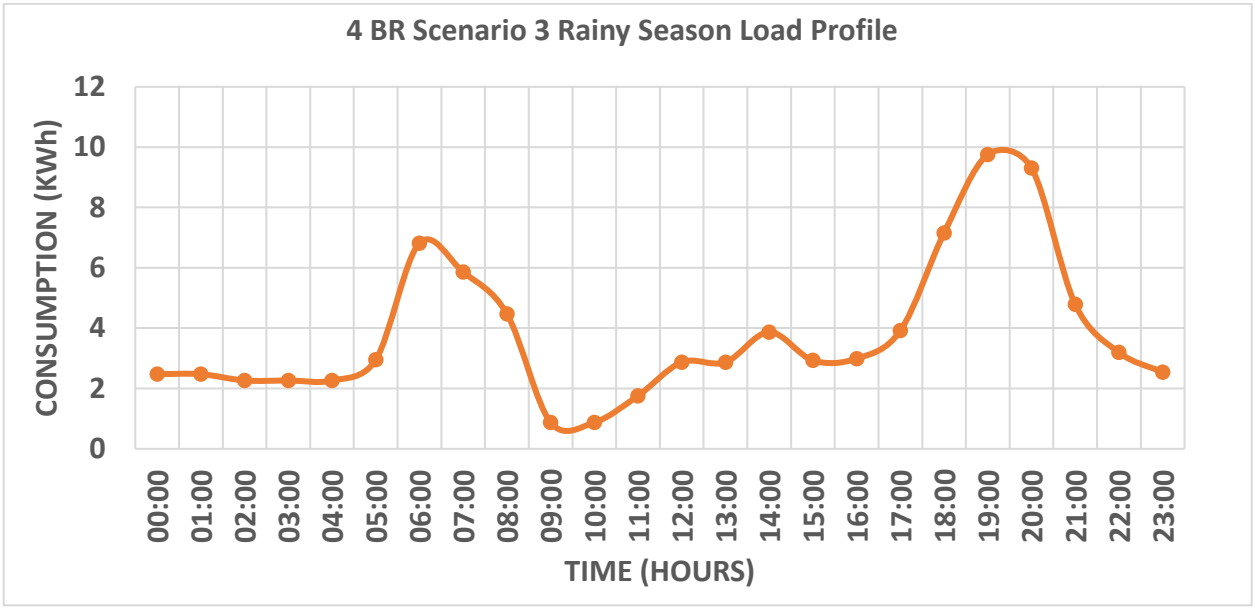

Fig. B1. 4 bedroom scenario 3 rainy season load profile.

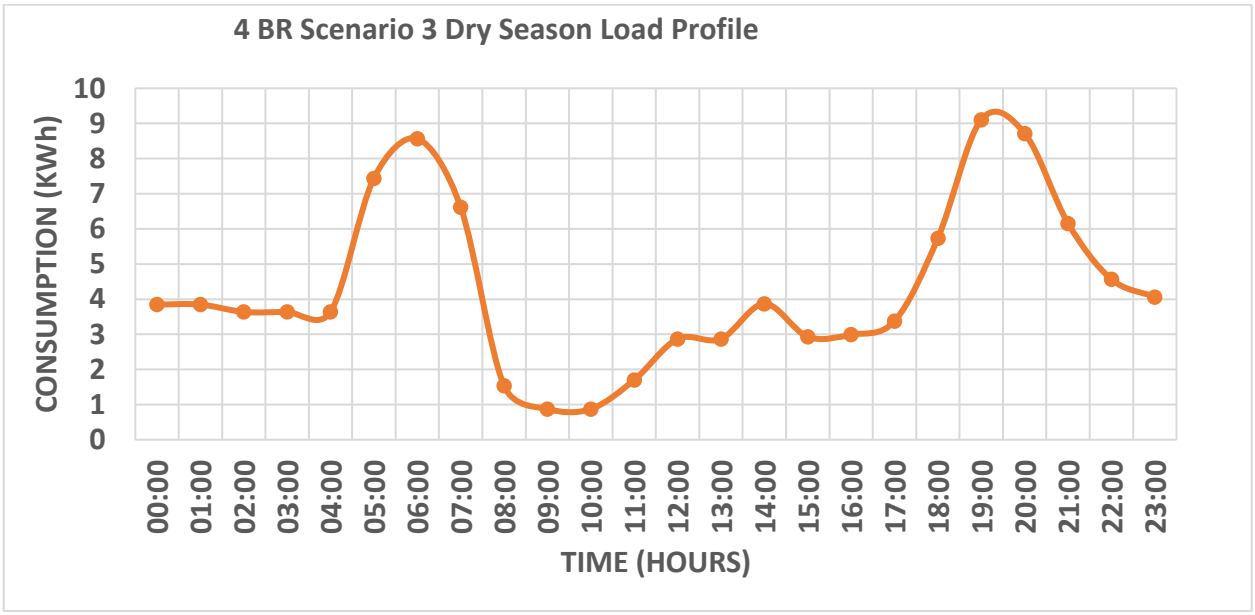

Fig. B2. 4 bedroom scenario 3 dry season load profile.

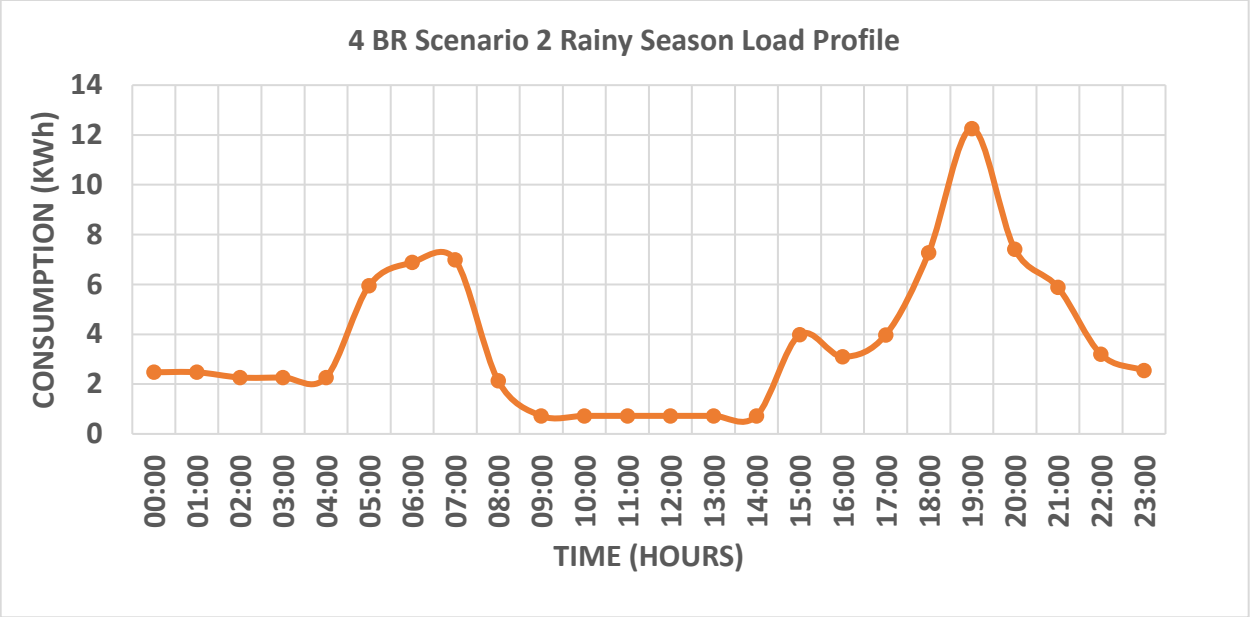

Fig. B3. 4 bedroom scenario 2 rainy season load profile.

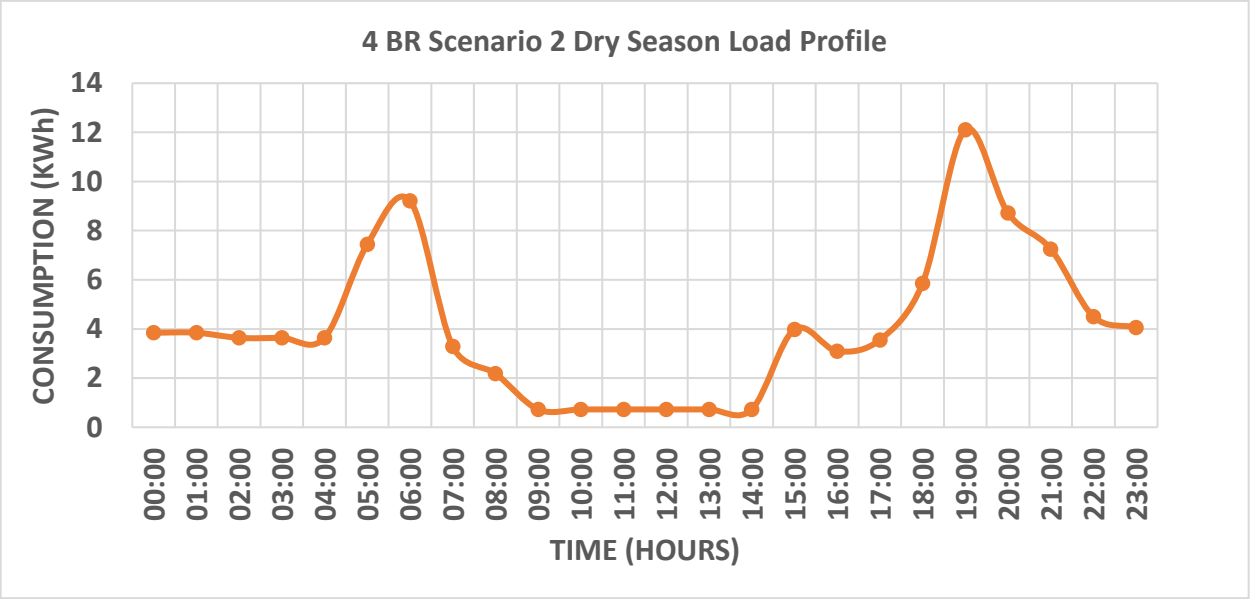

Fig. B4. 4 bedroom scenario 2 rainy season load profile.

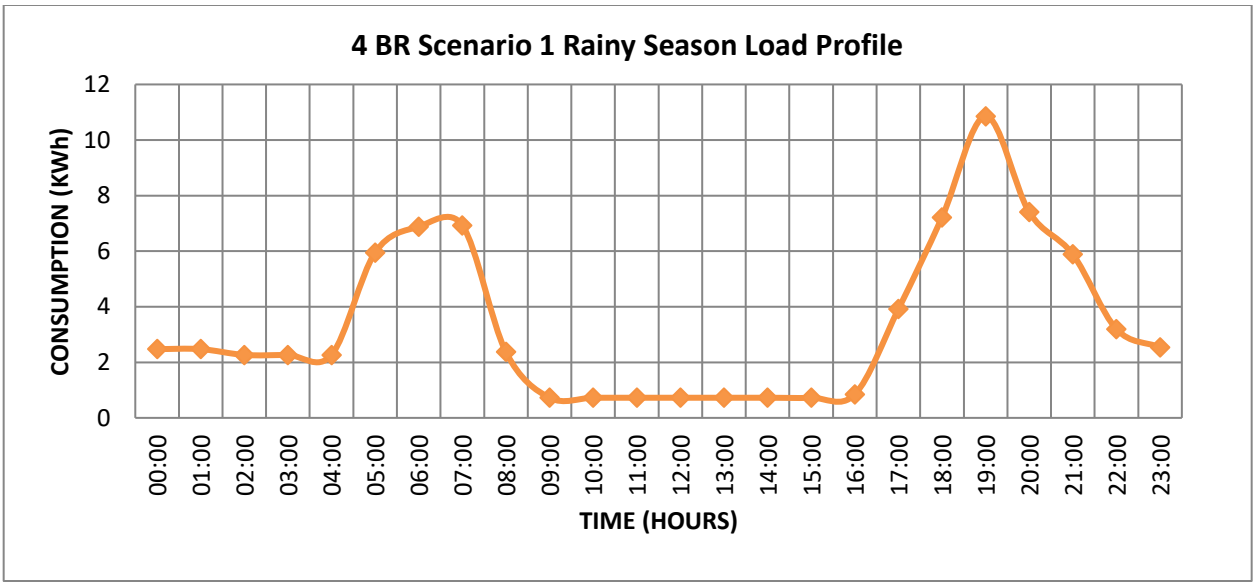

Fig. B5. 4 bedroom scenario 1 rainy season load profile.

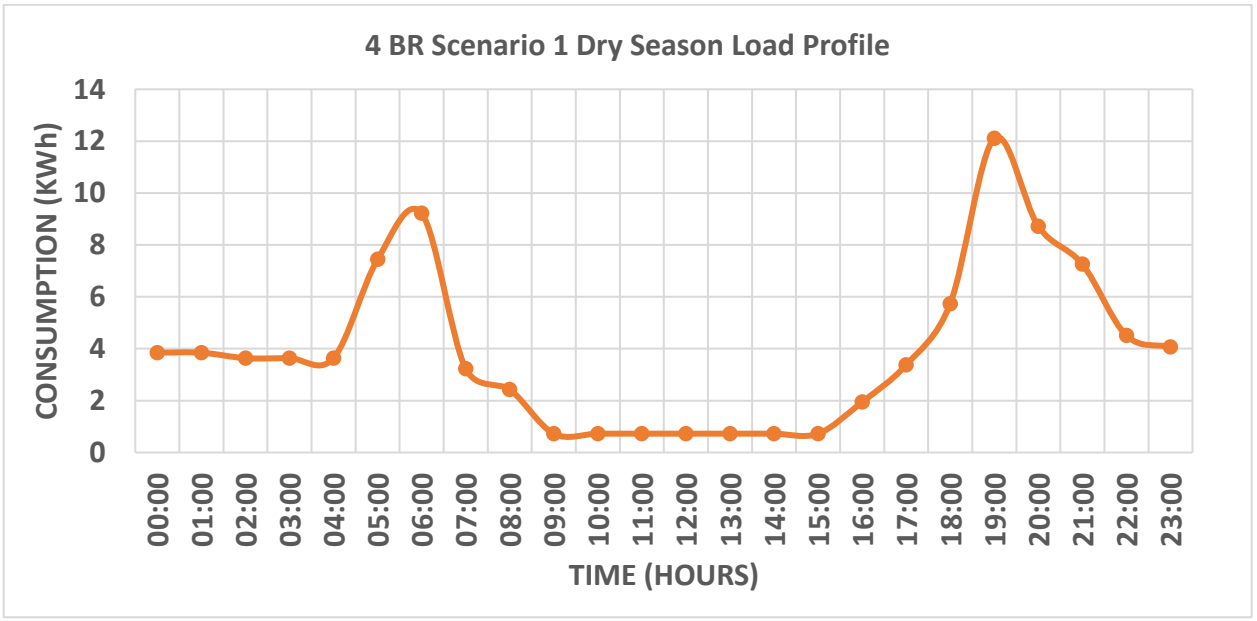

Fig. B6. 4 bedroom scenario 1 dry season load profile.

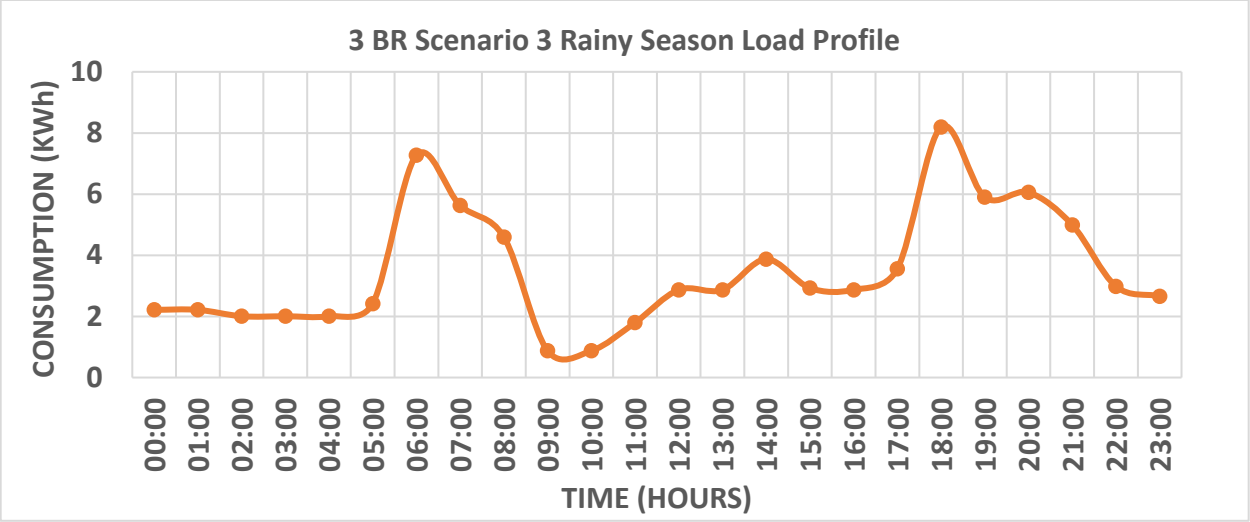

Fig. B7. 3 bedroom scenario 3 rainy season load profile.

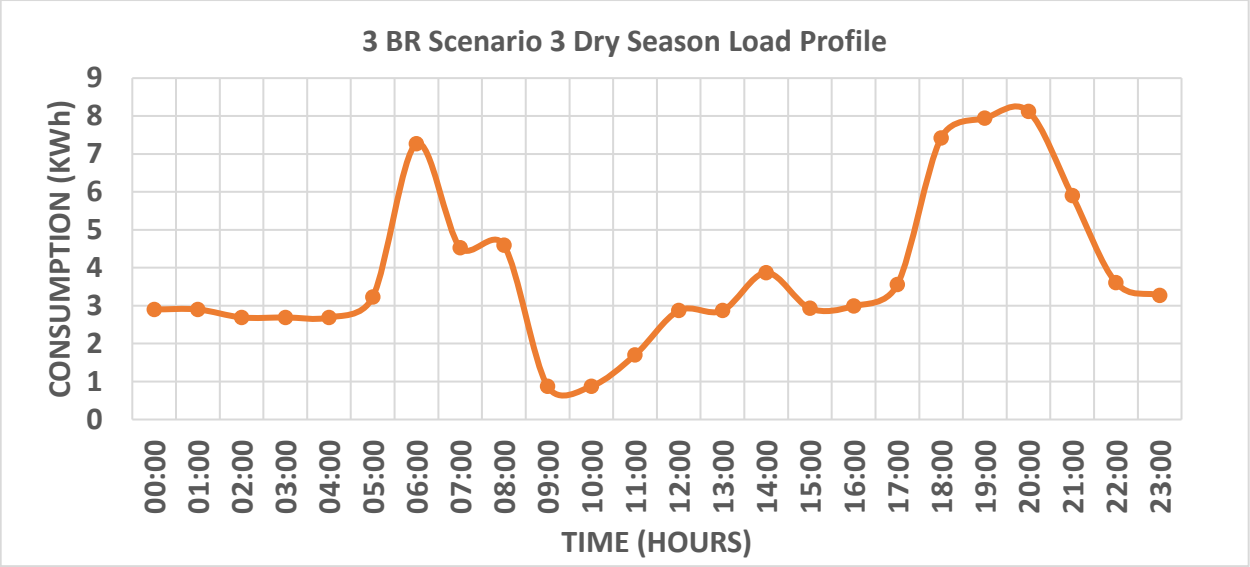

Fig. B8. 3 bedroom scenario 3 dry season load profile.

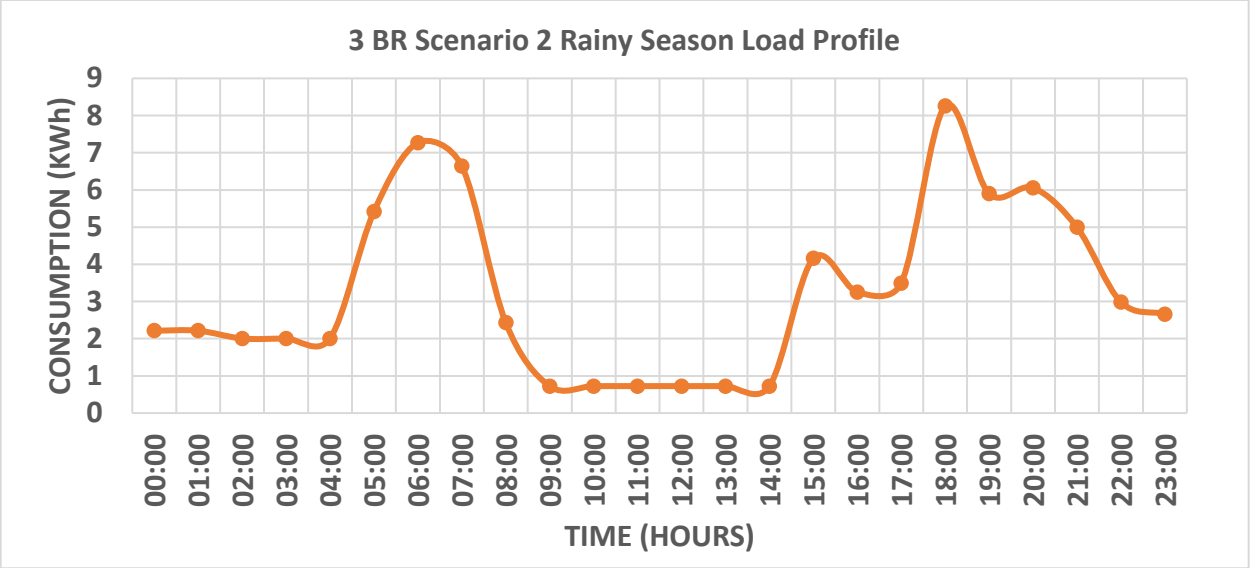

Fig. B9. 3 bedroom scenario 2 rainy season load profile.

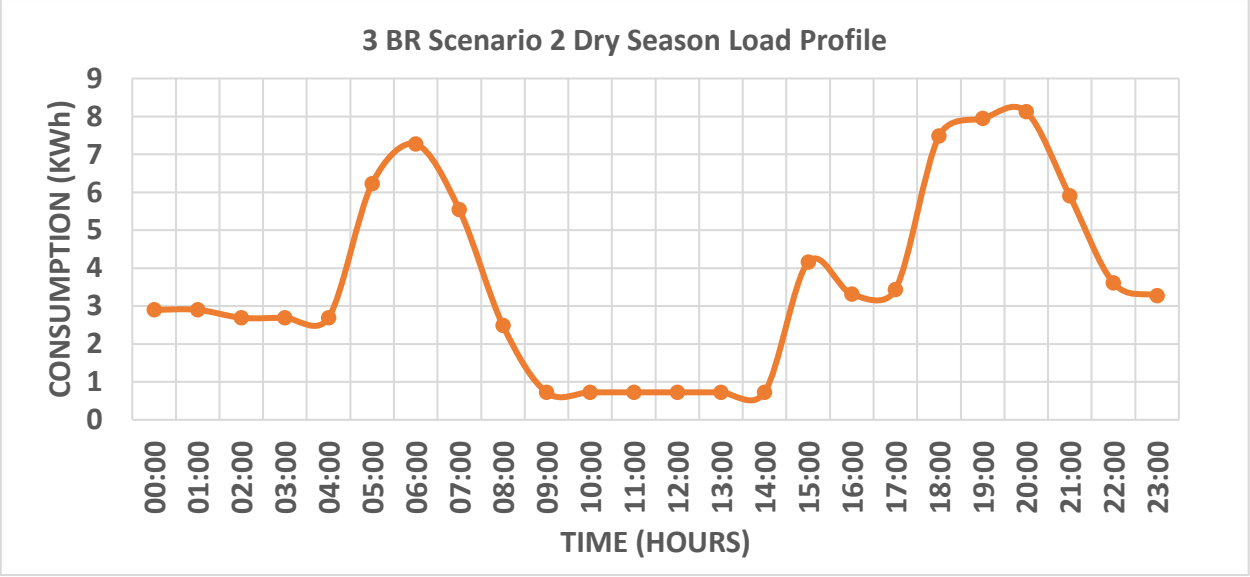

Fig. B10. 3 bedroom scenario 2 dry season load profile.

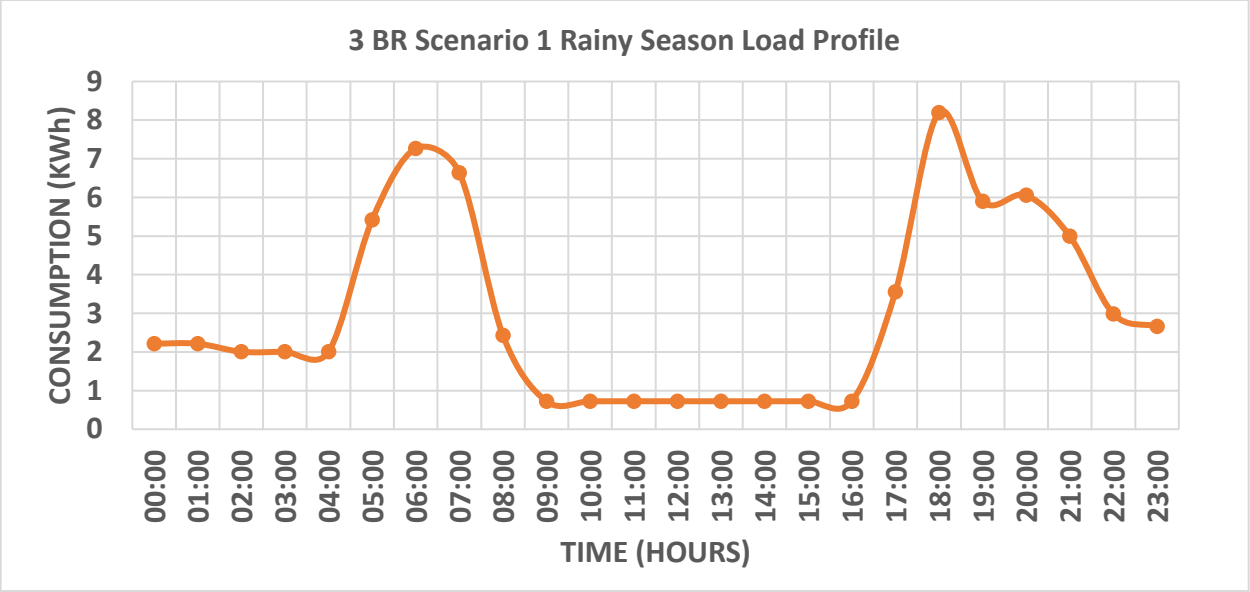

Fig. B11. 3 bedroom scenario 1 rainy season load profile.

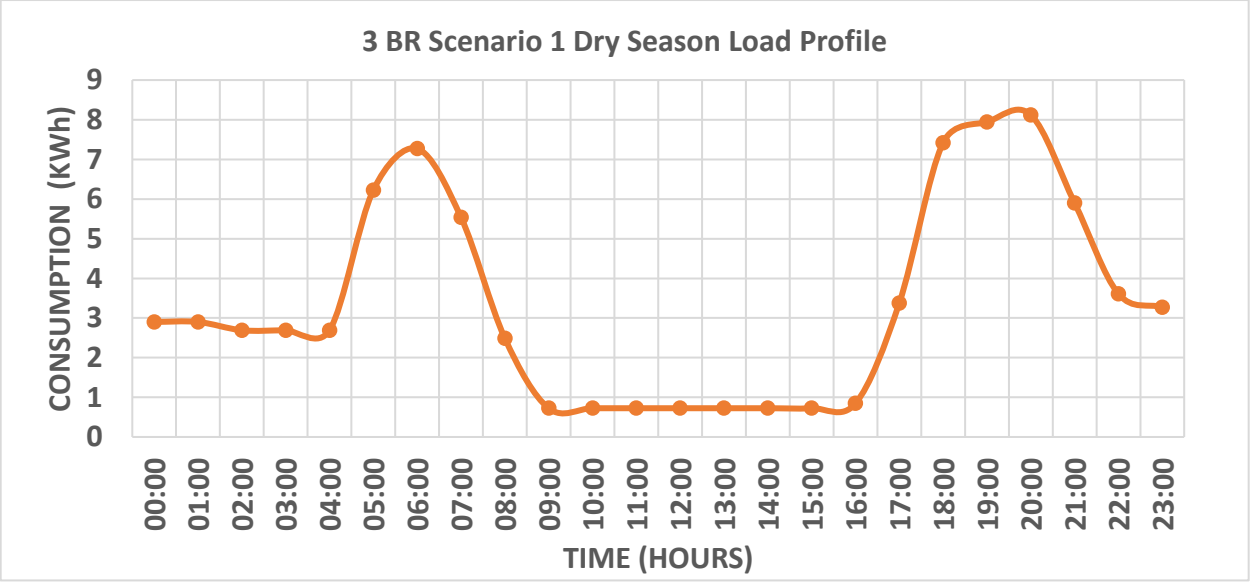

Fig. B12. 3 bedroom scenario 1 dry season load profile.

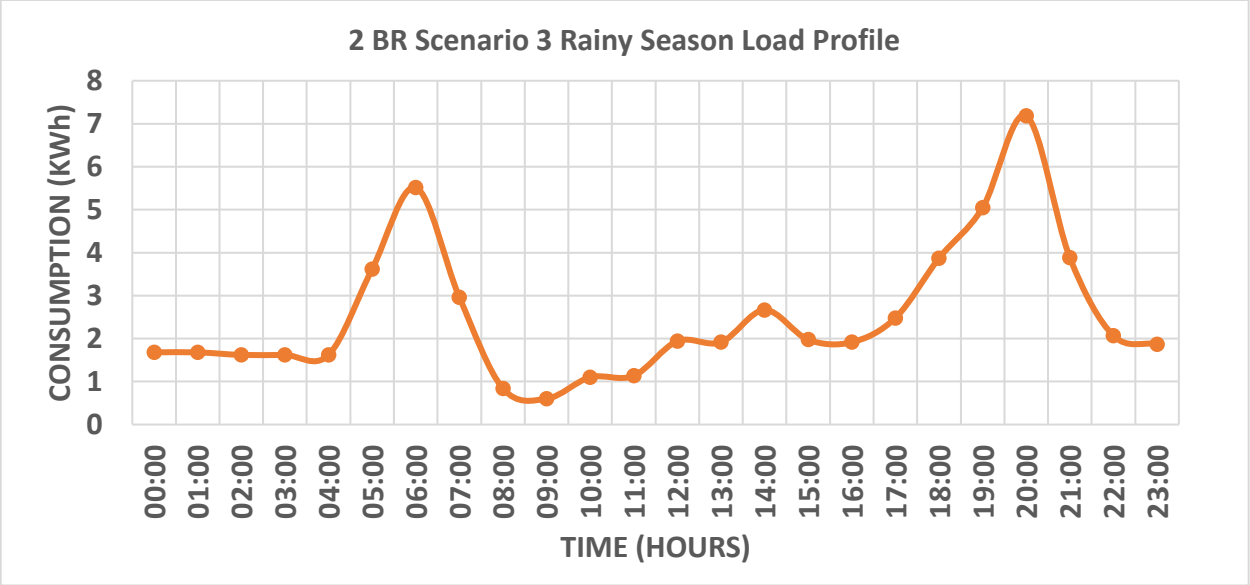

Fig. B13. 2 bedroom scenario 3 rainy season load profile.

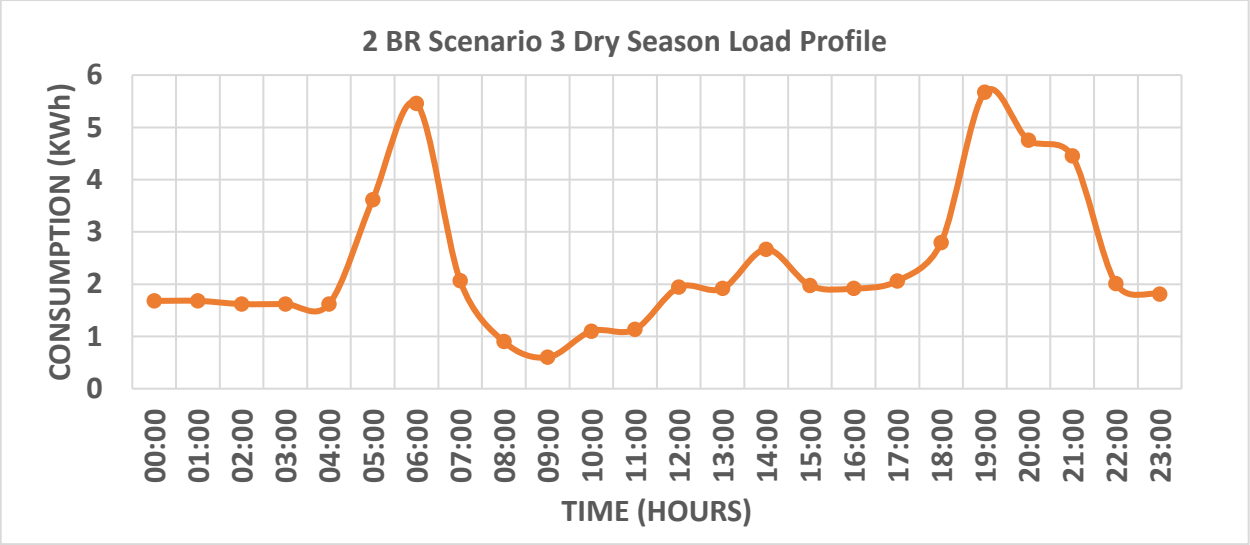

Fig. B14. 2 bedroom scenario 3 dry season load profile.

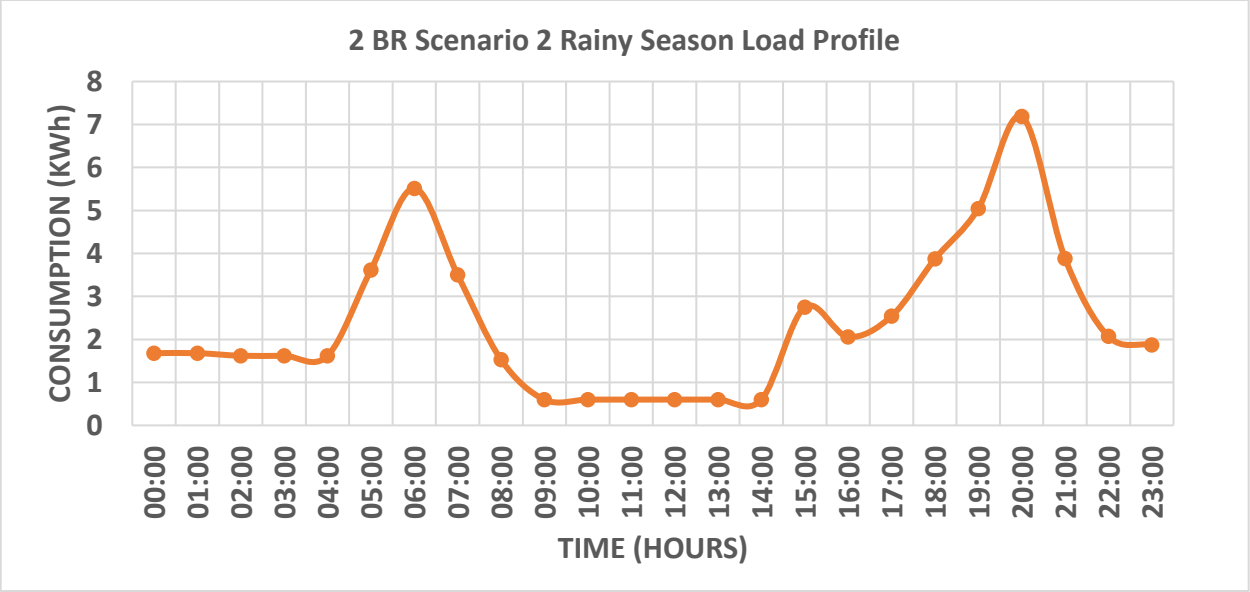

Fig. B15. 2 bedroom scenario 2 rainy season load profile.

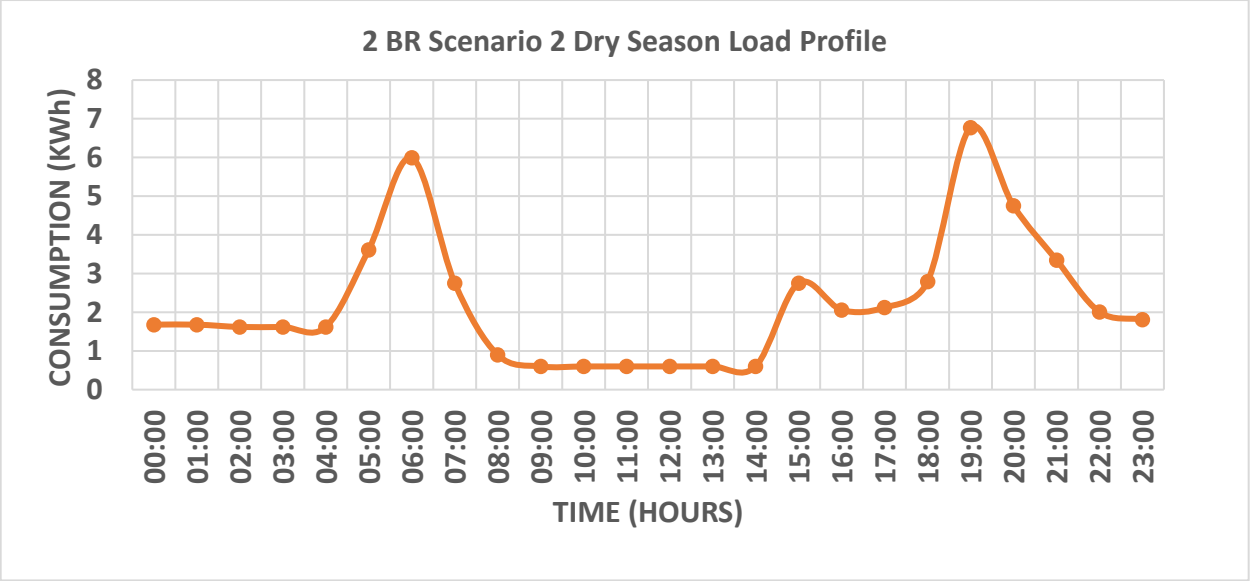

Fig. B16. 2 bedroom scenario 2 dry season load profile.

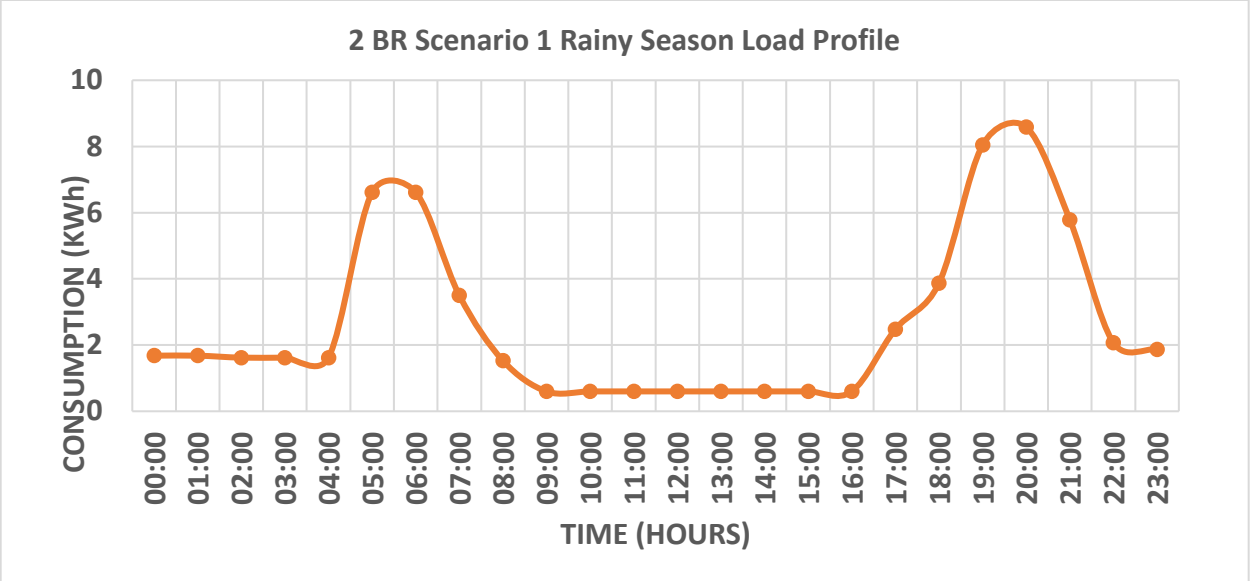

Fig. B17. 2 bedroom scenario 1 rainy season load profile.

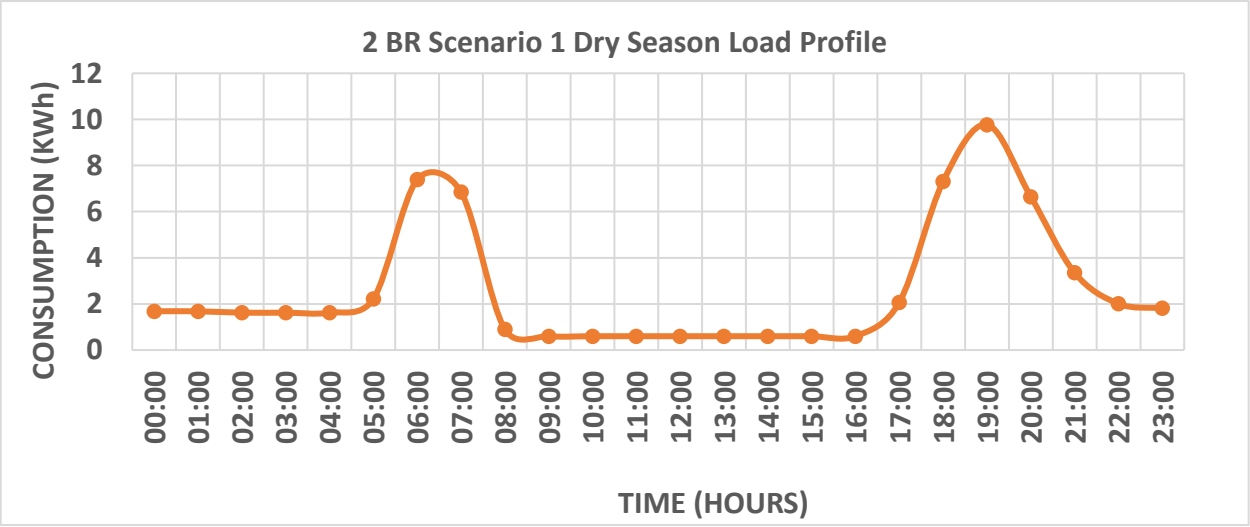

Fig. B18. 2 bedroom scenario 1 dry season load profile.

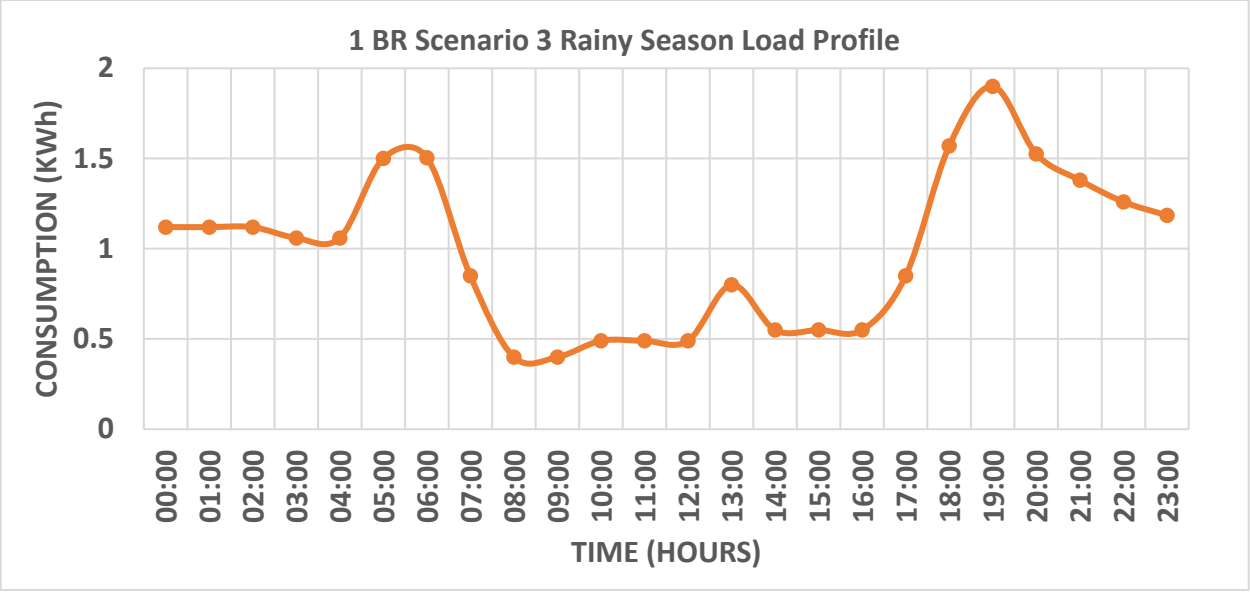

Fig. B19. 1 bedroom scenario 3 rainy season load profile.

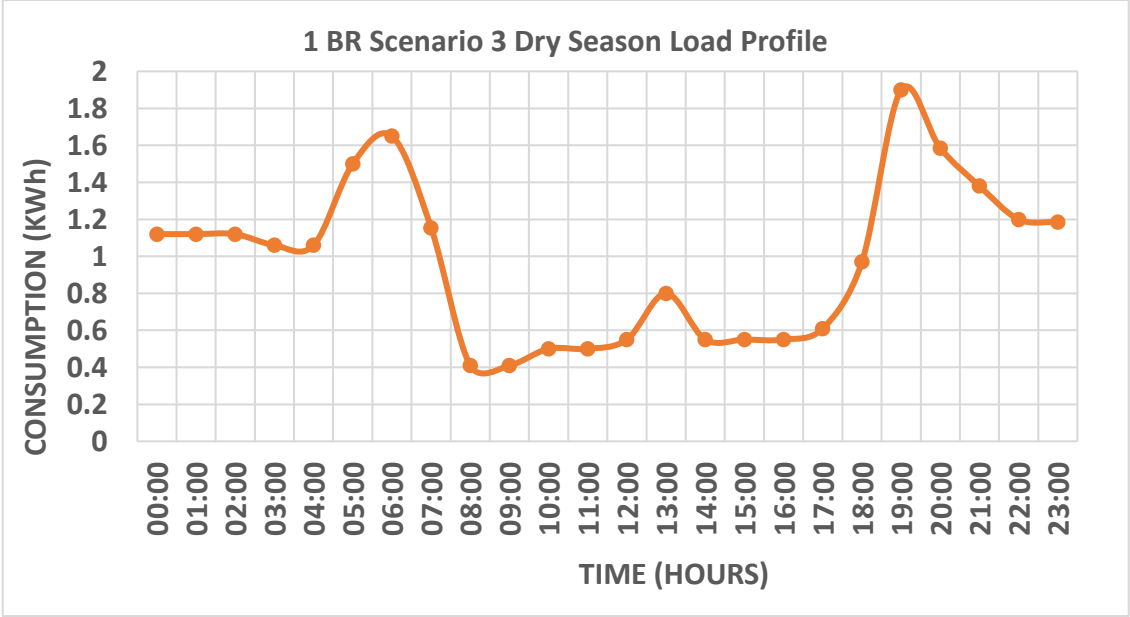

Fig. B20. 1 bedroom scenario 3 dry season load profile.

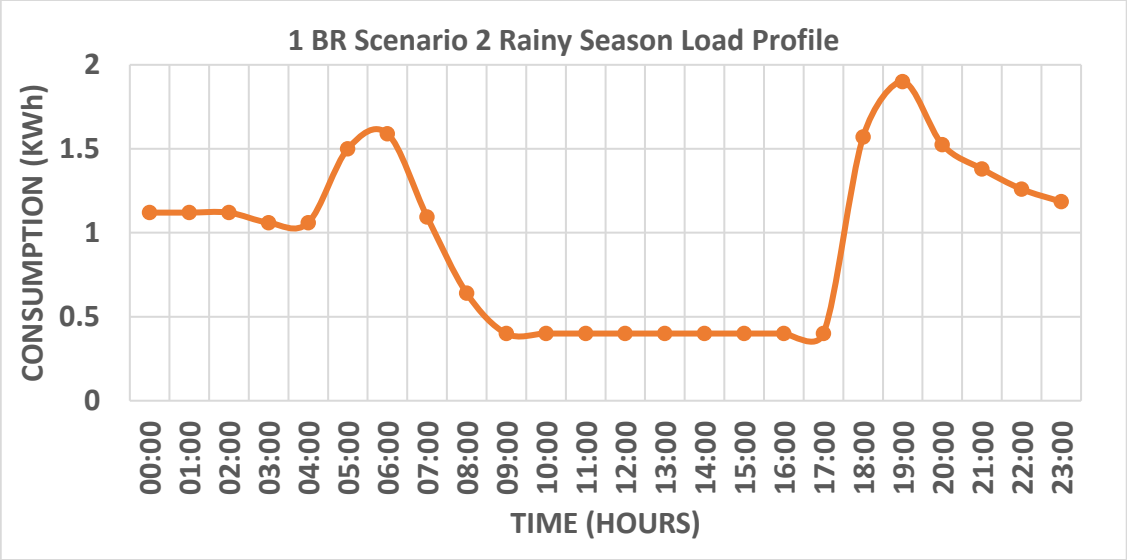

Fig. B21. 1 bedroom scenario 2 rainy season load profile.

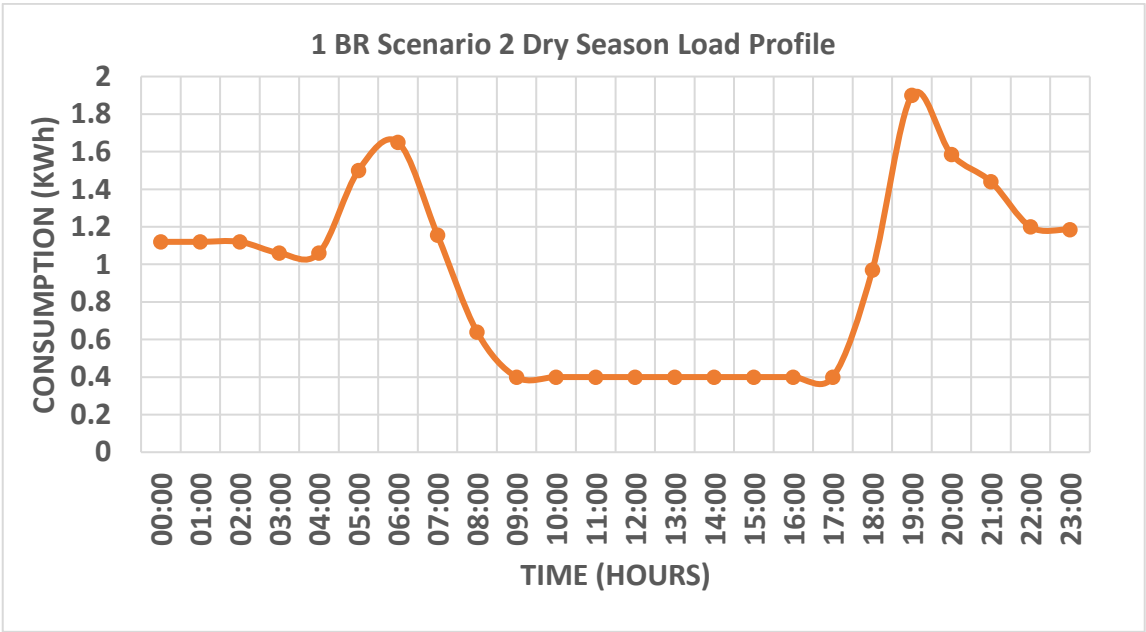

Fig. B22. 1 bedroom scenario 2 dry season load profile.

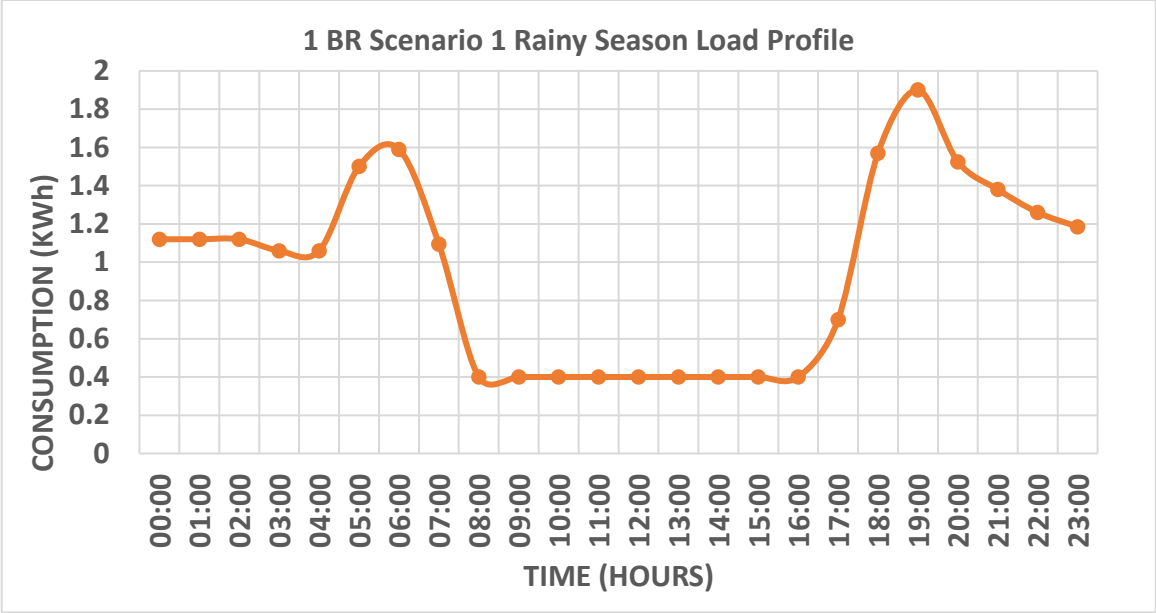

Fig. B23. 1 bedroom scenario 1 rainy season load profile.

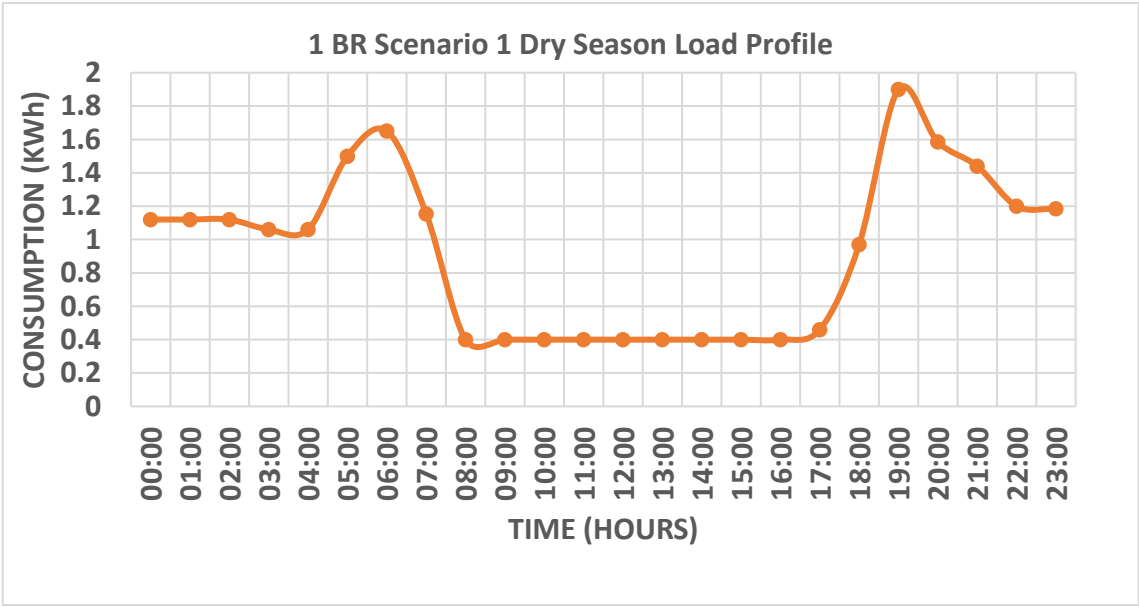

Fig. B24. 1 bedroom scenario 1 dry season load profile.

Appendix C Energy demand of various residential consumer types

Table C.1. Urban scenario 1 average demand

Urban scenario 1				
	LED		Incandescent	
Building	Rainy season load (w)	Dry season load (w)	Rainy season load (w)	Dry season load (w)
4 bedrooms	2,632.625	3,240.875	3,366.875	3,904.458
3 bedrooms	2,362.792	2,758.667	3,014.583	3,373.417
2 bedrooms	1,742.208	1,650.875	2,666.125	2,639.375
1 bedroom self-contain	662.500	656.125	947.375	921.875

Table C.2. Urban scenario 2 average demand

Urban scenario 2				
	LED		Incandescent	
Building	Rainy season load (w)	Dry season load (w)	Rainy season load (w)	Dry season load (w)
4 bedrooms	3,036.000	3,433.708	3,652.292	4,093.208
3 bedrooms	2,602.500	3,024.958	3,263.125	3,624.458
2 bedrooms	1,895.208	1,803.875	2,385.792	2,229.042
1 bedroom self-contain	662.042	657.500	946.875	929.375

Table C.3. Urban scenario 3 average demand

Urban scenario 3				
	LED		Incandescent	
Building	Rainy season load (W)	Dry season load (W)	Rainy season load (W)	Dry season load (W)
4 bedrooms	3,083.542	3,645.542	3,814.167	4,311.167
3 bedrooms	2,835.417	3,258.333	3,485.833	3,845.708

2 bedrooms	2,047.333	1,957.458	2,533.833	2,377.083
1 bedroom self-contain	705.750	719.042	988.542	976.458

Table C.4. Urban scenario 1 demand factor

Urban scenario 1				
	LED		Incandescent	
Building	Rainy season	Dry season	Rainy season	Dry season
4 bedrooms	0.413	0.470	0.450	0.502
3 bedrooms	0.377	0.461	0.415	0.411
2 bedrooms	0.672	0.621	0.825	0.939
1 bedroom self-contain	0.709	0.709	0.790	0.790

Table C.5. Urban scenario 2 demand factor

Urban scenario 2				
	LED		Incandescent	
Building	Rainy season	Dry season	Rainy season	Dry season
4 bedrooms	0.508	0.470	0.508	0.502
3 bedrooms	0.381	0.385	0.418	0.411
2 bedrooms	0.672	0.621	0.690	0.651
1 bedroom self-contain	0.709	0.709	0.790	0.790

Table C.6. Urban scenario 3 demand factor

Urban scenario 3				
	LED		Incandescent	
Building	Rainy season	Dry season	Rainy season	Dry season
4 bedrooms	0.363	0.333	0.405	0.378
3 bedrooms	0.377	0.382	0.415	0.411

2 bedrooms	0.672	0.500	0.690	0.545
1 bedroom self-contain	0.709	0.709	0.790	0.790

Table C.7. Urban scenario 1 load factor

Urban scenario 1				
	LED		Incandescent	
Building	Rainy season load	Dry season load	Rainy season load	Dry season load
4 bedrooms	0.291	0.315	0.310	0.322
3 bedrooms	0.353	0.337	0.368	0.415
2 bedrooms	0.285	0.293	0.311	0.270
1 bedroom self-contain	0.532	0.527	0.499	0.485

Table C.8. Urban scenario 2 load factor

Urban scenario 2				
	LED		Incandescent	
Building	Rainy season load	Dry season load	Rainy season load	Dry season load
4 bedrooms	0.273	0.333	0.298	0.338
3 bedrooms	0.385	0.442	0.395	0.446
2 bedrooms	0.310	0.320	0.332	0.329
1 bedroom self-contain	0.531	0.528	0.498	0.489

Table C.9. Urban scenario 3 load factor

Urban scenario 3				
	LED		Incandescent	
Building	Rainy season load	Dry season load	Rainy season load	Dry season load
4 bedrooms	0.388	0.500	0.391	0.473
3 bedrooms	0.423	0.480	0.425	0.474
2 bedrooms	0.335	0.431	0.353	0.419
1 bedroom self-contain	0.566	0.577	0.520	0.514

Table C.10. Urban scenario 1 unity power density

Urban scenario 1				
	LED		Incandescent	
Building	Rainy season (W/Ft^2)	Dry season (W/Ft^2)	Rainy season (W/Ft^2)	Dry season (W/Ft^2)
4 bedrooms	1.960	2.413	2.507	2.907
3 bedrooms	1.242	1.529	1.588	1.842
2 bedrooms	1.751	2.156	2.240	2.597
1 bedroom self-contain	5.162	6.354	6.601	7.655

Table C.11. Urban scenario 2 unity power density

Urban scenario 2				
	LED		Incandescent	
Building	Rainy season (W/Ft^2)	Dry season (W/Ft^2)	Rainy season (W/Ft^2)	Dry season (W/Ft^2)
4 bedrooms	2.260	2.557	2.719	3.048
3 bedrooms	1.432	1.620	1.723	1.931
2 bedrooms	2.019	2.284	2.429	2.723

1 bedroom self-contain	5.952	6.732	7.161	8.025

Table C.12. Urban scenario 3 unity power density

Urban scenario 3				
	LED		Incandescent	
Building	Rainy season (W/Ft^2)	Dry season (W/Ft^2)	Rainy season (W/Ft^2)	Dry season (W/Ft^2)
4 bedrooms	2.296	2.714	2.840	3.210
3 bedrooms	1.454	1.719	1.799	2.033
2 bedrooms	2.051	2.425	2.537	2.868
1 bedroom self-contain	6.046	7.147	7.478	8.452

Appendix D Assumed appliance wattages

Table D.1. 4 bedroom Urban with incandescent lights

4 bedrooms urban incandescent	
Appliances	Wattage (w)
Light bulb	60
Light bulb	11
Mobile phone charger	15
Laptop charger	65
Ceiling fan	60
DVD/DVR	25
Television	150
Home theatre	800
Cable decoder	35
Air conditioner (1 hp)	746
Air conditioner (1.5 hp)	1100

Refigerator/freezer	725
Microwave oven	700
Blender	300
Water pump (1.5 hp)	1100
Pressing iron	1400
Water heater	3000
Washing machine	400

Appendix E Street lighting computation Table

Table E.1. Generator powered HPS street lighting system

S/N	Description of materials with full specifications	Quantity	Rate ₦ ($)	Amount ₦ ($)	Remarks
A.)1	100KVA Mikano Generator	20	3,400,000.00 (93,922.65)	68,000,000.00 (187,845.30)	C_{GEN}
2	250W, 220V AC High Pressure Sodium Fittings	2,434	41,250.00 (113.95)	100,402,500.00 (277,354.97)	2 fittings per pole($C_{HPSFGEN}$)
3	250W, 220V AC High Pressure Sodium Lamps	2,434	12,670.00 (35.00)	30,838,780.00 (85,190.00)	2 lamps per pole ($C_{HPSLGEN}$)
4	4 - core 35mm^2 copper conductor armoured cable,	43,600 m	6,500.00 (17.96)	283,400,000.00 (782,672.93)	To interconnects ($C_{ACABHPSGEN}$)

	600V to earth and 100V between conductors				
5	4mm^2, double core flexible copper conductor cable	24,340 m	500.00 (1.38)	12,170,000.00 (33,618.78)	20m per pole ($C_{CABHPSGEN}$)
6	10m, double arm galvanized steel pole	1,217	72,400.00 (200.00)	88,110,800.00 (243,400.00)	$C_{POLEHPSGEN}$
7	Complete concrete reinforcement (cement, iron rod, sand, excavation, plank, nails, bolts and nuts, water) per pole	1,217	36,200.00 (100.00)	44,055,400.00 (121,700.00)	$C_{REINFORCEMENTHPSGEN}$
8	Installation cost	1,217	72,400.00 (200.00)	88,110,800.00 (243,400.00)	Installation of 1,217 light poles ($C_{INSTALLHPSGEN}$)
9	Labour cost	1,217	72,400.00 (200.00)	88,110,800.00 (243,400.00)	$C_{LABHPSGEN}$
10	Initial investment cost			**803,199,080.00 (2,218,781.99)**	ICC_{HPSGEN}
B.) 1	Replacement of complete High Pressure Sodium vapour	9,736		89,371,230.66 (246,881.85)	$C_{PWHPSLGEN}$

	lamp (four times) throughout the life span of the system (25 years).				
2	Present worth of workers' wages for the replacement of lamps throughout the life time of the project (25 years)	9,736		102,138,549.30 (282,150.69)	₦7240/pole ($20/pole for the cost of the installation) ($C_{PWHPSGENWW}$)
3	Replacement of oil and change of filter after 300 hours of operation of generator for twelve hours of operation of HPS streetlight lamps (three hundred and sixty five times) throughout the lifespan of the system (25 years)	7,300		5,754,297,530.00 (15,859,849.53)	10% of generator cost. (C_{PWOFC})

4	Decarbonization of generator after 1500 hours of operation of generator for twelve hours of operation of HPS streetlight lamps (seventy three times) throughout the lifespan of the system (25 years)	1,460		575,429,753.00 (1,589,584.95)	5% of generator cost. ($C_{PWGENDECARBON}$)
5	Engine overhaul of generating set after 6000 hours of generator operation for twelve hours of operation of HPS street light lamps (seventeen times) throughout the lifespan of the system (25 years).	340		1,349,760,164.00 (3,728,619.24)	50% of generator cost ($C_{PWENGOH}$)

6	Cost of Operation and Maintenance of Generator Powered Generator throughout the lifespan of the project			**7,870,997,226.96 (21,743,086.26)**	$C_{OMHPSGEN}$
C.)	Present Worth of the Cost of running generator using diesel using the minimum number of liters (3702) consumed per month by each generator as bench mark throughout the lifespan of the project	20		**3,359,259,895.00 (9,279,723.57)**	$C_{PWENERGYCOSTHPSGEN}$
D.)	Life Cycle Cost			**12,033,456,201.96 (33,241,591.81)**	LCC_{HPSGEN}
E.)	Annualized Life			**650,776,489.48 (1,797,725.11)**	$ALCC_{HPSGEN}$
F.)	COE			**244.17/kWh (0.675/kWh**)	COEHPSGEN

Table E.2. Grid powered HPS street lighting system

S/N	Description of materials with full specifications	Quantity	Rate ₦ ($)	Amount ₦ ($)	Remarks
A.)1	200KVA, 11/.415KV, 3-Phase Transformer	6	2,000,000.00 (5,524.86)	12,000,000.00 (33,149.17)	C_{TRANS}
2	250W, 220V AC High Pressure Sodium Fittings	2,434	41,250.00 (113.95)	100,402,500.00 (277,354.97)	2 fittings per pole ($C_{HPSFGRID}$)
3	250W, 220V AC High Pressure Sodium Lamps	2,434	12,670.00 (35.00)	30,838,780.00 (85,190.00)	2 lamps per pole ($C_{HPSLGRID}$)
4	4-core $35mm^2$ copper conductor armoured cable, 600V to earth and 100V between conductors	43,600 m	6,500.00 (17.96)	283,400,000.00 (782,872.93)	To interconnects ($C_{ACABHPSGRID}$)

5	$4mm^2$, double core flexible copper conductor cable	24,340 m	500 (1.38)	12,170,000.00 (33,618.78)	20m per pole ($C_{CABHPSGRID}$)
6	Materials required for the installation of transformer (including rod earthing, basement and three phase energy meter)	6	15,000,00.00 (41,436.46)	90,000,000.00 (248,618.78)	$C_{MATERIALINSTALLTRANS}$
7	10m, double arm galvanized steel pole	1,217	72,400.00 (200.00)	88,110,800.00 (243,400.00)	$C_{POLEHPSGRID}$
8	Complete concrete reinforcement (cement, iron, rod, sand, excavation plank, nails, bolts and	1,217	36,200.00 (100.00)	44,055,400.00 (121,700.00)	$C_{REINFORCEMENTHPSGRID}$

	nuts, water) per pole				
9	Installation cost	1,217	72,400.00 (200.00)	88,110,800.00 (243,400.00)	Installation of 1,217 light poles ($C_{INSTALLHPSGRID}$)
10	Labour cost	1,217	72,400.00 (200.00)	88,110,800.00 (243,400.00)	$C_{LABOURHPSGRID}$
11	Initial Investment Cost			**837,199,080.00 (2,312,704.64)**	$ICC_{HPSGRID}$
B.) 1	Replacement of complete high pressure Sodium Vapour Lamp (four times) throughout the life span of the system (25 years)	9,736		89,371,230.66 (246,881.85)	$C_{PWHPSLGRID}$
2	Present worth of worker's wages for the replacement of lamps throughout the life time of the protect (25years).	9,736		102,138,549.30 (282,150.69)	~~₦~~7,240/pole or $20/pole for the cost of installation ($C_{PWHPSGRIDWW}$)

3	Total cost of maintenance (replacement cost + workers' wages)			**191,509,780.00 (529,032.54)**	$C_{OMHPSGRID}$
C.)	Energy Consumption Cost			**1,267,300,915.00 (3,500,831.26)**	$C_{PWENERGYCOSTHPSGRID}$
D.)	Transformer Energy Losses			**16,953,328,794.93 (46,939,599.08)**	$C_{PWTRANSLOSSCOSTHPSGRID}$
E.)	Life Cycle Cost			**19,249,338,569.93 (53,282,127.51)**	$LCC_{HPSGRID}$
F.)	Annualized Life Cycle Cost			**1,041,015,712.28 (2,881,529.24)**	$ALCC_{HPSGRID}$
G.)	COE			**390.59/kWh (1.08/kWh)**	$COE_{HPSGRID}$

Table E.3. Solar PV powered street lighting system

S/N	Description of materials with full specifications	Quantity	Rate ₦ ($)	Amount ₦ ($)	Remarks
A.) 1	$180W_p$, 18VDC 4BB PV Solar Module	4,868	25,340.00 (70.00)	123,355,120.00 (340,760.00)	4 modules per pole (C_{SPV})
2	Complete super bright solar lamp 120w, 12-24VDC, LED, 80.110lm/m^2, > 75Ra,	2,434	78,375.00 (216.51)	190,764,750.00 (526,947.45)	2 per pole (C_{LED})

	Power Factor >95%, life span, >50,000hrs (Zhongshanttuijian Photoelectric Technology Co, Ltd.).				
3	200AH, 12VDC, Deep cycle sealed AGM battery, MIGHTY MAX	3,651	133,940.00 (370.00)	489,014,940.00 (1,350,870.00)	3 Batteries per pole (C_{BAT})
4	12/24 VDC, 48A MPPT Solar charge controller	1,217	56,834.00 (157.00)	69,166,978.00 (191,069.00)	1 charge controller per pole ($C_{CONTROLLER}$)
5	$4mm^{2,}$ double core flexible copper conductor cable	6,085m	500 (1,38)	3,042,500.00 (8,404.70)	5m per pole (C_{CABSPV})
6	Battery box	2,434	18,100.00 (50.00)	44,055,400.00 (121,700.00)	2 boxes per pole (C_{BOX})
7	Solar Rack	1,217	32,580.00 (90.00)	39,649,860.00 (109,530.00)	1 rack per pole (C_{SRK})
8	Complete concrete reinforcement (cement, iron, rod, sand, excavation plank, nails, bolts and nuts, water)	1,217	36,200.00 (100.00)	44,055,400.00 (121,700.00)	($C_{REINFORCEMENT}$)
9	10m, double arm galvanized steel pole	1,217	72,400.00 (200.00)	88,110,800.00 (243,400.00)	Each arm should be of 1.3m extension ($C_{POLESPV}$)
10	Labour cost	1,217	36,200.00 (100.00)	44,055,400.00 (121,700.00)	C_{LABSPV}

11	Installation cost (10% of PV cost)			113,527,114.80 (313,610.81)	$C_{INSTALL}$
12	Initial investment cost			**1,248,798,263.00 (3,449,718.96)**	ICC_{SPV}
B.) 1	Replacement of 200AH, 12VDC, Deep cycle sealed AGM battery, MIGHTY MAX for every five years throughout the life span of the system (25 years)	14,604		1,417,172,372.00 (3,914,840.81)	C_{BATPW}
2	Replacement of complete super Bright Solar Lamp 120w, 12-24VDC, LED, once throughout the life span of the system(25 years)	2,434		134,875,722.60 (372,584.87)	C_{PWLED}
3	Replacement of 12/24 VDC, 48A MPPT Solar charge controller once throughout the life span of the system (25 years)	1,217		50,224,581.95 (138,741.94)	$C_{PWCONTROLLER}$
4	Present Worth of Maintenance Cost			408,795,635.70 (1,129,269.71)	C_{PWM}
5	Replacement, Operation and Maintenance Cost throughout the lifetime of the project			**2,011,068,312.00 (5,555,437.33)**	C_{OMSPV}
C.)	Life Cycle Cost			**3,259,866,575.00 (9,005,156.28)**	LCC_{SPV}

D.)	Annualized Life Cycle Cost			**176,295,528.90 (487,004.22)**	$ALCC_{SPV}$
E.)	COE			**137.80/kWh (0.38/kWh)**	COE_{SPV}

Appendix F TCN geographical structure, generator, transmission and load data

Fig. F1. Geographical structure of TCN.

Table F.1. Existing 330 kV transmission line network circuit parameters

S/N	From Station Location	To Station Location	No of circuits	Length (Km)	S/N	From Station Location	To Station Location	No of circuits	Length (Km)
1	Afam G.S	Alaoji T.S	2	25	35	Ikot - Ekpene T.S	Alaoji T.S	2	57.9
2	Afam G.S	PH main T.S	2	8	36	Ikot - Ekpene T.S	Odukpani T.S	2	88.5
3	Ahoda T.S	Gbarian G.S	2	87.4	37	Jebba G.S	Jebba T.S	2	8
4	Aiyede T.S	Olorunsogo G.S	1	125	38	Jebba T.S	Ganmo T.S	1	70
5	Ajah T.S	Lekki T.S	2	5.5	39	Jebba T.S	Osogbo T.S	2	157
6	Ajah T.S	Alagbon T.S	2	21	40	Jebba T.S	Shiroro G.S	2	244
7	Ajaokuta T.S	Geregu G.S	1	75	41	Jos T.S	Makurdi T.S	1	285
8	Aladja T.S	Sapele G.S	1	93	42	Kaduna T.S	Shiroro G.S	2	95
9	Alagbon T.S	Lekki T.S	2	24.5	43	Kaduna T.S	Kano T.S	1	230
10	Alaoji G.S	Alaoji T.S	2	50	44	Kaduna T.S	Jos T.S	1	197
11	Alaoji T.S	Owerri T.S	2	77.1	45	Kainji T.S	Kainji G.S	2	0.47
12	Asaba T.S	Onitsha T.S	2	65.8	46	Kainji T.S	Jebba T.S	2	81
13	Benin T.S	Ajaokuta T.S	2	195	47	Katampe T.S	Gwagwalada T.S	1	60
14	Benin T.S	Delta G.S	1	107	48	lokoja T.S	Ajaokuta T.S	1	215
15	Benin T.S	Sapela G.S	2	50	49	New Haven T.S	Ugwaji T.S	2	65
16	Benin T.S	Asaba T.S	2	153.9	50	New Haven T.S	Onitsha T.S	1	96
17	Birnin – Kebbi T.S	Kainji T.S	1	310	51	Odukpani T.S	Adiabor T.S	2	10
18	Damaturu T.S	Maiduguri T.S	1	260	52	Okearo T.S	Egbin T.S	2	30
19	Delta G.S	Aladja T.S	1	30	53	Omotosho G.S	Benin T.S	1	120
20	Egbin G.S	Benin T.S	1	218	54	Onitsha T.S	Okpai G.S	2	56
21	Egbin G.S	Aja T.S	2	14	55	Onitsha T.S	Alaoji T.S	1	138
22	Ganmo T.S	Osogbo T.S	1	87	56	Osogbo T.S	Aiyede T.S	1	119
23	Gbarian G.S	Yenegoa T.S	2	25	57	Osogbo T.S	Ikeja west T.S	1	235
24	Gombe T.S	Damaturu T.S	1	160	58	Osogbo T.S	Ihovbor G.S	1	251
25	Gombe T.S	Yola T.S	1	240	59	Owerri T.S	Ahoda T.S	2	73.6
26	Gwagwalada	Shiroro G.S	1	144	60	PH main T.S	Omoko T.S	2	83
27	Gwagwalada T.S	Lokoja T.S	1	135	61	Sapele G.S	Delta G.S	1	93
28	Ihovbor G.S	Benin T.S	1	20	62	Shiroro G.S	Katampe T.S	1	144
29	Ikeja west T.S	Akangba T.S	2	18	63	Paras energy T.S	Sagamu T.S	2	4
30	Ikeja west T.S	Omotosho T.S	1	160	64	Trans amadi T.S	PH main T.S	2	8
31	Ikeja west T.S	Okearo T.S	2	32	65	Egbin G.S	Ikorodu T.S	2	17
32	Ikeja west T.S	Egbin T.S	1	62	66	Ikorodu T.S	Sagamu T.S	2	34
33	Ikeja west T.S	Olorunsogo G.S	1	50	67	Asco G.S	Ajaokuta T.S		50
34	Ikot - Ekpene T.S	Ugwaji T.S	2	174		Total			6717.67

Table F.2. Transmission line data

Line no.	From bus	To bus	R(p.u.)	X(p.u.)	B(p.u)
1	2	3	0.003183	0.023942	0.31
2	3	4	0.000287	0.002431	0.031373
3	3	4	0.000287	0.002431	0.031373
4	3	5	0.008543	0.073297	0.962559
5	3	6	0.005575	0.047487	0.617196
6	3	6	0.005575	0.047487	0.617196
7	3	10	0.002505	0.021255	0.274643
8	5	11	0.003773	0.028371	0.37

9	5	12	0.005121	0.043588	0.565870
10	5	13	0.004067	0.034560	0.447636
11	6	7	0.004102	0.034861	0.451573
12	6	8	0.008813	0.075657	0.972381
13	6	9	0.007570	0.064764	0.828210
14	6	10	0.003110	0.026403	0.341432
15	7	14	0.003430	0.029124	0.376815
16	8	14	0.003855	0.032749	0.414631
17	8	16	0.002437	0.018327	0.20
18	8	17	0.011005	0.082766	1.09
19	8	18	0.000369	0.003131	0.040387
20	11	21	0.007743	0.058231	0.77
21	12	13	0.001075	0.009116	0.117657
22	13	22	0.004981	0.042387	0.550090
23	16	18	0.001275	0.010818	0.139606
24	16	19	0.009865	0.074194	0.98
25	19	24	0.005384	0.040496	0.63
26	19	24	0.005384	0.040496	0.63
27	19	25	0.007664	0.057640	0.76
28	19	26	0.003817	0.032450	0.420027
29	19	27	0.001965	0.014780	0.19
30	19	27	0.001965	0.014780	0.19
31	21	28	0.010415	0.078332	1.04
32	21	28	0.010415	0.078332	1.04
33	22	25	0.001361	0.011547	0.149041
34	24	30	0.003773	0.028377	0.37
35	24	31	0.002130	0.018086	0.233596
36	24	32	0.006053	0.045521	0.60
37	25	33	0.004330	0.054152	0.019608
38	26	27	0.002476	0.018622	0.24

39	26	34	0.001022	0.007685	0.10
40	27	34	0.002476	0.018622	0.24
41	28	35	0.006485	0.055397	0.721889
42	28	35	0.006485	0.055397	0.721889
43	30	35	0.000346	0.002935	0.037867
44	32	38	0.000983	0.007390	0.09
45	32	39	0.001728	0.014668	0.189379
46	35	39	0.004921	0.041910	0.543796
47	38	39	0.002303	0.019550	0.252551
48	39	40	0.002188	0.018574	0.239914
49	40	41	0.000577	0.004891	0.063113

Table F.3. Generator characteristics

Generator	Connected bus	Power (MW)	Bus volt (kV)	Volt. mag (p.u.)
Kainji GS	1	259	16	1.0
Jebba GS	15	252	330	1.0
Shiroro	20	302	330	1.0
Olorunsogo	23	159	330	1.0
Geregu GS	36	120	330	1.0
Ihovor GS	37	240	330	1.0
Omotosho GS	42	188	330	1.0
Delta GS	43	281	330	1.0
Afam GS	44	280	330	0.973
Odukpani GS	45	260	330	1.0
Okpai GS	46	221	330	1.0
Alaoji GS	47	240	330	1.0
Sapele GS	48	170	330	1.0

Table F.4. Bus loading characteristics

S/N	Terminal Bus	Rating (MVA)	S/N	Terminal Bus	Rating (MVA)	S/N	Terminal Bus	Rating (MVA)
1	Afam	105.882	11	Delta	75.647	21	Kainji G.S	117.647
2	Aiyede T.S	117.647	12	Egbin G.S	1176.471	22	Kano T.S	217.529
3	Aja T.S	58.824	13	Ganmo T.S	75.882	23	Katampe T.S	235.294
4	Ajaokuta T.S	117.647	14	Geregu NIPP & G.S	164.706	24	Maiduguri T.S	58.824
5	Akangba T.S	131.765	15	Gombe T.S	235.294	25	New Haven T.S	294.118
6	Aladja T.S	96.588	16	Ikeja West T.S	352.941	26	Okaero T.S	117.647
7	Alaoji T.S	117.647	17	Jebba T.S	10.118	27	Okpia G.S	11.765
8	Alaoji G.S	52.588	18	Jebba G.S	117.647	28	Onitsha T.S	135.529
9	Benin T.S	184.471	19	Jos T.S	352.941	29	Oshogbo T.S	176.471
10	Birni-Kebbi T.S	117.647	20	Kaduna T.S	195.529	30	Shiroro G.S	72.353
						31	Yola T.S	117.647

Table F.5. Generator and bus data

Bus no.	Bus name	Bus volt (KV)	Volt. Mag. (PU)	Load		Generation	
				MW	MVAR	MW	MVAR
1	Kainji GS	16	1.0	-	-	259	-
2	Kainji SS	330	1.0	-	-	-	-
3	Jebba TS	330	0.988	260	119	-	-
4	Jebba SS	330	1.0	-	-	-	-
5	Shiroro SS	330	1.0	-	-	-	-
6	Oshogbo TS	330	1.0	107	56	-	-
7	Ayede TS	330	0.97	114	68	-	-
8	Ikeja West TS	330	1.0	447	195	-	-
9	Ihovbor SS	330	1.0	-	-	-	-
10	Ganmo TS	330	0.994	100	57	-	-
11	Kaduna TS	330	0.956	102	51	-	-
12	Katampe TS	330	1.0	201	107	-	-
13	Gwagwalada TS	330	0.956	120	65	-	-
14	Olorunsogo SS	330	1.0	-	-	-	-
15	Jebba GS	330	1.0	-	-	252	-
16	Egbin SS	330	1.0	-	-	-	-
17	Omotosho SS	330	1.0	-	-	-	-
18	Okearo TS	330	1.0	220	100	-	-
19	Benin TS	330	0.994	257	108		

20	Shiroro GS	330	1.0	-	-	302	-
21	Jos TS	330	0.939	232	110	-	-
22	Lokoja TS	330	0.97	100	60	-	-
23	Olorunsogo GS	330	1.0	-	-	159	-
24	Onitsha TS	330	0.982	180	85		
25	Ajaokuta TS	330	0.97	120	70	-	-
26	Delta SS	330	1.0	-	-	-	-
27	Sapele SS	330	1.0	-	-	-	-
28	Makurdi TS	330	0.939	160	72	-	-
29	Egbin GS	330	1.0	-	-	-	-
30	New Heaven TS	330	0.988	136	77		
31	Okpai SS	330	1.0	-	-	-	-
32	Alaoji SS	330	0.97	-	-	-	-
33	Geregu SS	330	1.0	-	-	-	-
34	Aladja TS	330	0.985	182	77	-	-
35	Ugwuaji TS	330	0.994	125	69		
36	Geregu GS	330	1.0	-	-	120	-
37	Ihovbor GS	330	1.0	-	-	240	-
38	Afam SS	330	1.0	-	-	-	-
39	Ikot Ekpene TS	330	0.948	165	74	-	-
40	Adiabor TS	330	0.97	90	48	-	-
41	Odukpani SS	330	1.0	-	-	-	-
42	Omotosho GS	330	1.0	-	-	188	-
43	Delta GS	330	1.0	-	-	281	-
44	Afam GS	330	0.973	-	-	280	-
45	Odukpani GS	330	1.0	-	-	260	-
46	Okpai GS	330	1.0	-	-	221	-
47	Alaoji GS	330	1.0	-	-	240	-
48	Sapele GS	330	1.0	-	-	170	-

Table F.6. Load bus data

Load bus	P (MW)	Q (MVar)	Voltage mag. (p.u.)	Bus name
3	260	119	0.988	Jebba TS
6	107	56	1.0	Oshogbo TS
7	114	68	0.97	Ayeda TS
8	447	195	1.0	Ikeja West TS
10	100	57	0.994	Ganmo TS
11	102	51	0.956	Kaduna TS
12	201	107	1.0	Katampe TS
13	120	65	0.956	Gwagwalada TS
18	220	100	1.0	Okearo TS
19	257	108	0.994	Benin TS
21	232	110	0.939	Jos TS
22	100	60	0.97	Lokoja TS
24	180	85	0.982	Onitsha TS
25	120	70	0.97	Ajaokuta TS
28	160	72	0.939	Makurdi TS
30	136	77	0.988	New Heaven TS
34	182	77	0.985	Aladja TS
35	125	69	0.994	Ugwuaji TS
39	165	74	0.948	Ikot Ekpene TS
40	90	48	0.97	Adiabor TS

Table F.7. Transformer data

S/N	From bus	To bus	MVA	KV	Hz	R (PU)	X (PU)	Pry/Sec volt (KV)
1	15	4	100	16	50	0.00	0.0586	16/330
2	1	2	100	16	50	0.00	0.0625	16/330
3	20	5	100	15.7	50	0.00	0.0625	15.7/330

4	23	14	100	10.5	50	0.00	0.0625	10.5/330
5	37	9	100	15	50	0.00	0.0625	15/330
6	36	33	100	15.8	50	0.00	0.0625	15.8/330
7	47	32	100	15	50	0.00	0.0625	15/330
8	42	17	100	10.5	50	0.00	0.0625	10.5/330
9	48	27	100	15.8	50	0.00	0.0625	15.8/330
10	43	26	100	11.5	50	0.00	0.0625	11.5/330
11	46	31	100	15.8	50	0.00	0.0625	15.8/330
12	44	38	100	10.5	50	0.00	0.0625	10.5/330
13	45	41	100	15	50	0.00	0.0625	15/330
14	29	16	100	18	50	0.00	0.0586	18/330

Appendix G Possible Load Switching Routes Via Transmission Line

Table G.1. Possible switching of load L3 on Jebba TS bus by participating generators

S/N	Name	Lines from Generators to Load 3 (Jebba TS) considering the entire network	
1	G1	L34	
2	G2	L23	
3	G3	L714, L67, L36	
4	G4	L35	
5	G5	L69, L36	
6	G6	L2533, L2225, L1322, L513, L35	L2533, L1925, L1619, L1618, L818,L68, L36
7	G7	L817, L68, L36	
8	G8	L2627, L1927, L1619, L816, L68, L36	L1926, L1925, L2225, L1322, L513, L35
9	G9	`L3238, L2432, L1924, L1619, L816, L68, L36	L3839, L3539, L2835, L2128,L1121,L511,L35
10	G10	L3940, L3539, L2835,L2128, L1121, L511,L35	L3839,L3238,L2432,L1924,L1619,L816,L68, L36
11	G11	L816, L68, L36	
12	G12	L1927,L1619, L1618, L818,L68, L36	L1927, L1925, L2225, L1322, L513, L35
13	G13	L2432, L1924, L1619, L816,L68, L36	L2432, L2430, L3035, L2835,L2128, L1121, L511,L35
14	G14	L2431,L1924,L1619,L816,L68,L36	L2431, L2430,L3035, L2835,L2128,L1121, L511,L35

Table G.2. Possible switching of load L6 on Oshogbo TS bus by participating generators

S/N	Name	Lines from Generators to Load 6 (Oshogbo TS) considering the entire network	
1	G1	L34, L36	
2	G2	L23, L36,	
3	G3	L714, L67	
4	G4	L35, L36	
5	G5	L69	
6	G6	L2533, L2235, L1322, L513, L35, L36	L2533, L1925, L1619, L816, L68
7	G7	L817, L68	
8	G8	L2627, L1927, L1619, L816, L68	L1926, L1619, L816, L68
9	G9	`L3238, L2432, L1924, L1619, L816, L68	
10	G10	L3839, L3539, L2835,L2128, L1121, L511,L35, L36	L3238,L2432,L1924,L1619,L816,L68, L36
11	G11	L816, L68	L1618,L818,L68
12	G12	L1927,L1619, L1618, L816,L68	L2734, L2627, L1925, L1619, L816,L68
13	G13	L2432, L1924, L1619, L816,L68	
14	G14	L2431,L1924,L1619,L816,L68	

Table G.3. Possible switching of load L7 on Ayede TS bus by participating generators

S/N	Name	Lines from Generators to Load L7 (Ayede TS) considering the entire network	
1	G1	L34,L36,L67	
2	G2	L23,L36,L67	
3	G3	L714	
4	G4	L35,L36,L67	
5	G5	L69, L67	
6	G6	L2533, L1925, L1619, L816, L68,L67	L2533, L1925, L1619, L816,L814, L714
7	G7	L817, L68, L67	L817, L814, L714
8	G8	L1926, L1619, L816, L814, L714	L1926, L1619, L816, L68, L67
9	G9	`L3238, L2432, L1924, L1619, L816, L814, L714	L3238, L2432, L1924, L1619,L816,L68,L67
10	G10	L4041, L3940, L3239, L2432,L1924, L1619, L816,L814,L714	L4041,L3940,L3239,L2432,L1924,L1619,L816 ,L68, L67
		L4041, L3940, L3539, L2835,L2128, L1121, L511,L35,L36,L67	
11	G11	L816, L68, L67	L816,L814,L714
12	G12	L1927,L1619, L816, L814,L714	L1927, L1619, L816, L68, L67
13	G13	L2432, L1924, L1619, L816,L814, L714	L2432, L1924, L1619, L816,L68, L67
14	G14	L2431,L1924,L1619,L816,L68,L67	L2431, L1924,L1619, L816,L814,L714

Table G.4. Possible switching of load L8 on Ikeja West TS bus by participating generators

S/N	Name	Lines from Generators to Load L8 (Ikeja West TS) considering the entire network
1	G1	L34,L36,L68
2	G2	L23,L36,L68
3	G3	L814
4	G4	L35,L36,L68
5	G5	L69, L68
6	G6	L2533, L1925, L1619, L816
7	G7	L817
8	G8	L1926, L1619, L816
9	G9	`L3238, L2432, L1924, L1619, L816
10	G10	L4041, L3940, L3239, L2432,L1924, L1619, L816
11	G11	L816
12	G12	L1927,L1619, L816
13	G13	L2432, L1924, L1619, L816
14	G14	L2431,L1924,L1619,L816

Table G.5. Possible switching of load L10 on Ganmo TS bus by participating generators

S/N	Name	Lines from Generators to Load L10 (Ganmo TS) considering the entire network	
1	G1	L34,L310	
2	G2	L23,L310	
3	G3	L714, L67,L610	L814, L68,L610
4	G4	L35,L310	
5	G5	L69, L610	
6	G6	L2533, L1925, L1619, L816, L68,L610	L2533,L2225,L1322, L513,L35, L310
7	G7	L817, L68, L610	
8	G8	L1926, L1619, L816, L68,L610	
9	G9	`L3238, L2432, L1924, L1619, L816, L68, L610	L3839,L3539,L2835,L2128,L1121,L511,L35,L310
10	G10	L4041, L3940, L3239, L2432,L1924, L1619, L816,L68,L610	L4041,L3940,L3239,L2432,L1924,L1619,L816,L68, L610
		L4041, L3940, L3539, L2835,L2128, L1121, L511,L35,L36,L610	
11	G11	L816, L68, L610	
12	G12	L1927, L1619, L816, L68, L610	
13	G13	L2432, L1924, L1619, L816,L68, L610	
14	G14	L2431,L1924,L1619,L816,L68,L610	

Table G.6. Possible switching of load L11 on Kaduna TS bus by participating generators

S/N	Name	Lines from Generators to Load L11 (Kaduna TS) considering the entire network	
1	G1	L34,L35,L511	
2	G2	L23,L35,L511	
3	G3	L714, L67,L36,L35,L511	L814, L68,L36, L35,L511
4	G4	L511	
5	G5	L69, L36,L35,L511	
6	G6	L2533, L1925, L1619, L816, L68, L36,L35,L511	L2533,L2225,L1322, L513,L511
7	G7	L817, L68, L36,L35,L511	
8	G8	L1926, L1925,L2225,L1322, L513,L511	
9	G9	L3839,L3539,L2835,L2128,L1121	
10	G10	L4041, L3940, L3539, L2835,L2128, L1121	
11	G11	L816, L68, L36, L35,L511	
12	G12	L1927, L1619, L816, L68, L36, L35,L511	L1927, L1925, L2225, L1322, L513, L511
13	G13	L2432, L1924, L1925, L2225, L1322, L513, L511	L3239,L3539,L2825,L2128, L1121
		L2432,L2430,L3035, L2835,L2128,L1121	
14	G14	L2431,L1924, L1925, L2225, L1322, L513, L511	L2431, L2430,L3035, L2835,L2128,L1121

Table G.7. Possible switching of load L12 on Katampe TS bus by participating generators

S/N	Name	Lines from Generators to Load L12 (Katampe TS) considering the entire network	
1	G1	L34,L35,L512	
2	G2	L23,L35,L512	
3	G3	L714, L67,L36,L35,L512	L814, L68,L36, L35,L512
4	G4	L512	
5	G5	L69, L36,L35,L512	
6	G6	L2533, L1925, L1619, L816, L68, L36,L35,L512	L2533,L2225,L1322, L513,L512
7	G7	L817, L68, L36,L35,L512	
8	G8	L1926, L1925,L2225,L1322, L513,L1213	
9	G9	L3839,L3539,L2835,L2128,L1121,L511,L512	L3238,L2432, L1924, L1925, L2225, L1322,L1213
10	G10	L4041, L3940, L3539, L2835,L2128, L1121,L511,L512	
11	G11	L816, L68, L36, L35,L512	
12	G12	L1927, L1925, L2225, L1322, L1213	
13	G13	L2432, L1924, L1925, L2225, L1322, L1213	L3239,L3539,L2825,L2128, L1121,L511,L512
14	G14	L2431,L1924, L1925, L2225, L1322, L1213	

Table G.8. Possible switching of load L13 on Gwagwalada TS bus by participating generators

S/N	Name	Lines from Generators to Load L13 (Gwagwalada TS) considering the entire network	
1	G1	L34,L35,L513	
2	G2	L23,L35,L513	
3	G3	L714, L67,L36,L35,L513	L814, L68,L36, L35,L513
4	G4	L513	
5	G5	L69, L36,L35,L513	
6	G6	L2533, L1925, L1619, L816, L68, L36,L35,L513	L2533,L2225,L1322
7	G7	L817, L68, L36,L35,L513	
8	G8	L1926, L1925,L2225,L1322	
9	G9	L3839,L3539,L2835,L2128,L1121,L511,L513	L3238,L2432, L1924, L1925, L2225, L1322
10	G10	L4041, L3940, L3539, L2835,L2128, L1121,L511,L513	
11	G11	L816, L68, L36, L35,L513	
12	G12	L1927, L1925, L2225, L1322	
13	G13	L2432, L1924, L1925, L2225, L1322	L3239,L3539,L2825,L2128, L1121,L511,L513
14	G14	L2431,L1924, L1925, L2225, L1322	

Table G.9. Possible switching of load L18 on Okearo TS bus by participating generators

S/N	Name	Lines from Generators to Load L18 (Okearo TS) considering the entire network
1	G1	L34,L36,L68,L818
2	G2	L23,L36,L68,L818
3	G3	L814,L818
4	G4	L35,L36,L68,L818
5	G5	L69, L68,L818
6	G6	L2533, L1925, L1618
7	G7	L817,L818
8	G8	L1926, L1619, L1618
9	G9	`L3238, L2432, L1924, L1619, L1618
10	G10	L4041, L3940, L3239, L2432,L1924, L1619, L1618
11	G11	L1618
12	G12	L1927,L1619, L1618
13	G13	L2432, L1924, L1619, L1618
14	G14	L2431,L1924,L1619,L1618

Table G.10. Possible switching of load L19 on Benin TS bus by participating generators

S/N	Name	Lines from Generators to Load L19 (Benin TS) considering the entire network
1	G1	L34,L36,L68,L816,L1619
2	G2	L23,L36,L68, L816,L1619
3	G3	L814, L816,L1619
4	G4	L35,L36,L68, L816,L1619
5	G5	L69, L68, L816,L1619
6	G6	L2533, L1925
7	G7	L817, L816,L1619
8	G8	L1926
9	G9	`L3238, L2432, L1924
10	G10	L4041, L3940, L3239, L2432,L1924
11	G11	L1619
12	G12	L1927
13	G13	L2432, L1924
14	G14	L2431,L1924

Table G.11. Possible switching of load L21 on Jos TS bus by participating generators

S/N	Name	Lines from Generators to Load L21 (Jos TS) considering the entire network	
1	G1	L34,L35,L511,L1121	
2	G2	L23,L35,L511, L1121	
3	G3	L714, L67,L36,L35,L511, L1121	L814, L68,L36, L35,L511, L1121
4	G4	L511, L1121	
5	G5	L69, L36,L35,L511, L1121	
6	G6	L2533, L1925, L1619, L816, L68, L36,L35,L511, L1121	L2533,L2225,L1322, L513,L511, L1121
7	G7	L817, L68, L36,L35,L511, L1121	
8	G8	L1926, L1925,L2225,L1322, L513,L511, L1121	L1926,L1924,L2430,L3035,L2835,L2128
9	G9	L3839,L3539,L2835,L2128	
10	G10	L4041, L3940, L3539, L2835,L2128	
11	G11	L816, L68, L36, L35,L511, L1121	
12	G12	L1927, L1619, L816, L68, L36, L35,L511, L1121	L1927, L1925, L2225, L1322, L513, L511, L1121
13	G13	L2432, L1924, L1925, L2225, L1322, L513, L511, L1121	L3239,L3539,L2825,L2128
		L2432,L2430,L3035, L2835,L2128	
14	G14	L2431,L1924, L1925, L2225, L1322, L513, L511, L1121	L2431, L2430,L3035, L2835,L2128

Table G.12. Possible switching of load L22 on Lokoja TS bus by participating generators

S/N	Name	Lines from Generators to Load L22 (Lokoja TS) considering the entire network	
1	G1	L34,L35,L513,L1322	
2	G2	L23,L35,L513,L1322	
3	G3	L714, L67,L36,L35,L513,L1322	L814, L68,L36, L35,L513,L1322
4	G4	L513,L1322	
5	G5	L69, L36,L35,L513,L1322	
6	G6	L2533, L1925, L1619, L816, L68, L36,L35,L513,L1322	L2533,L2225
7	G7	L817, L68, L36,L35,L513,L1322	
8	G8	L1926, L1925,L2225	
9	G9	L3839,L3539,L2835,L2128,L1121,L511,L513,L1322	L3238,L2432, L1924, L1925, L2225
10	G10	L4041, L3940, L3539, L2835,L2128, L1121,L511,L513,L1322	
11	G11	L816, L68, L36, L35,L513,L1322	L1619, L1925, L2225
12	G12	L1927, L1925, L2225, L1322	L1927, L1925, L2225
13	G13	L2432, L1924, L1925, L2225	L3239,L3539,L2825,L2128, L1121,L511,L513,L1322
14	G14	L2431,L1924, L1925, L2225	

Table G.13. Possible switching of load L24 on Onitsha TS bus by participating generators

S/N	Name	Lines from Generators to Load L24 (Onitsha TS) considering the entire network
1	G1	L34,L36,L68,L816,L1619,L1924
2	G2	L23,L36,L68, L816,L1619,L1924
3	G3	L814, L816,L1619,L1924
4	G4	L35,L36,L68, L816,L1619,L1924
5	G5	L69, L68, L816,L1619, ,L1924
6	G6	L2533, L1925,L1924
7	G7	L817, L816,L1619,L1924
8	G8	L1926,L1924
9	G9	`L3238, L2432
10	G10	L4041, L3940, L3239, L2432
11	G11	L1619,L1924
12	G12	L1927,L1924
13	G13	L2432
14	G14	L2431

Table G.14. Possible switching of load L25 on Ajaokuta TS bus by participating generators

S/N	Name	Lines from Generators to Load L25 (Ajaokuta TS) considering the entire network	
1	G1	L34,L35,L513,L1322,L2225	
2	G2	L23,L35,L513,L1322,L2225	
3	G3	L714, L67,L36,L35,L513,L1322,L2225	L814, L68, L816,L1619,L1925
4	G4	L513,L1322,L2225	
5	G5	L69, L68,L816,L1619,L1925	
6	G6	L2533	
7	G7	L817, L816, L1619,L1925	
8	G8	L1926, L1925	
9	G9	L3238,L2432, L1924, L1925, L2225	
10	G10	L4041, L3940, L3539, L3239,L2432,L1924,L1925	
11	G11	L1619, L1925	
12	G12	L1927, L1925	
13	G13	L2432, L1924, L1925	
14	G14	L2431,L1924, L1925	

Table G.15. Possible switching of load L28 on Makurdi TS bus by participating generators

S/N	Name	Lines from Generators to Load L28 (Makurdi TS) considering the entire network	
1	G1	L34,L35,L511,L1121,L2128	
2	G2	L23,L35,L511, L1121, ,L2128	
3	G3	L714, L67,L36,L35,L511, L1121,L2128	L814, L68,L36, L35,L511, L1121,L2128
4	G4	L511, L1121,L2128	
5	G5	L69, L36,L35,L511, L1121,L2128	
6	G6	L2533, L1925, L1924, L2430, L3035, L2835	L2533,L2225,L1322,L513,L511, L1121,L2128
7	G7	L817, L816, L1619,L1924,L2430, L3035, L2835	
8	G8	L1926,L1924,L2430,L3035,L2835	
9	G9	L3839,L3539,L2835	
10	G10	L4041, L3940, L3539, L2835	
11	G11	L1619,L1924,L2430, L3035, L2835	
12	G12	L1927, L1924, L2430, L3035, L2835	
13	G13	L2432,L2430,L3035, L2835	L3239,L3539,L2825
14	G14	L2431, L2430,L3035, L2835	

Table G.16. Possible switching of load L30 on New Heaven TS bus by participating generators

S/N	Name	Lines from Generators to Load L30 (New Heaven TS) considering the entire network	
1	G1	L34,L36,L68,L816,L1619,L1924,L2430	L34,L35,L511,L1121,L2128,L3035
2	G2	L23,L36,L68, L816,L1619,L1924,L2430	L23,L35,L511,L1121,L2128,L3035
3	G3	L814, L816,L1619,L1924,L2430	
4	G4	L35,L36,L68, L816,L1619,L1924,L2430	L511,L1121,L2128,L3035
5	G5	L69, L68, L816,L1619, ,L1924,L2430	
6	G6	L2533, L1925,L1924,L2430	
7	G7	L817, L816,L1619,L1924,L2430	
8	G8	L1926,L1924,L2430	
9	G9	`L3238, L2432,L2430	
10	G10	L4041, L3940, L3539, L3035	L4041, L3940, L3239, L2432,L2430
11	G11	L1619,L1924,L2430	
12	G12	L1927,L1924,L2430	
13	G13	L2432, L2430	
14	G14	L2431, L2430	

Table G.17. Possible switching of Load L34 on Aladja TS bus by participating generators

S/N	Name	Lines from Generators to Load L34 (Aladja TS) considering the entire network	
1	G1	L34,L36,L68,L816,L1619,L1926,L2634	L34,L36,L68,L816,L1619,L1927,L2734
2	G2	L23,L36,L68, L816,L1619 L1926,L2634	L24,L36,L68,L816,L1619,L1927,L2734
3	G3	L814, L816,L1619, L1926,L2634	L814, L816,L1619, L1927,L2734
4	G4	L35,L36,L68, L816,L1619, L1926,L2634	L35,L36,L68, L816,L1619, L1927,L2734
5	G5	L69, L68, L816,L1619, L1926,L2634	L69, L68, L816,L1619, L1927,L2734
6	G6	L2533, L1925, L1926,L2634	L2533, L1925, L1927,L2734
7	G7	L817, L816,L1619, L1926,L2634	L817, L816,L1619, L1927,L2734
8	G8	L2634	
9	G9	`L3238, L2432, L1924, L1926,L2634	`L3238, L2432, L1924, L1927,L2734
10	G10	L4041,L3940,L3239,L2432,L1924, L1926,L2634	L4041,L3940,L3239,L2432,L1924, L1927,L2734
11	G11	L1619, L1927,L2734	L1619, L1927,L2734
12	G12	L2734	
13	G13	L2432, L1924, L1926,L2634	L2432, L1924, L1927,L2734
14	G14	L2431,L1924, L1926,L2634	L2431,L1924, L1927,L2734

Table G.18. Possible switching of load L35 on Ugwuaji TS bus by participating generators

S/N	Name	Lines from Generators to Load L28 (Makurdi TS) considering the entire network	
1	G1	L34,L35,L511,L1121,L2128,L2835	
2	G2	L23,L35,L511, L1121, ,L2128,L2835	
3	G3	L714, L67,L36,L35,L511, L1121,L2128, ,L2835	L814, L816,L1619, L1924, L2430,L3035
4	G4	L511, L1121,L2128,L2835	
5	G5	L69, L36,L35,L511, L1121,L2128,L2835	L69, L816,L1619,L1924, L2430,L3035
6	G6	L2533, L1925, L1924, L2430, L3035	
7	G7	L817, L816, L1619,L1924,L2430, L3035	
8	G8	L1926,L1924,L2430,L3035	
9	G9	L3839,L3539	
10	G10	L4041, L3940, L3539	
11	G11	L1619,L1924,L2430, L3035	
12	G12	L1927, L1924, L2430, L3035	
13	G13	L2432,L2430,L3035	L3239,L3539
14	G14	L2431, L2430,L3035	

Table G.19. Possible switching of load L39 on Ikot Ekpene TS bus by participating generators

S/N	Name	Lines from Generators to Load L39 (Ikot EkpeneTS) considering the entire network	
1	G1	L34,L35,L511,L1121,L2128,L2835,L3539	L34,L36,L68, L816,L1619,L1924, L2432,L3239
2	G2	L23,L35,L511, L1121, ,L2128,L2835,L3539	L23,L36,L68, L816,L1619,L1924, L2432,L3239
3	G3	L814, L816,L1619,L1924, L2432,L3239	
4	G4	L511, L1121,L2128,L2835, ,L3539	
5	G5	L69, L36,L35,L511, L1121,L2128,L2835	L69, L816,L1619, L1619,L1924, L2430,L3035
6	G6	L2533, L1925, L1924, L2432, L3239	
7	G7	L817, L816, L1619,L1924, L2432, L3239	
8	G8	L1926,L1924, L2432, L3239	
9	G9	L3839	
10	G10	L4041, L3940	
11	G11	L1619,L1924, L2432, L3239	
12	G12	L1927, L1924, L2432, L3239	
13	G13	L3239	
14	G14	L2431, L2432, L3239	

Table G.20. Possible switching of load L40 on Adiabor TS bus by participating generators

S/N	Name	Lines from Generators to Load L40 (AdaborTS) considering the entire network	
1	G1	L34,L35,L511,L1121,L2128,L2835,L3539,L3940	L34,L36,L68, L816,L1619,L1924, L2432,L3239, L3940
2	G2	L23,L35,L511, L1121, ,L2128,L2835,L3539, L3940	L23,L36,L68, L816,L1619,L1924, L2432,L3239, L3940
3	G3	L814, L816,L1619,L1924, L2430,L3035,L3239, L3940	
4	G4	L511, L1121,L2128,L2835, ,L3539	
5	G5	L69, L36,L35,L511, L1121,L2128,L2835, L3539, L3940	L69, L816,L1619, L1619,L1924, L2430,L3035,L3539, L3940
6	G6	L2533, L1925, L1924, L2432, L3239, L3940	
7	G7	L817, L816, L1619,L1924, L2432, L3239, L3539, L3940	L817, L816, L1619,L1924, L2430, L3035, L3539, L3940
8	G8	L1926,L1924, L2432, L3239, L3539, L3940	L1926,L1924, , L2430, L3035, L3539, L3940
9	G9	L3839, L3940	
10	G10	L4041	
11	G11	L1619,L1924, L2432, L3239, L3940	L1619,L1924, L2430, L3035, L3539, L3940
12	G12	L1927, L1924, L2432, L3239, L3940	L1927, L1924, L2430, L3035, L3539, L3940
13	G13	L3239, L3940	
14	G14	L2431, L2432, L3239, L3940	

References

[1] *BP Statistical Review of World Energy 2022*. 2022 Available from: https://www.bp.com/content/dam/bp/business-sites/en/global/corporate/pdfs/energy-economics/statistical-review/bp-stats-review-2022-full-report.pdf. [Accessed November 2022].

[2] Q. Ma. *Greenhouse Gases: Refining the Role of Carbon Dioxide*. 1998 Available from: https://www.giss.nasa.gov/research/briefs/ma_01/. [Accessed November 2022].

[3] H. Ritchie, M. Roser, and P. Rosado. *CO_2 and Greenhouse Gas Emissions*. Our World in Data 2020 Available from: https://ourworldindata.org/co2-and-greenhouse-gas-emissions. [Accessed October 2022].

[4] Y. Jiang, S. Chen, C.C. Liu, W. Sun, X. Luo, S. Liu, N. Bhatt, S. Uppalapati, and D. Forcum, *Blackstart capability planning for power system restoration.* International Journal of Electrical Power & Energy Systems, 2017. **86**: p. 127-137.

[5] *Carbon Dioxide Information Analysis Center (CDIAC); Global Carbon Project (GCP)*. Available from: https://www.globalcarbonproject.org/. [Accessed October 2022].

[6] IEA. *Global Energy Review 2020*. The impacts of the Covid-19 crisis on global energy demand and CO2 emissions 2020 Available from: https://www.iea.org/reports/global-energy-review-2020. [Accessed October 2022].

[7] C.F. Kutscher and J.B. Milford, *Principles of sustainable energy systems*. 2018: CRC Press.

[8] P.K. Katti and M.K. Khedkar. *Towards sustainable energy systems: integrating renewable energy sources is the key for rural area power supply*. in *2005 International Power Engineering Conference*. 2005. IEEE.

[9] S. Imperatives, *Report of the World Commission on Environment and Development: Our common future.* Accessed Feb, 1987. **10**: p. 1-300.

[10] S. Solomon, *Contribution of Working Group I to the fourth assessment report of the Intergovernmental Panel on Climate Change 2007.* (No Title), 2007.

[11] *Household air pollution and health*. Available from: https://www.who.int/news-room/fact-sheets/detail/household-air-pollution-and-health. [Accessed October 2022].

[12] I.G. Unda, *Management of Electric Vehicle Battery Charging in Distribution Networks*, in *Electrical Engineering*. 2012, Cardiff University.

[13] G.I.E.C. GmbH. *The Nigerian Energy Sector - An Overview with a special emphasis on renewable energy, energy efficiency and rural*

electrification. 2015 Available from: https://www.bp.com/content/dam/bp/business-sites/en/global/corporate/pdfs/energy-economics/statistical-review/bp-stats-review-2022-full-report.pdf. [Accessed November 2022].
[14] *Record Growth in Renewables Achieved Despite Energy Crisis*. 2023 Available from: https://www.irena.org/News/pressreleases/2023/Mar/Record-9-point-6-Percentage-Growth-in-Renewables-Achieved-Despite-Energy-Crisis. [Accessed May 2023].
[15] H. Adair-Rohani, K. Zukor, S. Bonjour, S. Wilburn, A.C. Kuesel, R. Hebert, and E.R. Fletcher, *Limited electricity access in health facilities of sub-Saharan Africa: a systematic review of data on electricity access, sources, and reliability.* Global Health: Science and Practice, 2013. **1**(2): p. 249-261.
[16] J.S. Sachi Graber. *Boosting Community Resilience by Building Nigeria's First Solar- and Battery-Powered Undergrid Minigrid*. 2020 Available from: https://rmi.org/community-resilience-through-nigerias-first-undergrid-minigrid/. [Accessed November 2022].
[17] *Distributed Energy Resources*. Available from: http://www.ieso.ca/en/Learn/Ontario-Power-System/A-Smarter-Grid/Distributed-Energy-Resources. [Accessed October 2022].
[18] *The Future of the Electric Grid: The Impact of Distributed Generation and Electric Vehicles*. Available from: https://energy.mit.edu/wp-content/uploads/2011/12/MITEI-The-Future-of-the-Electric-Grid.pdf. [Accessed October 2022].
[19] M. Fila, D. Reid, G. Taylor, P. Lang, and M. Irving. *Coordinated voltage control for active network management of distributed generation*. in *2009 IEEE Power & Energy Society General Meeting*. 2009. IEEE.
[20] J.A. Lobão, T. Devezas, and J.P.S. Catalão, *Energy efficiency of lighting installations: Software application and experimental validation.* Energy Reports, 2015. **1**: p. 110-115.
[21] *Light's Labour's Cost*. 2006 Available from: http://www.iea.org/publications/freepublications/publication/light2006.pdf. [Accessed October 2022].
[22] D. Radulovic, S. Skok, and V. Kirincic, *Energy efficiency public lighting management in the cities.* Energy, 2011. **36**(4): p. 1908-1915.
[23] A.S. Scognamiglio, D .; Meloni, C .; Leonardi, G .; Gozo, N .; Giuliani, G .; Fumagalli, S .; DeLia, F .; Announced, M. *Guidelines: The fundamentals for efficient management of public lighting systems*. 2012 Available from: https://hdl.handle.net/20.500.12079/6524. [Accessed October 2022].

[24] É. Mata, A. Sasic Kalagasidis, and F. Johnsson, *Building-stock aggregation through archetype buildings: France, Germany, Spain and the UK.* Building and Environment, 2014. **81**: p. 270-282.
[25] A.C.a.N. Nakicenovic. *World energy outlook 2008*. 2008. [Accessed September 2022].
[26] *What's New in How We Use Energy at Home: Results from EIA's 2015 Residential Energy Consumption Survey (RECS)*. 2018 Available from: https://www.eia.gov/consumption/residential/reports/2015/overview/pdf/whatsnew_home_energy_use.pdf. [Accessed November 2022].
[27] A.P. Azodo, *Electric power supply, main source and backing: A survey of residential utilization features.* International Journal of Research Studies in Management, 2014. **3**(2).
[28] J. Yan, S.K. Chou, B. Chen, F. Sun, H. Jia, and J. Yang, *Clean, affordable and reliable energy systems for low carbon city transition.* Applied Energy, 2017. **194**: p. 305-309.
[29] J.-K. Choi, D. Morrison, K.P. Hallinan, and R.J. Brecha, *Economic and environmental impacts of community-based residential building energy efficiency investment.* Energy, 2014. **78**: p. 877-886.
[30] E. Ó Broin, É. Mata, A. Göransson, and F. Johnsson, *The effect of improved efficiency on energy savings in EU-27 buildings.* Energy, 2013. **57**: p. 134-148.
[31] G. Comodi, L. Cioccolanti, and M. Renzi, *Modelling the Italian household sector at the municipal scale: Micro-CHP, renewables and energy efficiency.* Energy, 2014. **68**: p. 92-103.
[32] S. Becker, B.A. Frew, G.B. Andresen, M.Z. Jacobson, S. Schramm, and M. Greiner, *Renewable build-up pathways for the US: Generation costs are not system costs.* Energy, 2015. **81**: p. 437-445.
[33] *Use of energy explained Energy efficiency and conservation*. Available from: https://www.eia.gov/energyexplained/use-of-energy/efficiency-and-conservation.php. [Accessed September 2022].
[34] *Checklists of Energy-Saving Measures Operations and Maintenance*. Available from: https://www.energystar.gov/buildings/save_energy_commercial_buildings/ways_save/checklists. [Accessed September 2022].
[35] *IEA (2018), World Energy Outlook 2018, IEA, Paris*. 2018 Available from: https://www.iea.org/reports/world-energy-outlook-2018.
[36] L.G. Swan and V.I. Ugursal, *Modeling of end-use energy consumption in the residential sector: A review of modeling techniques.* Renewable and Sustainable Energy Reviews, 2009. **13**(8): p. 1819-1835.
[37] J. Seryak and K. Kissock. *Occupancy and behavioral affects on residential energy use*. in *Proceedings of the Solar conference*. 2003. American Solar Energy Society; American Institute of Architects.

[38] Z. Yang, A. Ghahramani, and B. Becerik-Gerber, *Building occupancy diversity and HVAC (heating, ventilation, and air conditioning) system energy efficiency.* Energy, 2016. **109**: p. 641-649.
[39] R. Lacko, B. Drobnič, M. Mori, M. Sekavčnik, and M. Vidmar, *Stand-alone renewable combined heat and power system with hydrogen technologies for household application.* Energy, 2014. **77**: p. 164-170.
[40] Y.N. Udoakah and I.G. Okure, *Energy efficiency and sustainability: evaluation of electricity consumer's behaviour towards electricity usage and energy conservation.* AFRREV STECH: An International Journal of Science and Technology, 2017. **6**(2): p. 36-52.
[41] M. Muratori, M.C. Roberts, R. Sioshansi, V. Marano, and G. Rizzoni, *A highly resolved modeling technique to simulate residential power demand.* Applied Energy, 2013. **107**: p. 465-473.
[42] O. Guerra Santin, L. Itard, and H. Visscher, *The effect of occupancy and building characteristics on energy use for space and water heating in Dutch residential stock.* Energy and Buildings, 2009. **41**(11): p. 1223-1232.
[43] *Energy consumption in the United Kingdom.* 2002 Available from: https://www.thenbs.com/PublicationIndex/documents/details?Pub=DTI&DocID=261901. [Accessed September 2022].
[44] *Annual energy review 2006*. 2007. [Accessed October 2022].
[45] N.B.e. al., *Energy use data handbook, 1990 and 1998 to 2004*. 2006.
[46] *China statistical yearbook 2005*. 2005 Available from: http://www.stats.gov.cn/english/NewsEvents/200512/t20051219_25714.html. [Accessed October 2022].
[47] H.-x. Zhao and F. Magoulès, *A review on the prediction of building energy consumption.* Renewable and Sustainable Energy Reviews, 2012. **16**(6): p. 3586-3592.
[48] B.J. Johnson, M.R. Starke, O.A. Abdelaziz, R.K. Jackson, and L.M. Tolbert. *A method for modeling household occupant behavior to simulate residential energy consumption*. in *ISGT 2014*. 2014. IEEE.
[49] W. Li, Y. Zhou, K. Cetin, J. Eom, Y. Wang, G. Chen, and X. Zhang, *Modeling urban building energy use: A review of modeling approaches and procedures.* Energy, 2017. **141**: p. 2445-2457.
[50] E. Hirst, W. Lin, and J. Cope, *Residential energy use model sensitive to demographic, economic, and technological factors.* Q. Rev. Econ. Bus.;(United States), 1977. **17**(2).
[51] D. Oneal and E. Hirst, *An energy used model of the residential sector.* IEEE Transactions on Systems Man and Cybernetics, 1980. **10**: p. 749-755.
[52] H.K. Ozturk, O.E. Canyurt, A. Hepbasli, and Z. Utlu, *Residential-commercial energy input estimation based on genetic algorithm (GA) approaches: an application of Turkey.* Energy and Buildings, 2004. **36**(2): p. 175-183.

[53] R. Nesbakken, *Price sensitivity of residential energy consumption in Norway.* Energy economics, 1999. **21**(6): p. 493-515.
[54] K.S. Cetin, P.C. Tabares-Velasco, and A. Novoselac, *Appliance daily energy use in new residential buildings: Use profiles and variation in time-of-use.* Energy and Buildings, 2014. **84**: p. 716-726.
[55] R.A. Douthitt, *An economic analysis of the demand for residential space heating fuel in Canada.* Energy, 1989. **14**(4): p. 187-197.
[56] R. Pratt, C. Conner, B. Cooke, and E. Richman, *Metered end-use consumption and load shapes from the ELCAP residential sample of existing homes in the Pacific Northwest.* Energy and buildings, 1993. **19**(3): p. 179-193.
[57] A. Ozawa, R. Furusato, and Y. Yoshida, *Determining the relationship between a household's lifestyle and its electricity consumption in Japan by analyzing measured electric load profiles.* Energy and Buildings, 2016. **119**: p. 200-210.
[58] A. Kavousian, R. Rajagopal, and M. Fischer, *Determinants of residential electricity consumption: Using smart meter data to examine the effect of climate, building characteristics, appliance stock, and occupants' behavior.* Energy, 2013. **55**: p. 184-194.
[59] P. Wyatt, *A dwelling-level investigation into the physical and socio-economic drivers of domestic energy consumption in England.* Energy Policy, 2013. **60**: p. 540-549.
[60] T.F. Sanquist, H. Orr, B. Shui, and A.C. Bittner, *Lifestyle factors in U.S. residential electricity consumption.* Energy Policy, 2012. **42**: p. 354-364.
[61] F. McLoughlin, A. Duffy, and M. Conlon, *Characterising domestic electricity consumption patterns by dwelling and occupant socio-economic variables: An Irish case study.* Energy and Buildings, 2012. **48**: p. 240-248.
[62] C. Bartusch, M. Odlare, F. Wallin, and L. Wester, *Exploring variance in residential electricity consumption: Household features and building properties.* Applied Energy, 2012. **92**: p. 637-643.
[63] K. Olaniyan, B. McLellan, S. Ogata, and T. Tezuka, *Estimating Residential Electricity Consumption in Nigeria to Support Energy Transitions.* Sustainability, 2018. **10**(5).
[64] Y. Irimiya, I.A. Humphery, and I.I. Aondover, *Assessment of energy use pattern in residential buildings of Kano and Kaduna Northern Nigeria.* American Journal of Engineering Research, 2013. **2**(10): p. 271-275.
[65] S.E. Sunday, *Electricity: Over 50 % Customers Unmetered 4yrs after Privatisation*, in *Daily Trust Newspapers*. 03, October 2017.
[66] A. Sędziwy and L. Kotulski, *Towards Highly Energy-Efficient Roadway Lighting.* Energies, 2016. **9**(4).

[67] Y.O.N. Udoakah and U. Mfon David. *Sustainably meeting the energy needs of Nigeria: The renewable options*. in *2014 IEEE International Energy Conference (ENERGYCON)*. 2014.
[68] O.O. Ajayi and O.O. Ajayi, *Nigeria's energy policy: Inferences, analysis and legal ethics toward RE development.* Energy Policy, 2013. **60**: p. 61-67.
[69] C. Nwachukwu. *Nigerians maintain lead in generator imports in Africa*. The Vanguard 2013 Available from: http://www.vanguardngr.com/2013/09/nigeria-spends-n25bn-annually-on-generators-group/ . [Accessed May 2020].
[70] Y.O. Udoakah, E. Mudaheranwa, and L. Cipcigan. *Municipal Street Lighting Systems Energy Cost and Carbon Footprint Estimation in Uyo, Nigeria*. in *2019 IEEE PES/IAS PowerAfrica*. 2019.
[71] E. Usman. *Generator fume kills family of seven in Lagos*. The Vanguard 2014 Available from: http://www.vanguardngr.com/2014/05/generator-fume-kills-family-7-lagos/ [Accessed May 2020].
[72] L. Ikeji. *Generator fume kills man, wife and three children in Iko-rodu*. 2014 Available from: http://www.lindaikeji.blogspot.com/2014/09/graphic-pics-generato-fume-kill-man.html . [Accessed May 2020].
[73] R. Bisiriyu. *Generator fume kills 80 years old woman, four grandchildren*. Nigeria World News, 1–2 2014 Available from: http://www.nigeria-news-world.com. [Accessed May 2020].
[74] M.N. Postorino and L. Mantecchini, *A transport carbon footprint methodology to assess airport carbon emissions.* Journal of Air Transport Management, 2014. **37**: p. 76-86.
[75] M.D. Gupta, *Carbon footprint from road transport use in Kolkata city.* Transportation Research Part D: Transport and Environment, 2014. **32**: p. 397-410.
[76] X. Li, H. Tan, and A. Rackes, *Carbon footprint analysis of student behavior for a sustainable university campus in China.* Journal of Cleaner Production, 2015. **106**: p. 97-108.
[77] S. Zubelzu, R. Álvarez, and A. Hernández, *Methodology to calculate the carbon footprint of household land use in the urban planning stage.* Land Use Policy, 2015. **48**: p. 223-235.
[78] W.K. Biswas, *Carbon footprint and embodied energy consumption assessment of building construction works in Western Australia.* International Journal of Sustainable Built Environment, 2014. **3**(2): p. 179-186.
[79] F. Rossi, E. Bonamente, A. Nicolini, E. Anderini, and F. Cotana, *A carbon footprint and energy consumption assessment methodology for UHI-affected lighting systems in built areas.* Energy and Buildings, 2016. **114**: p. 96-103.

[80] H.S. Labo. *A Paper Presentation Current Status and Future Outlook of The Transmission Network*. 2010; Available from: http://www.nigeriaelectricityprivatisation.com/wpcontent/uploads/downloads/2011/02/Transmission_Company_of_Nigeria_Investor_Forum_Presentation.pdf
[81] M.O. Oseni, *An analysis of the power sector performance in Nigeria.* Renewable and Sustainable Energy Reviews, 2011. **15**(9): p. 4765-4774.
[82] E.D.T. Association, *Electric drive vehicle sales figures (US Market)-EV sales.* 2012.
[83] *Renewable Energy Master Plan 2013*, E.C.o.N. (ECN), Editor. 2013.
[84] D. Strohl. *Ford, Edison and the Cheap EV That Almost Was*. 2010 Available from: https://www.wired.com/2010/06/henry-ford-thomas-edison-ev/. [Accessed May 2020].
[85] W. Tang and Y. Jun, *Optimal charging control of electric vehicles in smart grids*. 2017: Springer.
[86] E.A. Nanaki and C.J. Koroneos, *Climate change mitigation and deployment of electric vehicles in urban areas.* Renewable Energy, 2016. **99**: p. 1153-1160.
[87] IEA. *Global EV Outlook 2022*. 2022 Available from: https://www.iea.org/reports/global-ev-outlook-2022. [Accessed November 2022].
[88] W. Kempton and J. Tomić, *Vehicle-to-grid power fundamentals: Calculating capacity and net revenue.* Journal of Power Sources, 2005. **144**(1): p. 268-279.
[89] *A Comprehensive Guide to Electric Vehicle Managed Charging*. 2019 Available from: https://sepapower.org/resource/a-comprehensive-guide-to-electric-vehicle-managed-charging/. [Accessed November 2022].
[90] P. Djapic, C. Ramsay, D. Pudjianto, G. Strbac, J. Mutale, N. Jenkins, and R. Allan, *Taking an active approach.* IEEE Power and Energy Magazine, 2007. **5**(4): p. 68-77.
[91] W.A. Braff, J.M. Mueller, and J.E. Trancik, *Value of storage technologies for wind and solar energy.* Nature Climate Change, 2016. **6**(10): p. 964-969.
[92] E.O.S.a.P.S. A. Kristen. *Coordinating Distributed Energy Resources for Grid Services: A Case Study of Pacific Gas and Electric*. 2018 Available from: https://www.nrel.gov/docs/fy19osti/72108.pdf. [Accessed 0ctober 2022].
[93] *Preparing for Distributed Energy Resources*. 2012 Available from: https://www.se.com/ww/en/download/document/998-2095-05-29-12AR0_EN/. [Accessed April 2022].
[94] *Advanced Distribution Management Systems (ADMS)*. 2018 Available from: https://www.gartner.com/en/information-

technology/glossary/advanced-distribution-management-systems-adms. [Accessed October 2022.
[95] P.E.J. Dirkman. *Enhancing utility outage management system (OMS) performance*. Available from: https://download.schneider-electric.com/files?p_Doc_Ref=998-2095-08-01-14BR0_EN, . [Accessed April 2022].
[96] A.S. Hassan, A. Firrincieli, C. Marmaras, L.M. Cipcigan, and M. Pastorelli. *Integration of electric vehicles in a microgrid with distributed generation*. in *2014 49th International Universities Power Engineering Conference (UPEC)*. 2014. IEEE.
[97] P. Papadopoulos, S. Skarvelis-Kazakos, I. Grau, L.M. Cipcigan, and N. Jenkins, *Electric vehicles' impact on British distribution networks.* IET Electrical Systems in Transportation, 2012. **2**(3): p. 91-102.
[98] Z.A. Obaid, L. Cipcigan, and M.T. Muhsin. *Analysis of the Great Britain's power system with Electric Vehicles and Storage Systems*. in *2015 18th International Conference on Intelligent System Application to Power Systems (ISAP)*. 2015. IEEE.
[99] A. Sani Hassan, L. Cipcigan, and N. Jenkins, *Impact of optimised distributed energy resources on local grid constraints.* Energy, 2018. **142**: p. 878-895.
[100] Z. Li, M. Shahidehpour, A. Alabdulwahab, and Y. Al-Turki, *Valuation of distributed energy resources in active distribution networks.* The Electricity Journal, 2019. **32**(4): p. 27-36.
[101] M. Daneshvar, B. Mohammadi-ivatloo, and K. Zare, *Integration of Distributed Energy Resources Under the Transactive Energy Structure in the Future Smart Distribution Networks*, in *Operation of Distributed Energy Resources in Smart Distribution Networks*. 2018. p. 349-379.
[102] M.B. Arias, M. Kim, and S. Bae, *Prediction of electric vehicle charging-power demand in realistic urban traffic networks.* Applied Energy, 2017. **195**: p. 738-753.
[103] L. Canals Casals, E. Martinez-Laserna, B. Amante García, and N. Nieto, *Sustainability analysis of the electric vehicle use in Europe for CO2 emissions reduction.* Journal of Cleaner Production, 2016. **127**: p. 425-437.
[104] H.B. Sonder, L. Cipcigan, and C.U. Loo. *Using electric vehicles and demand side response to unlock distribution network flexibility*. in *2019 IEEE Milan PowerTech*. 2019. IEEE.
[105] P. Nieuwenhuis, L. Cipcigan, and H. Berkem Sonder, *The Electric Vehicle Revolution*, in *Future Energy*. 2020. p. 227-243.
[106] D. Greenwood, S. Walker, N. Wade, S. Munoz-Vaca, A. Crossland, and C. Patsios, *Integration of High Penetrations of Intermittent Renewable Generation in Future Electricity Networks Using Storage*, in *Future Energy*. 2020. p. 649-668.

[107] Y.-O. Udoakah, S. Khalaf, and L. Cipcigan. *Blackout and black start analysis for improved power system resilience: The African experience*. in *2020 IEEE PES/IAS PowerAfrica*. 2020. IEEE.
[108] P. Pradhan, T. Deki, P. Wangmo, D. Dorji, D. Phuntsho, and C. Dorji. *Simulation and optimization of blackstart restoration plan in bhutan using digsilent*. in *2015 2nd International Conference on Recent Advances in Engineering & Computational Sciences (RAECS)*. 2015. IEEE.
[109] C. Abbey, D. Cornforth, N. Hatziargyriou, K. Hirose, A. Kwasinski, E. Kyriakides, G. Platt, L. Reyes, and S. Suryanarayanan, *Powering Through the Storm: Microgrids Operation for More Efficient Disaster Recovery.* IEEE Power and Energy Magazine, 2014. **12**(3): p. 67-76.
[110] *ECONOMIC BENEFITS OF INCREASING ELECTRIC GRID RESILIENCE TO WEATHER OUTAGES*. 2013 Available from: http://energy.gov/ [Accessed March 2022].
[111] S. Liu, B. Chen, T. Zourntos, D. Kundur, and K. Butler-Purry, *A Coordinated Multi-Switch Attack for Cascading Failures in Smart Grid.* IEEE Transactions on Smart Grid, 2014. **5**(3): p. 1183-1195.
[112] *Terrorism and the Electric Power Delivery System*. 2012. DOI: https://doi.org/10.17226/12050.
[113] L. Shanshan, H. Yunhe, L. Chen-Ching, and R. Podmore, *The Healing Touch: Tools and Challenges for Smart Grid Restoration.* IEEE Power and Energy Magazine, 2014. **12**(1): p. 54-63.
[114] N. Bhatt, S. Liu, and R. Podmore, *System Restoration Tools: System Restoration Navigator Integrated into EPRI Operator Training Simulator (SRN/OTS).* Journal of Power and Energy Engineering, 2015. **03**(04): p. 378-383.
[115] A.S.a.H.R. Renteria, *Electric Power Disruption: Toolkit for Local Government*, C.G.s.O.o.E. Services, Editor. 2020.
[116] D. Złotecka and K. Sroka. *The characteristics and main causes of power system failures basing on the analysis of previous blackouts in the world*. in *2018 International Interdisciplinary PhD Workshop (IIPhDW)*. 2018. IEEE.
[117] K.J. Rahman, M.M. Munnee, and S. Khan. *Largest blackouts around the world: Trends and data analyses*. in *2016 IEEE International WIE Conference on Electrical and Computer Engineering (WIECON-ECE)*. 2016. IEEE.
[118] M. Parihar and M. Bhaskar, *Review of power system blackout.* International Journal of Research and Innovation in Applied Science, 2018. **3**(6): p. 8-12.
[119] O.P. Veloza and F. Santamaria, *Analysis of major blackouts from 2003 to 2015: Classification of incidents and review of main causes.* The Electricity Journal, 2016. **29**(7): p. 42-49.

[120] Z. Bo, O. Shaojie, Z. Jianhua, S. Hui, W. Geng, and Z. Ming, *An analysis of previous blackouts in the world: Lessons for China's power industry.* Renewable and Sustainable Energy Reviews, 2015. **42**: p. 1151-1163.
[121] *Whole of Sri Lanka hit by power blackout*. The Guardian 2020 Available from: https://www.theguardian.com/world/2020/aug/18/whole-of-sri-lanka-hit-by-huge-power-blackout [Accessed February 2022].
[122] C. Owens. *The 11 Biggest Blackouts of all Times*. The blackout Report 2020 Available from: https://www.theblackoutreport.co.uk/2019/07/05/11-biggest-blackouts/. [Accessed February 2022].
[123] *Technical Report on the events of 9 August 2019*. 2019 Available from: https://www.ofgem.gov.uk/system/files/docs/2019/09/eso_technical_report_-_final.pdf. [Accessed February 2022].
[124] Y. Liu, H. Wang, and H. Ye, *Power system restoration theory and technology.* Science and Technology Press, Beijing, 2014.
[125] Y. Liu, R. Fan, and V. Terzija, *Power system restoration: a literature review from 2006 to 2016.* Journal of Modern Power Systems and Clean Energy, 2016. **4**(3): p. 332-341.
[126] D. Lindenmeyer, A. Moshref, M. Schaeffer, and A. Benge, *Simulation of the start-up of a Hydro Power plant for the emergency power supply of a nuclear power station.* IEEE Transactions on power systems, 2001. **16**(1): p. 163-169.
[127] M. Adibi, D. Milanicz, and T. Volkmann, *Remote cranking of steam electric stations.* IEEE transactions on power systems, 1996. **11**(3): p. 1613-1618.
[128] M. Braun, J. Brombach, C. Hachmann, D. Lafferte, A. Klingmann, W. Heckmann, F. Welck, D. Lohmeier, and H. Becker, *The Future of Power System Restoration: Using Distributed Energy Resources as a Force to Get Back Online.* IEEE Power and Energy Magazine, 2018. **16**(6): p. 30-41.
[129] T. Gonen, *Electric power distribution engineering*. 2015: CRC press.
[130] B. Chen, *Black start restoration for electric distribution systems and microgrids* 2017, Texas A&M University.
[131] *Cold Load Pickup Issues*. 2004 Available from: https://resourcecenter.ieee-pes.org/publications/technical-reports/PESTR0038.html. [Accessed February 2022].
[132] *Grid Reliability and Resilience Pricing (Document No. RM18-1-000), and Grid Resilience in Regional Transmission Organizations and Independent System Operations (Document No. AD18-7-000)*. 2018 Available from: https://www.google.com/url?sa=i&rct=j&q=&esrc=s&source=web&c

d=&ved=0CAIQw7AJahcKEwig3Za5k6eAAxUAAAAAHQAAAAAQAg&url=https%3A%2F%2Fwww.puc.pa.gov%2FGeneral%2Fpdf%2FFERC%2FAD18-7-000.pdf&psig=AOvVaw3i6YAbuytRo6B2slB4d4n9&ust=1690281233877492&opi=89978449. [Accessed February 2022].
[133] M. McGranaghan, M. Olearczyk, and C. Gellings, *Enhancing distribution resiliency: Opportunities for applying innovative technologies.* Electricity Today, 2013. **28**(1): p. 46-48.
[134] J.A.P. Lopes, C.L. Moreira, and A.G. Madureira, *Defining Control Strategies for MicroGrids Islanded Operation.* IEEE Transactions on Power Systems, 2006. **21**(2): p. 916-924.
[135] C. Chen, J. Wang, F. Qiu, and D. Zhao, *Resilient Distribution System by Microgrids Formation After Natural Disasters.* IEEE Transactions on Smart Grid, 2016. **7**(2): p. 958-966.
[136] M. Panteli and P. Mancarella, *The Grid: Stronger, Bigger, Smarter?: Presenting a Conceptual Framework of Power System Resilience.* IEEE Power and Energy Magazine, 2015. **13**(3): p. 58-66.
[137] N.G. ESO. *Distributed ReStart, Organisational, Systems and Telecommunications design stage 1*. 2020 Available from: https://www.nationalgrideso.com/document/178271/download. [Accessed February 2022].
[138] N.G. ESO. *Distributed ReStart, Procurement and Compliance Report – A high level outline of commercial and regulatory arrangements*. 2020 Available from: https://www.nationalgrideso.com/document/178266/download. [Accessed February 2022].
[139] J.A. Momoh, *Electric power distribution, automation, protection, and control*. 2017: CRC press.
[140] Y.-Y. Hsu, H.-M. Huang, H.-C. Kuo, S. Peng, C. Chang, K. Chang, H. Yu, C. Chow, and R. Kuo, *Distribution system service restoration using a heuristic search approach.* IEEE Transactions on Power Delivery, 1992. **7**(2): p. 734-740.
[141] S.P. Singh, G.S. Raju, G.K. Rao, and M. Afsari, *A heuristic method for feeder reconfiguration and service restoration in distribution networks.* International Journal of Electrical Power & Energy Systems, 2009. **31**(7-8): p. 309-314.
[142] Y. Jiang, J. Jiang, and Y. Zhang, *A Novel Fuzzy Multiobjective Model Using Adaptive Genetic Algorithm Based on Cloud Theory for Service Restoration of Shipboard Power Systems.* IEEE Transactions on Power Systems, 2012. **27**(2): p. 612-620.
[143] S. Wang and H.-D. Chiang. *Multi-objective service restoration of distribution systems using group-based two-stage methodology*. in *2014 IEEE PES T&D Conference and Exposition*. 2014. IEEE.

[144] Y. Kumar, B. Das, and J. Sharma, *Multiobjective, Multiconstraint Service Restoration of Electric Power Distribution System With Priority Customers.* IEEE Transactions on Power Delivery, 2008. **23**(1): p. 261-270.
[145] S. Srivastava and K.L. Butler-Purry, *Expert-system method for automatic reconfiguration for restoration of shipboard power systems.* IEE Proceedings - Generation, Transmission and Distribution, 2006. **153**(3).
[146] M.-S. Tsai, *Development of an Object-Oriented Service Restoration Expert System With Load Variations.* IEEE Transactions on Power Systems, 2008. **23**(1): p. 219-225.
[147] J.C. López, J.F. Franco, and M.J. Rider, *Optimisation-based switch allocation to improve energy losses and service restoration in radial electrical distribution systems.* IET Generation, Transmission & Distribution, 2016. **10**(11): p. 2792-2801.
[148] S. Khushalani, J.M. Solanki, and N.N. Schulz, *Optimized Restoration of Unbalanced Distribution Systems.* IEEE Transactions on Power Systems, 2007. **22**(2): p. 624-630.
[149] P.L. Cavalcante, J.C. Lopez, J.F. Franco, M.J. Rider, A.V. Garcia, M.R.R. Malveira, L.L. Martins, and L.C.M. Direito, *Centralized Self-Healing Scheme for Electrical Distribution Systems.* IEEE Transactions on Smart Grid, 2016. **7**(1): p. 145-155.
[150] A. Zidan, M. Khairalla, A.M. Abdrabou, T. Khalifa, K. Shaban, A. Abdrabou, R. El Shatshat, and A.M. Gaouda, *Fault Detection, Isolation, and Service Restoration in Distribution Systems: State-of-the-Art and Future Trends.* IEEE Transactions on Smart Grid, 2017. **8**(5): p. 2170-2185.
[151] N. Vlassis, *A concise introduction to multiagent systems and distributed artificial intelligence*. 2022: Springer Nature.
[152] P. Chiradeja and R. Ramakumar, *An Approach to Quantify the Technical Benefits of Distributed Generation.* IEEE Transactions on Energy Conversion, 2004. **19**(4): p. 764-773.
[153] *The Potential Benefits of Distributed Generation and Rate-Related Issues that May Impede Their Expansion: A Study Pursuant to Section 1817 of the Energy Policy Act of 2005 (Washington, DC, 2007)* Available from: https://www.google.com/url?sa=i&rct=j&q=&esrc=s&source=web&cd=&cad=rja&uact=8&ved=0CAIQw7AJahcKEwjoiMbr7amAAxUAAAAAHQAAAAAQAg&url=https%3A%2F%2Fwww.energy.gov%2Foe%2Farticles%2Fpotential-benefits-distributed-generation-and-rate-related-issues-may-impede-its&psig=AOvVaw1f0zWVcUmk5KNIjYF46u3Z&ust=1690374414545961&opi=89978449. [Accessed April 2022].

[154] A. Zidan and E.F. El-Saadany, *Incorporating load variation and variable wind generation in service restoration plans for distribution systems.* Energy, 2013. **57**: p. 682-691.
[155] C.L. Moreira, F.O. Resende, and J.A.P. Lopes, *Using Low Voltage MicroGrids for Service Restoration.* IEEE Transactions on Power Systems, 2007. **22**(1): p. 395-403.
[156] M. Vadari and G. StokeS, *Utility 2.0.* Public Utilities Fortnightly, 2013.
[157] H. Gao, Y. Chen, S. Mei, S. Huang, and Y. Xu, *Resilience-Oriented Pre-Hurricane Resource Allocation in Distribution Systems Considering Electric Buses.* Proceedings of the IEEE, 2017. **105**(7): p. 1214-1233.
[158] D.T. Ton and M.A. Smith, *The U.S. Department of Energy's Microgrid Initiative.* The Electricity Journal, 2012. **25**(8): p. 84-94.
[159] *Microgrids and Vehicle-Grid Integration*. Available from: https://gridintegration.lbl.gov/microgrids-vehicle-grid-integration. [Accessed May 2022].
[160] C. Marnay, S. Chatzivasileiadis, C. Abbey, R. Iravani, G. Joos, P. Lombardi, P. Mancarella, and J. Von Appen. *Microgrid evolution roadmap*. in *2015 international symposium on smart electric distribution systems and technologies (EDST)*. 2015. IEEE.
[161] Y. Xu, C.-C. Liu, K.P. Schneider, F.K. Tuffner, and D.T. Ton, *Microgrids for Service Restoration to Critical Load in a Resilient Distribution System.* IEEE Transactions on Smart Grid, 2018. **9**(1): p. 426-437.
[162] B. Zhao, X. Dong, and J. Bornemann, *Service Restoration for a Renewable-Powered Microgrid in Unscheduled Island Mode.* IEEE Transactions on Smart Grid, 2015. **6**(3): p. 1128-1136.
[163] H. Gao, Y. Chen, Y. Xu, and C.-C. Liu, *Resilience-Oriented Critical Load Restoration Using Microgrids in Distribution Systems.* IEEE Transactions on Smart Grid, 2016. **7**(6): p. 2837-2848.
[164] L.-J. Yang, Y. Zhao, C. Wang, P. Gao, and J.-H. Hao, *Resilience-Oriented Hierarchical Service Restoration in Distribution System Considering Microgrids.* IEEE Access, 2019. **7**: p. 152729-152743.
[165] Y. Xu, C.-C. Liu, Z. Wang, K. Mo, K.P. Schneider, F.K. Tuffner, and D.T. Ton, *DGs for Service Restoration to Critical Loads in a Secondary Network.* IEEE Transactions on Smart Grid, 2019. **10**(1): p. 435-447.
[166] B. Chen, C. Chen, J. Wang, and K.L. Butler-Purry, *Multi-Time Step Service Restoration for Advanced Distribution Systems and Microgrids.* IEEE Transactions on Smart Grid, 2018. **9**(6): p. 6793-6805.
[167] B. Chen, C. Chen, J. Wang, and K.L. Butler-Purry, *Sequential Service Restoration for Unbalanced Distribution Systems and Microgrids.* IEEE Transactions on Power Systems, 2018. **33**(2): p. 1507-1520.
[168] O. Bassey, K.L. Butler-Purry, and B. Chen, *Dynamic Modeling of Sequential Service Restoration in Islanded Single Master Microgrids.* IEEE Transactions on Power Systems, 2020. **35**(1): p. 202-214.

[169] S. Poudel and A. Dubey, *Critical Load Restoration Using Distributed Energy Resources for Resilient Power Distribution System.* IEEE Transactions on Power Systems, 2019. **34**(1): p. 52-63.
[170] Y. Zhao, Z. Lin, Y. Ding, Y. Liu, L. Sun, and Y. Yan, *A Model Predictive Control Based Generator Start-Up Optimization Strategy for Restoration With Microgrids as Black-Start Resources.* IEEE Transactions on Power Systems, 2018. **33**(6): p. 7189-7203.
[171] H.F. Habib, T. Youssef, M.H. Cintuglu, and O.A. Mohammed, *Multi-Agent-Based Technique for Fault Location, Isolation, and Service Restoration.* IEEE Transactions on Industry Applications, 2017. **53**(3): p. 1841-1851.
[172] J. Li, X.-Y. Ma, C.-C. Liu, and K.P. Schneider, *Distribution System Restoration With Microgrids Using Spanning Tree Search.* IEEE Transactions on Power Systems, 2014. **29**(6): p. 3021-3029.
[173] M. Khederzadeh and S. Zandi, *Enhancement of Distribution System Restoration Capability in Single/Multiple Faults by Using Microgrids as a Resiliency Resource.* IEEE Systems Journal, 2019. **13**(2): p. 1796-1803.
[174] Y. Wang, Y. Xu, J. He, C.-C. Liu, K.P. Schneider, M. Hong, and D.T. Ton, *Coordinating Multiple Sources for Service Restoration to Enhance Resilience of Distribution Systems.* IEEE Transactions on Smart Grid, 2019. **10**(5): p. 5781-5793.
[175] Y.-O. Udoakah, E. Mudaheranwa, and L. Cipcigan. *Dynamic modeling of energy consumption pattern of a typical Nigerian average urban and rural household for microgrid PV design*. in *2019 IEEE PES Innovative Smart Grid Technologies Europe (ISGT-Europe)*. 2019. IEEE.
[176] R. Yao and K. Steemers, *A method of formulating energy load profile for domestic buildings in the UK.* Energy and Buildings, 2005. **37**(6): p. 663-671.
[177] M.W. Strohbach, E. Arnold, and D. Haase, *The carbon footprint of urban green space—A life cycle approach.* Landscape and Urban Planning, 2012. **104**(2): p. 220-229.
[178] *Specification with guidance at the organizational level for quantification and reporting of greenhouse gas emission and removal 2006*. International Standards Organization.
[179] *Specification for the assessment of the life cycle greenhouse gas emissions of goods and services, 2008.* Available from: http://shop.bsigroup.com/upload/shop/download/pas/pas2050.pdf. [Accessed February 2022].
[180] *Guide to PAS 2050. How to assess the carbon footprint of goods and services*. Carbon Trust and Crown.
[181] A. Keyhani, *Design of smart power grid renewable energy systems*. 2016: John Wiley & Sons.

[182] G. Boyle, B. Everett, and J. Ramage, *Energy systems and sustainability.* 2003.
[183] *Illuminating the Benefits of LED Street Lights*.
[184] E.-S.A. Abd Nafeh, *Design and economic analysis of a stand-alone PV system to electrify a remote area household in Egypt.* The open renewable energy journal, 2009. **2**(1).
[185] C.B.o.N.C.B. N. *Current interest and inflation rates.* 2018 Available from: https://www.cbn.gov.ng/. [Accessed December 2018].
[186] J. Abaka, H. Iortyer, and T. Ibraheem, *Sizing and Economic Assessment of Photovoltaic and Diesel Generator for Rural Nigeria.*
[187] S.N.L.P.D.A. Center, *Stand Alone Photovoltaic Systems: A Handbook of Recommended Design Practices*. 1995: Sandia National Laboratories.
[188] R.A. Messenger and A. Abtahi, *Photovoltaic systems engineering*. 2018: CRC press.
[189] S.M. Lurwan, N. Mariun, H. Hizam, M.A.M. Radzi, and A. Zakaria. *Predicting power output of photovoltaic systems with solar radiation model*. in *2014 IEEE International Conference on Power and Energy (PECon)*. 2014. IEEE.
[190] T. Markvart, *Solar electricity*. Vol. 6. 2000: John Wiley & Sons.
[191] S.V. Kulkarni and S.A. Khaparde, *Transformer engineering: design, technology, and diagnostics*. 2017: CRC press.
[192] *Technical Specification of 200kVA, 315kVA, 630kVA, & 1600kVA, 11/0.433kV & 22/0.433kV Dry-Type (VPI) Distribution Transformer.* Available from: https://docplayer.net/40936526-Maharashtra-state-electricity-distribution-company-ltd.html. [Accessed December 2019].
[193] Y.-O. Udoakah, H.B. Sonder, and L. Cipcigan, *Low Voltage Distribution Network Simulation and Analysis for Electric Vehicle and Renewable Energy Integration*, in *2021 IEEE Power & Energy Society Innovative Smart Grid Technologies Conference (ISGT)*. 2021. p. 1-5.
[194] Y.-O. Udoakah, H.B. Sonder, and L. Cipcigan, *Nigerian Distribution Network Feeder Impact Assessment with Integration of Electric Vehicles*, in *2022 IEEE 7th International Energy Conference (ENERGYCON)*. 2022. p. 1-6.
[195] Y.-O. Udoakah, A. Inaolaji, L. Cipcigan, and S. Paudyal, *Volt-VAr Optimization of a Low Voltage Distribution Network in Nigeria*, in *2022 IEEE PES/IAS PowerAfrica*. 2022. p. 1-5.
[196] W.H. Kersting, *Distribution system modeling and analysis*, in *Electric power generation, transmission, and distribution*. 2018, CRC press. p. 26-1-26-58.
[197] G. Xydis and E. Nanaki, *Wind Energy Based Electric Vehicle Charging Stations Sitting. A GIS/Wind Resource Assessment Approach.* Challenges, 2015. **6**(2): p. 258-270.

[198] L. Wang, *Design of electric vehicle charging station based on wind and solar complementary power supply*. 2018.
[199] T. Ding, H. Chen, B. Wu, and P. Hu. *Harmonic characteristics analysis of PWM-based electric vehicle chargers considering control strategy*. in *2018 18th International Conference on Harmonics and Quality of Power (ICHQP)*. 2018. IEEE.
[200] K. Kim, C.S. Song, G. Byeon, H. Jung, H. Kim, and G. Jang, *Power demand and total harmonic distortion analysis for an EV charging station concept utilizing a battery energy storage system.* Journal of Electrical Engineering & Technology, 2013. **8**(5): p. 1234-1242.
[201] *Type-4 wind turbine model*. 2018 Available from: https://www.google.com/url?sa=i&rct=j&q=&esrc=s&source=web&cd=&cad=rja&uact=8&ved=0CAIQw7AJahcKEwiA19er9KmAAxUAAAAAHQAAAAAQAg&url=https%3A%2F%2Fwww.pscad.com%2Fknowledge-base%2Fdownload%2Ftype_4_wind_turbine_model_v46.pdf&psig=AOvVaw0CvSiuyNuHrZonEDcIP45z&ust=1690376206032129&opi=89978449. [Accessed December 2022].
[202] S. Heier, *Grid integration of wind energy: onshore and offshore conversion systems*. 2014: John Wiley & Sons.
[203] J. Sedo and S. Kascak, *Design of output LCL filter and control of single-phase inverter for grid-connected system.* Electrical Engineering, 2017. **99**(4): p. 1217-1232.
[204] *Design of LCL filter for three-phase grid connected inverter.* .
[205] M.B. Cain, R.P. O'neill, and A. Castillo, *History of optimal power flow and formulations.* Federal Energy Regulatory Commission, 2012. **1**: p. 1-36.
[206] Y.-O. Udoakah, H.B. Sonder, J. Liang, and L. Cipcigan, *Development of a Viable Black Start Restoration Pathway and Problem Formulation Sequence*, in *2022 IEEE 7th International Energy Conference (ENERGYCON)*. 2022. p. 1-6.
[207] A. Chiang, *Elements of dynamic optimization*. 1992, Waveland Press, Inc: Illinois.
[208] Z. Wang, B. Chen, J. Wang, and C. Chen, *Networked Microgrids for Self-Healing Power Systems.* IEEE Transactions on Smart Grid, 2016. **7**(1): p. 310-319.
[209] Z. Wang and J. Wang, *Self-Healing Resilient Distribution Systems Based on Sectionalization Into Microgrids.* IEEE Transactions on Power Systems, 2015. **30**(6): p. 3139-3149.
[210] A. Garces, *A Linear Three-Phase Load Flow for Power Distribution Systems.* IEEE Transactions on Power Systems, 2016. **31**(1): p. 827-828.

[211] G. Chicco, F. Corona, R. Porumb, and F. Spertino, *Experimental Indicators of Current Unbalance in Building-Integrated Photovoltaic Systems.* IEEE Journal of Photovoltaics, 2014. **4**(3): p. 924-934.
[212] L.H. Macedo, J.F. Franco, M.J. Rider, and R. Romero, *Optimal Operation of Distribution Networks Considering Energy Storage Devices.* IEEE Transactions on Smart Grid, 2015. **6**(6): p. 2825-2836.
[213] I.I. Cplex, *V12. 1: User's Manual for CPLEX.* International Business Machines Corporation, 2009. **46**(53): p. 157.
[214] G. Optimization, *LLC.(2022).* Gurobi Optimizer Reference Manual.
[215] Y.-O. Udoakah, E. Mudaheranwa, J. Liang, and L. Cipcigan, *Black Start Application in Power System Restoration using Distributed Energy Resources.* Energy. **2004**: p. 2965.
[216] O. Patrick, O. Tolulolope, and O. Sunny, *Smart Grid Technology and Its Possible Applications to the Nigeria 330 kV Power System.* Smart Grid and Renewable Energy, 2013. **04**(05): p. 391-397.
[217] *Nigeria Electricity and Gas Improvement Project December 2017, Transmission Expansion Plan Development of Power System Master Plan for the Transmission Company of Nigeria, Final Report.* 2018 Available from: https://www.google.com/url?sa=i&rct=j&q=&esrc=s&source=web&cd=&cad=rja&uact=8&ved=0CAIQw7AJahcKEwjQ8trz96mAAxUAAAAAHQAAAAAQAg&url=https%3A%2F%2Ftcnpmu.ng%2Fpmu_assets%2Fpmu_files%2F2018%2F02%2FFinal-Report-Text.pdf&psig=AOvVaw3XT7SIK7vZ657_o7lYOjUl&ust=1690377162613075&opi=89978449. [Accessed August 2022].
[218] P. Van den Bossche, F. Vergels, J. Van Mierlo, J. Matheys, and W. Van Autenboer, *SUBAT: An assessment of sustainable battery technology.* Journal of Power Sources, 2006. **162**(2): p. 913-919.
[219] H. Ibrahim, A. Ilinca, and J. Perron, *Energy storage systems—Characteristics and comparisons.* Renewable and Sustainable Energy Reviews, 2008. **12**(5): p. 1221-1250.